

Characterization of interlaminar fracture in composite materials : a case study approach
by Aaron Michael Cook

A thesis submitted in partial fulfillment of the requirements for the degree of Master of Science in Mechanical Engineering
Montana State University
© Copyright by Aaron Michael Cook (2001)

Abstract:
Composite materials are replacing standard engineering metals and alloys for many applications. Their inherent ability to be custom tailored for any application has made fiber reinforced composites a very viable material option. Their superior specific strength and stiffness characteristics have made them very competitive in the aerospace industry.

The primary limitation of fiber reinforced composites is fracture toughness, specifically delamination. Delamination failures are common due to the nature of composite construction. A variety of manufacturing techniques are available to make composites. Generally, all these methods employ a layered stacking of fibers in a primary plane. The interface between these layers is typically not reinforced with fibers and is the source of delamination or interlaminar fracture. Porosity and other manufacturing related defects also introduce nucleation sites for delamination.

Methods exist to evaluate and quantify inter-laminar fracture toughness, both experimentally and analytically. The material property that best represents resistance to delamination is the strain energy release rate (Gc). This can be experimentally obtained and analytically predicted with some success.

The primary focus of this study was the development of a process that would characterize and address interlaminar fracture in composites. This common mode of failure is not easily accounted for or mitigated. The design process developed considered two distinct approaches. Both methods required a database of material properties to compiled. The primary design approach was a “screening” methodology that employed comparative testing to down select composite architectures based on design drivers and applications. Another approach that was also investigated was a “predictive” or analytical approach. This process consisted of using closed form solutions or specifically finite element modeling methods to determine the strain energy release rate for given modes of failure. It was determined that analytically predicting crack growth or damage in complex structures will require research and study beyond this thesis. However, the screening approach provided meaningful results repeatedly.

This screening approach was applied to several case studies. Each case study was a separate project that investigated a unique topic relating to interlaminar fracture of composites. The process was used to satisfy sponsor needs and each project in turn provided a means to validate or improve the process. Each case study was also used to advance and validate the analytical techniques as well. Four case studies will be presented and the technical contributions of each will be discussed.

1. Evaluating composite Aerofan blade material for Pratt&Whitney 2. Investigating composite honeycomb fuel tanks for the X-33 3. Characterizing Aerospace resin systems for ACG 4. Understanding composite to metal bond behavior The four case studies were unique investigations that required interlaminar fracture characterization and analysis. In almost all cases delamination was the source of primary structure failure.

CHARACTERIZATION OF INTERLAMINAR FRACTURE IN COMPOSITE MATERIALS

A CASE STUDY APPROACH

by

Aaron Michael Cook

A thesis submitted in partial fulfillment
of the requirements for the degree

of

Master of Science

in

Mechanical Engineering

MONTANA STATE UNIVERSITY-BOZEMAN
Bozeman, Montana

July 2001

N378
C7711

APPROVAL

of a thesis submitted by

Aaron Michael Cook

This thesis has been read by each member of the thesis committee and has been found to be satisfactory regarding content, English usage, format, citations, bibliographic style, and consistency, and is ready for submission to the College of Graduate Studies.

Dr. Douglas Cairns Douglas S. Cairns (Signature) 7/10/01 Date

Approved for the Department of Mechanical & Industrial Engineering

Dr. Vic Cundy (Signature) 7/11/01 Date

Approved for the College of Graduate Studies

Dr. Bruce McLeod Bruce R. McLeod (Signature) 7-17-01 Date

STATEMENT OF PERMISSION TO USE

In presenting this thesis in partial fulfillment of the requirements for a master's degree at Montana State University-Bozeman, I agree that the Library shall make it available to borrowers under rules of the Library.

If I have indicated my intention to copyright this thesis by including a copyright notice page, copying is allowable only for scholarly purposes, consistent with "fair use" as prescribed in the U.S. Copyright Law. Requests for permission for extended quotation from or reproduction of this thesis in whole or in parts may be granted only by the copyright holder.

Signature Aaron Cook

Date 7/10/01

ACKNOWLEDGMENTS

I thank Dr. Douglas Cairns and Dr. John Mandell for their assistance and motivation in this research. I would also like to thank Dr. Ladean McKittrick for serving as a graduate committee member, and for providing guidance in the field of finite element analysis. Additional gratitude is offered to the sponsors involved in this study. Pratt & Whitney, AlliantechSystems, Advanced Composite Group, and the D.O.E. EPSCOR all provided funding and unique research opportunities. A special thanks is also extended to the members of the Composite Technology Research Team. Daniel Samborsky was especially helpful with his knowledge and suggestions for experimental testing. I am additionally thankful to Dr. Cundy and the Industrial and Mechanical Engineering Department's administrative team.

TABLE OF CONTENTS

LIST OF FIGURES xi

LIST OF TABLES xvii

ABSTRACT xix

1. INTRODUCTION 1

Composite Materials 1
Needs 2
Available Technology 2
Goals 3
Case Study Approach 3
Case I Carbon Fiber Aerofan Blades 5
Case II Honeycomb Sandwich Fuel Tanks 6
Case III Low Temperature Cure Composite Structures 7
Case IV Composite to Metal Interfaces 8
Evaluation Methodology 9

2. BACKGROUND 10

Composites 10
Advantages and Disadvantages 10
In-plane and Out of Plane Properties 11
Manufacturing 12
Failure Types and Related Theories 12
Strength of Materials Approach 13
Fracture Mechanics Approach Background and History 14
Interlaminar Fracture 15
Fracture Mechanics Overview 16
Mode I 17
Testing Procedure for DCB Specimen 19
Data Reduction Methods 21
Mode II 22
Testing Procedure for ENF Specimen 23
Data Reduction Methods 26
Finite Element Theory 27
Benefits 27
Models and Modeling Procedure 28
Step1 Geometry Development 29
Step 2 Element Choice 29
Step 3 Constitutive Properties 31

Step 4 Meshing 31
Step 5 and 6 Application of Constraints and Loads 32
Step 7 and 8 Solution and Results 32
Finite Element as Related to Fracture Mechanics 32
Strain Energy Release Rate Methods 33
Virtual Crack Closure Techniques 33
Crack Extension Techniques 36

3. INTERLAMINAR FRACTURE CHARACTERIZATION PROCESS 38

Needs 38
Optimization 39
Fracture Toughness Tips and Tradeoffs 39
Resin System 40
Fibers 40
Inhomogeneities 41
Porosity 41
Ply-drops and Dissimilar Material Interface 42
Interlaminar Zone and Other Inhomogeneities 43
Prediction and Screening Approach 44
Database 45
Screening Process 46
Screening Procedure 47
Prediction Approach 49
Composite Design 51

4. CASE STUDY I COMPOSITE AEROFAN BLADE EVALUATION 54

Project Introduction 54
Existing Work 55
Full Scale testing and Need for Screening Process 56
Problem Statement 57
Design Drivers and Material Limitations 58
Materials Provided and Specimen Description 58
Material Property Isolation 60
Test Matrix 61
Experimental Procedures 63
Basic In-plane and Interlaminar Properties 63
Delamination Mode II Testing 63
Apparatus 64
Procedure 66
Data Reduction 68
Dynamic Flexure Testing 74
Apparatus 75

Procedure 75
Data Reduction 75
Static Flexure Testing 78
Apparatus 78
Procedure 79
Data Reduction 80
Tensile Test 81
Apparatus 81
Procedure 81
Experimental Results 83
Mode II Delamination Resistance Results 83
Dynamic Flexure Results 86
Static Flexure Results 89
Tensile Test Results 91
Summary of Experimental Results 92
Numerical Analysis for Case Study I 94
Static Flexure Approach 94
Static Flexure Model 94
Static Flexure Numerical Results 96
End Notch Flexure Approach 98
End Notch Flexure Model 99
End Notch Flexure Results 101
Comparison 102
Test Specimen Validation 104
Summary for Case Study I 105

5. CASE STUDY II HONEYCOMB FUEL TANK INVESTIGATION 108

Project Introduction 108
Case Study Goal 109
Experimental Procedures 110
Flatwise Tension Testing 111
Specimen Preparation 113
Testing Procedure 114
Data Reduction Methods 115
Mode I Testing 118
Testing Procedure 119
Data Reduction Methods 119
Mode II Testing 121
Testing Procedure 122
Data Reduction Methods 122
Flatwise Compression Testing 125
Specimen Preparation 125
Testing Procedure 125

Data Reduction Methods 126
Experimental Results 127
Flatwise Tension Results 128
Discussion of Flatwise Tension Results 130
Mode I Results 131
Mode II Results 137
Discussion of Mode II Results 138
Flatwise Compression Results 140
Discussion of Flatwise Compression Results 140
Numerical Analysis of Honeycomb Fuel Tank Investigation 142
Motivation 142
Flatwise Tension 142
Approach 143
Model 143
Results 144
Solution and Mesh Convergence 145
Mode I 149
Approach 149
Model 150
Solution and Convergence 151
Comparison 152
Mode II 154
Summary for Case Study II 155
Epilogue 156

6. CASE STUDY III AEROSPACE RESIN EVALUATION 157

Project Introduction 157
Problem Statement 158
Material and Specimen Description 159
Test Matrix 160
Experimental Methods 161
Static Flexure 161
Static Flexure Apparatus 161
Static Flexure Testing Procedure 162
Static Flexure Data Reduction 163
Fracture Toughness Testing 163
DCB Testing Procedure 163
DCB Data Reduction Methods 165
Mode II 165
ENF Testing Procedure 165
ENF Data Reduction Methods 166
Dynamic Mode II Testing 167
Dynamic ENF Apparatus 167

Dynamic ENF Testing Procedure 167
Dynamic ENF Data Reduction 168
Scanning Electron Microscopy Evaluations 171
SEM Apparatus 171
SEM Testing Procedure 171
Experimental Results 173
Static Flexure Test Results 173
Mode I Results from DCB Testing 174
Mode II Results from Static ENF Testing 177
Mode II Results from Dynamic ENF Testing 179
SEM Results for Selected Systems 182
Summary for Case Study III 186

7. CASE STUDY IV METAL INTERFACE 188

Bond Characteristics 188
Chemical Bond 189
Structural Interlock 189
Need for Simpler Structure and Methodology 189
Lap Shear 190
Single Lap Shear 190
Shear Lap Construction 191
Shear Lap Configuration 191
Test Procedure 192
Data Reduction 192
Double Lap Shear 193
Double Lap Shear Configuration 193
Double Lap Shear Construction 194
Double Lap Shear Test Procedure and Data Reduction 194
Miniroot 195
Miniroot Construction 195
Miniroot Configuration 196
Testing Procedure 197
Data Reduction 198
Sample Results 198
Debonding 199
Pullout 200
Metal Interface Experimental Results 200
Parametric Study 200
Surface Treatment 201
Elastic Properties 201
Chemical Bond Characteristics 201
Mechanical Bond Characteristics 202
Knurling 202

Threading 202
Resin Systems 202
Layup Variations 203
Insert Material 203
Insert Coating 203
Test Matrix 204
Single Lap Shear Results 205
Double Lap Shear Results 207
Miniroot Experimental Results 209
Insert Coating Effects 209
Geometry Effects 211
Mechanical Interlock 213
Metal Interface Numerical Study 214
SLS Motivation and Approach 214
Model 215
Results 216
Miniroot Motivation and Approach 218
Model 218
Results 219
Summary for Case Study IV 221

8. CONCLUSIONS AND FUTURE WORK 223

Composite Material Design Process 224
Importance of the Screening Process 225
Case Study Review 225
Case Study I Composite Aerofan Blade Evaluation 226
Case Study II X-33 Fuel Tank Investigation 227
Case Study III Aerospace Composite Resin Characterization 228
Case Study IV Metal Interface Evaluation 228
Future Recommendations 229

REFERENCES CITED 230

APPENDIX A: FINITE ELEMENT CODES 235

LIST OF FIGURES

Figure Page

1.1 PW-4000-112 Aerofan Blade 5

1.2 Honeycomb Fuel Cell 6

1.3 Composite Applications for Resins Evaluated 7

1.4 Composite Wind Turbine 8

2.1 Fiber and Transverse Directions of a Composite 11

2.2 Laminate Construction 12

2.3 Three Modes of Fracture and Related Loading 17

2.4 DCB Test in Progress 18

2.5 DCB Testing Geometry 19

2.6 Mode I Fracture Propagation Behavior of a Composite Specimen 20

2.7 ENF Test in Progress 23

2.8 Mode II Fracture Specimen Geometry 24

2.9 Typical Mode II Crack Behavior 25

2.10 Mode II Crack Behavior with Hysteresis Captured 25

2.11 VCCT-1 Schematic with 8 Node Quadrilateral Elements 34

2.12 VCCT-2 Schematic for Mode I Closure 35

3.1 Porosity in a Composite Laminate 41

3.2 Sandwich Panel Material with Ply Drops 42

3.3 Resin Rich Region in a Laminated Composite 43

3.4 Database Construction Process 46

3.5 Screening Approach 48

3.6 Analytical Process for Fracture Modeling 50

4.1 Example of Impact and Dynamic Flex Testing Rectangular Specimen 60

4.2 Impact Testing Fixture 64

4.3 Data Acquisition Used for Experimental Testing 65

4.4 Force vs. Time Output for Series 5 Laminate 67

4.5 Acceleration vs. Time for 5 Series Laminate 69

4.6 Velocity Profile for 5 Series Laminate 70

4.7 Displacement vs. Time for 5 Series Laminate 72

4.8 Dynamic Load vs. Displacement Trace for Series 5 Laminate 73

4.9 Dynamic Flexure Behavior... 76

4.10 Static Flexure Test Fixture and Specimen 78

4.11 Static Flexure Behavior 79

4.12 Tensile Test Behavior 82

4.13 Delamination Results for 5 Series Material 84

4.14 Force vs. Time for Dynamic Flexure Tests 86

4.15 Force vs. Deflection for Dynamic Flexure Tests 87

4.16 Static Flexure Comparison 89

4.17 Tensile Test Results 91

4.18 Stress vs. Strain for 5 Series 92

4.19 FEA Static Flexure Model 95

4.20 Comparison of Experimental Static Flexure Results to Numerical 96

4.21 Longitudinal Stress Plot from FEA Solution 97

4.22 ENF Mesh with Refined Region and Boundary Conditions 100

4.23 Friction Effects on Predicted Mode II Fracture Toughness 103

5.1 Sampling of Panel 1 From Lobe 1 110

5.2 Sampling of Panel 2 From Lobe 4 111

5.3 Mounting (Glue) Fixture Used to Attach Tabs to Specimen 112

5.4 Flatwise Tension Specimen Complete with Attached Tabs 114

5.5 Testing Jig with Universal Pivoting Capability (flexible coupler) 115

5.6 Graphical Presentation of Flatwise Tension Specimen 117

5.7a Mode I Testing Apparatus 118

5.7b Test in Progress 118

5.8 Three Successive Loading Cases for Lobe 4 Material 120

5.9 Mode II Testing Apparatus In Progress 121

5.10 Mode II Test Results of Lobe 4 Material 123

5.11 Mode II Test Showing Constant Loading During Crack Growth 124

5.12 Compression Testing Configuration 126

5.13 Typical Compression Test Result for Lobe 4 127

5.14 Graphical Behavior of Lobe 4 Material in Flatwise Tension 129

5.15 Comparison of Failure Modes of Lobe 4 to Lobe 1 129

5.16 Peel-off Test Results for Lobe 1 Material L1-DCB-4 131

5.17 Lobe 1 Material Specimen Core Shear Failure 134

5.18 Failure Mode of Lobe 4 Material 135

5.19 Comparison of Static Flexure and ENF Results for Lobe 4 139

5.20 FWT Flatwise (Transverse) Tension Model 144

5.21 FWT Stress Distribution with Core Close-up 145

5.22 FWT Solution Convergence 146

5.23 Plane Stress vs. Plane Strain 147

5.24 Stress Profile Based on Offset Distance 148

5.25 Stress Profile without Singularities 148

5.26 DCB Model for Sandwich Material 151

6.1 Static Flexure Test Results for 6867 Material 162

6.2 Hysteretic Behavior of 6866 DCB – 3 Specimen 164

6.3 Mode II Crack Behavior with Hysteresis Captured 166

6.4 Force vs. Time Data for 6868 XHTM Material 168

6.5 Acceleration vs. Time for 6868 XHTM Material 169

6.6 Velocity Profile for 6868 XHTM Material 169

6.7 Displacement vs. Time for 6868 XHTM Material 170

6.8 Dynamic Load vs. Displacement Curve for 6868 XHTM Material 170

6.9 SEM Photo 172

6.10 Mode I Results for Varying Post Cure Temperatures 176

6.11 Mode II Fracture Toughness as a Function of Postcure Temperature 179

6.12A 6863 npc at 1500 183

6.12B 6863 npc at 500 183

6.12C 6863 pc177 at 1500 183

6.12D 6863 pc177 at 500 183

6.13A 6865 npc at 1500 184

6.13B 6865 npc at 500 184

6.13C 6865 pc177 at 1500 184

6.13D 6865 pc177 at 500 184

6.14A 6866 npc at 1500 185

6.14B 6866 npc at 500 185

6.14C 6866 pc177 at 1500 185

6.14D 6866 pc177 at 500 185

7.1 Fatigue Specimen, R112 Cross-Section 188

7.2 Single Lap Shear Specimen 191

7.3 Double Lap Shear Specimen (DLS) 194

7.4 Array of Miniroot Variations 196

7.5 Miniroot Anatomy 197

7.6 Lap Shear and Miniroot Test Approach 198

7.7 Miniroot Failure Characteristics 199

7.8 Effects of Using Epoxy Coating as an Intermediate Adhesive 210

7.9 Debond Behavior of Miniroots with Round Inserts 212

7.10 Failure of 45 Degree Diamond Knurled Steel Insert Miniroot 213

7.11 Shear Stress Singularity Effects 215

7.12 SLS FEA Model and Mesh Detail 216

7.13 Lap Shear Analytical and Numerical Results for Etched Vinylester 217

7.14 Miniroot FEA Shear Stress Plot for Vinylester 219

7.15 Shear Stress Data From Peak to Level Stress 220

LIST OF TABLES

Table Page

1.1 Case Study Evaluations 4

2.1 Catastrophies Due to Fracture of Statically Loaded Structures 15

4.1 Description of Specimen Architecture 59

4.2 Test Matrix of Aircraft Fan Blade Candidates 62

4.3 Results for Delamination Mode II Testing 85

4.4 Summary of Dynamic Flexure Data 88

4.4 Comparison of Static Flexure Results 90

4.5 Suggested Material Properties for Composite X 93

4.6 ENF Convergence for G_{IIc} cf = 0.35 101

4.7 FEA Results Compared to Analytical Methods 102

5.1 Test Development and Test Matrix 109

5.2 Comparison of Flatwise Tensile Tests for Lobe 1 128

5.3 Summary of Lobe 4 Transverse or Flatwise Tension Tests 130

5.4 Summary of Lobe 1 (L1) Mode I (DCB) Test Results 133

5.5 Mode I Results for Lobe 4 Material 136

5.6 Mode II Results for Lobe 4 137

5.7 Summary of Compression Test Results for Lobe 1 and Lobe 4 141

5.8 Convergence Results for FEA Techniques 152

5.9 Comparison of FEA and Experimental Results for G_c 153

5.10 Shear Effects of G_{II} compared to G_I 154

6.1 Specimen Description 159

6.2 Test Matrix 160

6.3 Summary of Static Flexure Results 173

6.4 Static Mode I Test Results 175

6.5 Summary of Mode II Test Results 177

6.6 Summary of Dynamic End Notch Flexure Results 180

6.7 Rate Dependency Comparison for Mode II Testing 181

7.1 Test Matrix for Composite and Metal Interface Investigation 204

7.2 Single Lap Shear Test Results for Shear Strength 206

7.3 Single Lap Shear Test Results for Load / unit width 206

7.4 Double Lap Shear Test Results for Shear Strength 208

7.5 Results of Including Epoxy Coating 211

7.6 Comparison of Aluminum and Steel Rod Miniroots 212

ABSTRACT

Composite materials are replacing standard engineering metals and alloys for many applications. Their inherent ability to be custom tailored for any application has made fiber reinforced composites a very viable material option. Their superior specific strength and stiffness characteristics have made them very competitive in the aerospace industry.

The primary limitation of fiber reinforced composites is fracture toughness, specifically delamination. Delamination failures are common due to the nature of composite construction. A variety of manufacturing techniques are available to make composites. Generally, all these methods employ a layered stacking of fibers in a primary plane. The interface between these layers is typically not reinforced with fibers and is the source of delamination or interlaminar fracture. Porosity and other manufacturing related defects also introduce nucleation sites for delamination.

Methods exist to evaluate and quantify inter-laminar fracture toughness, both experimentally and analytically. The material property that best represents resistance to delamination is the strain energy release rate (G_c). This can be experimentally obtained and analytically predicted with some success.

The primary focus of this study was the development of a process that would characterize and address interlaminar fracture in composites. This common mode of failure is not easily accounted for or mitigated. The design process developed considered two distinct approaches. Both methods required a database of material properties to compiled. The primary design approach was a "screening" methodology that employed comparative testing to down select composite architectures based on design drivers and applications. Another approach that was also investigated was a "predictive" or analytical approach. This process consisted of using closed form solutions or specifically finite element modeling methods to determine the strain energy release rate for given modes of failure. It was determined that analytically predicting crack growth or damage in complex structures will require research and study beyond this thesis. However, the screening approach provided meaningful results repeatedly.

This screening approach was applied to several case studies. Each case study was a separate project that investigated a unique topic relating to interlaminar fracture of composites. The process was used to satisfy sponsor needs and each project in turn provided a means to validate or improve the process. Each case study was also used to advance and validate the analytical techniques as well. Four case studies will be presented and the technical contributions of each will be discussed.

1. Evaluating composite Aerofan blade material for Pratt&Whitney
2. Investigating composite honeycomb fuel tanks for the X-33
3. Characterizing Aerospace resin systems for ACG
4. Understanding composite to metal bond behavior

The four case studies were unique investigations that required interlaminar fracture characterization and analysis. In almost all cases delamination was the source of primary structure failure.

CHAPTER 1

INTRODUCTION

This focus of this study is on the delamination and interlaminar fracture performance of composite materials. General testing methods and procedures were employed to evaluate the fracture performance of sponsor supplied materials. Additionally, various methods of analysis were used for fracture toughness evaluation, including FEA (finite element analysis). Guidelines were generated for improving design with regard to fracture toughness. A general methodology for the characterization of composite laminates was developed employing standard procedures and analysis techniques.

Composite Materials

Fiber reinforced composite materials are replacing standard isotropic materials in many applications. Aerospace vehicles, aircraft, marine equipment, and common items such as civil structures, prosthetic devices, and sports equipment are currently being constructed of such composite materials.

The primary advantage of composite materials is their inherent ability to be custom tailored to a specific design situation. Constituents like fibers and matrix material can be used in different combinations, amounts, and architectures to obtain an optimal material composition.

A major drawback to laminated composite materials stems from the manufacturing process used to construct them. Placing fabric or fibers in strata to obtain

a desired architecture allows resin rich layers to form between fabric layers. These regions are without reinforcement and are prone to develop discontinuities such as pores and voids. The performance of the composite material at these locations is dominated by the properties of the resin. Often the failure of a composite structure begins with the separation of these layers or delamination.

Needs

Composite designers and engineers recognize delamination as a primary failure mode. Unfortunately, modeling and predicting this behavior is not easy. In general, designers and engineers have the ability to implement a stress analysis and utilize this in parallel with empirically obtained strength data. In the case of engineering composites, fracture toughness and delamination resistance are not as easily accounted for. A general need exists for an organized approach that designers can use to evaluate and improve interlaminar fracture properties and capabilities. Both database-prediction and screening schemes are viable and will be discussed.

Available Technology

As stated previously, procedures regarding the design of laminated composites are abundant [Jones (1999), Hyer (1998), and Tsai (1988)]. Classical lamination theory can be applied to determine an appropriate composite architecture. However, techniques for designing a delamination resistant material with necessary interlaminar fracture toughness properties for service, are not as well established.

Testing procedures, failure criteria, and finite element analysis techniques are at the engineer's disposal to evaluate and predict interlaminar fracture toughness of

composite materials. These available technologies can be combined and expressed in terms of a general methodology for fracture performance evaluation. In turn, this methodology can be employed to enhance the performance of composite structures.

Montana State University's Composite Technology Team has routinely investigated delamination type failures [Orozco (1999)]. Standard test procedures have been applied to unidirectional laminated composites to evaluate and quantify fracture toughness. These procedures have been focused at the evaluation of resin performance in composite architectures. Significant effort has been directed at applying finite element analysis and fracture techniques to the evaluation of these baseline composites. Studies have also been extended towards applying these procedures to more complex structures, such as T-sections [Haugen (1998) and Morehead (2000)].

Goals

Ultimately the procedures and techniques used to quantify the fracture toughness performance of composite specimens can be used to predict failure of more complex composite structures. The goal of the current study is to provide a systematic engineering approach to help develop laminated architectures, evaluate interlaminar fracture properties, and improve performance of engineering composites in commercial applications.

Case Study Approach

Several investigations were conducted to address both the strength and fracture toughness characteristics of different composite candidates. Each project possessed individual specific needs imposed by the demands of the commercial sponsor. However,

a common theme was implemented to satisfy those needs. A basic methodology was developed to evaluate and improve fracture toughness properties and interlaminar performance.

Four individual case studies were performed where, each case involved a special class of composites. The material evaluated in each case was generally a more complex evolved composite than a standard longitudinal or quasi-isotropic composite. In all cases, steps were taken to improve the strength or stress performance of the material. It was suspected that certain sacrifices in fracture toughness may have been induced by these modifications. Table 1.1 contains descriptions of each case study including the sponsor, material description, use, and mode of failure investigated.

Table 1.1 Case Study Evaluations

	Case I	Case II	Case III	Case IV
Sponsor	Pratt & Whitney	Alliant Techsystems	Advanced Composite Group	Department of Energy
Material Architecture	Through thickness reinforced carbon fiber composites	Honey comb sandwich panels	Unidirectional carbon fiber laminates	metal reinforced composite root structures
Application	High bypass aerofan engine blade	Fuel cells for X-33 space shuttle	Aerospace low temperature cured structures	Root fittings for wind turbine root connections
Failure Mode Investigated	Dynamic GII, dynamic flexure, static flexure and tension	Flatwise tension and compression, GI and GII	GI, GII, dynamic GII, and strength properties	Bond threshold and damage tolerance
Numerical Study	Dynamic GII	Flatwise tension, GI and GII	None (used SEM technology to inspect damage)	Single and double lap shear and miniature root specimen

Each of the case studies focuses on a specific aspect of delamination or interlaminar fracture. The materials in these studies were evaluated for advanced aerospace applications.

Case I Carbon Fiber Aerofan Blades

Architecture variations were the primary focus of this case study. Through the thickness reinforced fabrics were used to reduce the probability of delamination. The degree of reinforcement was varied and appeared to have an effect on strength. These carbon fiber and epoxy laminates were resin transfer molded for high bypass aerofan blades shown in Figure 1.1.

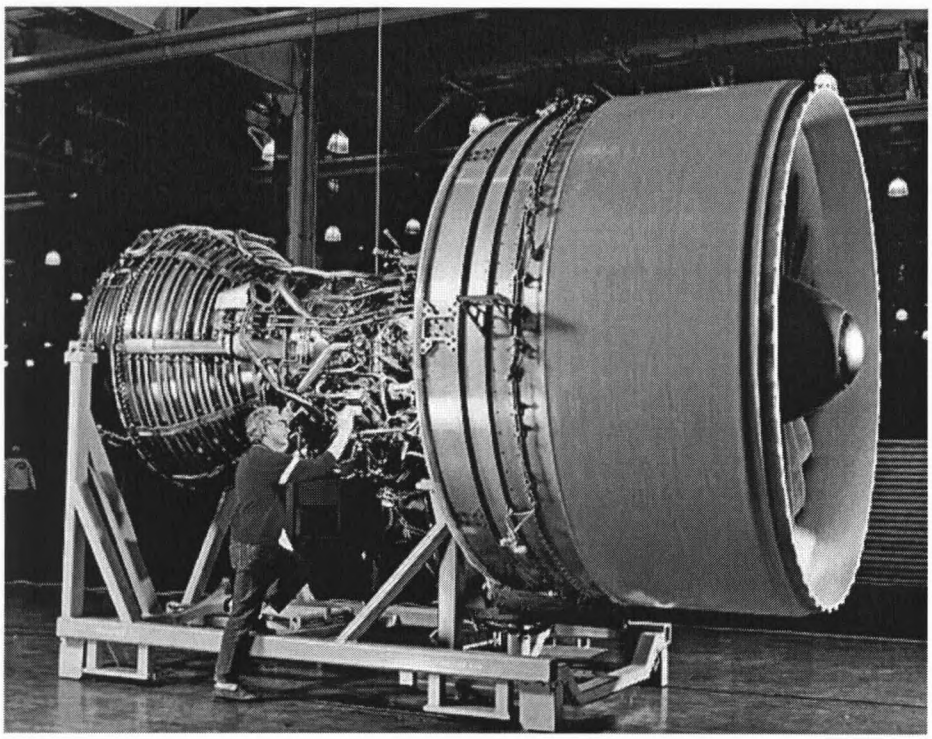


Figure 1.1 PW-4000-112 Aerofan Blade

Case II Honeycomb Sandwich Fuel Tanks

Inexpensive and lightweight core material was used with carbon fiber epoxy facesheets to construct a sandwich panel. Sandwich type construction was used with the intent of increasing bending strength and stiffness. However, in the process, a bond interface was introduced between the facesheets and the core material. This interface was investigated as a source for delamination and the limit of the performance of the material. These sandwich type composites were used in the construction of a lightweight fuel cell material shown in Figure 1.2.



Figure 1.2 Honeycomb Fuel Cell

Case III Low Temperature Cure Composite Structures

Several different resin systems were evaluated for interlaminar fracture toughness. The materials investigated were unidirectional carbon fiber pre-impregnated laminates. Nine separate material types were supplied and the formulated process was used to characterize the overall interlaminar fracture toughness of these systems. Post cure conditions were also varied for each system and the effect of this was quantified. Scanning electron microscopy was also used to inspect damage region and relate internal structure to fracture performance. The resin systems evaluated are used for the applications shown in Figure 1.3.

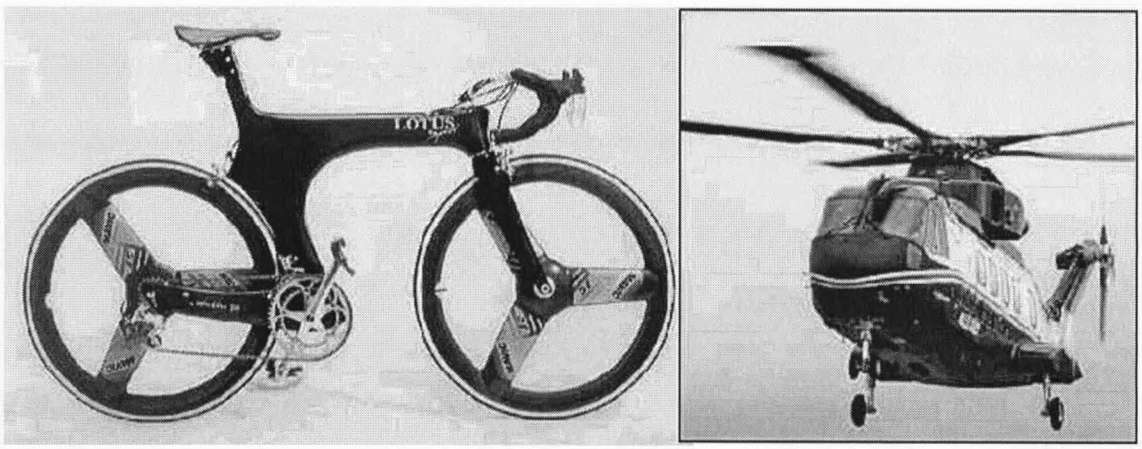


Figure 1.3 Composite Applications for Resins Evaluated

Case IV Composite to Metal Interfaces

In general, information regarding the bond characteristics between metal and composites is limited. The interface between the metal and composite or resin was identified as a potential delamination site. Experimental test methods were developed and implemented. FEA was also used to validate and interpret experimental findings. The metal inserts were in use for the root connections of a composite wind turbine blade in this case (shown in Figure 1.4). They were molded into a composite laminate and used for bolted connections to a hub.

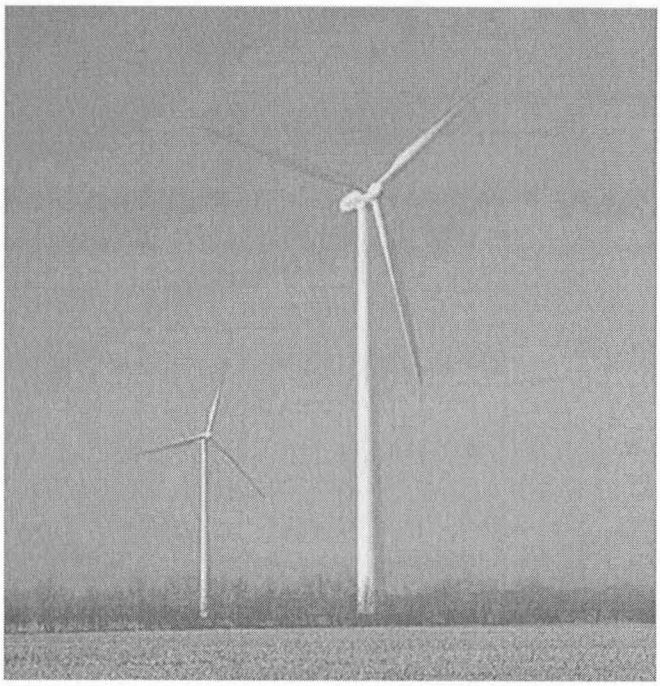


Figure 1.4 Composite Wind Turbine

Evaluation Methodology

A general methodology was developed that, employs predictive techniques and screening processes to evaluate a materials fracture toughness performance. The experimental methods used are presented, as well as analytical techniques. The process and related technology were then applied to the three case studies described above. Some of the results are specific to the sponsor and their specific demands. However, the approach was generalized and can be applied to other similar design situations.

CHAPTER 2

BACKGROUND

Composites

The first person to construct a home from mud and straw may have been the first composite designer. However, many people attribute the space race and its demand for higher flying, faster, and lighter aircraft to be the largest source of growth and development in composite materials [Hyer (1998)]. Aerospace applications have provided knowledge and technology that have spread to commonalities such as sports equipment and simple civilian structures.

Advantages and Disadvantages

The overall advantage of composite materials is the inherent ability to customize or tailor the directional capabilities of the component materials to meet the demands of specific design loads. Utilizing the strength of the fibers can provide structures that have superior strength and stiffness in the fiber direction. Typically, this comes at the expense of reduced strength and stiffness properties in the transverse direction. Decreased transverse properties or properties normal to the fiber direction are considered to be a large weakness of composites. Examples of fiber direction and transverse directions are shown in Figure 2.1

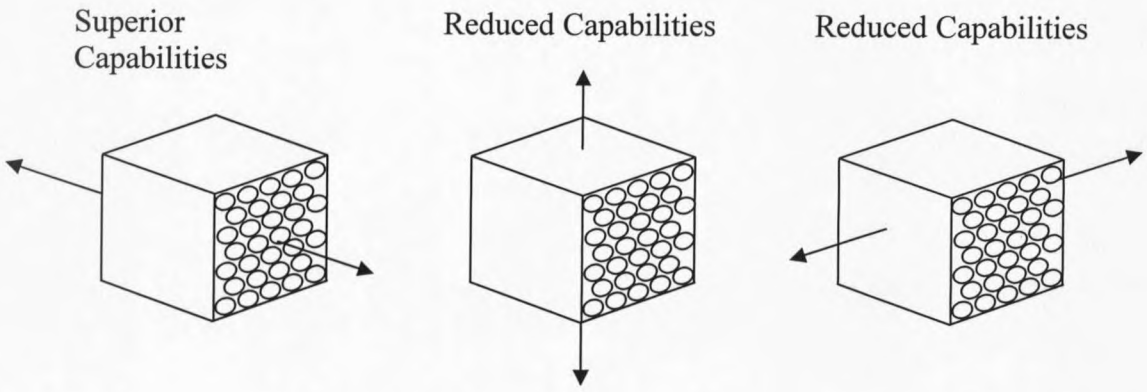


Figure 2.1 Fiber and Transverse Directions of a Composite

In-plane and Out of Plane Properties

The performance of laminated composite materials is typically divided into two groups, in-plane and out of plane. In plane properties are those that relate to the plane of the predominant fiber direction. Typically fibers are oriented in a specific direction to support expected loads. The direction or plane in which the majority of the fibers or fabric lay is referred to as in-plane. The direction perpendicular to the fibers, or transverse is out of plane.

The overall layup or design of a laminated composite material is the architecture. The architecture accounts for the intended loading with fiber volume, fiber type, orientation of each layer of fiber fabric, resin type, and any other reinforcement. Any combination of the above variables is composite or material architecture.

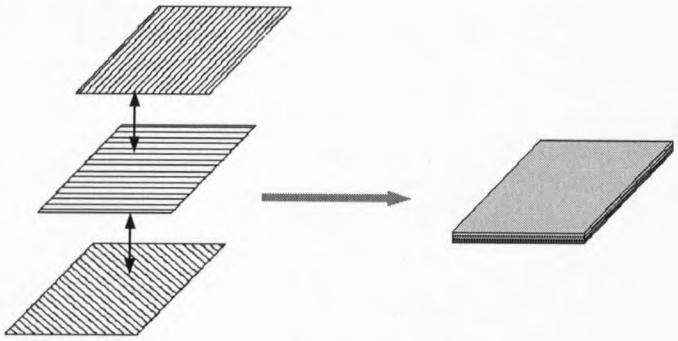


Figure 2.2 Laminate Construction

Manufacturing

A major weakness of laminated composite architectures stems from the way in which they are constructed or manufactured. Three common methods are utilized for the manufacture of composite materials. They are hand lay-up, resin transfer molding and vacuum assisted resin transfer molding. For all three of these techniques, plies or layers of fabric are placed on top of one another to construct an architecture. The interface between these layers is a resin-rich, fiber-absent region that has diminished resistance to shear forces. As a result, delamination is one of the most common types of failure in composites.

Failure Types and Related Theories

Failure modes are typically categorized as either static or dynamic failures. Static failures occur typically when a materials stress exceeds it strength [Gere (1984)]. This mode of failure is commonly termed the "strength of materials criterion". Materials often fail well below this strength; this reduction in strength is often attributed to the presence

of cracks and flaws. When the stress intensity at a crack front exceeds the material's critical stress intensity factor, failure occurs. Accounting for or predicting this type of failure is the science of fracture mechanics. Examples of dynamic or time dependent failures are creep and fatigue. These types of failures and analysis will not be addressed in this study.

Strength of Materials Approach

Static stress failure criteria exist for both ductile and brittle materials. Typically a maximum combined stress state is analyzed and compared to the material's strength [Norton (1996)]. The material's design strength is usually based on a published value or a quantity obtained empirically. A variety of experimental methods are available for determining material strength and depend mostly on material type. Ductile materials, such as steel and aluminum, are traditionally evaluated with the maximum distortion energy criterion, often referred to as the Henky-von-Mises Criterion. Brittle materials are not accurately represented by this criterion. As a result, the Coulomb Mohr theory is usually preferred for evaluating and assessing limiting stresses of brittle materials such as cast iron [Norton (1996)]. Composite material strengths are not accurately represented by either of the above failure criterion, primarily due to their anisotropic nature.

Although composite materials are not usually classified as ductile materials and are not isotropic, often the maximum stress or a modification of the von-Mises criterion is employed to estimate the failure stress [Norton (1996)]. This method can be accurate depending on the application, but not for general cases. An improved criterion for evaluating limiting stresses for composites is the Tsia-Wu criterion [Hyer (1998), Jones

(1999) and Tsai (1971)]. This method accounts for the anisotropic construction and behavior of composites. The Tsia-Wu criterion offers a unique advantage. This method can be used to analyze each layer or laminae of the structure individually. Then, the limiting layer of entire architecture is isolated, and the corresponding limiting stress is found. An overview summarizing and comparing these criteria can be found in Tsai (1971).

Fracture Mechanics Approach Background and History

The strength of materials approach to static failure assumes a material to be homogenous in some cases, isotropic in some cases, and free of defects such as micro-cracks and voids in all cases. These assumptions are not always valid. With the case of metals and alloys, cracks are typically caused by manufacturing and processing treatments. Small cracks are almost always present and should be accounted for in analysis. Components can fail at stresses well below the material's strength when cracks are present. When the critical amount of energy is present or when the stress intensity is adequate, crack propagation occurs. Brittle type fracture in ductile materials has been the cause of many catastrophic disasters [Broek (1996) and ASM (1997)]. A brief timeline of noteworthy fracture induced failures is offered below in Table 2.1.

Table 2.1 Catastrophies Due to Fracture of Statically Loaded Structures

Date	Event
March 19th 1830	Montrose Suspension bridge chains gave way during a boat race resulting in many deaths
1860-1870	200 deathes/year due to wheel and axle fractures in England
January 19th 1919	Boston Molasses Tank Rupture killed 21 people
January 16th 1943	WWII tankers cracked in half due to residual stresses and cracking from welding.

The failures in Table 2.1 are all fracture failures of metal structures. The stress-state during the catastrophe was below the critical strength of the structure's material. The cause of failure in each of these events is commonly believed to be the result of brittle fracture. Interestingly enough, steel is known to exhibit a ductile to brittle transition in behavior at low temperatures. Most of the above failures occurred during winter or colder months.

Interlaminar Fracture

Metals are not the only materials susceptible to failure due to fracture or crack propagation. Composite materials are often vulnerable to fracture type failure called interlaminar fracture. Interlaminar fracture occurs when the plies or layers separate. Often voids, pores, or other small defects are present between layers. These

discontinuities provide nucleation or initiation points for separation to occur. Interlaminar fracture is a common mode of failure for composite materials, especially in laminated architectures [Hyer (1998), Broek (1996), and Jones (1999)]. This failure phenomenon will be a focus of this study.

Fracture Mechanics Overview

As stated previously, failure can occur in a material or structure at stresses well below the yield or ultimate strength. Griffith stated that "crack propagation will occur if the energy released upon crack growth is sufficient to provide all the energy that is required for crack growth [Griffith (1920)]." Griffith's criterion can be mathematically expressed as:

$$\frac{dU}{da} \geq \frac{dW}{da} \tag{2.1}$$

where U is the elastic energy,

W is the energy required for crack growth,

a is the crack length and (da) is the change in crack length.

G is the strain energy release rate or crack driving force and is equal to (dU/da).

The energy consumed in crack propagation is denoted by R=dW/da, which is called the crack resistance [Broek (1996)].

There are three distinct modes of fracture that are related directly to the manner of loading. These modes are denoted as mode I, mode II, and mode III type fractures. All three modes are shown in Figure 2.3, as well as the loading required to induce them.

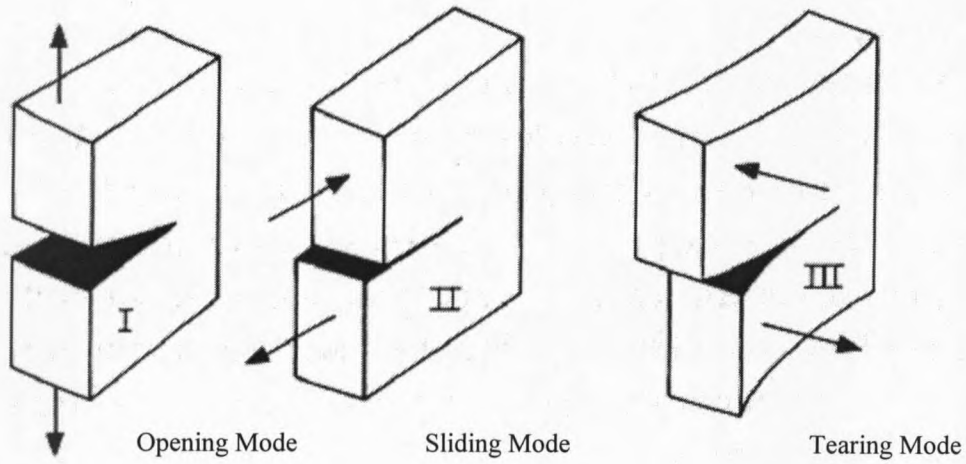


Figure 2.3 Three Modes of Fracture and Related Loading

Mode I

Mode I type fracture has typically been accepted as the most common and important mode of crack propagation. A normal stress field induces an opening or "wish-bone" effect. This type of behavior is common in structure and substructures such as skin stiffeners, I beams, or bonded connections of separate structures [Broek (1996)]. Brittle metals such as cast iron typically fail from mode I type fracture in service. This is one reason that some homogeneous materials possess a compressive strength that is significantly greater than their tensile strength.

Mode I fracture toughness can be evaluated a variety of ways. For engineering polymers and metals, an ASTM standard compact tension sample (similar to Figure 2.3) is used [ASTM E 399-90 (1992)]. These test specimens have prescribed dimensions that simulate plain strain type loading. Ultimately K_{Ic} is obtained based on initial crack length and remote stress field. K_{Ic} is a stress intensity factor that accounts for the reduced load

handling capability of a material based on stress concentrations from cracks. Some iterations may be necessary to provide valid test results. This type of testing is usually only valid for high strength-brittle materials and homogenous materials in general.

In the case of laminated composites, the Griffith criterion is employed to evaluate G_{Ic}, the critical amount of energy required to propagate a crack. The DCB or double cantilever beam test is used [ASTM D 5528-94 A (1997)] to obtain this material property. A DCB test in progress is shown in Figure 2.4 below. A generalized configuration of a DCB test is shown in Figure 2.5. Several dimensions need to be measured prior to testing and typically force vs. deflection is recorded during crack initiation and propagation. A variety of reduction techniques are available to calculate G_I or Mode I fracture toughness.

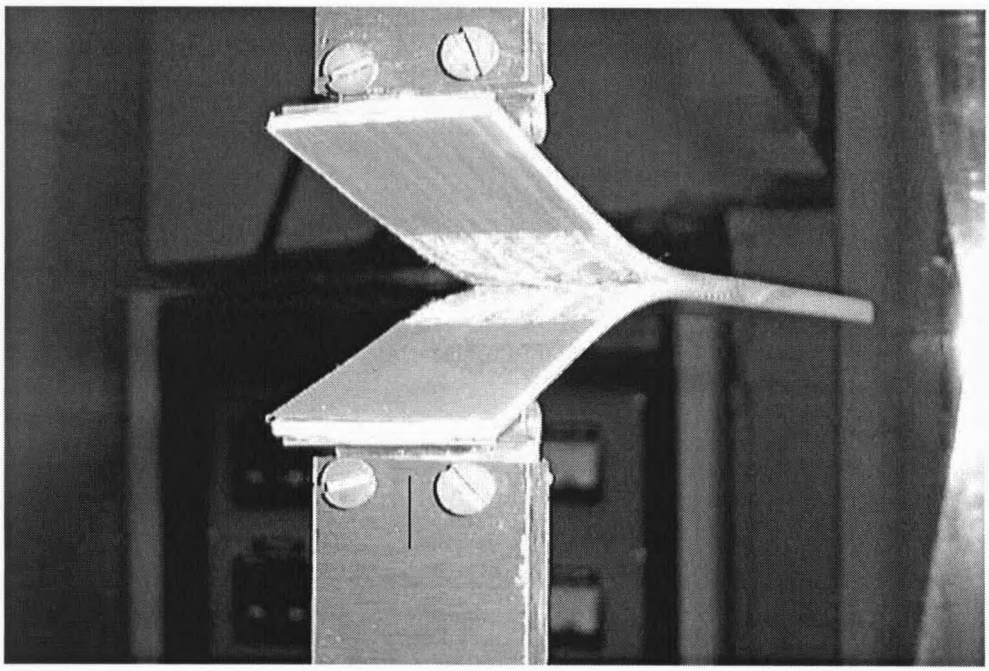


Figure 2.4 DCB Test in Progress

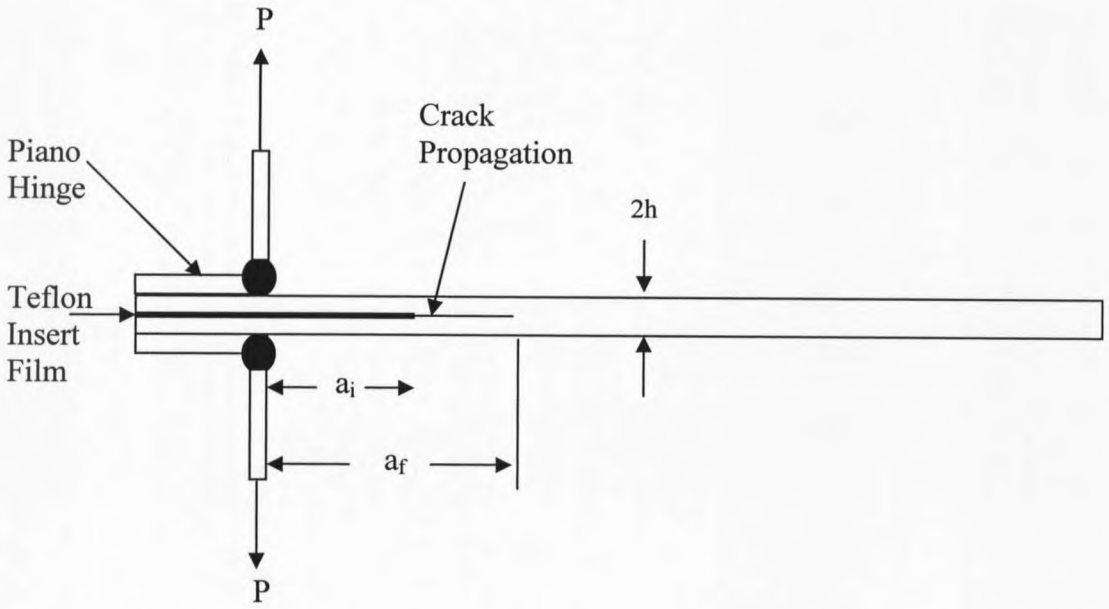


Figure 2.5 DCB Testing Geometry

Testing Procedure for DCB Specimen

DCB specimens can be sectioned from a plate where a teflon strip has been inserted to represent a flaw or crack. Once the specimens have been cut from the plate, hinges are attached at the crack end of each specimen as shown in Figure 2.5. A fixture is used to connect the hinges on each DCB specimen to standard Instron grips. The gripped hinges are then pulled slowly apart in displacement control until satisfactory crack growth has occurred in the specimen. At this point, the test machine's actuator is

reversed to allow specimen unloading. During this entire process, force and corresponding actuator displacement are recorded. The area enclosed by the force – displacement curve represents the energy absorbed by the specimen. Provided that no damage has occurred beyond crack growth, this energy is directly responsible and related uniquely to crack growth, or propagation [Broek (1996)]. Once the specimen is unloaded, the procedure can be repeated to extend the crack further. A more compliant force – displacement graph will result. Results from five crack propagations of the same specimen are shown in Figure 2.6.

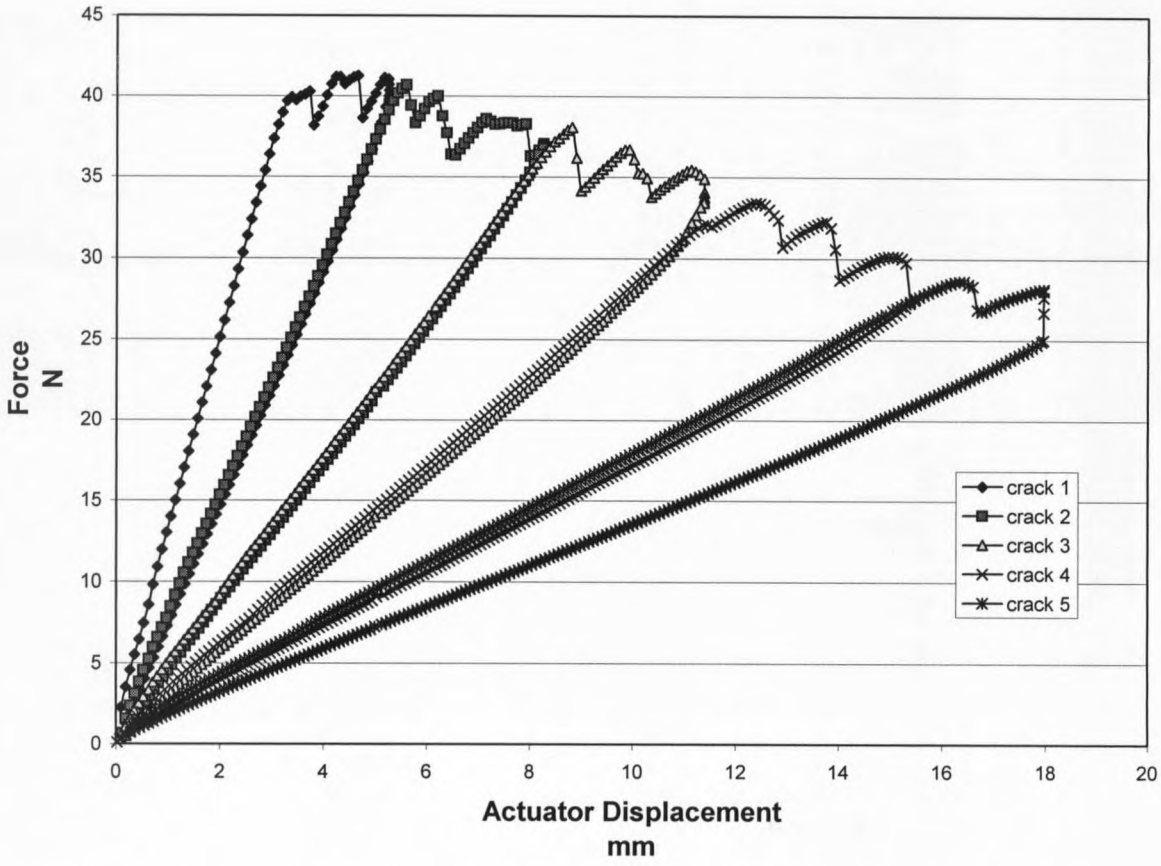


Figure 2.6 Mode I Fracture Propagation Behavior of a Composite Specimen

Data Reduction Methods

A common method to evaluate mode I fracture toughness is to simply calculate the energy a specimen has absorbed during loading and unloading and divide that quantity by the crack damage area. The crack damage area in the case of a DCB specimen is the width of the specimen multiplied by the propagated crack length. The Energy method used to calculate mode I fracture toughness[Broek (1997)] can be written as:

$$G_I = \frac{SE}{b(a_f - a_i)} \tag{2.2}$$

where

SE is the dissipated energy, numerically integrated from the force – displacement curve, b is the specimen width, as shown in Figure 2.5,

a_f is the final crack length and a_o is the initial crack length, as shown in Figure 2.5.

This is the most fundamental method for acquiring a G_I value from experimental data. Other methods are available to evaluate G_I. One such method is the modified beam theory method. This method (2.3), like the area method, doesn't require material properties to be known a priori.

$$G_I = \frac{3P\delta}{2ba} \tag{2.3}$$

where

P is load corresponding to initial crack onset,

δ is the deflection (actuator displacement) corresponding to initial crack onset,

a is the initial crack length at crack onset (a_I in Figure 2.5),

b is the specimen width from Figure 2.5.

It should be noted that this equation is valid anywhere the crack length and corresponding load and deflection values are known, while crack growth is occurring. The load and deflection at crack arrest could also be applied to equation (2.3), with the final crack length used for a. This approach would provide conservative results since it requires a slight increase in load to regenerate crack growth. This is evident from viewing the fracture propagation curve in Figure 2.6.

Mode II

Mode II fracture is caused by in plane shear or a sliding motion between two surfaces. Bending is the load scenario that typically induces mode II fracture. This failure mode is more prevalent in laminated composites than metals due to the layered construction [Russel (1987) and Carlsson (1986)]. To evaluate mode II fracture toughness, a three point bending apparatus is used to conduct an end notch flexure (ENF) test. A typical test apparatus is shown in Figure 2.7 below.

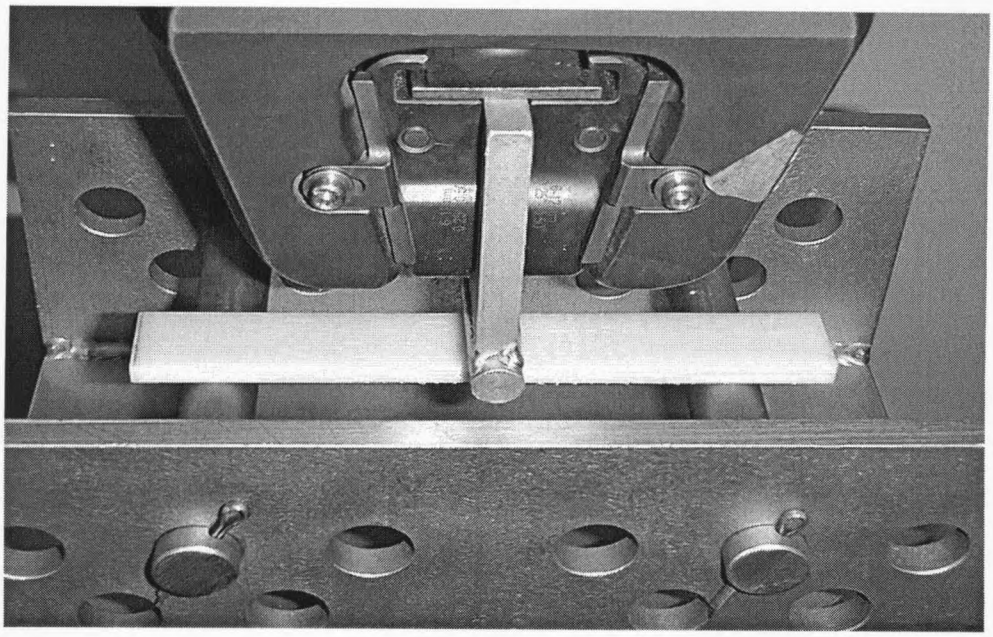


Figure 2.7 ENF Test in Progress

Testing Procedure for ENF Specimen

As with the DCB specimen, an initial crack is required and is typically created during manufacture with the insertion of a teflon strip. An ENF or end notch flexure specimen is supported by two rollers, which are separated by about 125 mm. The supported specimen is then loaded at midspan by a loading nose to ensure line contact. A model ENF specimen is shown in Figure 2.8.

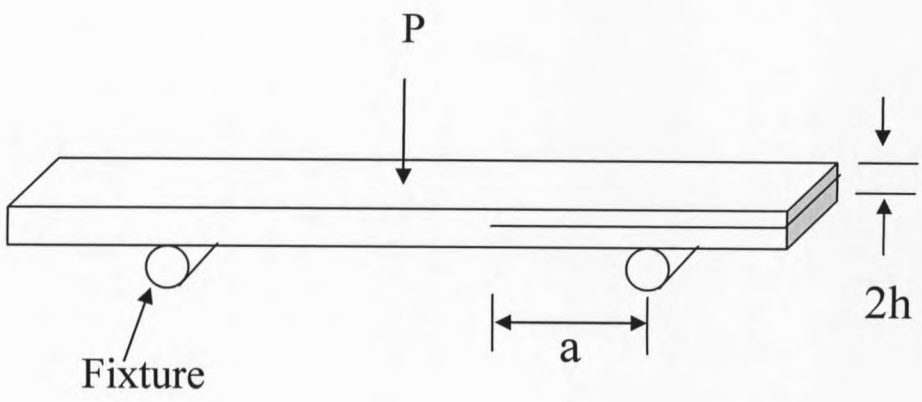


Figure 2.8 Mode II Fracture Specimen Geometry

The load is incremented in displacement control until the crack propagates. Mode II crack propagation is typically confirmed by the presence of audible cracking and is generally not stable. The crack propagates to the midspan or further, in a very sudden fashion. As a result, repeat crack growths are generally not possible because the crack will generally extend between the entire span of the supports. The hysteretic behavior of unloading is generally not captured. Instead, a straight line is assumed back to the origin, and the bounded area again approximates the energy absorbed as shown in Figure 2.9. The unloading behavior can be captured and provides assurance that delamination was the only failure mode. An example is shown in Figure 2.10.

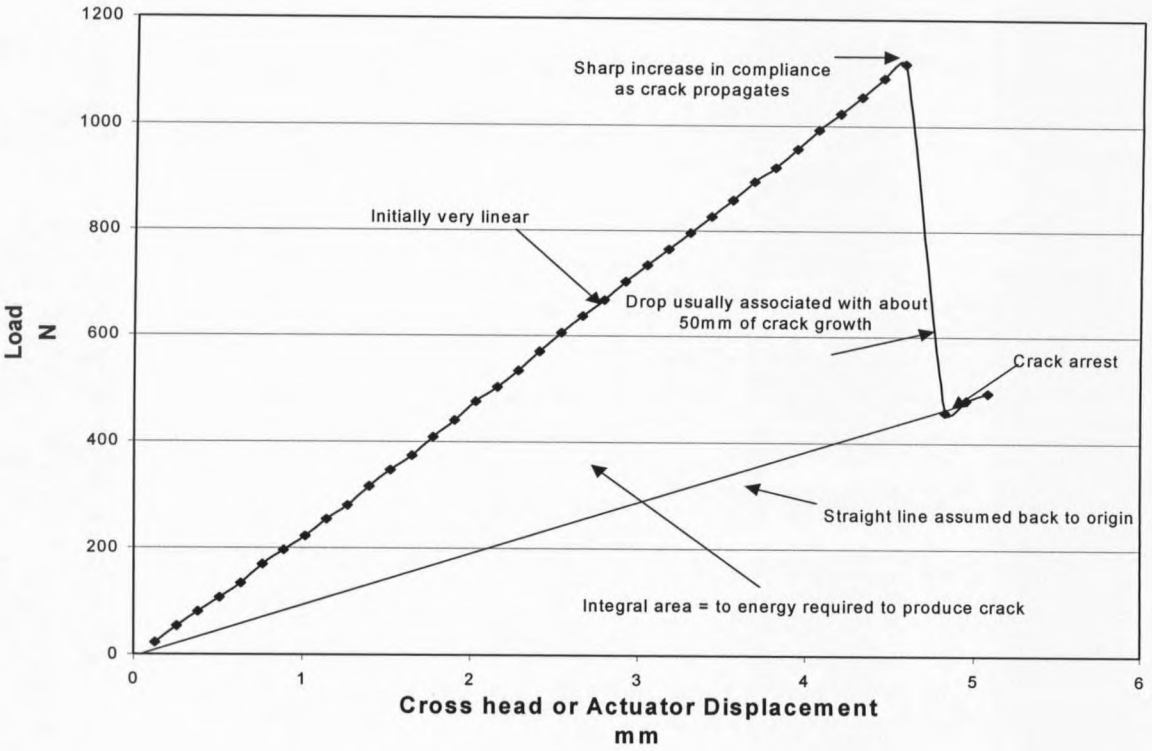


Figure 2.9 Typical Mode II Crack Behavior

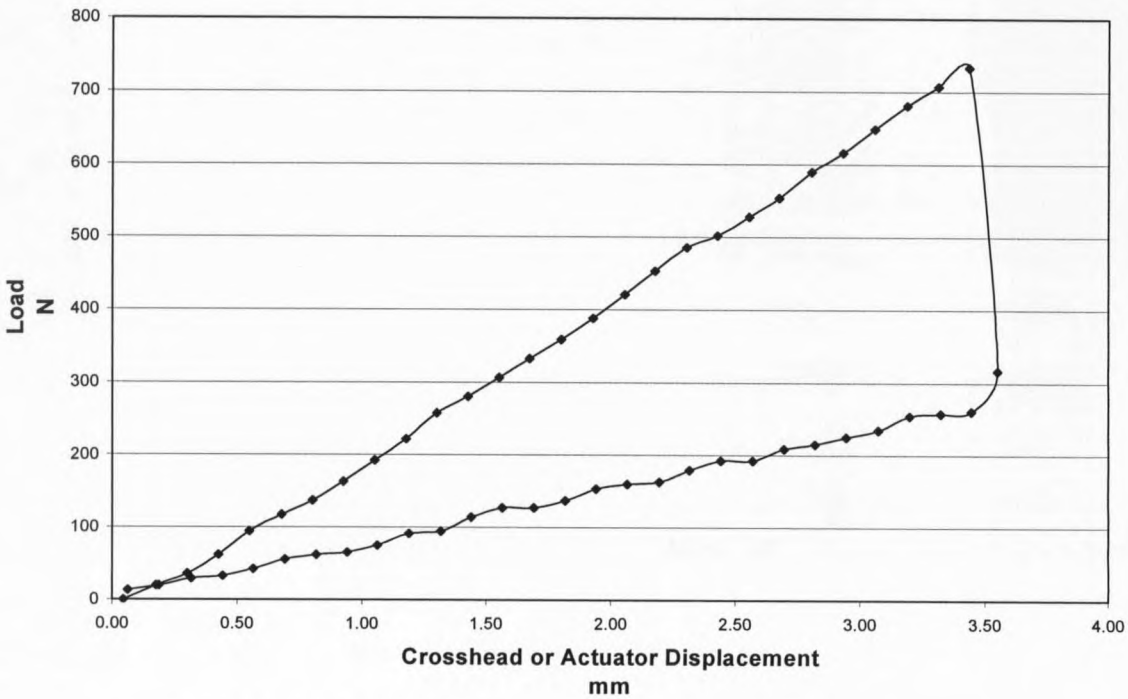


Figure 2.10 Mode II Crack Behavior with Hysteresis Captured

Data Reduction Methods

As in the case of mode I type fracture, the driving element of crack growth is strain energy. The energy method, equation (2.2), is valid for mode II fracture as well. The load displacement data can be integrated and divided by the crack damage area to calculate a G_{II} or mode II fracture toughness.

There is another method available to evaluate G_{II} that is based on beam theory. This method is called the compliance method. The following series of equations demonstrate the use of this method [Cairns (1992) and Carlsson and Gillespie (1986)].

$$G_{II} = \frac{9P^2Ca^2}{2w(2L^3 + 3a^3)} \tag{2.4}$$

where P is the critical load or the force at crack initiation,

C is the compliance of a simple supported beam with a crack extending to one, edge of length (a),

a is the initial crack length,

w is the width of the specimen,

L is the span length of the specimen.

The compliance (C) can be found by

$$C = \frac{2L^3 + 3a^3}{8Ewh^3} \tag{2.5}$$

where E is the elastic modulus and h is half of the total specimen thickness.

A simplified expression for the mode II fracture toughness that neglects shear contributions is as follows:

$$G_{II} = \frac{9 \cdot P^2 a^2}{16 \cdot Ew^2 h^3} \tag{2.6}$$

Finite Element Theory

The finite element (FEA) method essentially solves the basic spring equation for segmented regions of a larger body. Then secondary quantities such as strain and stress are derived from approximation functions and basic constitutive relations. This method is an approximation that generally provides improved results as the number of regions or elements used to represent a body is increased. This is increased subdivision is called mesh refinement.

Benefits

The role of finite element analysis is potentially unlimited. Finite element simulations are generally used to model experimental phenomena. In the case of costly experiments with limited material and facilities, finite element simulations can reduce the number of iterations required to perfect experimental procedures. The primary function of FEA is modeling complex geometries that can not easily be tested or represented by simpler methods. Modeled stresses can be compared to material strengths to predict failure. Other forms of failure such as buckling and fracture can be modeled as well.

Models and Modeling Procedure

A model is simply a representation of a behavior. Where possible, 2-D simulations were used to conserve computer resources. Symmetry was employed to model half or quarter specimens, which also conserved on elements and computer resources.

Depending on the FEA code that is employed the procedure may vary. However, the following procedure is consistent with most texts and works well with ANSYS code [ANSYS (1998)].

1. Generate geometry of problem or structure being investigated. Isolate behavior that is to be captured, because some simplification may be implemented in the model to conserve computer resources. 1-D, 2-D, or 3-D approximations can be used where appropriate.
2. Choose an interpolation function or element type that best represents the loading conditions, constraints, and material behavior that occurs.
3. Assign constitutive properties or material properties such as elastic moduli, Poisson's ratios, and shear moduli. For composite materials these parameters can vary depending on the laminate's material directions or architecture.
4. Mesh the geometry with the chosen elements. Some strategy is necessary to maintain a good aspect ratio and to provide adequate resolution to model physical behavior.
5. Boundary conditions or constraints should be applied next. This step is probably the most difficult step to apply accurately.

6. Apply loads in the form of forces, pressures, moments, etc.
7. Solve model for primary unknowns, which are typically nodal forces and displacements. Calculate secondary quantities such as strains and stresses.
8. Interpret results and evaluate convergence by increasing elemental divisions, increasing order of existing elements, or by adding integration points at locations of high gradient. Additionally FEA solutions should be compared to experimental findings or rudimentary analytical solutions. In this study, FEA solutions were typically validated by experimental findings.

Step 1 Geometry Development

Most of the models constructed for the case studies evaluated were two-dimensional approximations. Strength or Fracture type failure was being modeled and parametric models were constructed and used to evaluate stresses or fracture

Step 2 Element Choice

Interpolation functions are used to represent behavior internal to each element. One or more elements are then used to mathematically represent a structure and its behavior. Typically, in 2-D simulations ANSYS plane82 8 noded elements were utilized. This element type provides quadratic approximation capabilities. Both plane strain and plane stress options were implemented.

Plane strain assumes that when deformation is completely restricted in the z direction. In response to this restriction, there is a stress in the z direction. The loading is

biaxial and no shear stresses result. This assumption typically produces conservative results, or predicts larger than expected stresses.

Plane stress is useful for modeling relatively thin cross-sections. For plane stress it is assumed that the strain in the z direction is completely unrestricted so that the stress in the z direction is 0. Out of plane shear stresses are neglected also in this case.

In 3-D simulations, continuum type elements were used. The ANSYS versions of these elements that were used in this study are solid45 and solid95. They are typically referred to as brick elements.

The solid45 element is an eight noded brick element that uses a linear approximation to represent variations in displacement and force. It is composed of 8 corner nodes, where each node has 3 degrees of freedom. The 3 degrees of freedom are translations in each of the three dimensions. A special version of this element type is the solid46 element, which allows for layered properties throughout the element.

The solid95 is a 20 noded brick element and uses a quadratic approximation function. However this element has 2.5 times as many degrees of freedom as the solid45, which increases computation time.

A special class of finite elements are available that represent sliding at a boundary. These elements are generically referred to as contact elements. Sliding and contact surfaces can be modeled and friction can be accounted for with these elements. Contact elements were required for the mode II fracture simulations due to the sliding at the shear induced crack initiation.

ANSYS has several contact elements available. The contact169 and target171 elements are specially adapted for two-dimensional surface-to-surface contact. These elements are capable of handling motion along curved constraints and account for friction at the sliding interface. Additionally, with these elements both sliding surfaces can be deformable and possess elastic properties. Other variations of contact elements are available for different applications.

Step 3 Constitutive Properties

Constitutive properties are material properties such as elastic modulus, Poisson's ratio, shear modulus, thermal conductivity, density, and other properties that relate to the behavior being modeled. For composites, the elastic properties are not always the same in each direction. For the interlaminar fracture simulations an equivalent modulus or material stiffness was used. This is called a smeared elastic modulus, and is generally only used when the transverse properties are not directly related to the behavior simulated.

Step 4 Meshing

Meshing is simply the process of discretizing a given geometry into elements. The density of the elements should increase where change is occurring most. In fracture analysis the element density is always greatest around the crack and the crack front. This is often called the a/da ratio, which is the crack length divided by the amount of element divisions.

Step 5 and 6 Application of Constraints and Loads

In the case of solid mechanics or structural models, displacement boundary conditions are generally used. Translations and rotations were restricted to simulate the constraints on the actual structure. A force was typically applied to represent the load that would promote crack growth or cause stress failure. When the models were used to verify experimental behavior the force responsible for crack initiation was used. This is referred to as the critical load, or load that initiated a mode of failure.

Step 7 and 8 Solution and Results

Primary unknowns are forces and displacements. These values are solved for and then used to derive strain and stress. Generally, contour stress plots can be used to locate local high stress regions. Stress should be inspected on an elemental basis, and an appropriate failure criterion can be applied. Stiffness requirements can also be evaluated by inspecting displacements at key locations. Special techniques are available to model fracture and delamination and are discussed.

Finite Element as Related to Fracture Mechanics

There are three basic approaches for the assessment of fracture toughness using finite element analysis. The stress intensity, strain energy release rate, and the J integral are methods available [ANSYS (1998)]. Typically, the stress intensity approach is not used for use with composites, because composites are not isotropic and this complicates the analysis [Sun (1997)]. The strain energy release rate methods work well with

smeared properties and are easiest to implement. The J integral method is also a viable method for composite fracture mechanics analysis [ASTM E 813-89 (1991)].

Strain Energy Release Rate Methods

Several approaches have been implemented to evaluate the strain energy release rate using FEA. Two of the more common are the virtual crack closure method and the virtual crack extension method. These methods are an extension of the fundamental Griffith criterion.

Virtual Crack Closure Techniques

The virtual crack closure method stems from an assumption that the energy required to drive, or propagate, a crack is equal to the energy required to close the same crack [Irwin (1949)]. This theory was first postulated by Irwin and has been used to develop the single step and the two step virtual crack closure techniques (VCCT). These techniques have been employed in conjunction with FEA, by Rybicki and Kanninen (1977). Typically a specimen is modeled with the critical load or displacement applied to an initial crack setting. After completing an elastic static analysis, nodal forces and displacements are used to estimate the energy required to close the crack state.

In the case of the single or one step VCCT, only one computation or solution case is required. Typically the one step version is employed for complicated solutions, to reduce computational burden. In this method, the critical load associated with crack growth is applied to specimen geometry. A static solution is produced and the forces at the crack tip are multiplied by the resulting displacements behind the crack tip. The

location of these forces and displacement nodes are shown in Figure 2.11. Different reduction schemes are available and depend on the element used for the solution. A schematic used to for ANSYS plane82 eight noded 2-D elements is shown in Figure 2.11.

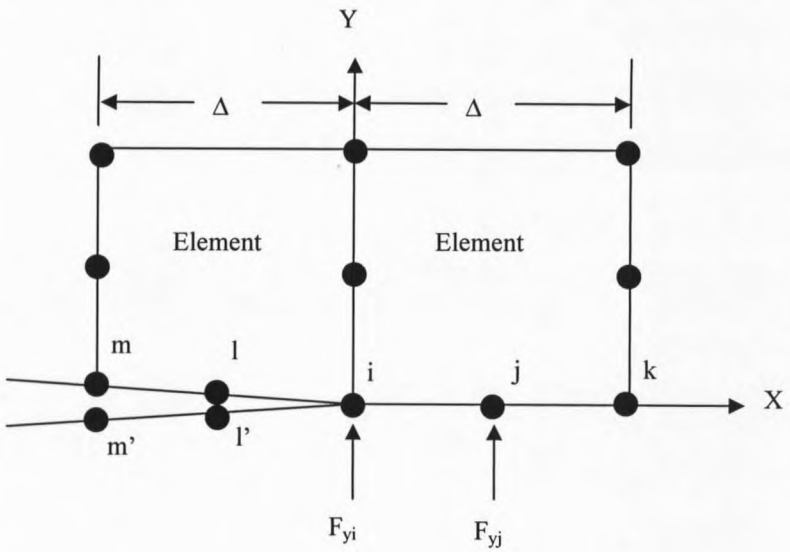


Figure 2.11 VCCT-1 Schematic with 8-Node Quadrilateral Elements

The equations used to calculate the strain energy release rate G_c are similar for mode I (G_I) and mode II (G_{II}) and can be written as:

$$G_I = -1/(2\Delta)[F_{yi}(v_m - v_{m'}) + F_{yj}(v_l - v_{l'})] \quad (2.7)$$

$$G_{II} = -1/(2\Delta)[F_{xi}(u_m - u_{m'}) + F_{xj}(u_l - u_{l'})] \quad (2.8)$$

where u and v are x and y displacements, respectively,

Δ is the element width,

and F represents nodal forces at locations indicated in Figure 2.11.

More information can be found regarding the derivation of this equation in references mentioned.

The two step method employs the same principal as the single step method. The model is first solved with the critical load applied, and displacements at key nodes are recorded. The model is then re-solved after unit loads have been applied to partially close the crack. The unit loads are applied at the corner of the elements at the immediate opening of the modeled crack. Details regarding the application of the unit loads for mode I are shown in Figure 2.12. The unit loads or forces should always be applied to the corner node, even when higher order elements are used. In the case of mode II, the location of the unit loads is the same as for mode I. However, the direction of the unit loads should provide relative closure between the two corner nodes.

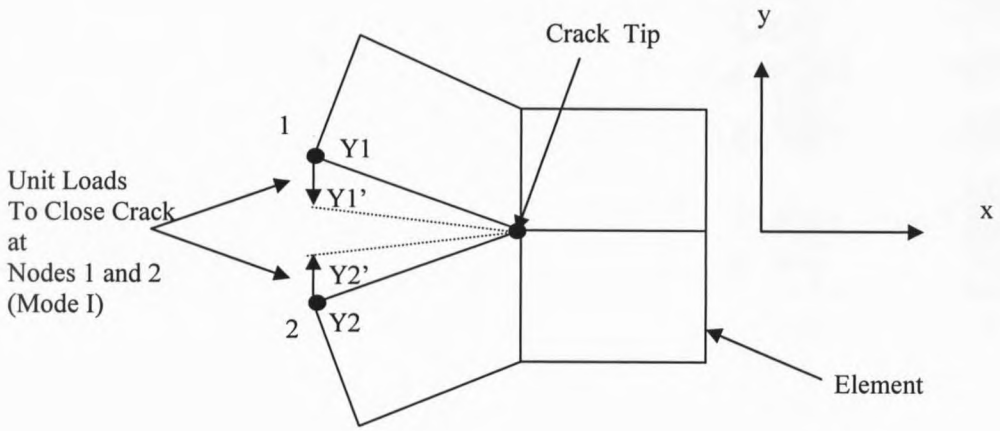


Figure 2.12 VCCT-2 Schematic for Mode I Closure

The initial displacements are used in accordance with the reduced displacements from the unit load case to evaluate G_c. The equation for this operation follows:

$$G_I = \frac{\dfrac{(Y_1 - Y_2)^2}{(Y_1 - Y_2) - (Y'_1 - Y'_2)}}{2(Element\ width)} \tag{2.9}$$

$$G_{II} = \frac{\dfrac{(X_1 - X_2)^2}{(X_1 - X_2) - (X'_1 - X'_2)}}{2(Element\ width)} \tag{2.10}$$

where X_i and Y_i are displacements at nodes i,

And X' and Y' are displacements at the same nodes after the unit loads have been applied.

Crack Extension Techniques

The crack extension technique uses total strain energy stored by the specimen at two states to find the energy required to produce crack growth. Typically the first solution case is with the critical load or displacement applied that initiated crack propagation. The second solution case is evaluated with the same load or displacement, and the crack is extended by either a single node or an element. The residual load or displacement at crack arrest and corresponding crack length could also be used for the

second state. The total strain energy for the second case is subtracted from the first, and divided by the crack damage area. The method can be expressed as:

$$G = \frac{U_a - U_{a+\Delta a}}{b(\Delta a)} \tag{2.11}$$

where U is the total strain energy,

a is the initial crack length,

Δa is the length of crack extension,

and b is the specimen width.

A variation of this technique was developed as part of this study, which simply uses the final known crack length and corresponding displacement or load for the energy at the second state.

The FEA methods outlined can be applied to structures and used as a predictive tool. These methods require material properties such as G_c to be known. The experimental procedures used to obtain these properties for mode I and and mode II were presented. Ultimately before these FEA techniques are used they should be validated. In this study the experimental test conditions were modeled and compared to experimental results obtained by traditional means. While it is suggested that these models be expanded to more complex substructures and structures, such activity exceeds the scope of this study.

CHAPTER 3

INTERLAMINAR FRACTURE CHARACTERIZATION PROCESS

Basic experimental procedures and analytical techniques have been presented. This chapter addresses the formulation of a fracture toughness optimization process, incorporating experimental and analytical procedures into a methodology. Industry needs are summarized, tips and tradeoffs are discussed, and design processes are presented.

Needs

The two most basic needs in current composite manufacturing industries are:

1. Understand the importance of interlaminar fracture of composites.
2. Balance strength and interlaminar fracture toughness and other properties as well as cost.

To meet these needs it is necessary to:

- Establish testing methodology to evaluate strength and fracture toughness.
- Employ basic data reduction techniques and methods to evaluate material performance. Additionally inspection techniques should be utilized to interpret failure modes and reasons for limiting performance of laminated architectures.
- Develop screening processes to reduce full scale testing and associated expenses. Screening processes can be an incremental evolution of tests.

- Implement FEA fracture techniques as modeling tool to understand and minimize fracture or delamination failures with G_c material properties.

Optimization

It has been established that structures and their constituent materials should satisfy strength and fracture toughness requirements. In the case of homogeneous isotropic materials, strength and fracture toughness are often inversely proportional. Altering the micro-structure of steel and other metals to enhance strength generally reduces the fracture toughness or makes the material more brittle.

The structure of a composite material is based on a number of variables. Each combination of resin system, fiber type, fiber volume, and manufacturing method affect and alter the strength and fracture performance. It is then necessary to conduct a constrained optimization evaluation to achieve the best blend of properties. Such an evaluation will assure that the material does not have excessive strength at the expense of inadequate fracture toughness.

Fracture Toughness Tips and Tradeoffs

Alterations can be made to constituent materials of a composite to improve fracture and delamination performance. Often some sacrifice is made for the improvement. Suggestions are offered that can help improve fracture performance. The primary elements affecting the delamination resistance are: the resin system used, architecture and fibers, and inhomogeneities. A more detailed overview of factors that relate to fracture toughness performance is provided in this section.

Resin System

The interlaminar fracture toughness of a composite is generally thought to be resin dominated. Different resin systems are available and the primary difference is generally chemical composition [Orozco (1999)]. Epoxy systems are used with carbon fiber composites and are usually considered the toughest. Polyester resins are affordable but are typically brittle in behavior when compared to epoxy systems. Vinylesters offer improved performance over the polyester system with significant savings relative to epoxy systems. Polyurethane resins are also viable. Important tradeoffs to consider are the glass transition temperature (T_g) and the relative stiffness (elastic modulus).

Fibers

The contribution of G_c from the fibers is not negligible. It is generally accepted that purely uniaxial architectures will possess the worst fracture toughness characteristics. Alternating the orientation of the fiber layers provides mechanical interlock from layer to layer and combats delamination. In cases where bending and torsional loading are expected. An architecture of [0,+45,-45,0] would be advised to separate $0 - 0$ combinations.

Out of plane reinforcement also mitigates interlaminar fracture. Varying degrees of cross-stitching fibers can enhance fracture performance. Layer to layer stitching, Through thickness reinforcement, bed of nails scheme, and woven fabrics are examples of out of plane reinforcement [Freitas (1995)]. The primary tradeoff with this scheme is that fewer fibers can be placed in the in-plane direction, which can reduce strength and stiffness properties.

Inhomogeneities

Pores, ply-drops, interface between dissimilar materials, stitching, resin-rich regions, and interlaminar zones all contribute to material variances and flaws. The flaws can serve as nucleation sites for fracture [Cairns (1990)].

Porosity

Pores can be reduced, but not eliminated by cautious manufacturing techniques. Excessive flow speeds can induce porosity by introducing air "bubbles." These air bubbles become voids. Porosity can actually increase interlaminar toughness by distributing damage. Cracks can detour away from the interlaminar zone and spread in a more tortuous path. Regardless, porosity is still a potential source for crack growth and delamination. Porosity is shown in Figure 3.1.

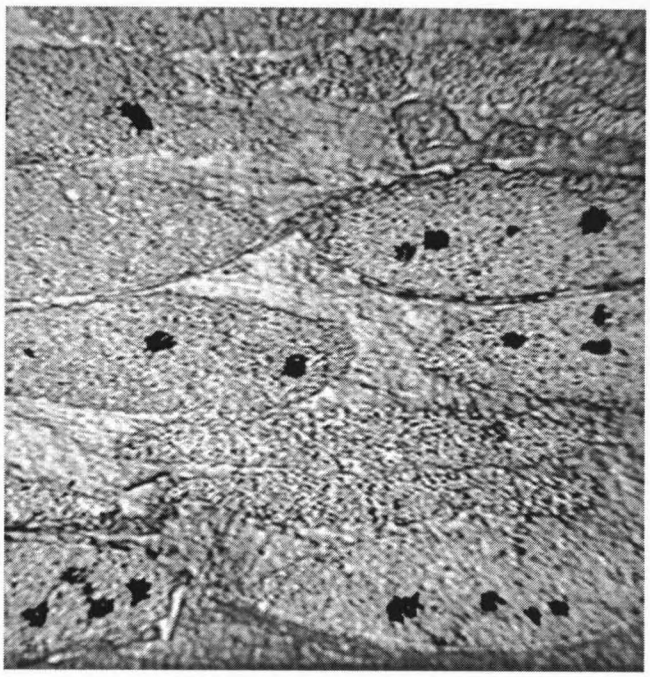


Figure 3.1 Porosity in a Composite Laminate

Ply-drops and Dissimilar Material Interface

Ply-drops are used where composite structure thickness is varied. In order to maintain consistent fiber volume, layers can be eliminated gradually to correspond with decreases in thickness. It is difficult to due this in a subtle manner. Generally there is a stress concentration associated with the abrupt transition where the ply is discontinued.

Sandwich theory is used to exploit the moment of inertia to resist bending loads. To accomplish this an inferior core material is typically used that is light in weight. When this is done an interface of dissimilar materials is introduced. The variation in stresses due to change in stiffness could be a weakness and potential source for delamination. Additionally, some sort of bond region is required to mate the face sheet and core material. This area or region is also prone to delamination. The specimen shown in Figure 3.2 has both a material dissimilarity and a ply drop region at the taper.

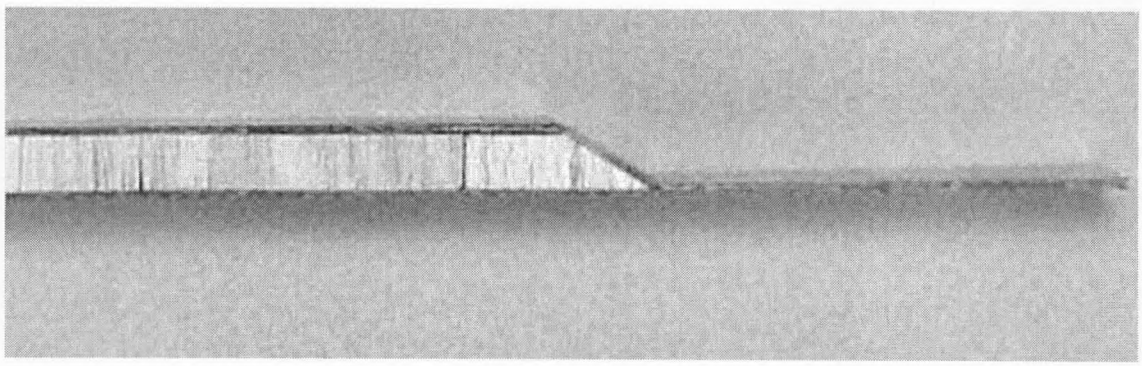


Figure 3.2 Sandwich Panel Material with Ply Drops

Interlaminar Zone and Other Inhomogeneities

Stitching, resin rich regions and the interlaminar zone itself are all inhomogeneities. The interlaminar zone is a region or layer of unreinforced material between strata of fibers or fabric. This is a specific case of a resin rich region. A resin rich region is any place where the fibers and resin are not distributed evenly. All laminated composites possess resin rich regions and interlaminar zones due to the nature of their construction. A good example of a resin rich region is shown in Figure 3.3.

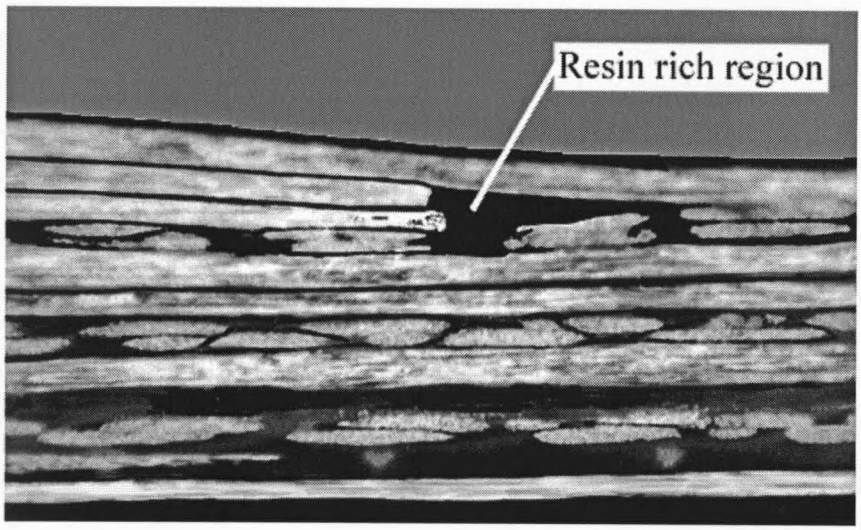


Figure 3.3 Resin Rich Region in a Laminated Composite

Avoiding the introduction of the inhomogeneities discussed, and using a resin with infinite toughness and bondability would eliminate the need for the fracture mechanic procedures and the delamination analysis techniques discussed. At this point, this is not possible, so a means to account for, quantify, and improve fracture

performance is required. The solution proposed is an engineering design process for composite candidate materials.

Prediction and Screening Approach

Two approaches were investigated, predictive modeling and screening. Failure of a structure due to fracture and delamination can be modeled. The methods outlined can be employed to determine the delamination resistance G_c of a material. The strain energy release rate (SERR) or G_c is a material property that can then be used to evaluate maximum allowable load for a structure given a flaw size and location. Conversely, given an operating load a maximum flaw size can also be determined and inspected for. Local and global analysis schemes are available and mixed mode type analysis is achievable with the FEA methods provided. The crack closure and crack extension techniques work well for 2-D structures where the type of damage is known. Without prior knowledge of the damage and location these techniques become unwieldy. Additionally, as the architecture is modified to combat fracture or delamination failure, modeling can become more complex.

However, provided that a database of material properties was gathered, these materials could be compared at a fundamental level. From simple experiments, elastic modulus, tensile strength, T_g, G_I, and G_{II} properties can be obtained. In the case where analytical modeling is not reasonably possible, the best material candidate can be selected and used based on material parameter evaluations. In this case a screening approach is taken. Additional testing of substructures and incremental or evolutionary experimental development can also be used. This is where experiments are performed to evaluate

specific structural behavior. Before either a prediction or screening approach can be taken, a database plan needs to be established.

Database

A database is simply a compilation of data or information. In this case a database would consist of pertinent material properties of a given material or composite. Databases can range in size; MSU in an effort with the D.O.E. [Mandell et al (1997)], has generated a substantial database in an effort to ascertain composite properties for wind turbine blades. Ideally, companies developing composites should emulate this effort on a smaller scale.

The primary reason for this database development is to provide an aid in the selection of resins, fibers, and other architectural components. Most of the industry has embraced the database philosophy for materials, but should consider extending it to include interlaminar fracture properties, for composites. Once a database has been established both screening and analysis techniques are feasible for material selection and architecture development. A process that could be used to establish a database is shown in Figure 3.4.

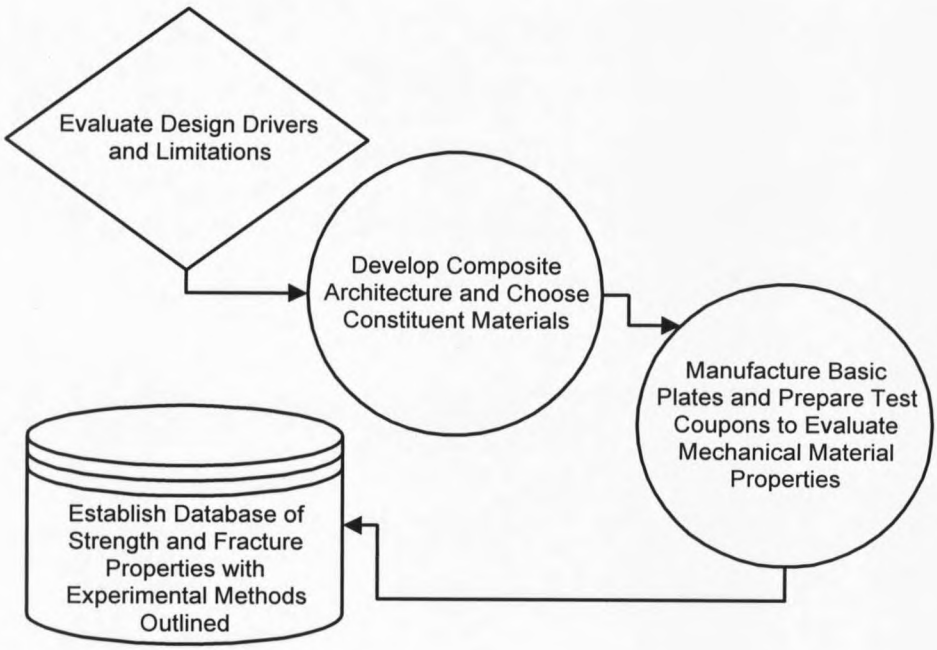


Figure 3.4 Database Construction Process

Screening Process

The four individual projects investigated in this study used screening processes to evaluate composite architectures for large scale structures. Due to the complexity of the full scale composite structures, it was necessary to perform tests on simpler sub-structures and coupons to obtain an understanding of the behavior of the larger structure. Ideally certain material properties can be quantified and related to the structure's behavior. In the cases presented, the sponsors constructed full-scale structures without evaluating substructure or material properties. At some point the structure exhibited

unacceptable performance. These unexpected responses lead to a need for increased understanding of the material properties of the candidate materials and architectures.

Screening Procedure

Screening is simply a process of isolating and comparing properties of something to aid in the selection. Screening can occur at a material level. Coupons can be constructed and submitted to appropriate testing to construct a database of pertinent material properties. At this point, based on limiting elements of design, the best material can be chosen based on qualitative comparison of quantified properties. With this approach, the behavior of the structure is not confidently known. However, at minimum, the designer has a better chance of choosing the best material to manufacture the structure and meet its in service needs.

Various experiments can be developed to address potential problems and behavior. Simple substructures can be constructed of rival materials and tested at incremental levels. Confidence can then be gained at various levels regarding the performance of the material. An evolution of successfully constructed and tested sub-structures can then lead to a successful construction and performance of the final structure as shown in Figure 3.5.

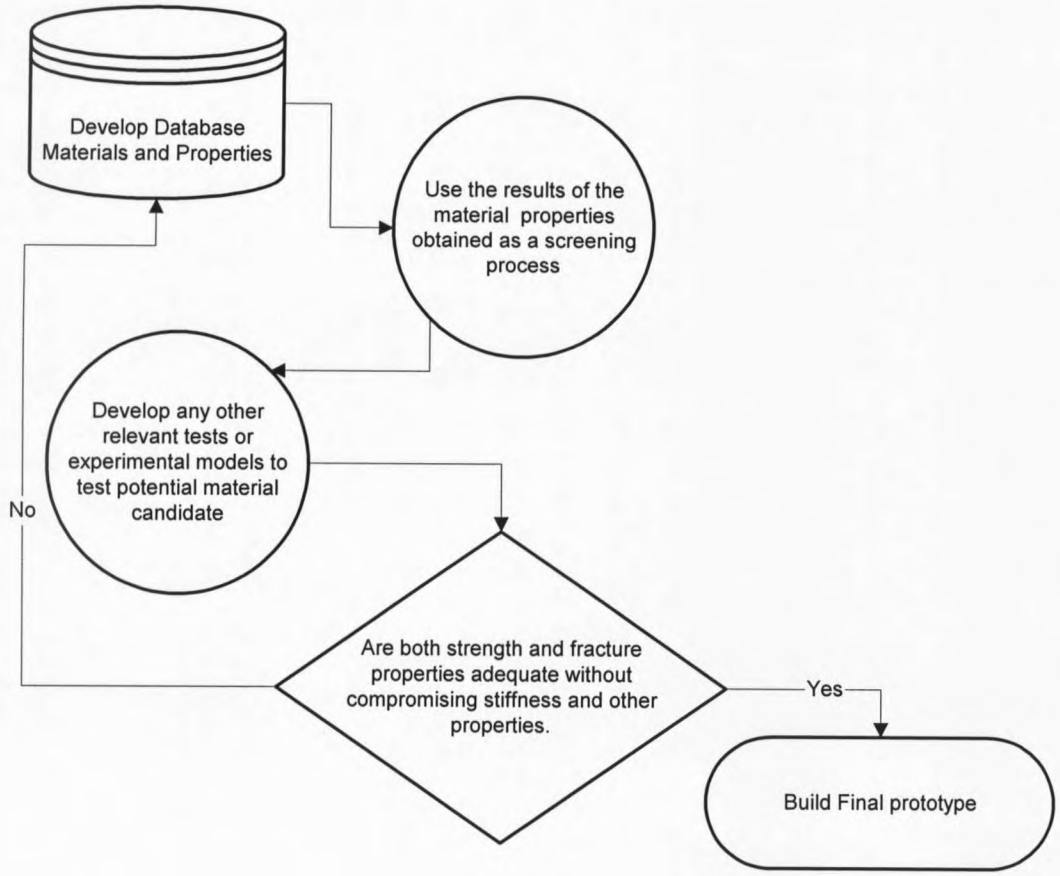


Figure 3.5 Screening Approach

Prediction Approach

The roles of finite element analysis (FEA) were discussed in the previous chapter. This analytical technique has the potential to be used as a predictive tool. With the inclusion of key constitutive and strength properties, models can be constructed that represents the behavior and failure of structures. These models are not prophecy and need to be "anchored" or compared to other analysis and generally experimental results to establish confidence. When FEA models are accurate, significant expense and resources can be saved. Ultimately FEA and other analysis techniques can be used to forecast the performance of a potential structure. The performance typically includes stiffness and strength capabilities.

Analytical methods capable of predicting fracture and delamination in test coupons have been presented. Significant effort has been invested to extend these methods to substructures and ultimately to structures. The goal of obtaining material properties at a coupon level and using these values to model structural behavior has been a focus of the Composite Technology Team at Montana State University (MSU). Currently, predicting delamination in complex structures is not a simple science. To accurately model fracture in these situations requires some additional development. Some advancement was made with composite T sections by Morehead (2000) and Haugen (1998). In these studies, FEA models were used to model and predict the delamination of composite T sections. From these investigations a basic methodology was formed and is presented in Figure 3.4. This process ensures strength and stiffness performance and attempts to evaluate fracture performance at a structural level.

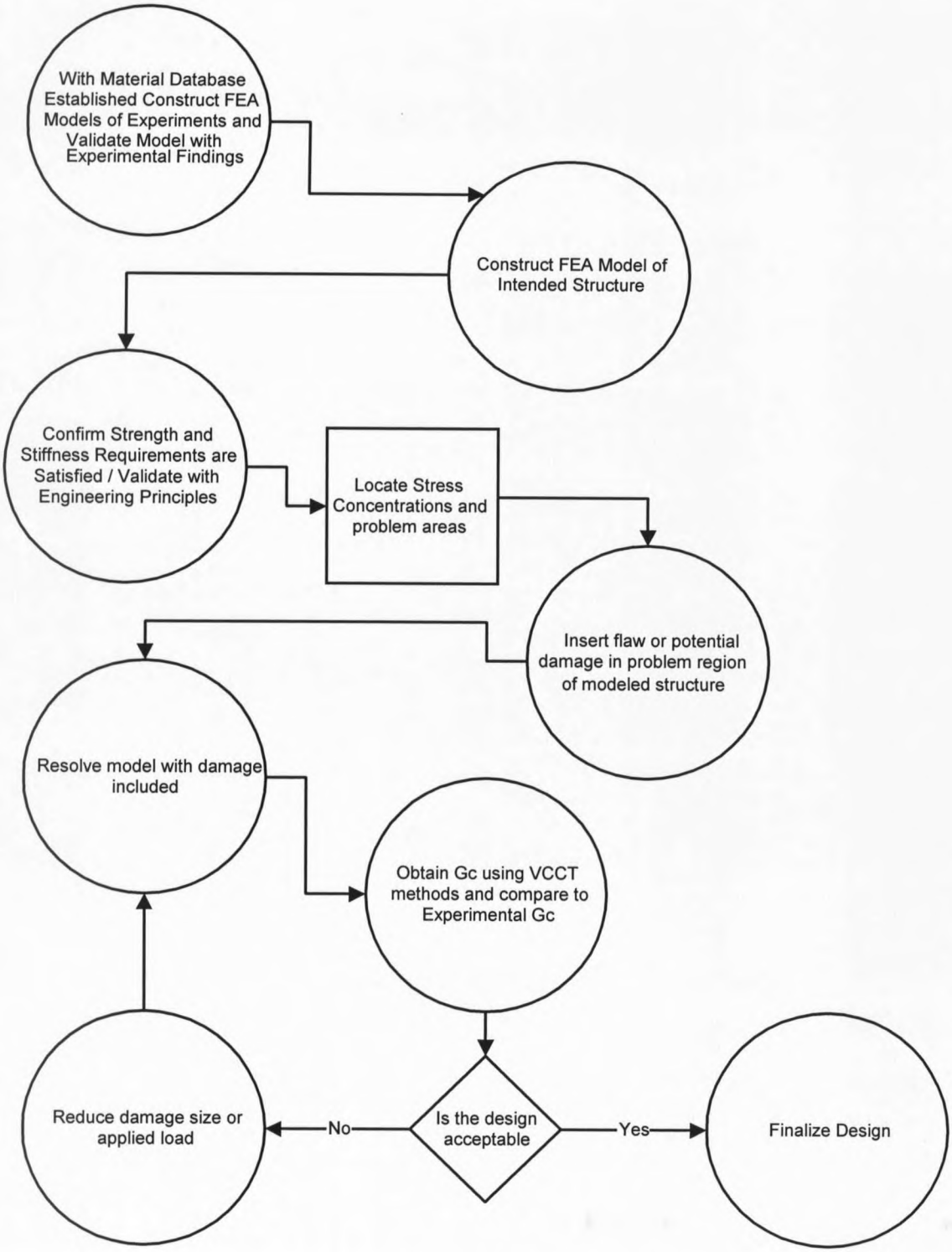


Figure 3.6 Analytical Process for Fracture Modeling

Composite Design

A systematic approach to designing laminated architectures that ensures adequate strength and resistance to interlaminar fracture is offered. These following steps should be followed to produce an optimized strong and tough composite. The process is as follows.

1. Apply analytical methods available to evaluate forces and stresses on component desired. Establish and evaluate potential design drivers and limitations.
2. With the aid of classical lamination theory, develop an architecture scheme that best addresses loading conditions. Details such as fiber type, resin system, fiber volume, and fiber orientation should be considered at this stage.
3. With a set of architecture candidates established, the initial construction of simple plates should be conducted. Specimens can be sectioned from these plates, which can then be subjected to tensile testing, mode I fracture testing, static flexure testing, etc. Some considerations to effectively address interlaminar fracture toughness are listed below.
    - Mode I tests are generally used as a fundamental characterization of fracture toughness.
    - In applications where bending type loading is present, mode II should be evaluated also. G_{II} is not always directly proportional to G_I. This type of failure is common in composites and should not be overlooked.

- When possible, during testing, the full hysteresis should be captured. This provides some confirmation with regard to validity of the data and the experimental intent. Additionally, using the area method provides an estimate of resistance to crack growth (R-curve behavior) [Broek (1996)]. R-curve behavior can be used to establish whether or not a material can sustain stable crack growth and possess some inherent crack arresting properties [Cairns (1990)].
- Where dynamic or impulse loading is expected, high strain rate testing should be employed. The resins in composites are usually polymers. Polymers are generally accepted as being strain rate dependent, and the fracture toughness of composite laminates could be affected by this sensitivity.

4. All of the information obtained can be used to establish a material property database. At this point two paths are available. The properties in the material database can be used as a selection tool, or strictly as a comparison, or both.
5. Material properties can be used as a screening process, or evolutionary tests can be developed and used to compare material performance. FEA modeling may be required to confirm experimental techniques. Additionally, FEA models can be anchored or validated with the experimental data obtained.
6. FEA models of an actual structure can be constructed. The solutions from these models can be compared to basic coupon properties. Both fracture and

strength requirements can be optimized. Other properties such as T_g can be optimized in this fashion as well.

The basic needs presented were shared by four separate projects. Each project possessed a unique facet or delamination situation. The design processes discussed were applied to each project to solve individual project needs and to establish confidence in and the validity of the processes. The following chapters are case study evaluations of the projects outlined.

In almost all cases the screening comparison path was chosen. However, significant effort was also focused on the development and application of analytical techniques and models. This effort was done to advance the technology associated with the prediction approach. Applying database material properties and FEA analysis as a predictive tool is ideal, but the confidence associated with these analyses is limited. An interactive design process that includes incremental screening tests and FEA validation is most desirable.

CHAPTER 4

CASE STUDY I
COMPOSITE AEROFAN BLADE EVALUATION

This project employed a database – screening approach. Basic material properties were identified that related to structural performance. Experimental procedures were developed to test these properties for several composite material candidates. These materials properties and parameters were then compared as a screening process to find the best suited candidates for potential composite structural architectures. Additionally, some research was conducted regarding fracture modeling. Numerical mode II simulations were developed to substantiate and help explain experimental findings. The numerical study employed several analysis techniques to predict G_{IIc} values. Friction at the sliding interface was accounted for and results were compared for varying friction coefficients.

Project Introduction

Traditionally, fan blades for turbofan engines have been constructed from materials such as titanium, high strength aluminum alloys, and steels. The demand for reduction in component weight and cost has spurred interest in the use of high strength composites as alternative materials. Minimizing the weight of the blades in turn reduces the associated weight of supporting bearings, journals and shaft-mounted components [Cairns (1999)].

Composite materials that have the potential of replacing metals for blade use exist. However, many of these candidates have trouble passing the "bird strike test" [Weeks (1998)] and other durability requirements.

Bird impact is a primary design consideration of fan components for turbofan engines. The actual bird strike test consists of the engine ingesting four 2.5 pound birds in sequence at operational speeds that would correspond to 85,000 pounds of thrust. The engine and related components have to be effectively sized to meet the bird strike requirements. The weak transverse properties of composites have often lead designers to the continued use of materials such as titanium. Only the GE90 motor is currently equipped with a composite Aerofan blade. This motor is used to power the Boeing 747 and the details of its architecture and properties are proprietary and unknown. It is believed that dynamic mode II fracture would be the major cause of blade failure for composite blades subjected to birdstrike conditions.

Existing Work

To combat the possibility of delamination, significant effort was spent evaluating through thickness reinforced composites [Jarmon (1998), Naik (1998), and Weeks (1998)]. Pratt & Whitney conducted several investigations to develop a composite material that would have improved transverse properties and greater delamination resistance.

Soft body impact testing was conducted with gelatin bird-like replicas [Weeks (1998)]. These 110 gram birds were projected at prepared panels at a speed of about

400 m/s. Typically the impact energy was increased with incremented impact speeds until damage formed. The impact conditions were increased further to evaluate damage tolerance. It was concluded that the stitched laminates possessed an increased damage tolerance and delamination resistance, but with a reduced initial damage threshold.

Additional investigations were conducted regarding the implementation of micro-mechanical architectural analysis [Naik (1998)] and mechanical properties of standard 2-D and 3-D RTM composites [Jarmon (1998)]. The two dimensional (2-D) composites were standard baseline laminates without through thickness reinforcement. The three dimensional (3-D) composites were similar but included cross-stitching or weaving to reduce delamination tendencies. The mechanical properties evaluated were in-plane tension (strength and modulus), in-plane compression (strength and modulus), and flexural and shear strengths. Some increase was noted in the tensile and compressive moduli for 2-D stitched variations. However, all other properties suffered when any through thickness or layer to layer reinforcement was added.

Some hybrid (S-2 glass-IM7 carbon) reinforced architectures were also produced and tested. The hybrid versions showed no improvement over the baseline 2-D satin weave (non-reinforced) carbon fiber epoxy composite.

Full Scale Testing and Need for Screening Process

Bird strikes are a predominant hazard faced by jet engine blades in use. Standard procedures have been developed to simulate bird collision events using full-scale blade assemblies as discussed. However, the destructive testing of full-scale assemblies is time-consuming and costly. A series of test procedures are therefore desired to provide

quantitative data for the component materials rather than for the entire composite structure. A material testing hierarchy would permit refinement of component materials and related properties. The components fabricated from these materials would be more likely to pass bird strike tests and meet other in-service durability requirements. A generalized problem statement to summarize project goals follows.

Problem Statement

Pratt & Whitney, under the DARPA sponsored Affordable Composites for Propulsion (ACP), has pursued the challenge of developing a composite aircraft engine fan blade. Toward this goal, Pratt & Whitney needs an economical method of evaluating mechanical properties of composites. Montana State University was tasked to assist in this effort by addressing the following tasks.

1. Isolate material properties and characteristics that apply to aerofan blade design and typical in service load scenarios.
2. Develop appropriate test methods to evaluate these properties.
3. Present and compare results from testing actual specimens.
4. Make recommendations for modifications of material composition, by providing actual minimum design specifications.

To address these considerations, a parametric study was performed to evaluate individual composites. Based on characteristics found, appropriate materials for blade usage can be selected. Such a study requires a test methodology, experimental results, and ultimately interpretation of those results: Each of these topics are addressed in subsequent sections of this case study evaluation.

Jet engine aerofan blades must meet very demanding specifications. Among these are stiffness requirements, tensile strength and various durability requirements. The goal of this study was to investigate the durability aspects of the candidates provided and either choose the best candidate for blade design or determine appropriate specifications to improve durability without sacrificing original design requirements.

Design Drivers and Material Limitations

Durability properties that were investigated fall into two categories: in-and out-of-plane strength. Often, measures taken to increase interlaminar strength sacrifice in plane strength. Heavy cross-stitching, for example increases out of plane strength by providing resistance to delamination. However, in-plane strength is lost when in-plane fibers are replaced by cross-stitching. Acceptable in-plane and out-of-plane strengths are both required for impact survival and durability. Delamination is a significant out of plane mode of failure for composites, and was addressed during testing. In plane metrics include bending stress, bending modulus, energy absorbed during impact, as well as threshold and ultimate dynamic strength.

Materials Provided and Specimen Description

To support completion of the stated goals, a small assortment of approximately 40 rectangular specimens and 12 "dog bone" tensile specimens were supplied by Pratt and Whitney. These specimens were tested, evaluated, and compared. Four distinctly different compositions were represented in these specimen configurations. Variations included different degrees of cross-stitching and unstitched versions. The cross-stitched laminates are generally referred to as '3-D composites" and the unstitched are termed "2-

D composites." Typically these architectures were given an identification code: Codes and corresponding compositions are shown in Table 4.1. Details of each type of specimen follow in the 'Specimen Description' section of this study as well as in other sources [Jarmon (1998) and Weeks (1998)].

The architectures were fabricated with 3M PR-520 toughened epoxy resin using the RTM (Resin Transfer Molding) process [Naik (1998)]. The layup consisted of a quasi-isotropic or transversely- isotropic schedule composed of IM7 carbon fibers. Each specimen was numerically coded: The first digit of the code sequence denoted the architecture type. All other components of the designation are part of the specimen serial number, and have no significance. Major differences included the absence or presence of cross-stitching, and the hybridization of fibers. The 5 series was a 2D baseline composite, which did not possess reinforced cross-stitching. All others were reinforced with some degree of cross-stitching either layer to layer, or through the entire cross-section. The 4 series differed from all others because it had silicon glass fibers as well as IM7 carbon fibers. Table 4.1 has descriptions of the specimens provided to MSU for testing.

Table 4.1 Description of Specimen Architecture

Panel Type	Fibers	Resin	Description
1 series	IM7 Graphite	PR520	layer to layer interlock
2 series	IM7 Graphite	PR520	through thickness interlock
4 series	IM7 and S2 Glass	PR520	hybrid fibers through thickness interlock
5 series	IM7 Graphite	PR520	five harness satin cross-ply (no cross-stitching)
Resin Transfer Molding was used in all cases			

Experimental materials will be referred to by their series ID numbers in the remaining portion of this document. The materials were configured to dimensions of 171.5 mm x 25.4 mm x 6.35 mm. An example of the supplied rectangular specimens is shown in figure 7. Note identification code and visible pattern from cross stitching.

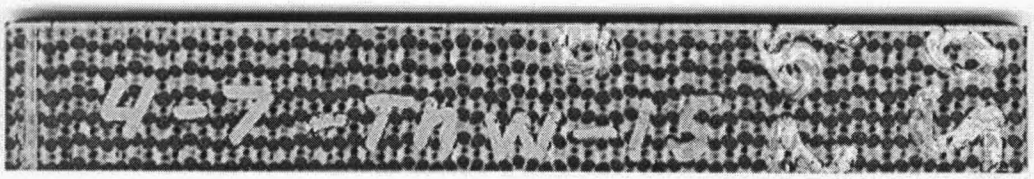


Figure 4.1 Example of Impact and Dynamic Flex Testing Rectangular Specimen

Additionally, two plates made of carbon fiber unstitched material were supplied. These plates along with MSU-manufactured fiberglass epoxy resin stock were fabricated into coupons that resembled the rectangular architectures provided. These specimens were subjected to an array of testing conditions to develop initial testing procedures. The small sample size of the specimens made it necessary to use additional materials to develop test methodology procedure before testing of materials supplied was initiated.

Material Property Isolation

The probability of success for surviving birdstrike is based on several material properties. Specific material properties must be selected for evaluation before preliminary screening tests can be conducted. A variety of screening tests can then be conducted to evaluate specific properties. Finally, based on all properties, the materials can be compared and selected. In the event that none of the material candidates provided

meet minimum requirements, specifications and suggested modifications in architecture can be developed. Four experiments were chosen to evaluate the material properties that directly relate to the design drivers discussed. The 3-point bend test or static flexure test establishes static strength properties and stiffness properties. The dynamic flexure test evaluates strength properties at high strain rates, while the delamination testing addresses fracture toughness. The delamination tests conducted were at high strain rates also. The primary goal with testing is to relate material properties to design drivers. Since bird strike is the in service threat, dynamic or impact type tests were conducted.

Test Matrix

An array of different tests were required to investigate all of the above mentioned quantities. No one test could reveal all of these mechanical properties. A test matrix Table 4.2 was developed that lists candidate identification and tests conducted (where a * indicates a single test). Specific descriptions of test procedures, equipment used, and the results are provided in following sections. A description of nomenclature is included only the first digit relates to the specimen architecture. All other numbers and letters relate to the specimen identification.

Table 4.2 Test Matrix of Aircraft Fan Blade Candidates

Rectangular Laminate Architectures				
Specime	3-point bend test	Dynamic Flex test	Delamination	Level II flex test
1-7-tnw	**	**	*	
1-8-tnw	**	*		*
1-8-bw		*		
2-7-tnw	**	**		*
2-8-tnw	*	**		
2-8-bw		*		
4-7-tnw	*	***	*	
4-8-tnw	*	*	*	*
4-8-bw	**	*	*	*
5-2-tnw	*	*	****	
5-3-bw		*		

Tensile Test Coupons ("Dog bones")		
Specimen	Static tests	Fatigue
1-9-ffw	*	
1-11-ffw	**	**
2-9-ffw	**	
2-11-ffw	*	
5-2-ffw	***	

Key to Fabrication and Nomenclature:	
IM7=Graphite fibers; S2=glass fibers; PR520 Resin With RTD used throughout	
1-series	IM7 Layer to Layer Interlock
2-series	IM7 Through Thickness Interlock
4-series	IM7/S2 Hybrid Through Thickness Interlock
5-series	IM7 Five Harness Satin Cross Ply (2-D Baseline)

Experimental Procedures

Based on the expected structural requirements, related material properties to achieve them, and the test matrix formed, a series of experiments were conducted. Each test was related to a material property of interest. The material property is explained as well as the apparatus used, procedure followed, and data reduction methods employed to evaluate said property.

Basic In-plane and Interlaminar properties

In-plane properties and interlaminar properties were used to characterize the supplied specimens. In-plane properties included ultimate tensile strength, elastic modulus, and fatigue life. Interlaminar characteristics were evaluated using mode II type test methods [Cairns (1992), Russel (1987) and Carlsson (1986)]. Two separate testing devices were used to obtain the associated properties.

Delamination Mode II Testing

Delamination resistance was evaluated using dynamic mode II testing. Delamination resistance to impact is considered one of the most significant parameters, since composites generally possess poor interlaminar fracture properties. Due to the nature of loads imposed by potential birdstrike, a dynamic version of the mode II fracture test was conducted. The metric of delamination resistance from this experiment was still G_{IIc}, but for dynamic loading conditions. This property accounts for any strain rate dependencies of the material [Cairns (1992)].

Apparatus

To conduct a dynamic version of the mode II fracture toughness test, special equipment was required. An impact tower was employed to supply the force and energy to induce crack growth. High-speed data acquisition equipment was also used. Details regarding the equipment used follow.

The impact test apparatus consisted of a Dynatup (8200) Drop-Weight Tester, retrofitted with a Kistler (9342A) piezo-electric load cell and a custom designed impact tip (shown in Figure 4.2).

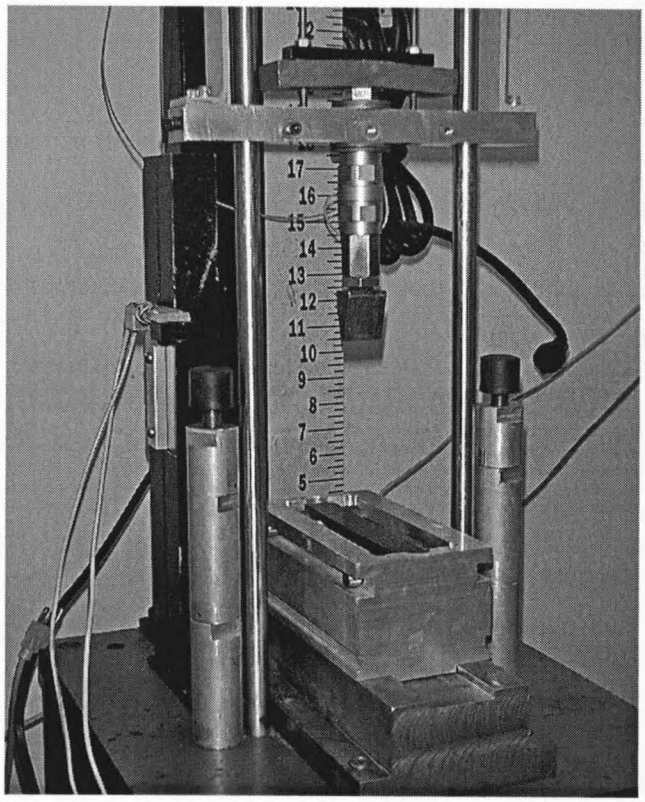


Figure 4.2 Impact Testing Fixture

A Kistler variable-gain charge amplifier used to condition load cell voltage output signals, which were then collected using a modular National Instruments SCXI Data

Acquisition system. Using a 200MHz Pentium II computer, National Instruments LabVIEW was programmed to control data acquisition and sample, convert, and store sampled data. The hardware and acquisition components are shown in Figure 4.3. The measurement capacity (load range) of the system was 0-32000 N. At the maximum 68 kHz sampling rate, about 1000 data points could be collected during a typical 16 millisecond impact event. It was necessary to obtain a multitude of discreet data points to represent the impact, and to support the numerical integration data reduction procedure [Mackin (1992) and McMichael (1989)].

Impact crosshead drop velocity at the point immediately before impact was also needed for data reduction. Drop velocity was determined using a dual photoelectric element knife-gate system, mounted and adjusted to provide impact velocity data for a range of specimen thicknesses.



Figure 4.3 Data Acquisition Used for Experimental Testing

A special purpose fixture was designed to support the impact specimens and prevent translation before or during impact. This fixture supported the specimens in a simple (three point bending) configuration. The fixture was adjustable to provide a variety of spans, and possessed enough clearance to allow for deflections of up to 1 inch. The installed impact fixture is shown in Figure 4.2.

Procedure

Some of the procedure and data reduction techniques are similar to the mode II fracture toughness methods outlined in Chapter 2. The test specimen geometry is the same. In this case the initial crack was induced by means of a specially constructed jig and chisel tool. The material was supplied by the project sponsor and was not manufactured on site. This made it impossible to incorporate a teflon strip for the initial flaw or crack. As a result the initial crack was induced with a precision chisel and guiding fixture.

Typically, in fracture testing, crack fronts can be measured visually with a caliper. The specimens provided were constructed of IM7 carbon fiber. This dark colored laminate made it difficult to determine the location of the crack fronts visually. Instead the crack fronts were located through the use of an ultrasonic transducer. Once located, they were marked and the distance from the support location to the crack front was measured with a standard caliper. The initial crack length is critical because the compliance method for the analysis of G_{IIc} depends solely on the initial crack length.

With the initial crack length, width, thickness, and span length of the specimen known, it was then supported in test fixture described above. With the aid of an assistant,

the crosshead latch was deployed and the data acquisition was initiated. The impact tup was then allowed to fall and strike the specimen. The specimen would accumulate load until the strain energy stored exceeded the fracture toughness capacity of the material. At that point, the crack would propagate in a rapid and unstable manner. The specimen would continue to deform and then would unload. After unloading the impactor would rebound. The crosshead was caught to prevent additional unmeasured impact damage to the specimen. During the impact event, force and time indexes, were recorded. Based on the known sampling frequency, the time increment could be determined. From this, a force versus time graph was constructed, as shown in Figure 4.4. Further data reduction had to be implemented to achieve a standard force versus deflection graph.

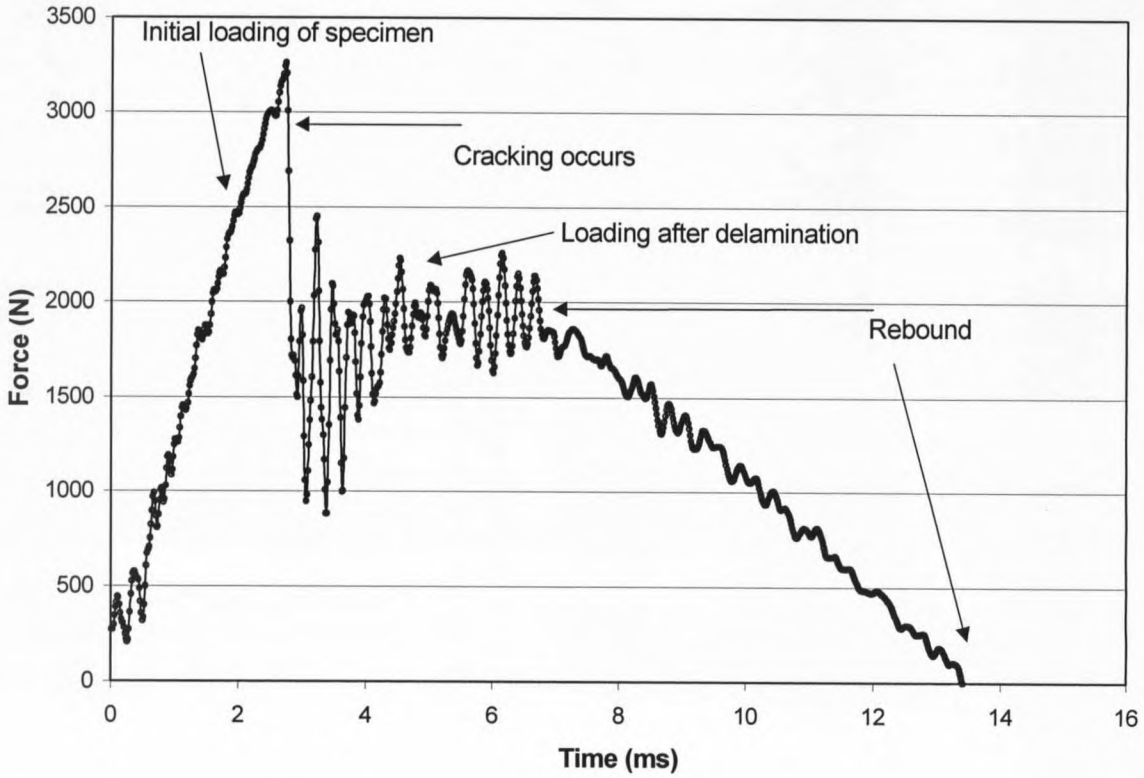


Figure 4.4 Force vs Time Output for Series 5 Laminate

Data Reduction

Impact tests provided force vs. time data of the form represented in Figure 4.4. This information was converted to force vs. deflection data by employing a series of numerical integration routines. The force data were used to obtain acceleration, velocity, and displacement all as functions of time. To accomplish this reduction required only the original force versus time trace and boundary conditions regarding velocity and displacement during the impact.

Newton's 2nd law was used to determine acceleration as a function of time from the initial force data. The force data F(t) was divided by the mass of impact crosshead assembly to provide acceleration versus time data. This equation is expressed as:

$$a(t) = \frac{F(t)}{m} \tag{4.1}$$

where F(t) is the experimentally obtained Force – time data,

and m is the moving mass of the impactor.

Little information was gained from the acceleration versus time data, but it was then used to determine velocity. It should be noted that the curvature or trace of the acceleration versus time graph (Figure 4.5) is no different than the force versus time curve. The acceleration data differs by only a constant, the crosshead mass (m).

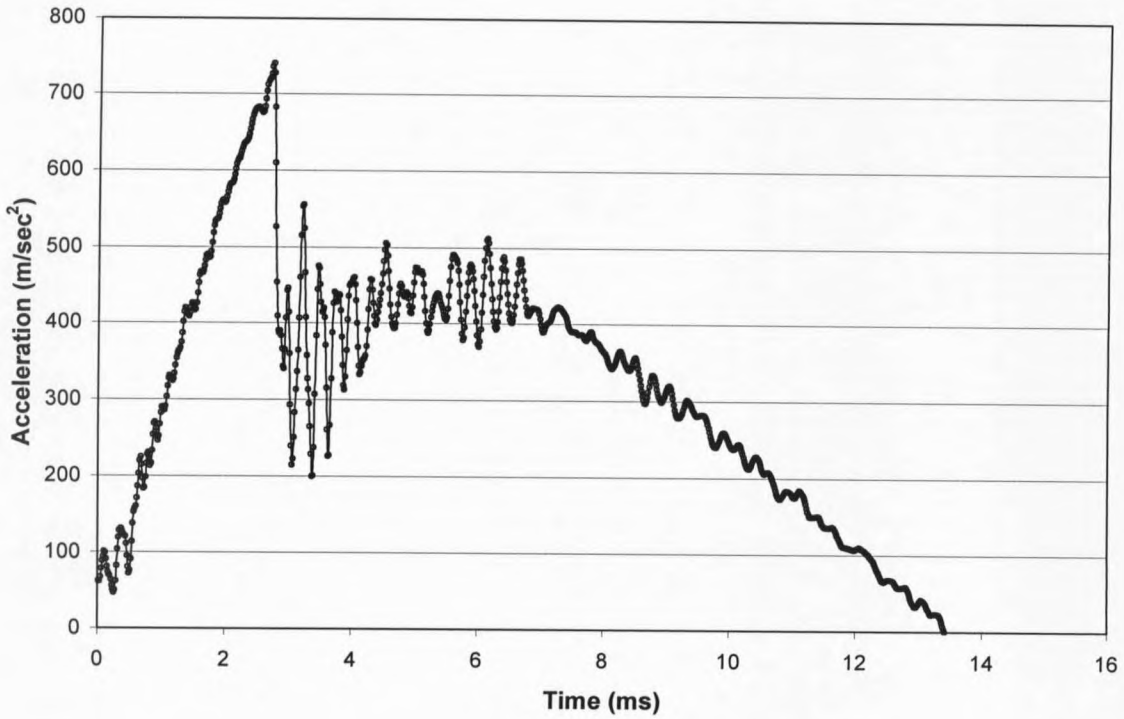


Figure 4.5 Acceleration vs. Time for 5 Series Laminate

The acceleration data a(t) was integrated using a trapezoidal rule and incrementally subtracted from initial velocity taken from Labview velocity program. From this basic relationship of motion, the velocity was then known as:

$$v(t) = \int_{t_i}^{t_f} a(t) + v_0 \tag{4.2}$$

where a(t) is acceleration as a function of time,

t_I and t_o are initial and final times respectively,

and v_o is an integration constant, which is the initial impact velocity.

The initial velocity (v_0) is the velocity of the crosshead immediately before it strikes the specimen. This velocity was found by conducting a series of test drops from the test height and recording velocity readings from the knifegate assembly. There is typically some variance associated with this technique, so the average was used. Another approach used, and recommended by the author, was to guess the initial velocity until the velocity profile crossed the abscissa at the same time the force versus time curve began to unload. For this approach, the average value obtained from the knifegate was used for an initial guess. A representative velocity profile is shown in Figure 4.6.

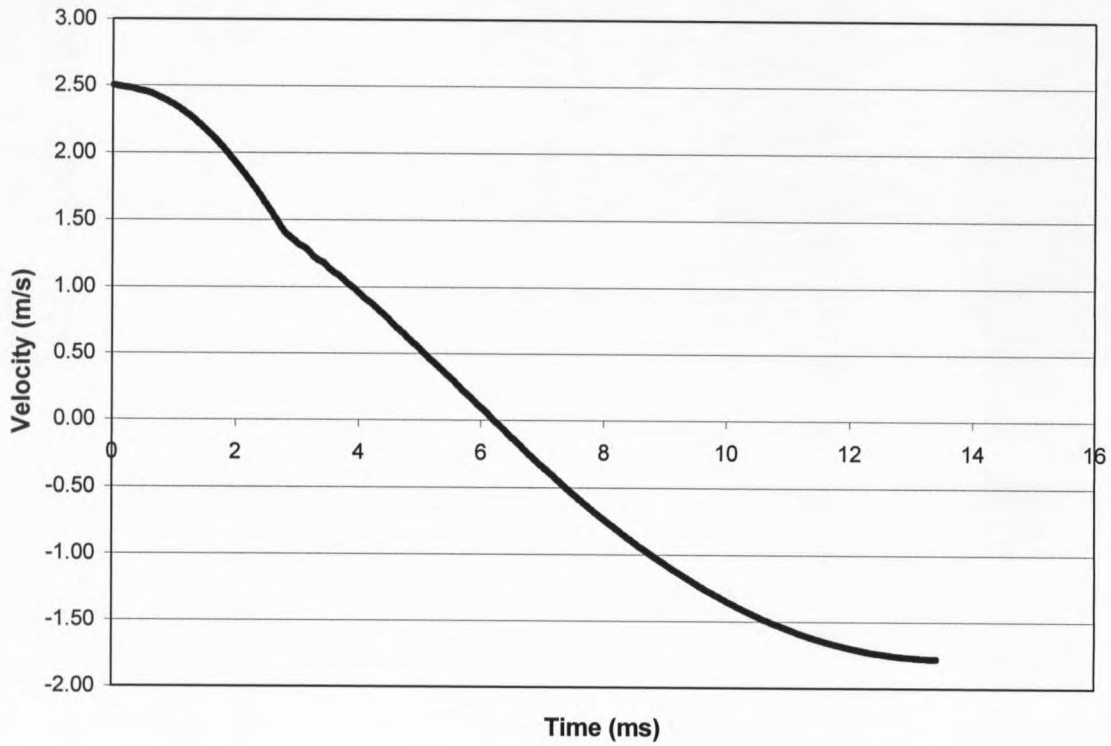


Figure 4.6 Velocity Profile for 5 Series Laminate

Note the velocity profile crosses the abscissa indicating that the crosshead stops at bottom dead center and rebounds upward as specimen unloads. Also the negative rebound velocity is less than initial impact velocity. This indicates that energy has been lost due to material damage.

Using the surface of the impact candidate as a datum, the velocity data, v(t), can be integrated and incrementally added to the initial displacement of zero. This was accomplished with the following relationship:

$$d(t) = \int_{t_i}^{t_f} v(t) + d_0 \qquad (4.3)$$

where v(t) is the velocity as a function of time,

t_I and t_F are initial and final time respectively,

and d_0 is an integration constant equal to 0 or the datum.

The result of this reduction is a displacement vs. time data set (Figure 4.7)

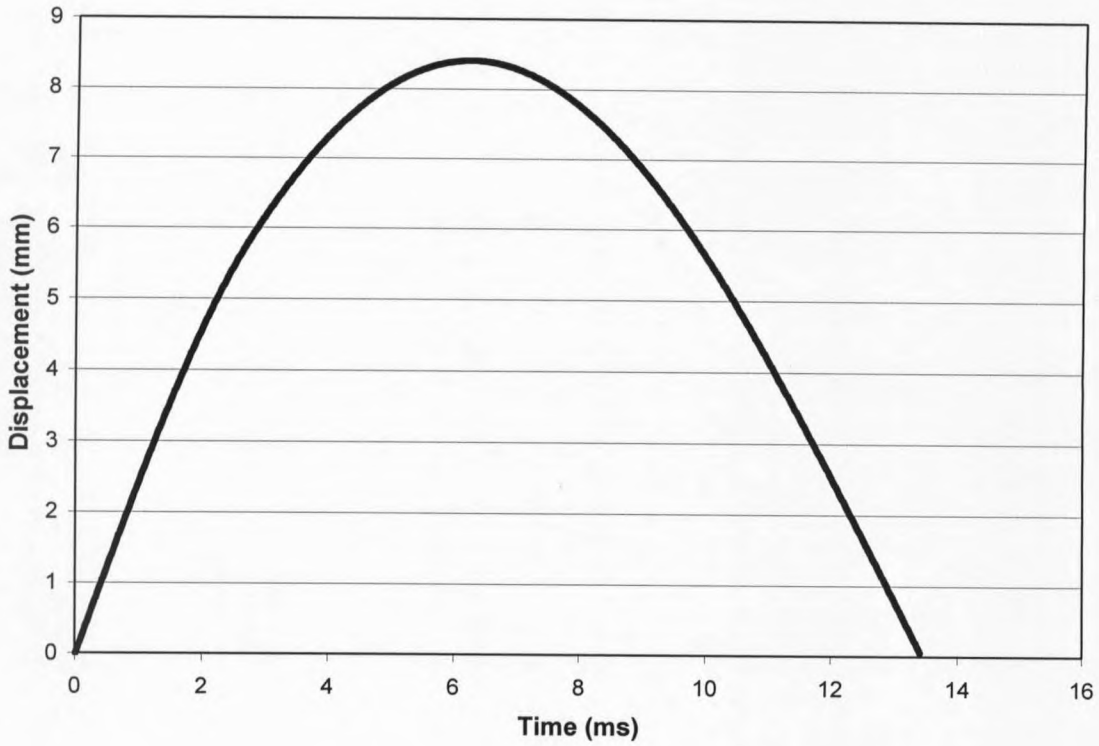


Figure 4.7 Displacement vs. Time for 5 Series Laminate

The corresponding force vs. time and deflection vs. time can then be plotted, or force can then be plotted vs. corresponding deflection. The sharp drop in Force shown in Figure 4.8 is due to crack propagation. When the crack propagates through the material, the specimen becomes more compliant and the force therefore reduces drastically as shown. It should be noted that the fractured specimen will accumulate load after crack propagation, but at a decreased slope. The location where this behavior takes place is typically assumed to be the crack arrest phase (Figure 4.8). This is due to the compliance increase associated with crack growth. This slope eventually levels off and then decreases.

Two important quantities are required for further characterization of fracture toughness. The critical load that initiated crack propagation is required for compliance approximations for crack initiation resistance, Equation (2.6). This load can be obtained from the force versus time graph as well.

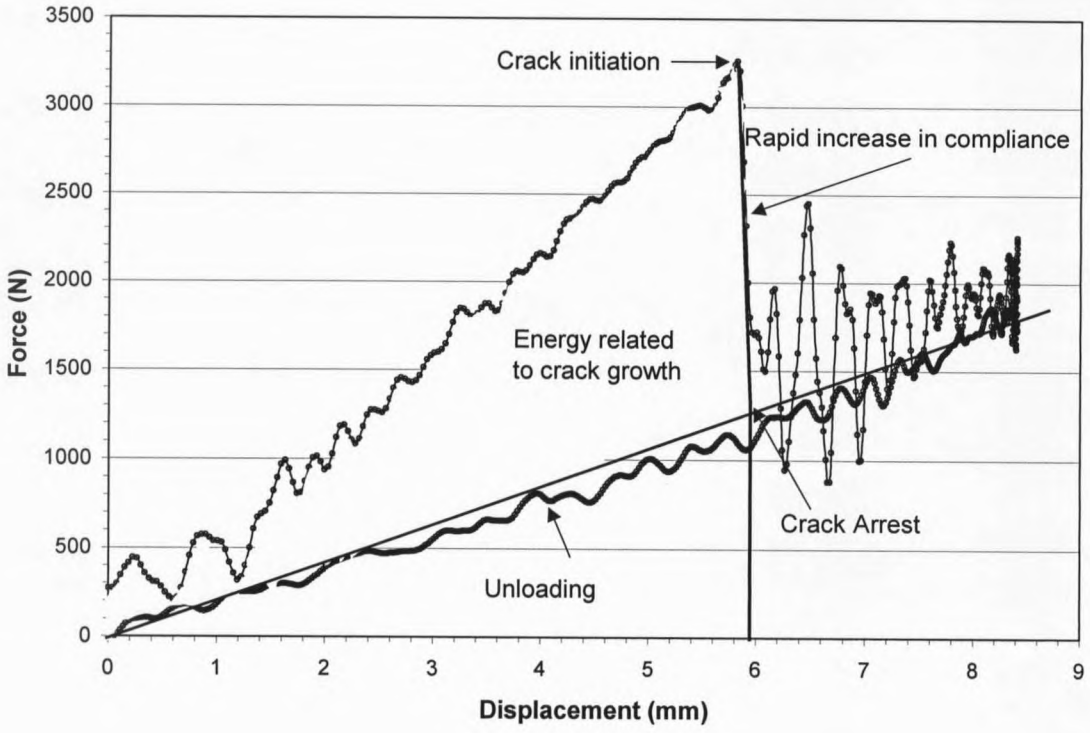


Figure 4.8 Dynamic Load Displacement Trace for Series 5 Laminate

The second important quantity is the area bounded by the force versus displacement trace. This region represents the energy that was associated with crack growth. This area can be numerically integrated and related to the crack damage area

using Equation (2.2). This quantity is typically used as a measure of resistance to crack growth, not resistance to crack initiation. Generally the area method, Equation (2.2) yields larger values than the compliance method, Equation (2.6). This difference is due to fiber bridging and other phenomenon that can act as crack deterents. This type of R curve or resistance curve behavior is common. Materials which provide reduced G_c results for the area method relative to the compliance method are generally not good for durability. This is because without R curve behavior, cracks can grow unstably and rapidly once they are initiated.

Dynamic Flexure Testing

The dynamic flexure test is used to measure the threshold, or flexural strength, and the energy absorbed before damage and after damage initiates. The threshold strength is defined as the flexural stress at which damage initiates. The term tolerance is used to describe the ability of a material to continue structural performance after sustaining damage. Threshold strength is the more significant of the two because ideally, the blade should withstand birdstrike type impact without becoming damaged or permanently deformed. Typically materials with a considerable threshold exhibited lower damage tolerances [Cairns and Lagace (1989)]. Since most composites have low strain to failure values, threshold strengths are viewed as important parameters related to durability during impact. Of the parameters discussed only the flexural strength obtained is considered a material property. The energy absorbed before damage and total energy absorbed during impact can be used to compare materials, but are not considered material properties.

Apparatus

The same apparatus was used for the dynamic flexure testing as was used for the dynamic delamination testing. All of the same equipment, data acquisition, fixtures and impact tups were used.

Procedure

Dynamic Flexure testing consisted of using similar specimens as the static delamination tests. The same fixture was used to support the specimens and the test procedure was the same with the exception of not including a pre-crack. The specimen was impacted until damage occurred. The dominant mode of failure was typically transverse compression from bending or flexure. Crack lengths were not measured and generally delamination failure did not result.

Data Reduction

The numerical integration scheme, described earlier, was implemented in the same manner. Initial velocity had to be known, the mass of the crosshead, and the force versus time trace, were needed. Equations 4.1-4.4 were used to generate the same plots as in the case of delamination testing. Typically the data from this test varied in appearance from the delamination data. The data did not have a sharp increase in compliance, continued loading, and then unloading. Instead there was usually a bell shaped loading and unloading. Nonlinear behavior would occur that corresponded to damage initiation. Cracking and fracture observed were generally in the transverse

direction not the in-plane or longitudinal direction. A representative response from this test is shown in Figure 4.9.

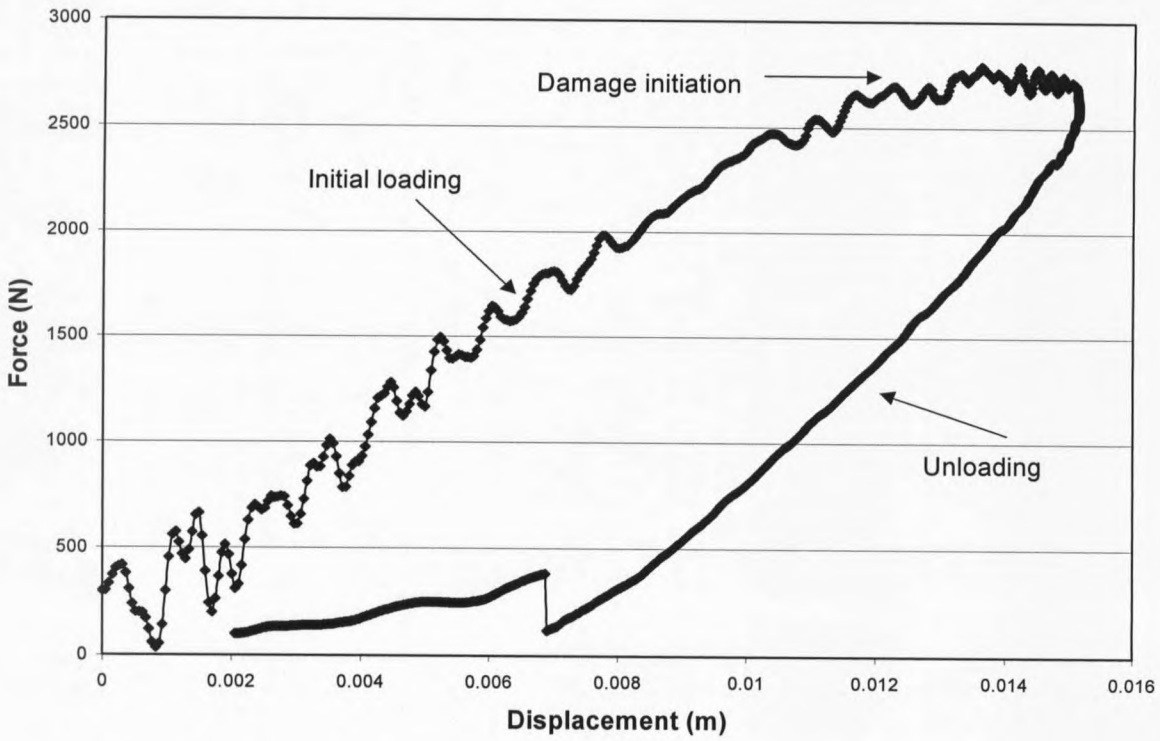


Figure 4.9 Dynamic Flexure Behavior

The bending stress was calculated at two different levels using the following relationship:

$$\sigma = \frac{My}{I} \tag{4.4}$$

where M is the maximum bending moment,

y is the distance from the neutral axis to the outermost fiber,

and I is the moment of inertia for a rectangular beam section.

The largest force and related stress in the linear range represents the reversible limit or the stress at which damage initiates. The maximum load and related stress represent the ultimate limits of the material. The first quantity is the most useful. Ideally a blade should be able to survive birdstrike and continue operating safely. A blade with significant damage would not possess the required stiffness and balance for safe operation.

The energy absorbed was calculated at both the damage initiation and ultimate load levels. This was done with the following relationship:

$$SE = \int_{x_i}^{x_f} F \cdot dx \tag{4.5}$$

where

SE is the Strain energy absorbed by crack growth,

F is the force, x_i and x_f are initial and final displacements respectively,

and dx is an incremental displacement.

The most pertinent energy absorption metric would be the quantity relating to the damage initiation level. As with stress, it was considered optimal that an aerofan blade would sustain the kinetic energy associated with birdstrike and continue to operate. However some damage tolerance is needed, because a material that promptly detonates when the reversible limit is exceeded is not desirable.

Static Flexure Testing

Static flexure testing provided key properties such as flexural modulus and flexural strength. Static flexure testing is commonly evaluated with bending tests which are simply a static version of the dynamic flexure tests.

Apparatus

A 3-point fixture, manufactured in-house, was used in combination with an Instron (model 4206) screw type test device. The device is screw driven and was operated in displacement control. The static test apparatus is shown in Figure 4.10.

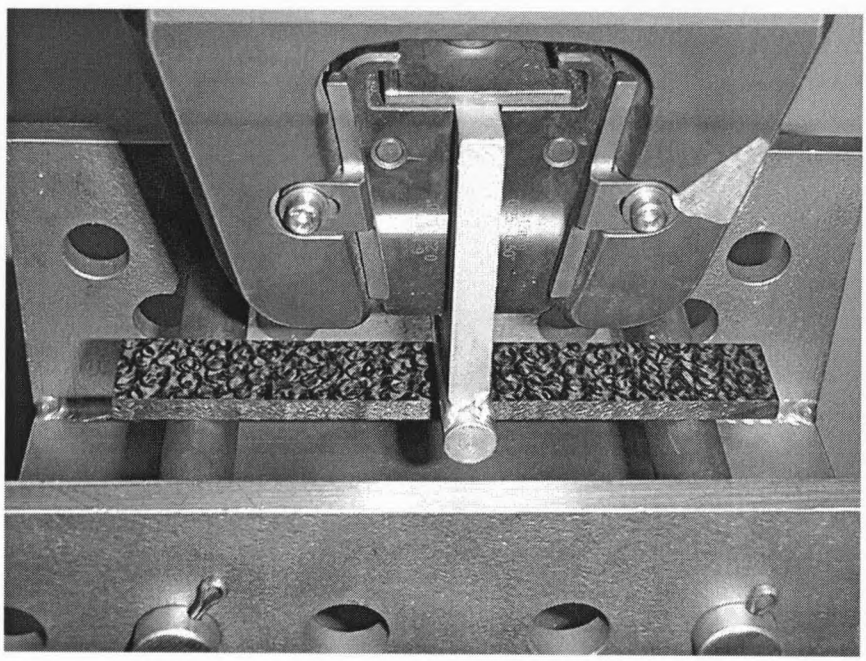


Figure 4.10 Static Flexure Test Fixture and Specimen

Voltages proportional to the applied load and crosshead displacement were output and sampled by a Labview SCXI-1200 data acquisition system.

Procedure

The specimen was measured for width and thickness and then supported in the fixture as shown in Figure 4.10. The crosshead was then activated to apply forces in displacement control. An array of force and corresponding displacement was measured via data acquisition described above. Data was recorded until the specimen failed. The force was then plotted vs. displacement as displayed in Figure 4.11. From this, bending modulus, maximum bending stress, and energy absorbed were determined. The static flexure test provided a comparative basis for the dynamic flexure test as well.

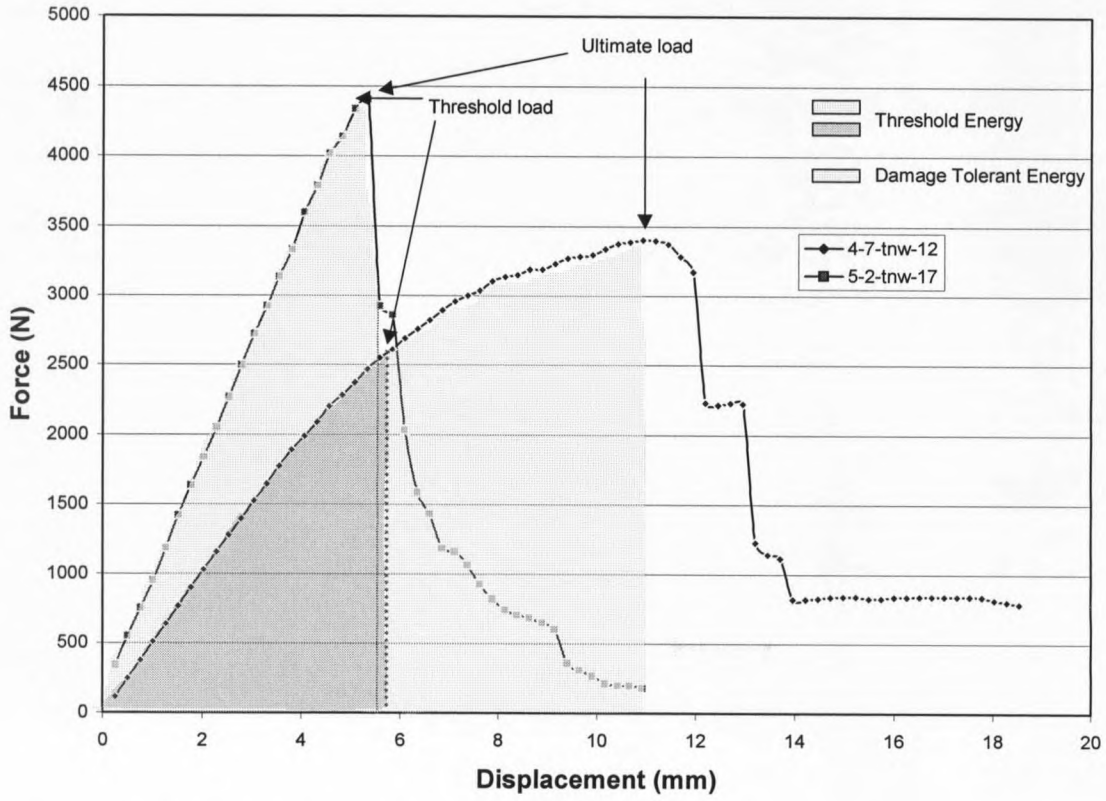


Figure 4.11 Static Flexure Behavior

Data Reduction

The bending modulus was obtained by performing a curve fit on the linear portion of the flexure data. This slope represents the equivalent of spring stiffness. Using standard beam theory, the bending modulus can be isolated and solved for. The deflection for a simple span beam can be expressed as:

$$\delta = \frac{PL^3}{48EI} \tag{4.6}$$

where P is the load,

L is the spanned length of the beam,

E is the Elastic modulus,

and I is the moment of inertia.

This relationship can be rearranged as follows:

$$E = \frac{P}{\delta} \cdot \frac{L^3}{48I} \tag{4.7}$$

This metric can vary from the modulus obtained from a standard tensile test and was used as a smeared property for finite element analyses.

The bending stress was calculated at the same two levels using Equation (4.4) as was done for the dynamic flexure. The largest force or stress in the linear range represents the reversible limit or the stress at which damage initiates. The maximum load

and related stress represent ultimate limits of the material. Again, the first quantity is the most useful. While some degree of damage tolerance was desired, resistance to initial damage was viewed as the primary objective.

Tensile Testing

Several standard tensile test "dog bone" shaped specimens were supplied. These were subjected to tensile testing to find elastic modulus and ultimate tensile strength. These properties were not the focus of this investigation, however they were evaluated in an effort to verify that improvements in durability performance were not causing reduced strength and stiffness properties.

Apparatus

The Instron (model 4206) screw machine was employed to load the tensile specimens. Each specimen was equipped with a strain gage, that was incorporated into a standard Wheatstone bridge circuit with an excitation voltage supplied. Load and corresponding strain were sampled with a Labview program capable of sampling load and strain proportional voltage.

Procedure

Specimens were measured for width and thickness at the narrow portion of the "dog bone" sample. They were then secured into the Instron 4206 by means of the universal clamp type grips. Load was applied in displacement control. The load and strain were recorded until the specimen failed. Stress and strain were then plotted to characterize the tensile characteristics of the material. It should be noted that the strain

measured is representative of the entire material, but the load is not distributed uniformly due to the alternating layers of the laminated architecture. Generally the stress – strain responses were very linear. An example is shown in Figure 4.14. Some of the materials possessed damage tolerance, while others failed immediately upon exceeding a given threshold.

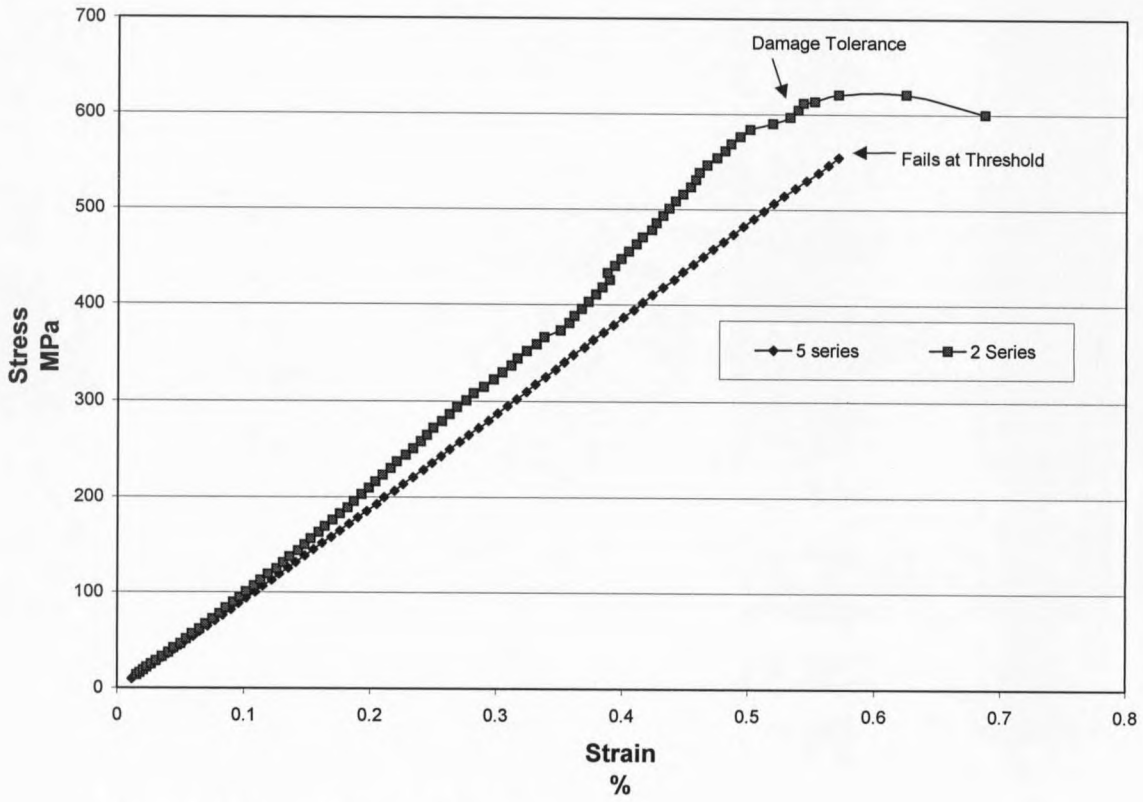


Figure 4.12 Tensile Test Behavior

Experimental Results

Generally, the results obtained are preliminary and do not represent a statistically significant data set. However based on these results some conclusions can be drawn. Current results suggest that materials supplied need further development to satisfy the minimum design requirements for aerofan blades. The 5 series (2-D baseline) composite showed the most promise in regards to ultimate tensile strength. However, this material exhibited the worst delamination resistance. Plots comparing all specimen types for each test conducted are shown in this section. Additionally, a tabular comparison of preliminary results is included. The results are presented based on tests conducted and properties evaluated.

Mode II Delamination Resistance Results

Mode II delamination tests were conducted to evaluate G_{IIc} values. Series 1 and 2 under no circumstances would accept a pre-crack. While this indicates very good delamination resistance, the goal of the test is to measure load and energy required to propagate an existing crack. The physical inability to initiate a crack made it impossible to obtain meaningful results from Mode II delamination tests for series 1 and 2 materials. The 4 series material was pre-cracked, but the crack would not propagate under bending or shear loading under any circumstances. Only minimal results could be obtained for this material. Mode II fracture did occur in the 5 series material. Typical fracture behavior is shown in Figure 4.13 for this material.

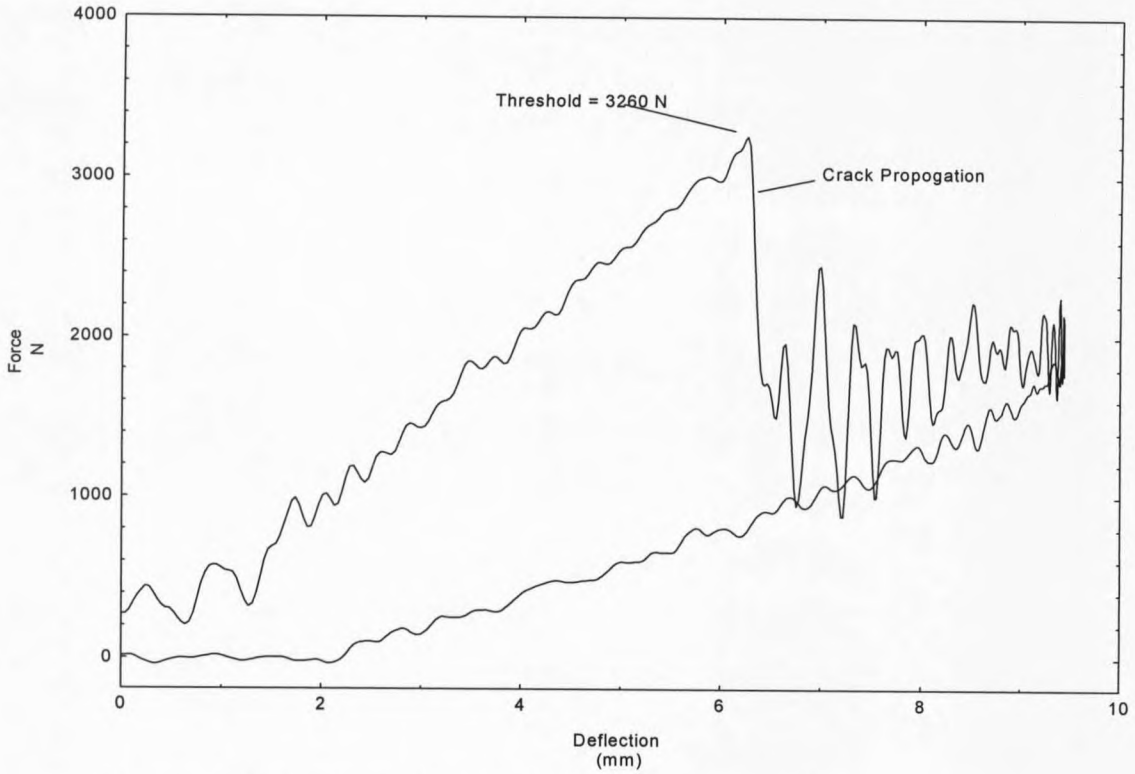


Figure 4.13 Delamination Results for 5 Series Material

Table 4.3 below is a comparison of the G_{IIc} results. By virtue of the fact that series 1 and 2 would not accommodate pre-crack, and would not exhibit delamination under any other test environment, these materials were qualitatively the best for delamination resistance but could not be quantified. Similarly, the 4 series material would only produce minimum values. G_{II} values are included for the 5 series material. Both the compliance (initiation) and area (average) methods were used to evaluate G_{IIc}. Typically, materials that exhibit a lower average G_{IIc} than an initial G_{IIc} value have poor impact

properties [Cairns (1990)]. This type of response indicates that once propagation initiates; the resistance to delamination decreases.

Table 4.3 Results for Delamination Mode II Testing

Material Type	Description	Dynamic GIIc Initiation (J/m^2)	Dynamic GIIc Average (J/m^2)
1	IM7 layer to layer interlock	Could not initiate precrack	No propagation
2	IM7 through thickness interlock	Could not initiate precrack	No propagation
4	IM7/S2 Hybrid	1832+ (no precrack propagation)	No propagation
5	IM7 5 harness satin cross ply	2070	(1697)[1]
[1] lower average dynamic indicative of poorer impact properties			

The tabulated values for series 5 are an average of three tests. Series 1 and 2 would not accept pre-cracking and under no other testing environment experienced delamination. It has been assessed that the through thickness reinforced series 1 and 2 are over designed with respect to delamination resistance. While these two specimen types exhibit superior resistance to delamination, their out-of-plane strength has been sacrificed significantly. The 4 series is cross-stitched layer to layer only. Resistance to mode II failure is beyond adequate for this material as well. Series 4 material would accept a pre-crack but would not propagate the initial crack under any circumstances. Series 4 always failed from bending stresses and showed no potential to delaminate. The G_{IIc} value displayed was based on one test and is a minimum value. It is suspected that the series 4 material is also excessively reinforced against delamination. The 5 series

material fractured in the interlaminar zone and values for the Mode II interlaminar fracture toughness are provided.

Dynamic Flexure Results

Results obtained from dynamic flexure tests are the most revealing. The primary difference in this test is the mode of failure evaluated. Specimens are not pre-cracked prior to impact. The mode of failure is typically tension or compression from bending stresses induced by transverse impact. All supplied specimens were subjected to this test with comparable results. Figure 4.14 shows representative force – time data for all 4 specimen types.

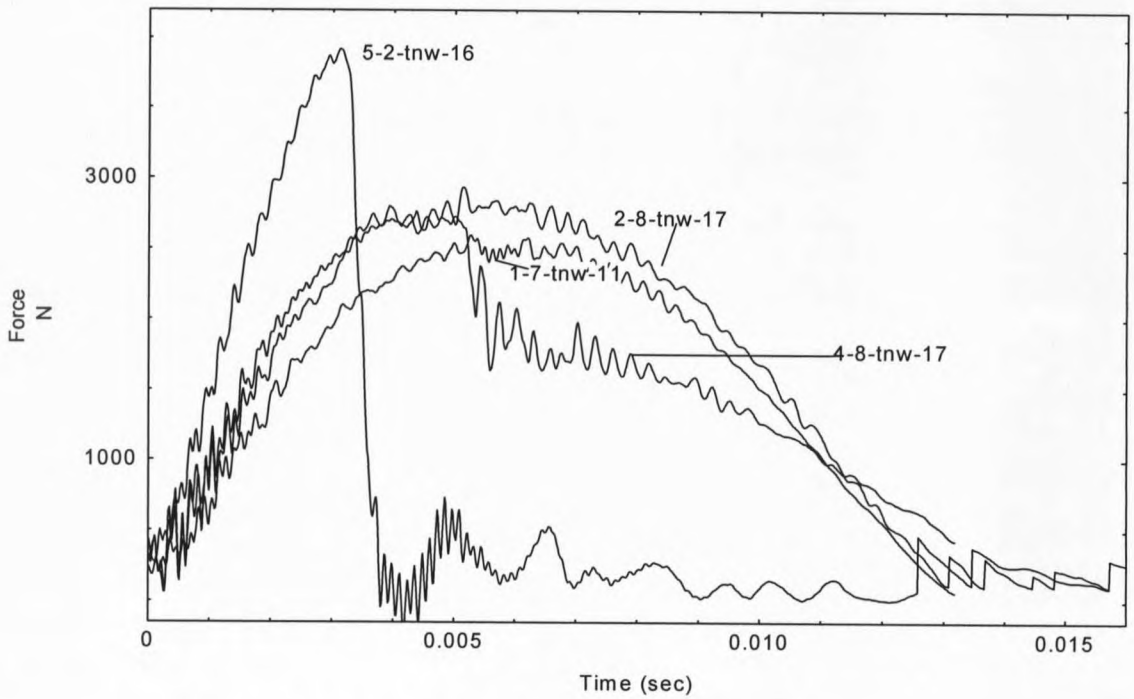


Figure 4.14 Force vs. Time for Dynamic Flexure Tests

The bell-shaped graphs demonstrate damage tolerant material behavior. All of the materials except for the 5 series exhibited this behavior. With the basic data reduction scheme presented in experimental procedures, the force-time date was converted into force-displacement data. The force-displacement data shown in Figure 4.15 and equation 2.6 were then used to find energy absorbed.

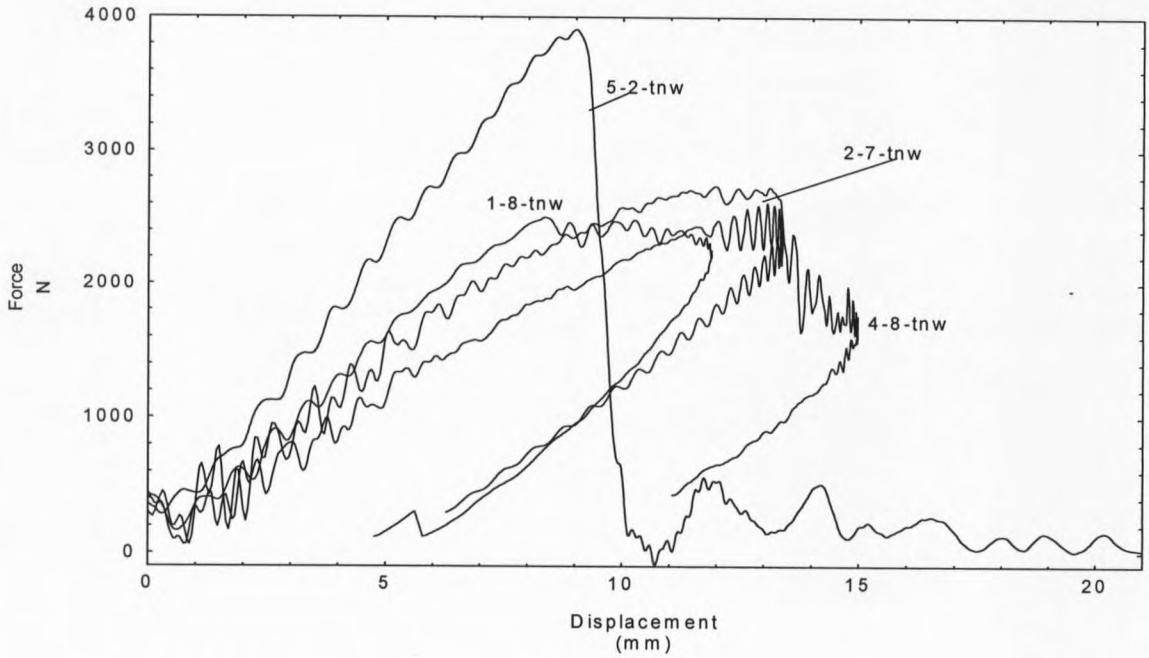


Figure 4.15 Force vs. Deflection for Dynamic Flexure Tests

From Figure 4.15, it is apparent that the 5 series had the highest threshold, but fails catastrophically at after damage onset. This threshold is a significant parameter for evaluating a material's impact resistance. The 4 series had the next highest threshold and the largest total absorbed energy. This balance of characteristics is more desirable but the flexural strength is inadequate. Total energy absorbed and ultimate bending stress were

evaluated. Additionally energy absorbed before onset of damage, and bending stress at onset of damage, were evaluated. The (before onset of damage) metrics are the most significant because any damage to an Aerofan blade is assumed unacceptable. For total damage resistance, the 5 series non-reinforced material was found to be superior. Other materials exceeded the 5 series in regard to total energy absorbed. This is due to large amounts of energy being dissipated after damage is initiated. The dynamic flexure results for each type of specimen are summarized in Table 4.4.

Table 4.4 Summary of Dynamic Flexure Data

specimen ID	Energy absorbed (Tolerance)	Max Stress	Energy absorbed before onset of damage	Threshold Max load before onset of damage
	Joules	Mpa	Joules	Mpa
1-7-tnw-11	25	608	14	586
1-7-tnw-17	21	513	11	512
1-8-bw-5	21	596	16	596
1-8-tnw-17	23	491	13	491
1-8-tnw-20	26	511	12	510
2-7-tnw-14	16	542	14	482
2-7-tnw-15	20	508	18	474
2-8-tnw-17	16	571	17	544
2-8-tnw-18	16	556	18	557
4-7-tnw-13	17	533	13	465
4-8-bw-4	25	473	16	452
4-8-bw-5	25	537	14	496
4-8-tnw-17	21	534	14	503
4-8-tnw-19	23	472	11	402
5-2-tnw-16	24	765	18	765

Static Flexure Results

Results from the static flexure tests support the dynamic flexure tests as was intended. Important data obtained from these tests were bending modulus, static threshold, and static tolerance. Graphical representation of these test results is shown in Figure 4.16.

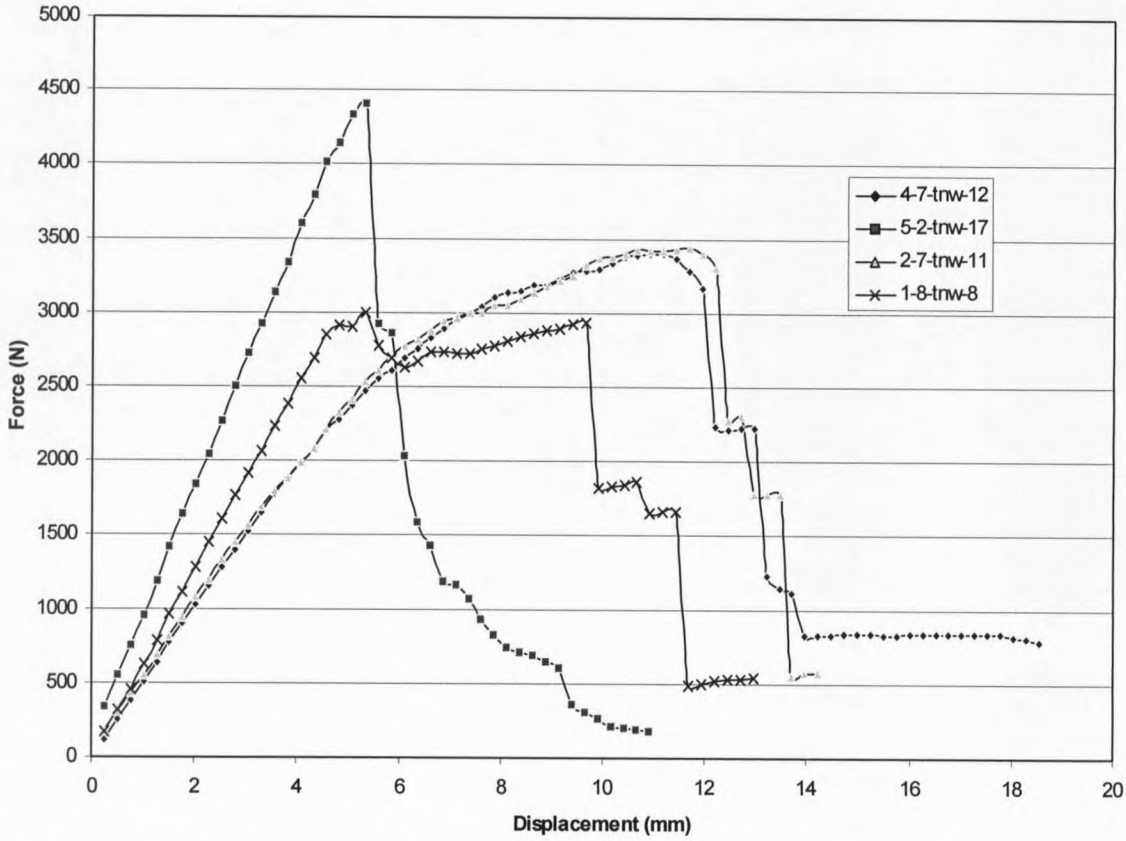


Figure 4.16 Static Flexure Comparison

Table 4.5 is a summary of static flexure results. It is apparent that as in the case of dynamic flexure test, that the 5 series has the highest threshold and the 4 series boasts the highest total absorbed energy.

Table 4.5 Comparison of Static Flexure Results

Material ID	Static Flexure Strength	Static Flexure Modulus	Energy Absorbed During Static Test	Stress at level of damage
1,2,4,5 series materials	MPa	GPa	Joules	Mpa
1-7-tnw-12	619	48.4	23.3	558
1-7-tnw-13	615	52.2	26.3	528
1-8-tnw-18	595	54.7	24.5	558
1-8-tnw-19	565	53.2	23.6	518
2-7-tnw-11	685	40.5	32.0	458
2-7-tnw-12	685	41.6	31.1	438
2-8-tnw-16	686	40.9	27.8	558
4-7-tnw-12	677	41.7	34.9	438
4-8-bw-2	664	44.6	29.6	558
4-8-bw-3	618	42.5	27.3	498
4-8-tnw-18	576	41	25.1	438
5-2-tnw-17	876	74.4	18.5	797

Several observations can be made regarding tabulated and graphical comparisons. Comparing ultimate bending strengths can be misleading. Several of the reinforced specimens exhibited strengths that rivaled the 2-D baseline composite. However it should be noted that the strength associated with initial onset of damage was highest for the 2-D baseline composite.

Tensile Test Results

Several "dog bone" specimens were supplied and subjected to previously described testing. The ultimate tensile strength and tensile modulus are the only metrics extracted from this test. A comparison graph is shown in Figure 4.17 of other parameters. Each major type of material variation was tested except for 4 series. No 4 series dog bones were supplied. The 2 and 5 series remained linear to about 600 MPa, the 1 series became damaged at stress levels of about 450 MPa.

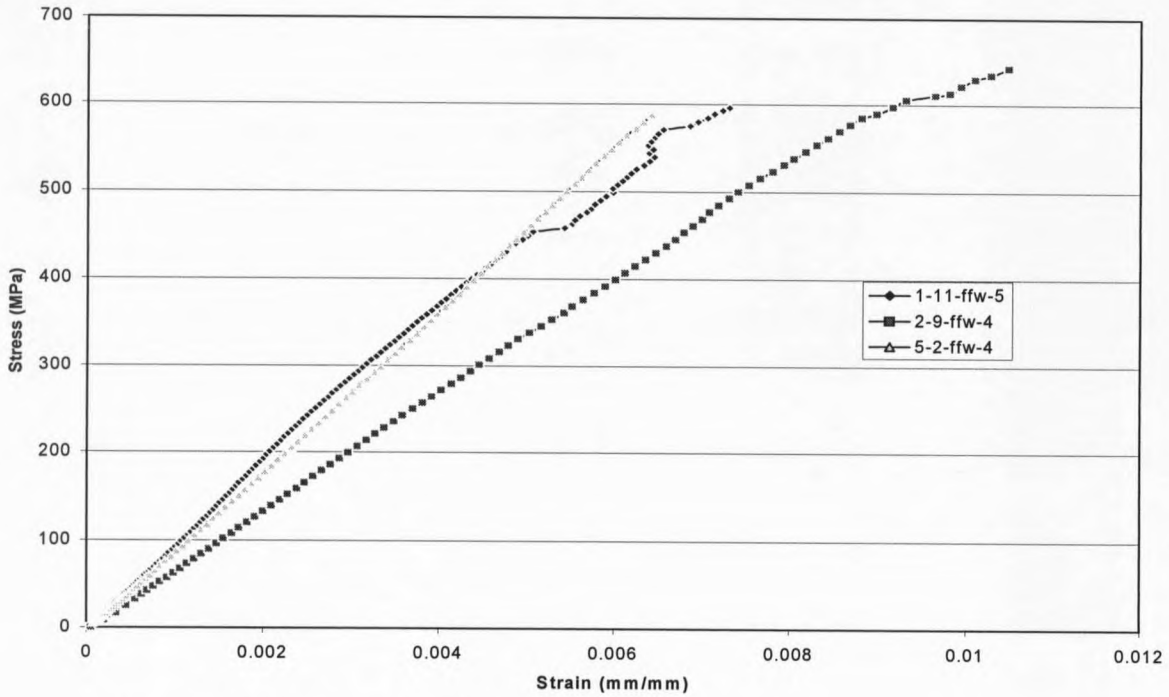


Figure 4.17 Tensile Test Results

The 5 series material shown in figure 4.18, maintained linearity complete to failure. Typically the other reinforced materials exhibited cracking and other acoustic emmissions that indicated damage at about 75 to 80% of ultimate tensile strength.

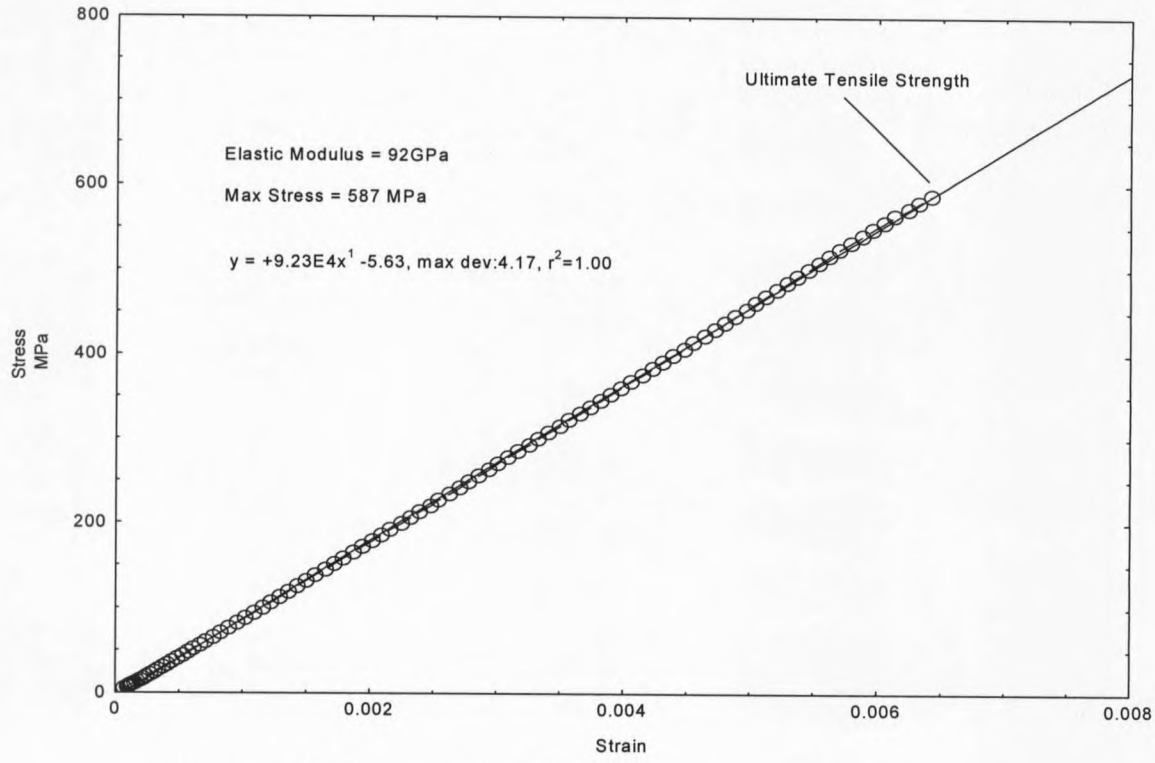


Figure 4.18 Stress vs. Strain for 5 Series

Summary of Experimental Results

Several results are evident from this study. The original goals of isolating material characteristics that effect aerofan blade durability and test method development were achieved. Preliminary results have been obtained and compared. All of the materials submitted for testing have some compromise regarding in-plane and out-of-plane properties. It is also evident that the heavily reinforced architectures, with through

thickness cross-stitching, compromised out of plane strength. Most of the reinforced materials had larger tolerance or absorbed more total energy than the 2-D version. However this may be of little use since this energy value and area under the curve correspond to permanent damage. This justifies the additional calculation of energy absorbed and other bending strength before the onset of damage. In service it would be required that a blade withstand an impact and complete the intended flight. Once this requirement is satisfied, delamination resistance is the next most important consideration when dealing with composites. Dynamic threshold and delamination requirements must be met while simultaneously maintaining stiffness, tensile strength and bending strength. It is additionally necessary to exceed the strength to weight ratio of rival materials such as titanium before material can be considered a valid candidate.

Suggested material properties are supplied below in Table 4.6. These values are a blend of properties from the architectures tested in this study. The testing procedures discussed can be used as a screening process to refine existing material properties.

Table 4.6 Suggested Material Properties for Composite X

	Suggested	Current best	Current best ID
Dynamic Flex Strength threshold	> 800 MPa	765 MPa	5 series
Dynamic GIIc value	> 2700 J/m^2	>2700 J/m^2	All but 5 series
Static Bending Strength	> 850 MPa	797.2 MPa	5 series
Bending Modulus	> 69 GPa	74.4 GPa	5 series
Tensile Modulus	> 70 GPa	> 70 GPa	All exceed
Tensile Strength	> 650 MPa	655 MPa	2 series
Strength to weight ratio	undecided	not known	5 series

Numerical Analysis for Case Study I

Two separate but similar models were developed. One model was meant to represent flexure testing and the other was designed to simulate ENF or end notch flexure test. These models were intended to substantiate data reduction techniques used to calculate material properties such as flexural strength, flexural modulus, and dynamic mode II fracture toughness. Mode II fracture is generally not as well understood as mode I. The friction at the sliding interface of the crack could affect the results [Gillespie (1986)]. Non-conservative values could be produced, by disregarding the friction at the crack interface.

Static Flexure Approach

From previously conducted static flexure tests the flexure modulus was obtained experimentally. This modulus was input as a constitutive property in a finite element model of the specimen tested. This model was then solved for incremental loads up to the limit of the material. From this, a load – displacement graph could be generated and compared to the experimental data. Additionally, the bending stress at max load could be obtained and compared to the bending stress predicted by standard beam formulations.

Static Flexure Model

For the case of the static flexure model a 2-D analysis was conducted. Half symmetry was employed to reduce the computational burden. A state of plane stress was assumed and Ansys plane82 elements were used. Typically the mesh consisted of six elements through the thickness of the modeled static flexure specimen. The aspect ratio was held to 1x1. The material properties were smeared and obtained from experimental

results. The boundary conditions at the plane of symmetry were simply to restrict thickness edge from translating in the horizontal or (x) direction. This prevented the specimen from translating and also maintained the 0-curvature restriction required for symmetry. The reaction boundary condition was addressed by implementing contact elements. The static flexure specimens were supported at each end by rollers, which were an integral part of the entire static flexure fixture. The actual contact of the static flexure specimen with the roller was modeled and this addressed the support or reaction boundary condition. The roller to fixture contact surface was modeled, since the roller was not press fit and was allowed to rotate and follow the curvature of the fixture support holes. The specimen was loaded in steps in displacement control. Corresponding nodal loads were found at each displacement increment and were compared to experimental data. The model is shown in Figure 4.19.

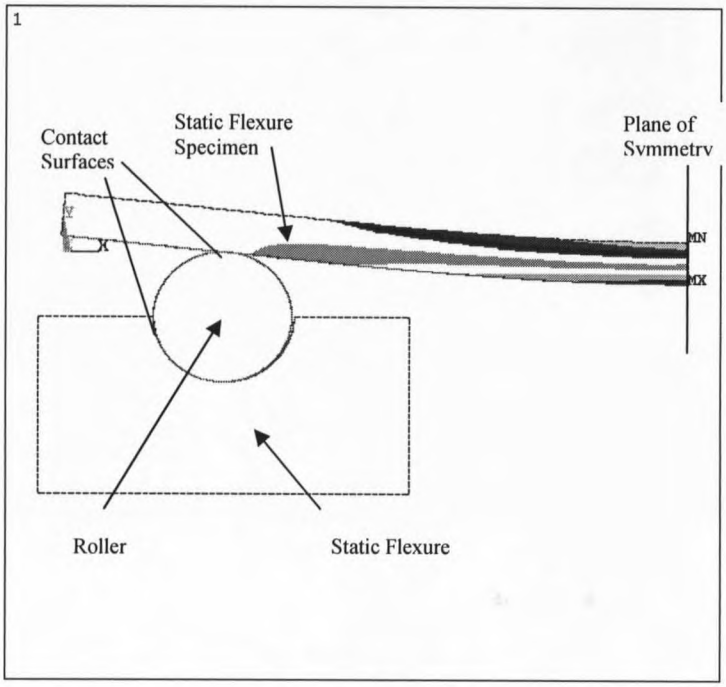


Figure 4.19 FEA Static Flexure Model.

Static Flexure Numerical Results

The load displacement data from the FEA model matches the experimental data closely as shown in Figure 4.20. At about a load of 3000 N, the experimental data becomes nonlinear. The FEA model does not capture this affect because damage thresholds have not been modeled.

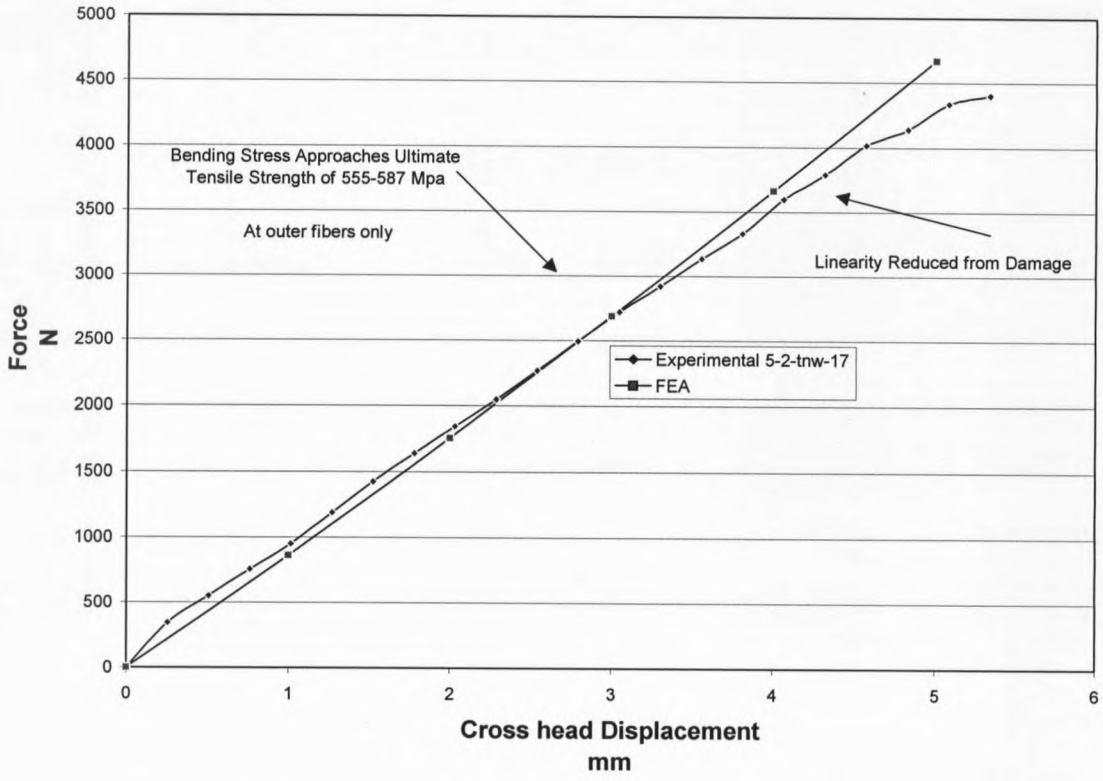


Figure 4.20 Comparison of Experimental Static Flexure Results to Numerical

It is interesting to note that the bending stress corresponding to the initial nonlinearity is close to the experimental tensile strength. When comparing reduced experimental data, the tensile strength of the 5 series composite was about 600 MPa, this

conflicted greatly with the bending strength of 874 MPa. However when using a displacement of 3 mm, the FEA model predicted a stress of about 600 MPa at the outer tensile fibers. At a displacement slightly greater than 3mm is where the data skews from linear. Most likely at about 3mm of displacement the fibers at the outer edge of the flexure specimen begin to fail which reduces the stiffness but still allows the specimen to accumulate load.

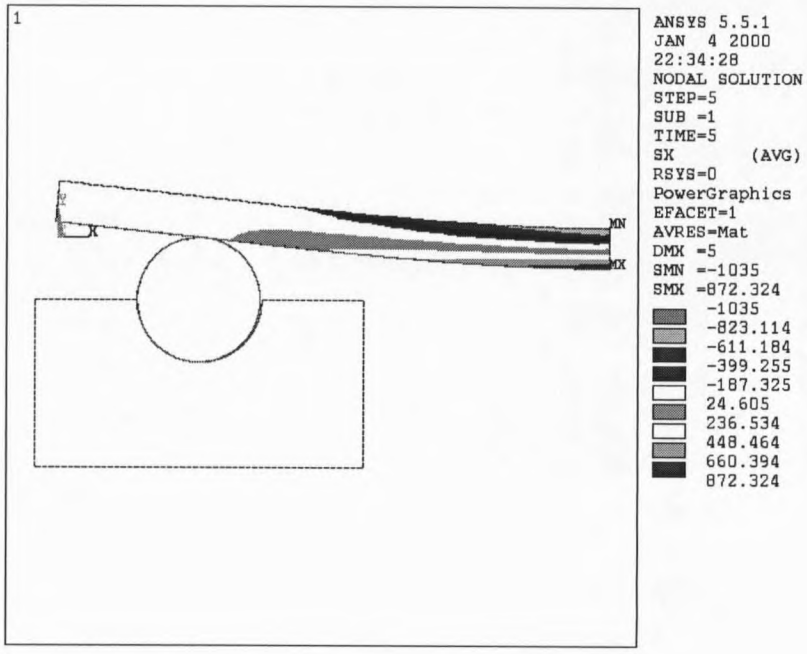


Figure 4.21 Longitudinal Stress Plot from FEA Solution

End Notch Flexure Approach

From previously conducted static flexure tests the flexure modulus was obtained experimentally. This modulus was input as a constitutive property in a finite element model of an ENF test specimen. Both crack closure techniques and crack extension methods were used to evaluate G_c numerically. Four solutions were required. Initially the model was solved with the critical load applied. The total strain energy was output as well as required nodal data for the single step virtual crack closure technique (VCCT 1). The model was then resolved with unit loads applied so that relative motion between the corner nodes immediately behind the crack front would be closed. Nodal displacements at the corner nodes were output and used with the initial displacements to calculate G_c (equation 2.10) with the two step method (VCCT 2).

Two crack extension methods were also used. The crack in the original model was extended by the length of an element. The critical load was held constant and the model was resolved. The total strain energy was output and used with equation (2.11) and the original strain energy to calculate G_c. This method is called crack extension 1 (CE 1). A similar technique was applied. Instead of using an incremental extension, the final crack extension was used from the experimental data. The actual displacement was applied to the model instead of assuming a constant load. This approach is CE 2.

Friction was accounted for at the crack surface. The validity of the mode II test has been questioned, mainly due to the effect of friction on these results [Gillespie (1986)]. This model was evaluated in two steps. Initially the load corresponding to crack initiation was used with the initial crack length modeled. The model was solved and total strain energy was output. The model was then resolved in displacement control with the

final crack length supplied and the displacement at crack arrest input. The total strain energy was then output for this load step. The difference in strain energy between the two states is the strain energy required to induce crack growth. The standard area method can then be used to reduce the strain energy to a G_{II} value. This G_{II} value could then be compared to that obtained by fracture mechanics via beam formulations.

End Notch Flexure Model

The model used for the ENF simulation was similar to the static flexure model. A two dimensional model was developed and symmetry was abandoned due to the asymmetric nature of an ENF specimen. The geometry was constructed of eight rectangular areas. This was done to provide regions of mesh refinement near the crack. The actual crack was constructed by superimposing two lines on top of another.

The primary material property used for the ENF model was the "smeared" flexural modulus obtained from the static flexure experiment. This modulus was verified by the load – displacement curve produced with the static flexure model. A Poisson's ratio of 0.33 was assumed. Only two material properties were required for an isotropic approximation.

The areas were meshed with plane82 elements and plane stress loading conditions were declared. At the crack front the two lines shared an end point. One line was assigned to the area immediately above the crack and the other line was used for the area below the crack. Contact elements were used on these crack surfaces. A flexible – flexible contact pair was created using the target169 and contact171 elements described. This allowed both surfaces to have elastic properties. The top line was assigned to be the

target and the bottom line was assigned to be the contact surface. The assignment of the contact and target surface was not critical because a flexible – flexible contact pair was constructed. A static coefficient of friction was assigned to the target and contact elements. Mesh details and boundary conditions are shown in Figure 4.22

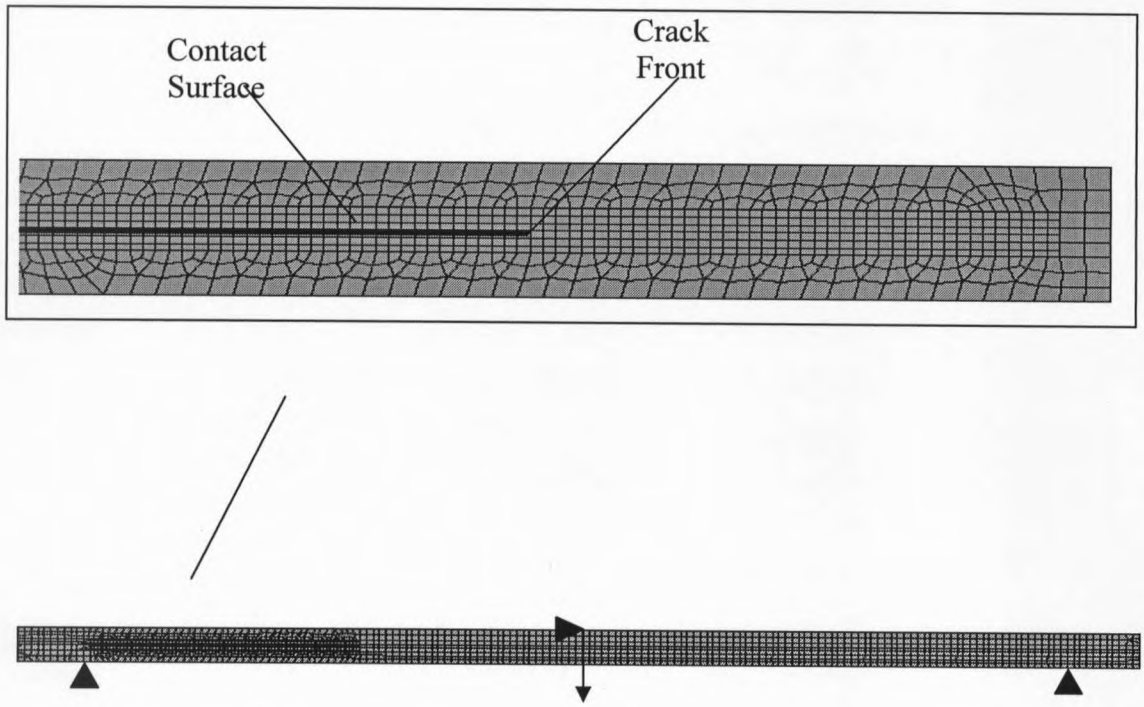


Figure 4.22 ENF Mesh with Refined Region and Boundary Conditions

The nodes corresponding to the location of the experimental supports were restricted from vertical motion. An additional displacement restriction was required to provide stability to the ENF model. A horizontal restriction was placed on the loaded

node to prevent the stability problems. The critical load responsible for crack initiation was applied to the node at midspan. A nonlinear solution was required and appropriate quantities such as strain energy, force and displacements at key nodes were output to obtain G_c.

End Notch Flexure Results

The model constructed was evaluated for three different a/da ratios. The four methods discussed were used to calculate G_{IIc}. Once convergence was confirmed and a confident solution was obtained the results were compared to those from the experimental findings and analytical techniques. The results from the FEA crack extension and crack closure methods are in table 4.7 for each a/da refinement.

Table 4.7 ENF Convergence for G_{IIc} cf = 0.35

load	mesh	VCCT 1	VCCT 2	CE 1	CE 2
N	a/da	N/m	N/m	N/m	N/m
2410	58	1717	1366	1890	2092
2410	97	1675	1679	1655	2093
2410	145	1683	1681	1261	2093

The VCCT 1 method provided a reasonable estimate for G_{IIc} at all a/da ratios. The solution converged and compared closely to the VCCT 2 method. The VCCT 2 method required improved refinement but was very self-consistent. The CE 1 method

seemed to provide accurate results at the 97 a/da ratio but was not consistent and did not show improvement with refinement. The CE 2 method converged immediately.

Comparison

The finite element (FEA) two-step crack extension (CE 2) method was bounded by the other methods. The only difference between the area method and the two-step strain energy method is the manner in which, the energy required to promote crack growth was obtained. The Area method uses numerically integrated experimental data. The two-step strain energy method calculates the energy using the FEA procedure outlined.

Table 4.8 FEA Results Compared to Analytical Methods

	VCCT 1	VCCT 2	CE 1	CE 2	Beam Method	Area Method
	N/m	N/m	N/m	N/m	N/m	N/m
cf=0	1791	1791	1182	2130	1845	2163
cf=0.35	1683	1681	1261	2093	1845	2163

The VCCT 1 method compares closely to the VCCT 2 method and the beam method for a friction coefficient of 0. These methods provide an approximation of the energy required to initiate cracking. The CE 1 method also is a measure of the initiation SERR. This method does not compare well to the others. At an increased value of friction the FEA model predicts lower G values. This is because the analytical methods can not account for the effects of friction. Assuming the FEA results are correct, the

analytical methods are non-conservative by a significant amount. This downfall prompted additional study. As a result the VCCT 1 and VCCT 2 methods were used to evaluate G_{IIc} at a range of friction coefficients. The results are shown in Figure 4.23.

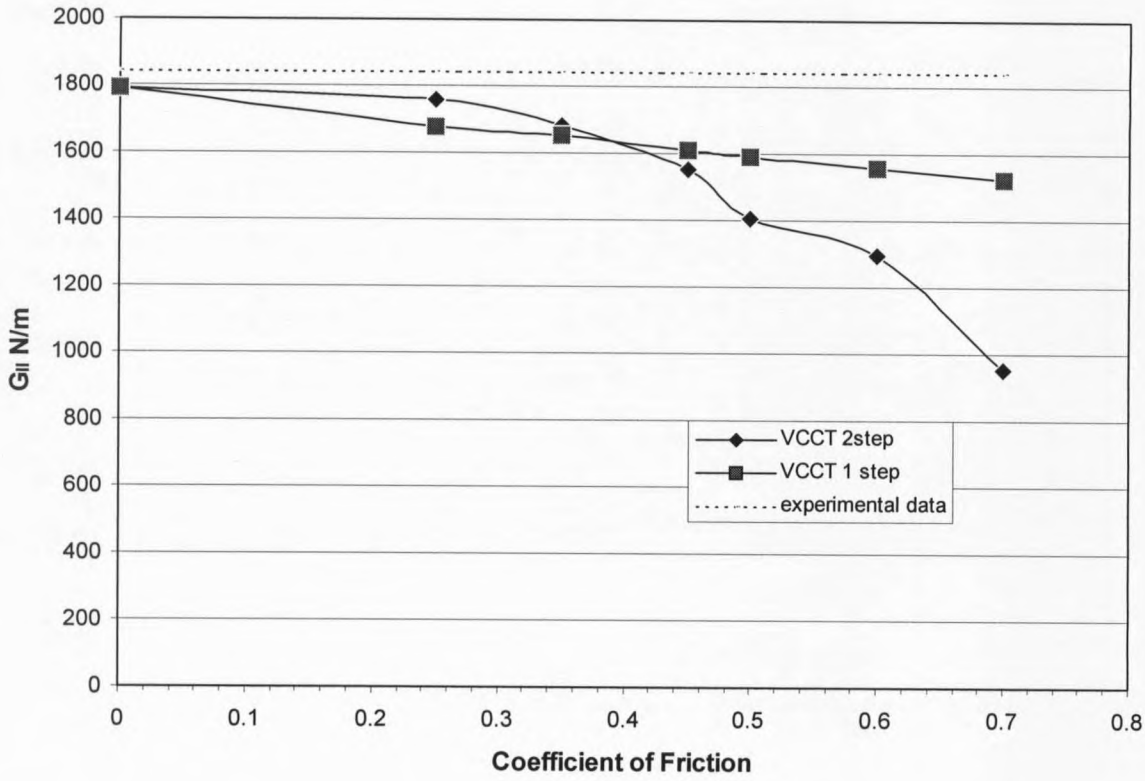


Figure 4.23 Friction Effects on Predicted Mode II Fracture Toughness

As the coefficient of friction is increased the analytical method over-predicts G_{IIc}. Additionally, the two FEA methods agree up to a friction value of about 0.4. At that point the two methods diverge. The VCCT 1 method is most likely correct because coulomb friction should behave linearly. This should be substantiated by some other calculation.

Simple slope tests were conducted to evaluate the friction coefficient between the two sliding surfaces. The results of these experiments suggest that the friction coefficient was between 0.45 and 0.55. Based on this approximation the analytical G_{IIc} value was probably non-conservative by at least 10%. A teflon strip was not used during the manufacture of the laminates, as a result the crack interface was considerably rough and consistent with the propagated region.

The Area method and the CE 2 method average the G_{IIc} over a known crack growth region. These methods account for R-curve behavior and generally predict larger values for G_{IIc} than the initiation methods.

Test Specimen Validation

The FEA model also provided an immediate inspection tool for stresses. It was stated earlier that the Area method relates energy absorbed to crack damage. However, if damage occurs in addition to crack growth, an inflated G_{II} value would result.

The experimental data had two similar test results. These were the 5-tnw-13 and 14 specimens. However the 5-2-tnw-18 specimen varied from these others exceptionally. The 5-2-tnw-18 specimen possessed a G_{II} value that was twice as much as the others. This data point indicated that possibly additional damage could have been induced, beyond crack growth and stimulated further investigation. When consulting with bending stress and VMS values from the FEA analysis, stress values of 700+ MPa were predicted for this specimen. These values exceed both the tensile strength and the experimentally predicted dynamic bending strength. When specimens 13 and 14 were evaluated with the FEA model, stress levels around 550 to 580 MPa were predicted. This suggests that most

likely, specimen 13 and 14 produced reliable G_{II} test results. Possibly a blunt crack was formed in specimen 18 and before ample energy could be absorbed to initiate crack growth, parallel modes of failure resulted.

The two-step FEA model was not applied to the other specimens because only the series 5 material would accept pre-cracking and fail in fracture. However, any additional material candidates generated (that failed from delamination), could be simulated by this model.

Summary for Case Study I

In this case study the database-screening approach worked well to isolate key properties and compare them on a material level. The tests outlined could be used to evaluate potential composite candidates or refine existing ones. It was noted that excessive reinforcement through the thickness compromised in plane strength. The through thickness reinforcement could be optimized to improve fracture toughness without sacrificing strength. Additionally, the 90 degree fibers could be replaced by 45 degree or 0 degree fabric. This would increase the strength in the primary direction to compensate for the loss from the addition of the through thickness fibers. This would allow for increased strength and interlaminar fracture toughness. When converting a typical stress intensity factor for titanium to a strain energy release rate the G_c for titanium is 10 times greater than that of the 5 series composite. This suggests that some through thickness reinforcement is needed to compete with titanium with regards to toughness. The strength of titanium can be rivaled by making above changes to the architecture, but only in the primary or longitudinal direction, where needed. The tests

provided and methodology presented can be used to optimize and develop composite candidate materials for this application.

The numerical study focused on evaluating G_{II} for a coupon subjected to flexure. The analysis used smeared constitutive properties and employed various strain energy approaches to evaluate G. From the work completed it was found that the crack closure methods work and compare well to the analytical equation for G_{IIc}. The crack closure methods can also account for friction at the crack interface. When including friction on the crack interface in the models, it was found that both the VCCT 1 method and the VCCT 2 method agreed well for friction coefficients below 0.3. At friction values above 0.3 the G values diverged and from each other, as well as from the analytical equation which does not address friction effects. A two-step crack extension method was also applied that included friction affects. This method was compared to the energy method, which averages G over some distance of crack growth. The two-step strain energy method compared well with the experimental area method, which indicates that not accounting for friction when applying the area method is actually less errant than when using the compliance method. The primary revelation from this study is that the analytical method used to quantify G_{II} over-predicts the fracture toughness. Models like the ones presented should be used to isolate G_{II} from experimental tests and the friction should be included in any model where discrete crack damage modeling is taking place. The VCCT 1 method was easiest to use and provided reasonable results through a range of friction coefficients.

Overall the database-screening approach proved sufficient to compare composite material candidates on a qualitative and quantitative level. Design drivers or key

properties were isolated and appropriate tests were formulated to determine these properties. Once obtained, the experimental properties were compared. The tests outlined could be used determine material limitations and assist in improving them. The experiments conducted are part of a general methodology formulated to evaluate interlaminar fracture performance.

When investigating the database – prediction approach it was found that when attempting to model mode II fracture behavior, friction needs to be accounted for. Some sort of friction knock-down factor should be used for the original G_{II} obtained from experiments, or an FEA model should be employed to evaluate the actual G_{II}.

CHAPTER 5

CASE STUDY II
HONEYCOMB FUEL TANK INVESTIGATION

This project employed a database – screening approach as in case study I. Basic material properties were identified that related to structural performance. Experimental procedures were developed to test these properties. These materials were then compared as a screening process to find the limiting source of performance for the honeycomb composite material. Both interlaminar fracture and strength properties were evaluated.

Additionally, some advancement was made regarding analytical modeling. Flatwise tension models were used to confirm validity of experimental procedures. Mode I simulations were developed to substantiate experimental findings and to validate a compliance equation derived for sandwich panel G_I testing. Mode II models were also developed to confirm experimental technique and interpret results.

Project Introduction

The X-33 was the most recent generation of spacecraft. A significant effort was made to reduce the weight of the fuel cells, which contain liquid helium and liquid hydrogen. The solution was to make the fuel cells from a honeycomb type sandwich panel. These honeycomb fuel tanks were originally constructed full scale and little was known about the properties of the honeycomb sandwich material.

A catastrophic failure occurred during bond processing of Lobe 1 of Tank-1 of the X33 liquid hydrogen tank assembly [HPC (2000)]. Many curing stages are necessary for final assembly, and failure occurred during Cure 4a. On January 13 and 14, 1999, the

failed Lobe 1 was removed to reveal extensive, core/face sheet debonding. The nominal materials are Hexcel's IM7/8552 for the face sheets, Korex^{tm} core material, with 3M EA 9394 film adhesive. The Lobe 1 portion of the tank was later repaired.

Case Study Goal

In this study, mechanical properties were evaluated for Tank-1of the X-33 space shuttle. Tank-1 Lobe 1 repair material was selected as the baseline material, and Tank-1 Lobe 4 was chosen for studies on nominal, as built lobes. The material was sent by Alliant Techsystems, Bacchus Works for testing at Montana State University.

Four tests were chosen for studying mechanical behavior. Each test that was developed and the motivation for its development are included in Table 5.1. Table 5.1 also serves as a test matrix and included the number of tests conducted during this study. Only limited quantities of the control material was available from Lobe1 repair material. Hence, only transverse tension, Mode I interlaminar fracture, and transverse compression testing was conducted on these samples.

Table 5.1 Test Development and Test Matrix

Tests Developed		Motivation	# of tests on Lobe 1	# of tests on Lobe 4
1	Transverse Tension	Evaluates Interlaminar Tensile Strength	5	6
2	Mode I Interlaminar Fracture (G_I)	Mode I Fracture Properties	6 specimens 10 tests	10 specimens 26 tests
3	Mode II Interlaminar Fracture (G_{II})	Mode II Fracture Properties	0	9 specimens 11 tests
4	Transverse Compression	Through Thickness Compression	3	10

The testing techniques for the above tests were developed uniquely for this study. Test fixtures, tabs, and a bonding fixture were designed and constructed as needed. Test procedure and results are summarized in following sections of this document.

Experimental Procedures

Four testing approaches were taken to characterize the honeycomb sandwich material from Lobe 1 and Lobe 4. The testing techniques applied were flatwise or transverse tension, Mode I Fracture (peel-off), Mode II shear fracture, and transverse compression tests. Each of these testing methods will be described in their own section.

Three plates were supplied to Montana State University for testing. Two of the plates, sectioned from Lobe 4, were curved. The remaining panel, sectioned from Lobe 1, was mostly flat. It should be noted that Lobe 1 material was a repair section and was chosen to represent baseline data. These panels were divided into 38 x 38mm squares and 38 x 152mm rectangles as shown in Figure 5.1 and 5.2. The square shaped specimens were used for flatwise tension testing, and the rectangular specimens were used for fracture toughness tests. Limited material was available, so an optimization was performed to maximize the number of samples.

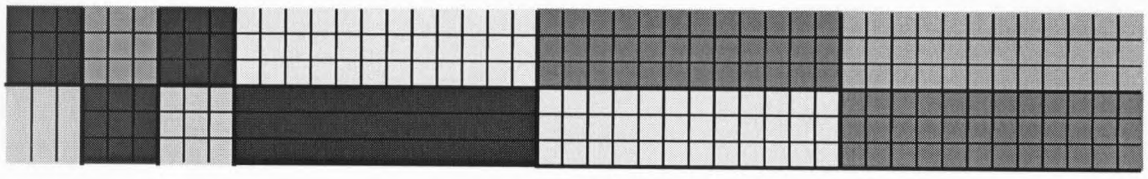


Figure 5.1 Sampling of Panel 1 From Lobe 1

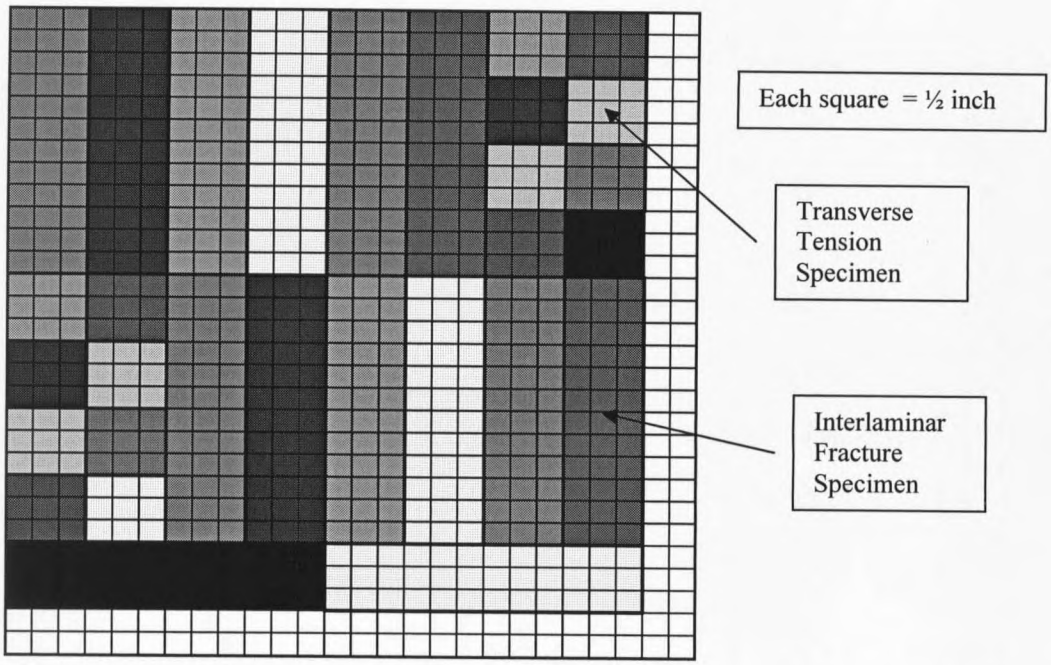


Figure 5.2 Sampling of Panel 2 from Lobe 4

The Montana State University (MSU) machine shop cut panels to the prescribed dimensions with the use of a carbide cutter. Special care was taken to provide a dry environment for machining and storage.

Flatwise Tension Testing

A substantial concern was to achieve precise alignment of the specimens with their tab fixtures. It was decided that the most crucial point was to have applied loads always be directly opposite of each other. This way, moments created from being off center would be minimized. Hence, significant care was expended to get these loads

applied through the center of the specimen. One approach that might accomplish this would be to precision machine an exact set of tab fixtures and re-use these for the testing of each specimen. This approach was not taken for several reasons. Due to variation of actual specimen size, lack of access to precision equipment, and the fact that specimens were to be preserved, a precision bonding fixture was fabricated instead. The fixture shown below in Figure 5.3 uses the V-block and slotted region to center the specimen with both tabs.

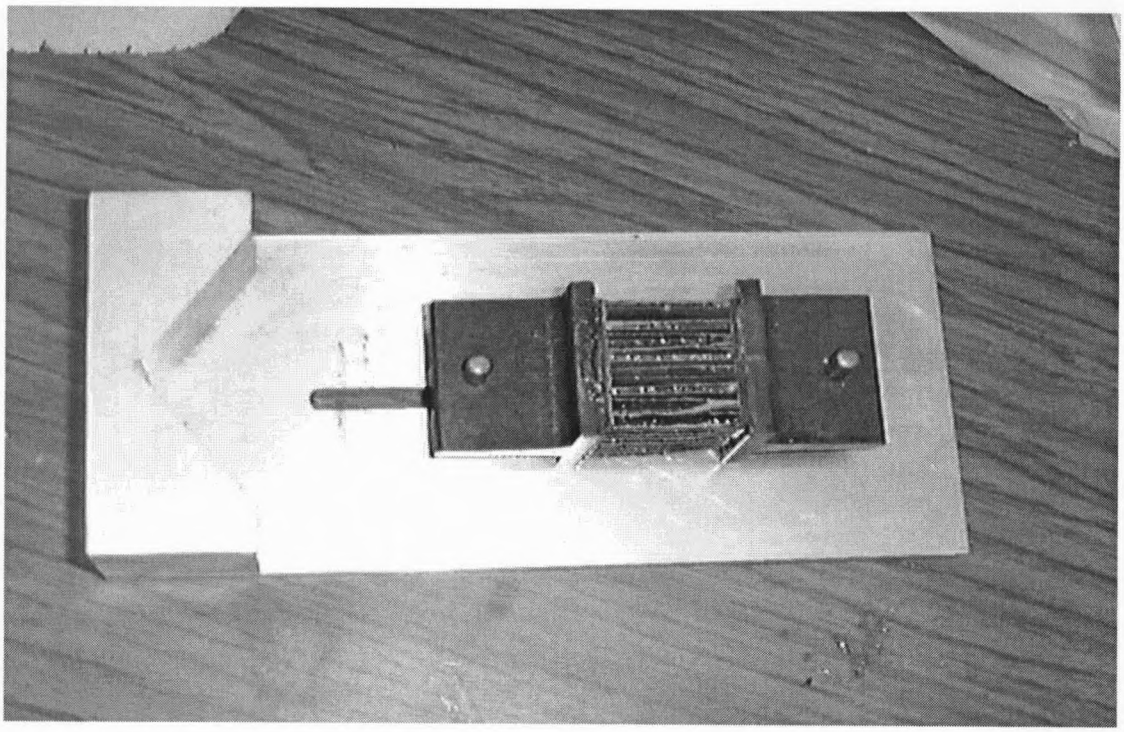


Figure 5.3 Mounting (Glue) Fixture Used to Attach Tabs to Specimen

The specimen was glued to top tab first using the V block and slot. Then the partially glued assembly was slid upward and the bottom tab was attached with aid of an alignment pin. This aligned the holes of each fixture with the center of the specimen. This system can be used with a range of specimen sizes and tab dimensions. This allowed the tab fixtures to be mass-produced and attached in a precise and accurate fashion. The specimens could then be glued and oven cured at 65 degrees Celsius. This was done in batches of about four.

Specimen Preparation

Approximately 6 specimens were tested from each lobe. The 38 x 38mm square specimens were pulled apart in the direction transverse to the face sheet layers. This was accomplished by attaching fabricated tabs to the top and bottom of the specimens. The fixtures were simply pieces of steel T-section crosscut to at least 38mm. The tabs were very stiff to preclude any distortion during testing. These T-sections were then fitted with a 6mm hole through the web. The tabs were held to the specimen by means of various glues. The most common adhesive used was Hysol.EA 9309.2NA QT System. This two-part epoxy had excellent bond strength of about 27 MPa, but was difficult to work with. Other epoxies used were over the counter glues made by Devcon. These were easier to apply but did not always have the strength of Hysol. A specimen ready to be aligned and tested is shown in Figure 5.4.

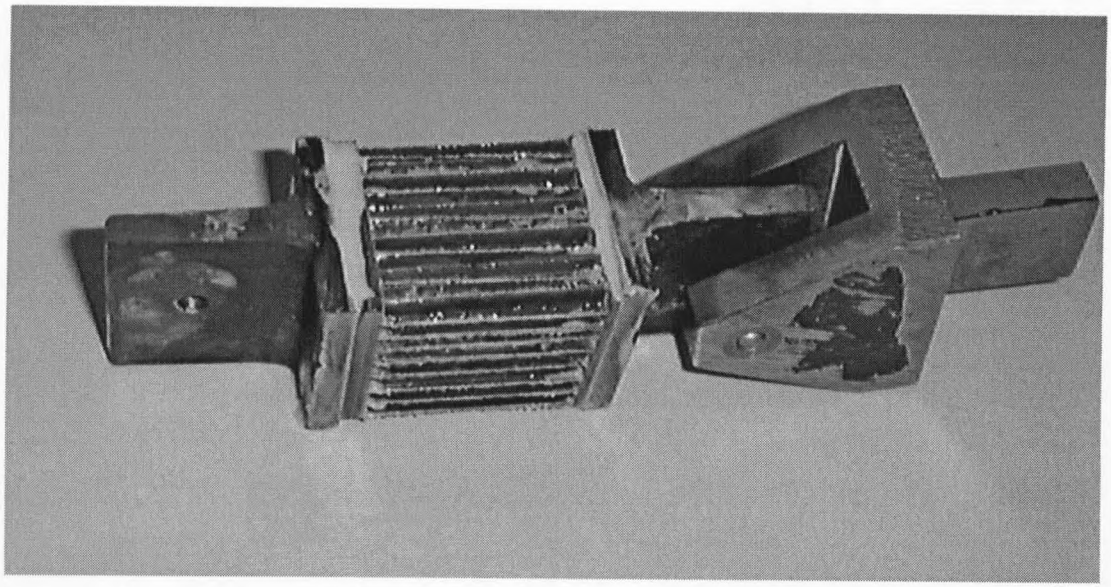


Figure 5.4 Flatwise Tension Specimen Complete With Attached Tabs

Testing Procedure

Data sheets were used to manually record coupon dimensions. Specimens were labeled with a prefix L1 or L4, which indicates whether they were a Lobe 1 or a Lobe 4 sample. Once these specimens were prepared, testing took place with use of an Instron 8562 Screw machine [ASTM C 297-94 (1997)]. Specimens were tested in displacement control at rate of 0.08 mm / min. An additional flexible apparatus was used to secure the specimen into the Instron. The intent was to combat the possibility of inducing moments from eccentric loading. The flexible coupler consists of two clevise type ends with a universal joint at one end. The flexible coupler is shown in Figure 5.5.

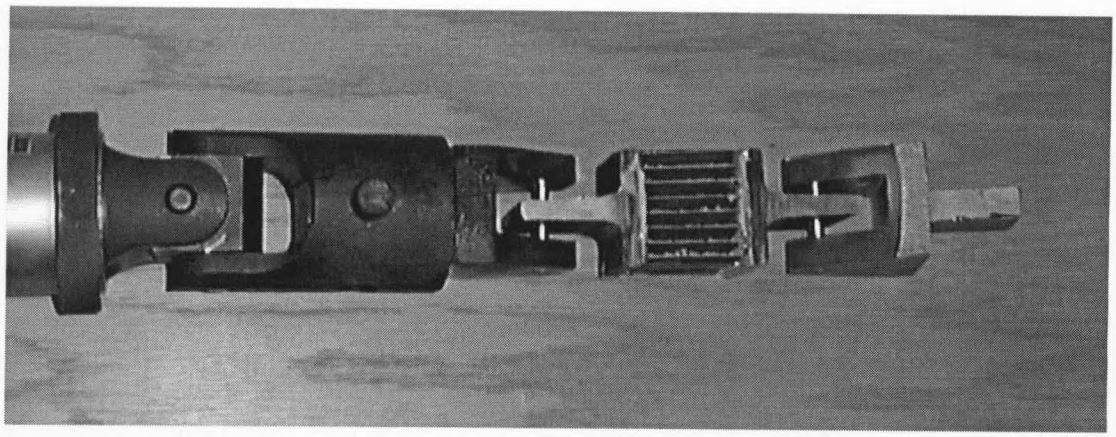


Figure 5.5 Testing Jig with Universal Pivoting Capability (flexible coupler)

Adding any bending loads would create a combined stress state that would not be accounted for in simple data analysis. The presence of any moments would not be an accurate assessment of flatwise tensile strength. The flexible link used allowed the specimen to pivot in both planes, with limited friction, to minimize bending moments.

Data Reduction Methods

While the specimens were tested to failure, Instron Series 9 software was used to record force and deflection. Occasionally, a specialty Labview program and Nidaq data acquisition setup was used instead. The force and deflection data were then used to obtain a stress-strain plot.

Stress was represented as:

$$\sigma = \frac{P}{A} \tag{5.1}$$

where P was the recorded force in Newtons,

and A was the overall cross sectional area.

Strain was determined as:

$$\varepsilon = \frac{\delta}{L} \tag{5.2}$$

where δ was the crosshead displacement,

and L was the core thickness.

The ultimate tensile strength the value of the largest load seen by material divided by the cross-sectional area. It should be again noted that the cross-sectional area was based on the outermost dimensions, not actual core paper area. The "effective" elastic modulus was found from linear regression and was based on the assumption that all of the displacement read corresponded to the extension of the paper core. The strain at failure was evaluated based on cross-head displacement measurements. All of these values are labeled on each individual graph. A sample graphical representation is shown in Figure 5.6. All tests conducted were later compiled and compared on a tabular basis. Statistical

information in form of mean and standard deviation is also presented in the Results section of this chapter.

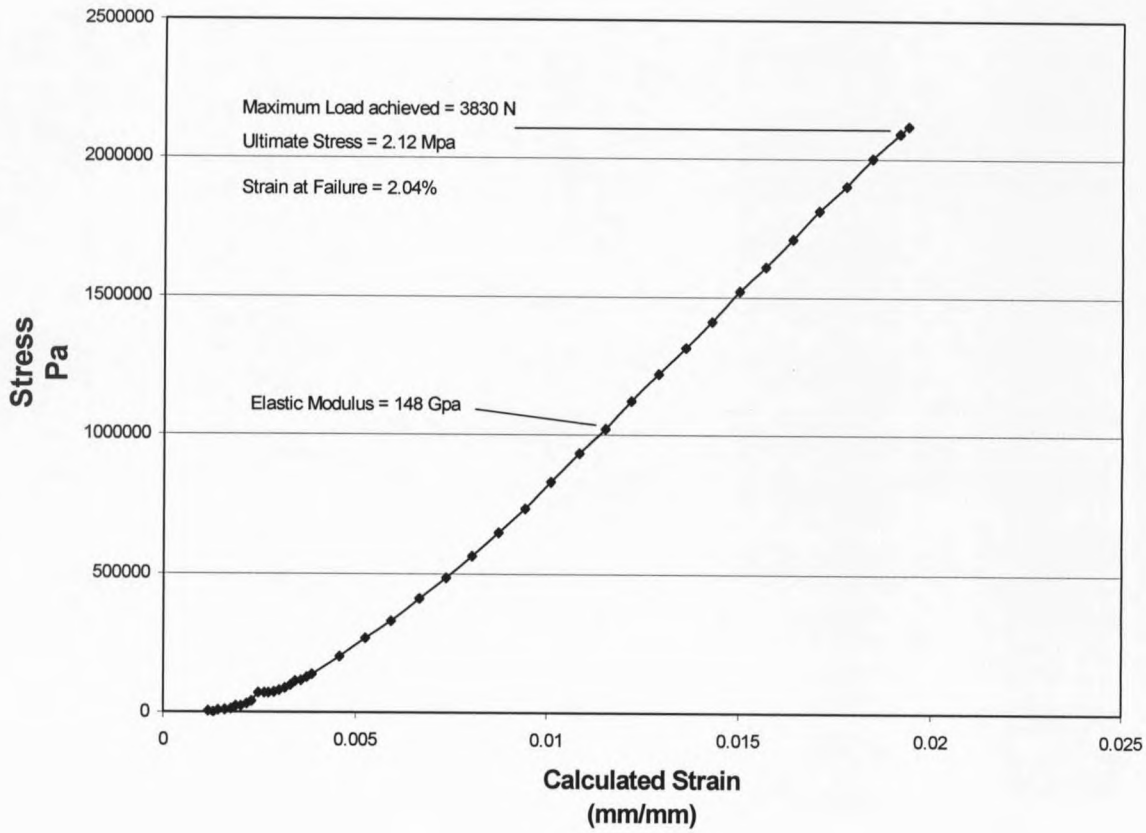


Figure 5.6 Graphical Presentation of Flatwise Tension Specimen

Mode I Testing

Mode I Peel-off tests were conducted to evaluate the material's resistance to separation at the core or at the core bond. These tests were executed in the same fashion as a double cantilever beam test used for Mode I fracture toughness [ASTM D 5528-94A (1997) and Carlsson (1986)]. As stated earlier the 38 x 152mm specimens were subjected to peel off testing. Each coupon was pre-cracked at one end at the composite core interface with razor blade. Both face sheet (inner and outer) interfaces were tested. Two hinges were attached to these specimens at the cracked end with Hysol adhesive. At this point, the specimens were measured and ready to be tested. A simple test fixture had to be constructed, so that the standard Instron grips could accommodate the hinge fitted peel off specimens. The test apparatus is shown in Figures 5.7a and 5.7b.

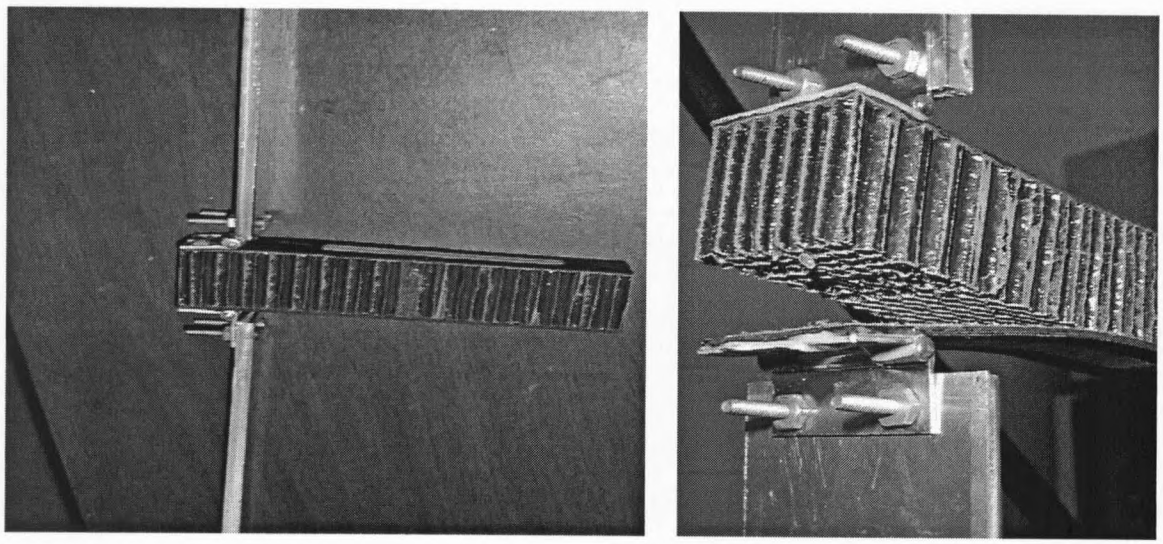


Figure 5.7a Mode I Testing Apparatus and Figure 5.7b Test in Progress

Testing Procedure

Force and deflection were obtained via Labview data acquisition. Initial and final crack lengths were measured by means of visual inspection with the use of 4 digit-precision calipers. Each specimen was initially given a pre-crack of about 40mm. Forces were applied, in displacement control at 0.025 mm/sec until the crack propagated approximately one inch. The peel-off specimen was then unloaded to obtain a complete hysteresis. Once the specimen was completely relaxed and the final crack measured, the test was repeated until crack extended past the mid-plane of the sample. Testing would be stopped and crack growth or new crack length was measured. This was repeated up to three times for each specimen. The panels presented to MSU for testing had face sheets of varying thickness. Tests were conducted with the initial crack on the thin side as well as the thick side.

Data Reduction Methods

Ultimately, some measure of peel off resistance was desired. The approach taken to achieve this was an energy method. The force deflection data was integrated resulting in total energy absorbed for each crack session. This total energy was then divided by the specimen width multiplied by crack length (eq2.2). The result was the Mode I critical strain energy release rate [Broek (1996) and ASTM D 5528-94A (1997)].

Since each specimen was subjected to repeated crack growth, 3 to 4 G_I values were obtained for each rectangular specimen. Usually, the first G_I values obtained were larger than subsequent values. The information from the first test was probably not valid

because the pre-crack may not have been initiated in the path of least resistance. In later test cases, the crack initiation process was refined enough that the values obtained from the first crack were used. Three loading sequences for a Lobe 4 material are shown in Figure 5.8.

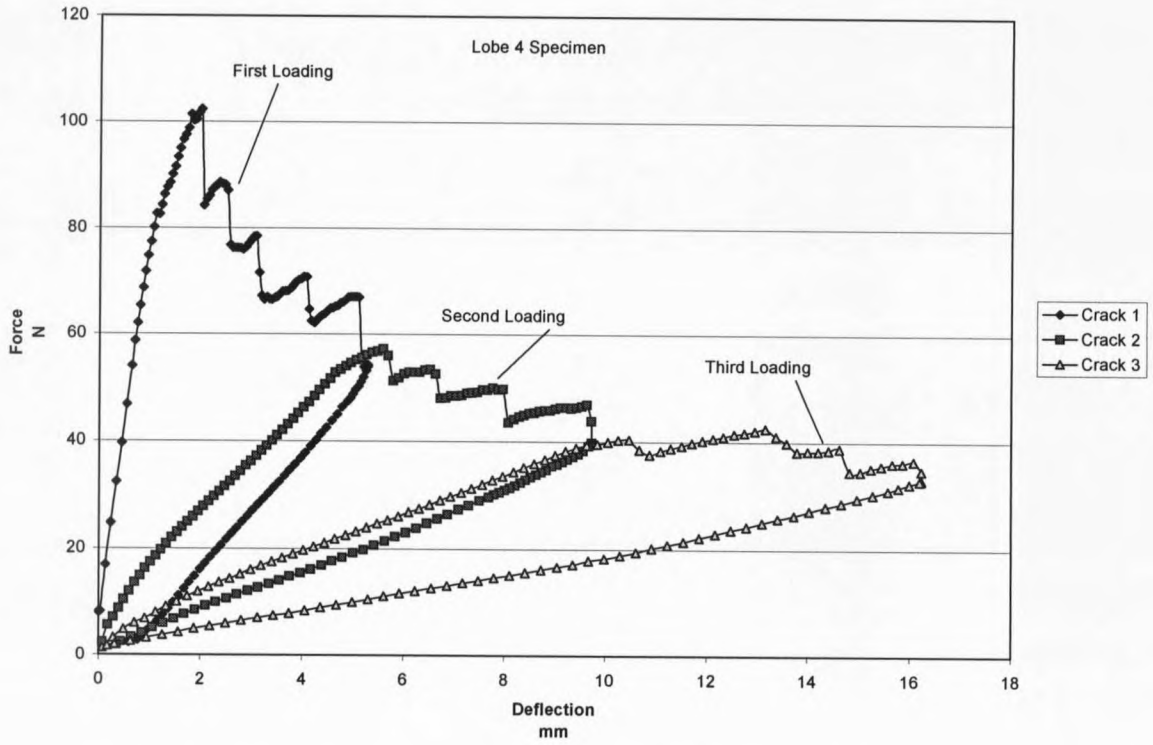


Figure 5.8 Three Successive Loading Cases for Lobe 4 Material

A closed form solution based on compliance relationships was also developed that can be used to determine G_{Ic}. It was also shown that the modified beam theory equation is valid for asymmetric sandwich panels.

Mode II Testing

In addition to Mode I type peel testing and flatwise tensile testing, Mode II type fracture evaluation was also desired. The main difference in this mode of crack propagation is the driving force. Mode I crack propagation is a function of direct separation of the face sheet from the core material. Mode II crack propagation is a result of shear stresses, and was induced from bending. As a result, the testing configuration varies. Mode II tests were conducted in three point bending fashion. Two rollers provide support while a loading nose provides the driving force to induce in plane fracture [Carlsson (1986) and Carlsson (1991)]. The actual testing fixture and machine used are shown in Figure 5.9. Loading tabs were used to distribute loading and reaction forces. When this was not done, compression crushing of core material was experienced.

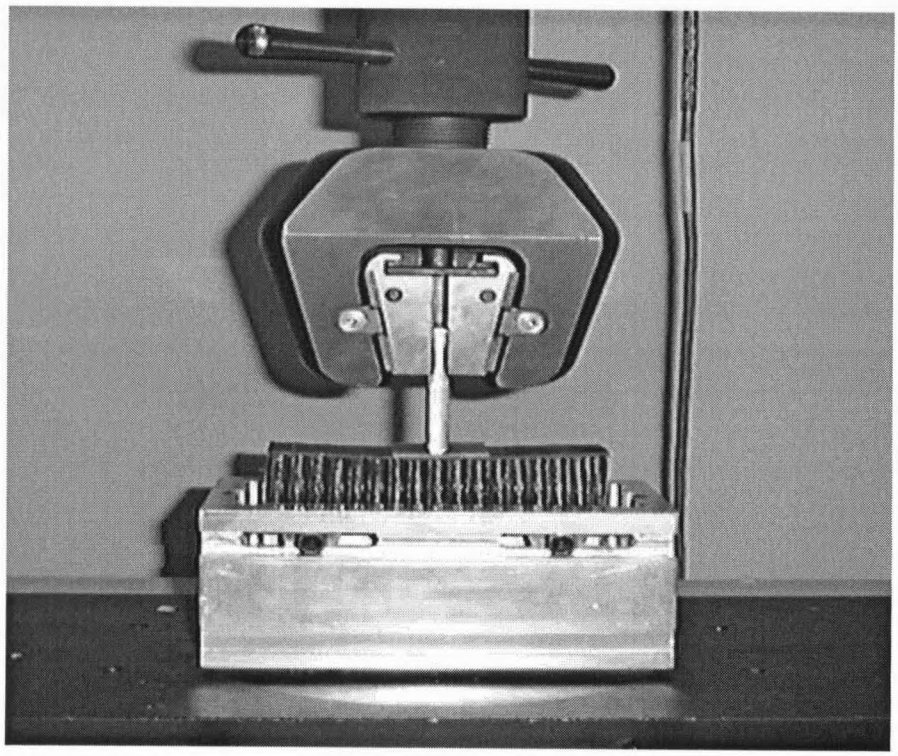


Figure 5.9 Mode II Testing Apparatus In Progress

Testing Procedure

The specimens were loaded in a 3 point bending configuration at a rate of about 0.8 mm/minute. Load and cross-head displacement were sampled by means of Labview data acquisition. When sharp cracking was heard, or when the load suddenly decreased, the specimen was unloaded. Testing in this fashion allowed hysteretic behavior to be captured. Crack growth was measured by means of visual inspection and calipers. Repeat testing was rarely made on mode II specimens. The crack typically propagated to at least the mid-span, and only core crushing would result from further testing. For valid G_{II} tests, crack propagation must be the primary failure mode. If various modes of failure are present, then the energy measured corresponds to crushing, crack propagation, and bending failure.

Data Reduction Methods

Data reduction for Mode II tests are the same as for Mode I. A variety of beam-theory type equations exist [Cairns (1992) and Carlsson (1991)]. However, these usually apply to a material with a crack in the center. The area method described before was used instead. The area method is dependable as long as the damage region is known. The graphical output differs from Mode I and is illustrated in Figure 5.10. The sharp drop shown above was a result of a sudden increase in compliance, as a consequence of crack growth. Hysteresis was not always captured for the Mode II tests. The specimen would begin to load after the crack has propagated and arrested. This occurred because the specimen was tested in displacement control. These data points were disregarded because they were not related to crack growth.

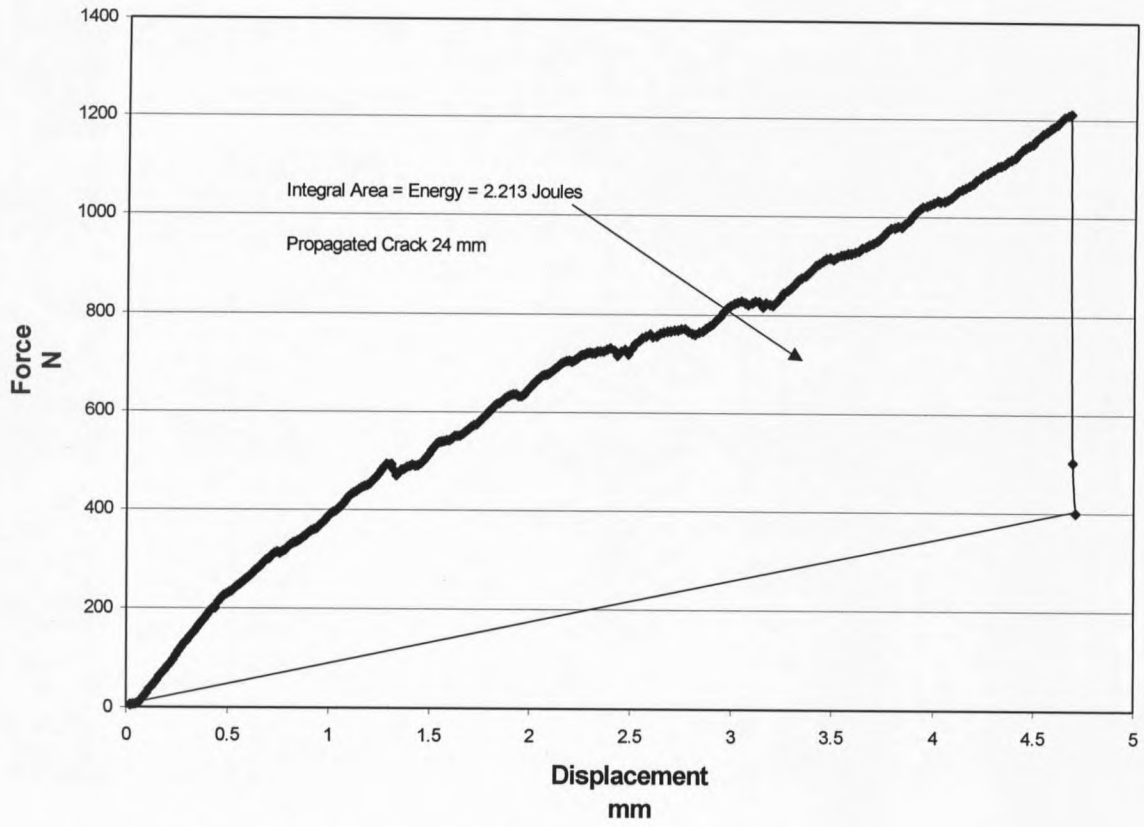


Figure 5.10 Mode II Test Results of Lobe 4 Material

A straight line is assumed back to the origin instead of recording hysteresis. Figure 5.10 is typical Mode II behavior, but not all specimens behaved in this fashion. Many of the Mode II tests conducted yielded results similar to Mode I as far as graphical load versus deflection output. A more representative graph is shown in Figure 5.11.

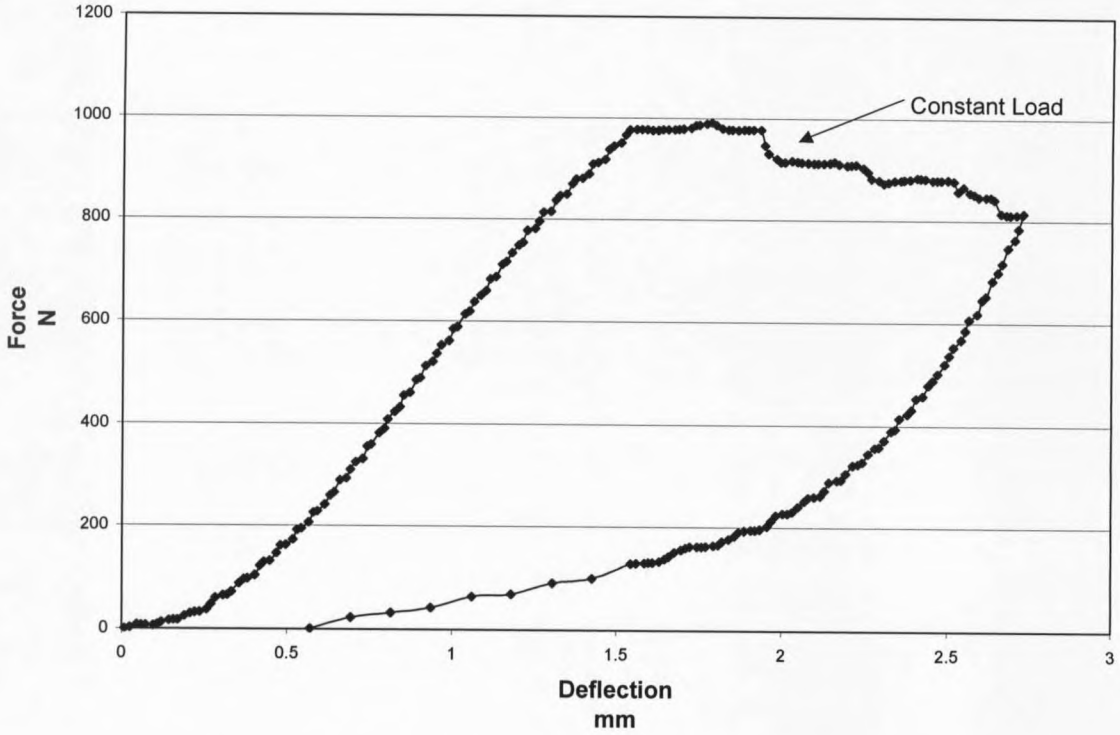


Figure 5.11 Mode II Test Showing Constant Loading During Crack Growth

Except for the first test case, hysteresis was always recorded. It is an interesting note that only the first test case behaved as shown in Figure 5.10. Subsequent tests behaved either like Figure 5.11, or as combinations of both.

Flatwise Compression Testing

Flatwise compression tests were also conducted on recycled specimens [ASTM C 365-94 (1997)]. Usually, the Mode I specimens would have about 50mm of virgin material left after three to four crack propagations. Due to excess bending of the face sheets only four cracks could be obtained for the Mode I specimens. The remaining untested material was sectioned from the Mode I specimens and used for compression testing. This testing was not originally requested, however, compressive strength and compressive modulus can be relevant properties [Astrom (1997)] depending on applied stresses.

Specimen Preparation

The compression specimens were cut to approximately 38 x 38mm squares. This size was chosen because these dimensions were used for flatwise tension. Additionally, these dimensions were the largest that would fit the compression fixtures of the Instron 4206. Once salvaged, they were then simply labeled and measured. They were carefully inspected to insure that no prior damage existed.

Testing Procedure

Special testing fixtures were used with the Instron 4206 machine for flatwise compression. Load and Displacement were sampled at a test rate of about 1.0 mm/minute. Testing was conducted in displacement control until the load peaked and the specimen collapsed. All data were recorded using Labview data acquisition. A representative graph of the test apparatus is shown in Figure 5.12.

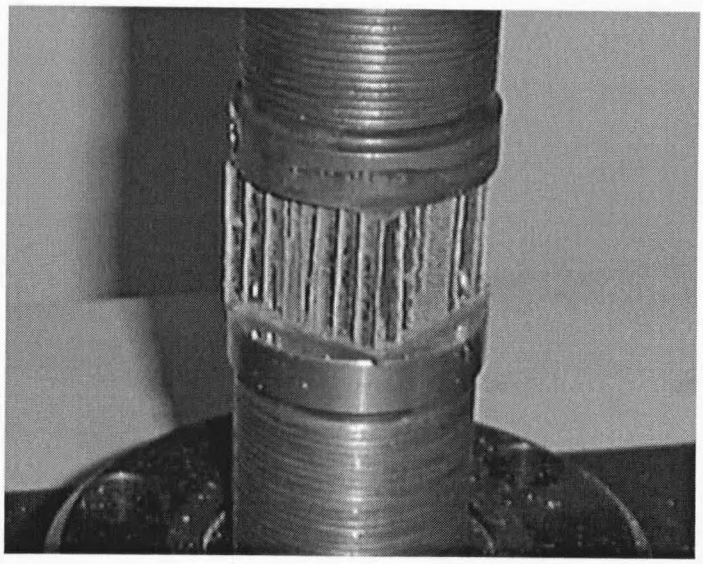


Figure 5.12 Compression Testing Configuration

Data Reduction Methods

The force and deflection output were handled in a similar fashion as flatwise tension. The stress was based on dividing loads by overall cross-sectional area (equation 5.1). As in the case of flatwise tension tests, the displacement read was assumed to be primarily the extension of the paper core. As a result, the strain was calculated based on the division of cross-head extension by the core thickness (equation 5.2). Compressive modulus as well as ultimate compressive strength were the key metrics gained from these tests.

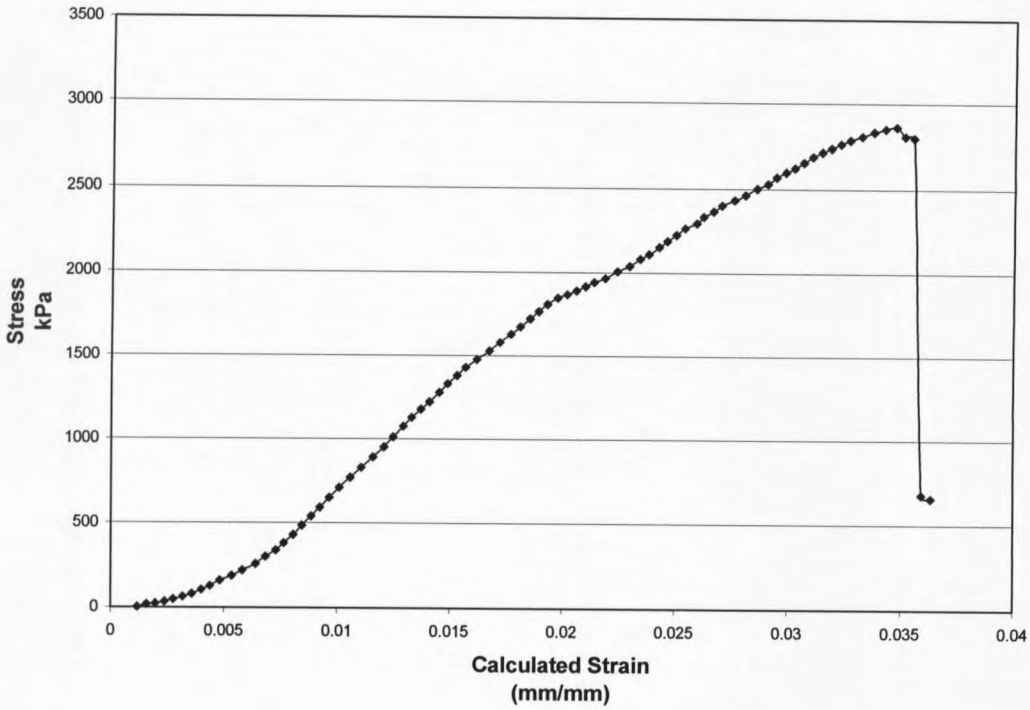


Figure 5.13 Typical Compression Test Result for Lobe 4

Experimental Results

Results were obtained for two different materials by four different test methods. Flatwise tension, Mode I peel-off tests, and compression tests were conducted on Lobe 1 and Lobe 4 material. Mode II shear induced peel tests were conducted on Lobe 4 material only, due to limited material.

Flatwise Tension Results

Tabular comparisons were made regarding flatwise tension samples. The ultimate tensile strength, modulus, percent strain at failure, and failure mode were compiled. Some statistical results were obtained. The mean and standard deviation are included in Table 5.2. Graphical behavior of the Lobe 1 material was shown in Figure 5.6.

Table 5. 2 Comparison of Flatwise Tensile Tests for Lobe 1

	Ultimate Tensile Strength	Elastic Modulus	Strain to Failure	Failure Mode
	kPa	MPa	%	
L1-FWT-1	2861	170	1.89	Failure at midplane of core
L1-FWT-2	3241	162	2.21	Failure at midplane of core
L1-FWT-3	2710	148	2.04	Failure in core at adhesive interface
L1-FWT-4	2979	157	2.79	Failure in core at adhesive interface
L1-FWT-5	2786	151	2.36	Failure in core at adhesive interface
Average	2915	158	2.26	
Standard Deviation	207	9	0.35	

Lobe 4 material was tested in the same fashion as Lobe 1. Figure 5.14 is a representative graph of Lobe 4 material. The modulus and strain at failure are similar to the Lobe 1 material, but the ultimate tensile strength was much lower. The failure mode was also different than the Lobe 1 material. The Lobe 4 material failed at the adhesive boundaries in all cases. A comparison of the two failure modes is shown in Figure 5.15 below. Lobe 4 usually failed at the adhesive layer, while Lobe 1 failed in the paper core.

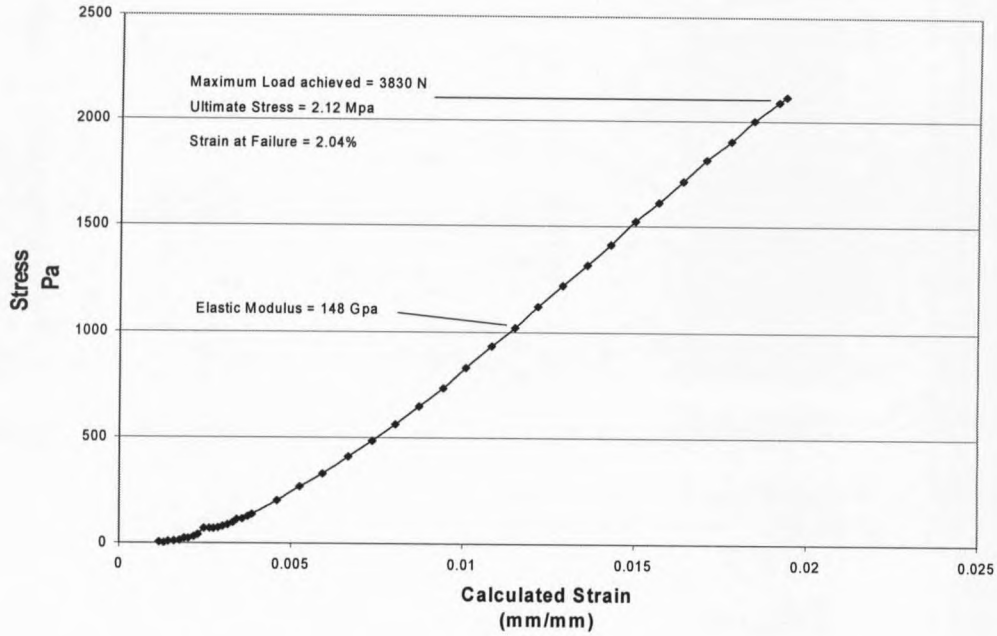


Figure 5.14 Typical Behavior of Lobe 4 Material in Flatwise Tension

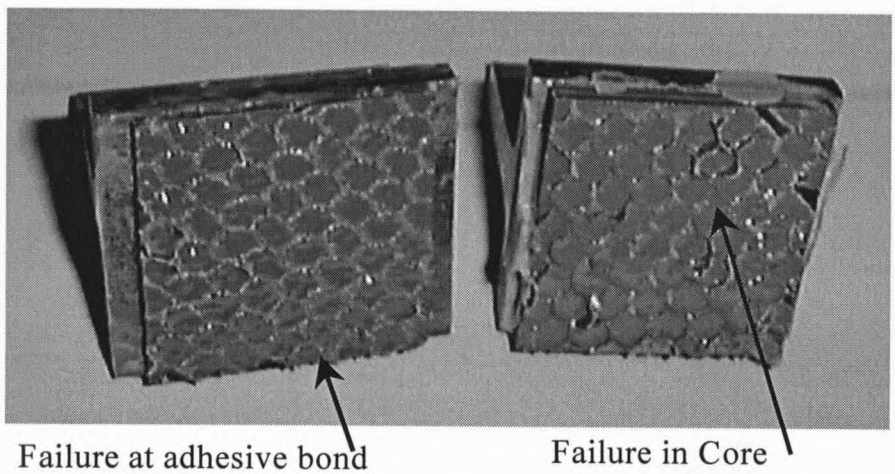


Figure 5.15 Comparison of Failure Modes of Lobe 4 to Lobe 1

Six specimens were tested for Lobe 4 material and data summaries are included in Table 5.3. The same quantities are displayed as before, however, some noticeably different results were obtained. The average ultimate tensile strength was over 830 MPa

lower than Lobe 1. The modulus and strain at failure were slightly lower. The ultimate tensile strength had more deviation but the strain to failure and moduli were more consistent.

Table 5.3 Summary of Lobe 4 Transverse or Flatwise Tension Tests

	Ultimate Tensile Strength	Elastic Modulus	Strain to Failure	Failure Mode
	kPa	MPa	%	
L4-FWT-C-1	2365	140	2.07	sudden even fracture at interface between core and adhesive layer
L4-FWT-C-3	2096	141	1.92	sudden even fracture at interface between core and adhesive layer
L4-FWT-C-4	2241	135	1.92	sudden even fracture at interface between core and adhesive layer
L4-FWT-C-5	2006	137	1.69	sudden even fracture at interface between core and adhesive layer
L4-FWT-C-6	1662	136	1.44	sudden even fracture at interface between core and adhesive layer
L4-FWT-C-7	1965	136	1.73	sudden even fracture at interface between core and adhesive layer
Average	2056	137	1.80	
Standard Deviation	244	2	0.22	

Discussion of Flatwise Tension Results

The most noted difference was the fact that the ultimate tensile strength was significantly lower and the failure mode was different. Clearly, the Lobe 4 material had some problems with bonding at the adhesive interface where failure occurred. This caused the reduced tensile strengths as well. The only added difference not present for Lobe 1 is the fact that Lobe 4 material possessed some curvature. The Lobe 1 material was relatively flat. Conversely, Lobe 4 specimens had visible curvature at a specimen size of 38 x 38mm.

Mode I Results

Mode I tests were conducted as outlined previously. Both Lobe 1 and Lobe 4 materials were asymmetric in nature. This was due to the fact that one face sheet had different thickness from opposite side. It was suspected and observed that the results would vary based on the thickness of material adjacent to the crack. As a result, pre-cracks were initiated on either the thick or the thin side before testing. Typically, G_I values for cracks initiated on the thin side were higher than samples with cracks on the thick side for Lobe 4 and Lobe 1 material. G_I values were compared separately for each lobe based on crack location. A sample depiction of Mode I test data of Lobe 1 is shown below in Figure 5.16.

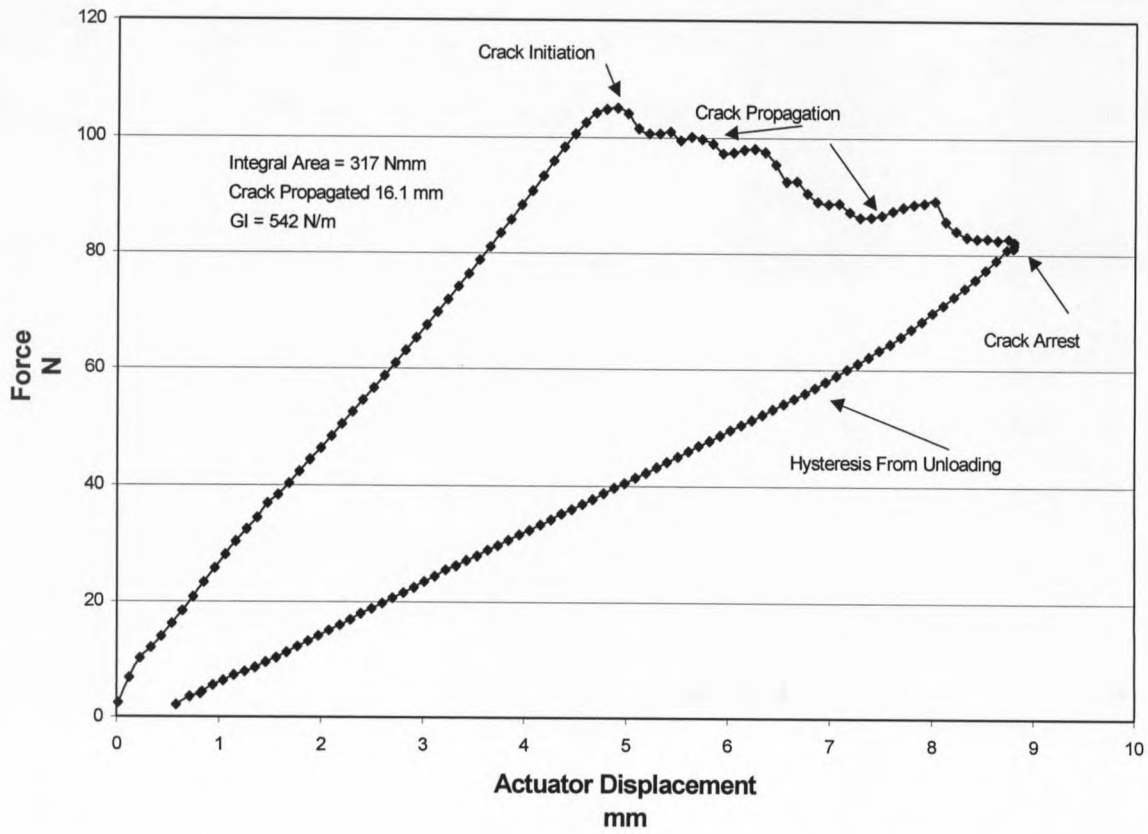


Figure 5.16 Peel-off Test Results for Lobe 1 Material L1-DCB-4

The results above are from a test where the crack was initiated on the thin side. These results are from the propagation of the second crack. Typically, the data from the first crack propagation was thought to be non-conservative. The initial crack medium was most likely a more tortuous path than what would be typical. However, all subsequent cracks were assumed to follow the path that provided the least crack resistance. The secondary cracks are more likely to possess a more realistic crack tip, as opposed to the initial pre-crack. All data for each crack session were recorded but some crack 1 data were not included in average. The variance of the data was reduced when these values were discarded. The data also maintained its identity regarding whether the crack was initiated on the thin side or the thick side. Energy absorbed, initial crack length, final crack length, and G_I values are displayed in Table 5.4. Average G_I and standard deviation for both crack conditions are tabulated as well.

Table 5.4 Summary of Lobe 1 (L1) Mode I (DCB) Test Results

	energy	width	crack final	crack initial	G1eq	crack
	N*m	mm	mm	mm	N/m	location
* L1-DCB-1 crack 1	0.24	37.1	70.8	42.1	**229**	Thin
L1-DCB-1 crack 2	0.56	37.1	86.0	70.8	**997**	Thin
* L1-DCB-2 crack 1	0.42	37.1	58.0	39.7	**623**	Thick
L1-DCB-2 crack 2	0.42	37.1	72.7	58.0	**771**	Thick
	0.00	0.0	0.0	0.0		
* L1-DCB-3 crack 1	0.97	37.1	72.1	44.4	**947**	Thick
* L1-DCB-4 crack 1	0.23	36.4	43.0	36.2	**913**	Thin
L1-DCB-4 crack 2	0.32	36.4	59.1	43.0	**542**	Thin
L1-DCB-4 crack 3	0.30	36.4	74.2	59.1	**536**	Thin
L1-DCB-4 crack 4	0.38	36.4	90.4	74.2	**644**	Thin
L1-DCB-5 crack 2	0.52	37.0	50.8	37.5	**1064**	Thick
L1-DCB-5 crack 3	0.61	37.0	65.5	50.8	**1113**	Thick
L1-DCB-5 crack 4	0.36	37.0	76.5	65.5	**879**	Thick
L1-DCB-5 crack 5	0.47	37.0	99.6	76.5	**544**	Thick
L1-DCB-6 crack 2	0.41	37.5	63.2	49.6	**797**	Thin
L1-DCB-6 crack 3	0.66	37.5	88.2	63.2	**707**	Thin

Lobe 1 Thick side	Lobe 1 Thin side
Averate GI = 685 N/m	Average GI = 704 N/m
Standard Deviation = 150 N/m	Standard Deviation = 173 N/m

Note * denotes blunt crack fronts. This data not included in average

The Lobe 1 thin side G_I was slightly larger than the Lobe 1 thick side. Cracks initiated on the thicker side always progressed towards the thinner side for the Lobe 1 material. Usually, the crack would follow a 45 degree path until the crack front reached the thin side. The crack would continue to propagate in the core material parallel to the face sheet until testing ceased. For the cases when the crack was induced on the thick side, the entire crack length was estimated by following the actual curved path. A specimen exhibiting the aforementioned lobe 1 phenomenon is shown in Figure 5.17.

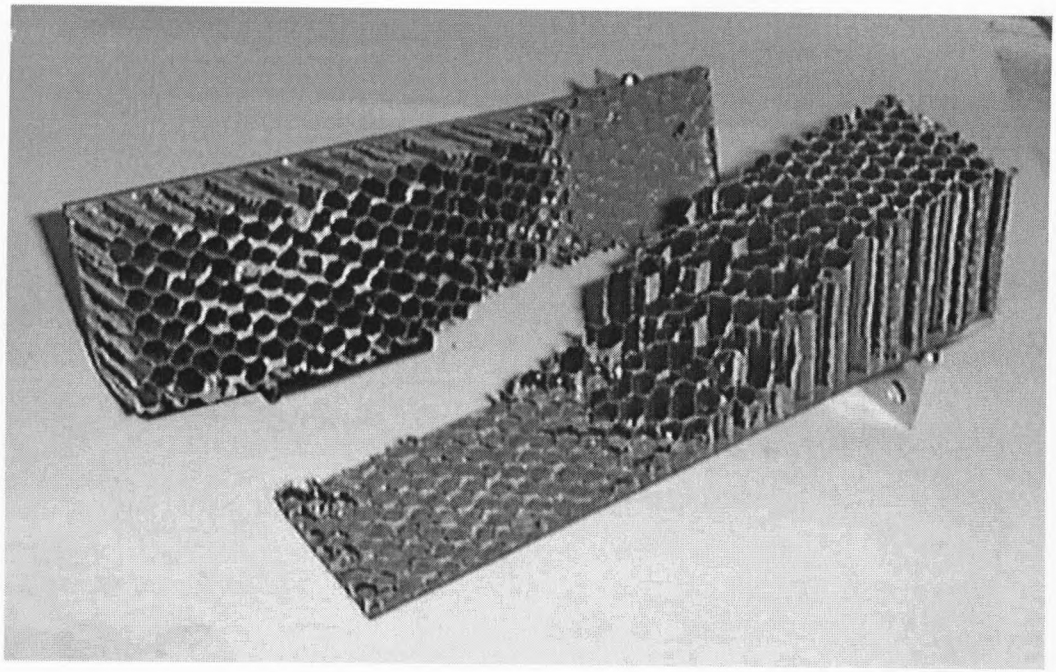


Figure 5.17 Lobe 1 Material Specimen Core Shear Failure

Cracks that were initiated on the thin side stayed on the thin side and propagated in the core paper parallel to the face sheet near the adhesive layer. All Lobe 1, Mode I fractures were in the core material, not at the adhesive layer. This is similar to the flatwise tensile failure mode of the Lobe 1 material. A typical failure of Lobe 4 material is shown in Figure 5.18.

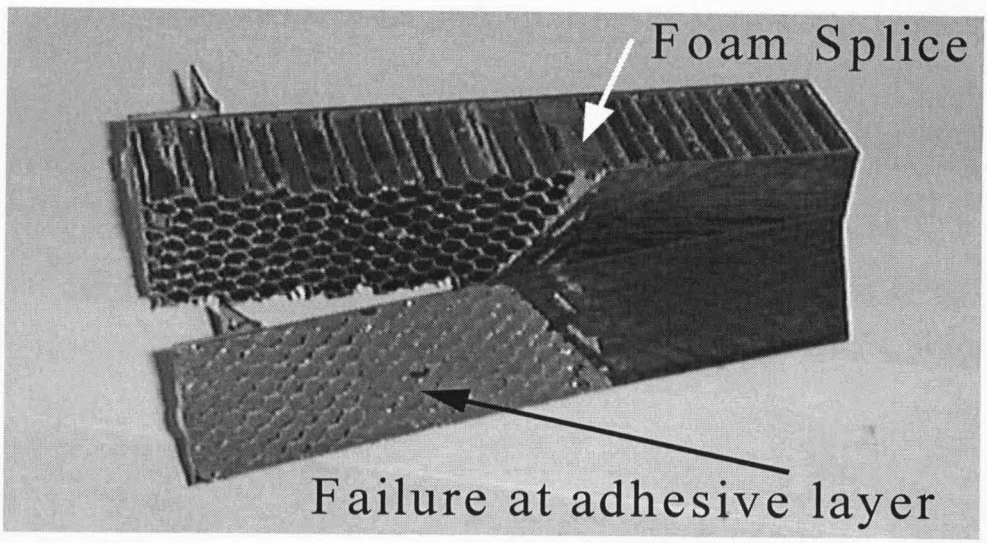


Figure 5.18 Failure Mode of Lobe 4 Material

Lobe 4 material was tested in the same manner. The failure mode was always at the core/adhesive layer interface. The cracks propagated parallel to the face sheet in all cases. The Mode I values were considerably less for Lobe 4 than Lobe 1. Test results are shown in Table 5.5 for Lobe 4 below.

Table 5.5 Mode I Results for Lobe 4

		energy	width	crack final	crack initial	G1eq	Crack
		N*m	mm	mm	mm	N/m	location
*	L4-DCB-1-C crack 1	0.185	37.2	46.7	35.2	**432**	Thick
	L4-DCB-1-C crack 2	0.201	37.2	75.0	46.7	**191**	Thick
	L4-DCB-1-C crack 3	0.257	37.2	111.6	75.0	**188**	Thick
*	L4-DCB2-C crack 1	0.196	36.1	46.0	39.4	**823**	Thick
	L4-DCB2-C crack 2	0.230	36.1	75.8	46.0	**214**	Thick
	L4-DCB2-C crack 3	0.216	36.1	96.4	75.8	**292**	Thick
*	L4-DCB4-C crack 1	0.266	36.0	46.5	35.1	**645**	Thin
	L4-DCB4-C crack 2	0.402	36.0	71.1	46.5	**454**	Thin
	L4-DCB4-C crack 3	0.332	36.0	88.2	71.1	**538**	Thin
*	L4-DCB-7-C crack 1	0.246	36.2	54.9	37.6	**393**	Thick
	L4-DCB-7-C crack 2	0.205	36.2	75.3	54.9	**277**	Thick
	L4-DCB-7-C crack 3	0.211	36.2	93.5	75.3	**320**	Thick
*	L4-DCB-8-C crack 1	0.218	36.5	48.4	35.7	**473**	Thick
	L4-DCB-8-C crack 2	0.207	36.5	68.6	48.4	**279**	Thick
	L4-DCB-8-C crack 3	0.201	36.5	91.4	68.6	**241**	Thick
	L4-DCB-8-C crack 4	0.108	36.5	100.1	91.4	**343**	Thick
	L4-DCB-8-C crack 5	0.150	36.5	114.0	100.1	**294**	Thick
	L4-DCB-9-C crack 1	0.182	36.0	51.1	30.5	**245**	Thick
	L4-DCB-9-C crack 2	0.337	36.0	78.3	51.1	**343**	Thick
	L4-DCB-9-C crack 3	0.206	36.0	97.2	78.3	**303**	Thick
Panel 2	L4-P2-DCB-1 crack 1	0.289	37.6	63.2	42.2	**366**	Thin
Panel 2	L4-P2-DCB-1 crack 2	0.163	37.6	73.2	63.2	**432**	Thin
Panel 2	L4-P2-DCB-2 crack 1	0.267	37.0	63.5	34.2	**246**	Thick
Panel 2	L4-P2-DCB-2 crack 2	0.312	37.0	89.5	63.5	**324**	Thick
Panel 2	L4-P2-DCB-2 crack 3	0.364	37.0	116.8	89.5	**360**	Thick
Panel 2	L4-P2-DCB-3 crack 1	0.247	37.6	49.4	30.9	**356**	Thin
Panel 2	L4-P2-DCB-3 crack 2	0.490	37.6	80.4	49.4	**421**	Thin
Panel 2	L4-P2-DCB-3 crack 3	0.331	37.6	110.2	80.4	**295**	Thin
Panel 2	L4-P2-DCB-4 crack 1	0.243	37.6	51.9	38.6	**487**	Thin
Panel 2	L4-P2-DCB-4 crack 2	0.490	37.6	86.6	51.9	**376**	Thin
Panel 2	L4-P2-DCB-4 crack 3	0.479	37.6	109.4	86.6	**560**	Thin

Note * denotes blunt crack fronts. This data not included in average

Lobe 4 Thick side	
Average GI	**278 N/m**
Standard Deviation	**54 N/m**

Lobe 4 Thin side	
Average GI	**429 N/m**
Standard Deviation	**84 N/m**

Mode II Results

Due to the limited supply of Lobe 1 material, Mode II tests were only conducted on Lobe 4 material. Tests were conducted with the initial crack either adjacent to the thin or the thick face sheet, based on Mode I test results. As for Mode I, the G_{II} values were larger for the thin side than for the thick side. Tabulated results of all testing conducted are shown in Table 5.6.

Table 5.6 Mode II Results for Lobe 4

	Energy	width	crack final	crack initial	GII	crack
	N*m	mm	mm	mm	N/m	location
L4-P1-MII-1 crack 1	2.18	36.5	61.7	38.1	2530	Thick
L4-P2-MII-1 crack 1	1.97	37.4	64.5	52.1	4226	Thin
L4-P2-MII-2 crack 1	0.51	37.5	45.2	33.3	1137	Thick
L4-P2-MII-2 crack 2	1.69	37.5	79.0	45.2	1340	Thick
L4-P2-MII-4 crack 1	1.27	37.6	56.9	49.3	4404	Thick
L4-P2-MII-4 crack 2	1.00	37.6	74.9	56.9	1487	Thick
L4-P2-MII-5 crack 1	3.71	37.3	70.3	33.3	2687	Thick
L4-P2-MII-6 crack 1	3.72	37.7	57.7	32.6	3933	Thin
L4-MII-7-T crack 1	0.46	37.6	55.9	51.3	2623	Thin
L4-MII-8-F crack 1	2.03	37.4	76.5	48.5	1941	Thick
L4-MII-9-F crack 1	1.81	37.8	74.7	34.7	1199	Thick

Mode II Fracture Toughness of All Lobe 4 = 2503 N/m

Mode II Fracture Toughness of Thick side only = 2083 N/m

Mode II Fracture Toughness of Thin side only = 3588 N/m

Discussion of Mode II Results

When only small cracks were grown, a second crack propagation was attempted. Occasionally, the results from these tests were much larger than for the first. The results of the repeated crack attempts were less representative than the results from the original crack session. This case is exactly opposite of Mode I. In Mode I the first crack can be the least representative, because the initial crack is too blunt or not in path of least resistance. For the case of Mode II it was very important to ensure that the initial crack was not blunt, and was following the path of least resistance. As a result, the first attempt at Mode II delamination had to be perfect. This is because subsequent attempts of crack propagation typically induced multiple modes of damage other than delamination. When a material is subjected to multiple modes of failure; the energy absorbed becomes very large and is not uniquely related to Mode II delamination. This would indicate a much larger G_{II} value than the material actually possessed.

The average Mode II strain energy release rate for Lobe 4 when the crack was induced on the thin side was 3590 N/m, and only 2083 N/m for the thick side. The thick side G_{II} was about 58 % of the thin side G_{II}. This is similar to the Mode I results. The standard deviation for Mode II was 850 N/m and 1100 N/m for thin and thick respectively. Despite the large deviation in the results, one point can be made. It is most likely that the Lobe 4 material would not fail from Mode II fracture. The G_{II} value was approximately eight times larger that the G_I value for each crack configuration. This indicates that the ability of the material to resist Mode II delamination is approximately eight times greater than its ability to resist Mode I fracture. If significant bending stresses

were applied, Mode II could become more dominant. The dominating mode of failure relates to the type of loading as well as crack resistance in each mode. However, based on static flexure tests conducted [ASTM C 393-94 (1997)], the Lobe 4 material would most likely not fail from transverse stresses and exhibit Mode II fracture if loaded in a bending configuration. Essentially, the Mode II fracture toughness is probably low enough that the stresses or energy required to propagate a crack would not exceed the crushing threshold of the material. Load pads were used on Mode II specimens as a precaution regardless. There is some evidence that would suggest that the Lobe 4 material may have enough transverse toughness to withstand energy levels capable of inducing Mode II fracture. However, G_I is much lower than G_{II}. A static flexure test of Lobe 4 compared with Mode II fracture test results is shown in Figure 5.19.

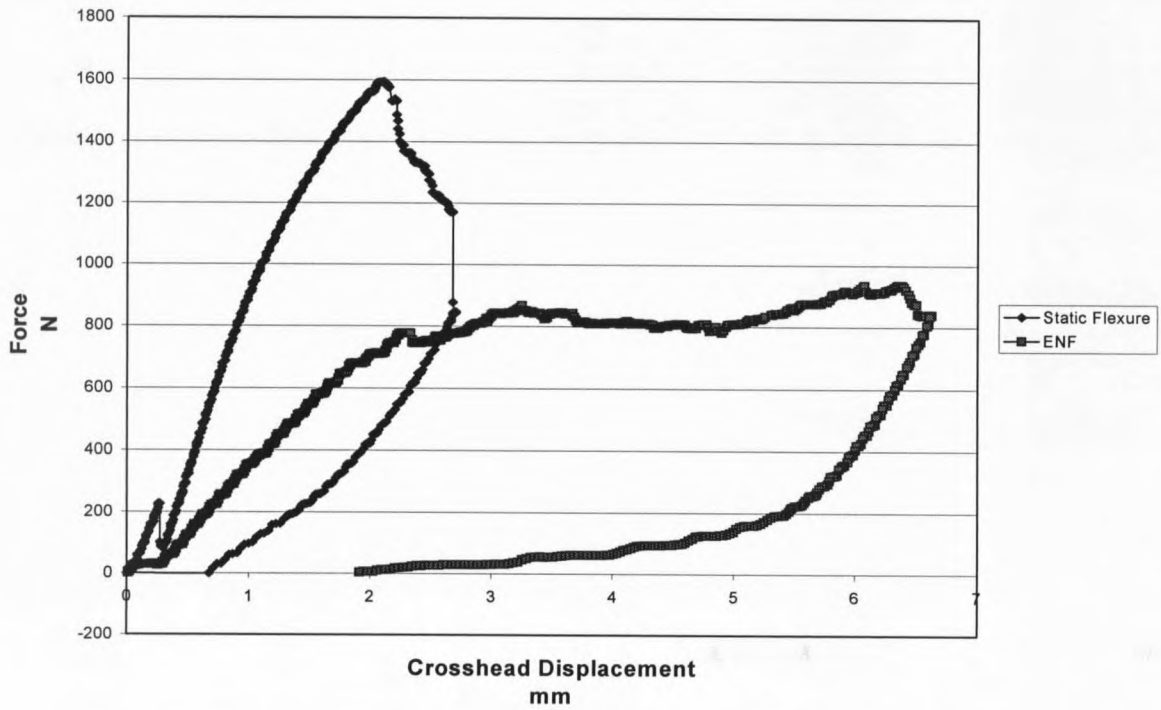


Figure 5.19 Comparison of Static Flexure and ENF Results for Lobe 4

Flatwise Compression Results

Flatwise compression tests were also performed as outlined previously. These results indicated that neither Lobe 1 or Lobe 4 material were equal in compression and tension. The compressive modulus was lower for compression than for tension. As expected, the compressive strength for Lobe 4 was larger than its tensile strength. Lobe 1 was opposite with a substantially lower compressive strength. Lobe 4 had approximately the same compressive strength as Lobe 1 (shown in Table 5.7). If compressive strength were to be required in addition to tensile strength for combined loading cases, Lobe 4's significantly lower tensile strength may not be the limiting property. Three specimens were recycled from Mode I DCBs for Lobe 1 and used for compression testing. Two Lobe 4 specimens were recycled from panel 1 DCBs and 5 virgin specimens were also tested. Four virgin Lobe 4 specimens were also taken from panel 2 and tested. The results for these tests are shown in Table 7. The H/D quantity is the ratio of core thickness / approximate specimen width.

Discussion of Flatwise Compression Results

The low compression strength of Lobe 1 could be related to the fact that Lobe 1 was thicker than Lobe 4. Having a larger H/D ratio could have caused lower core buckling loads to occur. Conversely Lobe 4's performance may be due to its lower H/D ratio. The compressive failure was most likely simultaneous buckling of cell walls and was core thickness dependent.

The recycled specimens were probably not affected by the recycling process, since no damage was present in these regions. Two of Lobe 4's better data points regarding modulus and compressive strength are from recycled specimens. These

compression test results could be substantiated with tests conducted on larger cross-section specimens. It is the opinion of the author that these are valid data points and should be considered for the X33 structural analysis.

Table 5.7 Summary of Compression Test Results for Lobe 1 and Lobe 4

	Modulus E	Compressive Strength	H/D	
Material I.D.	MPa	kPa	m/m	
L1-P1-1-R-DCB-3	119	2440	1	Lobe 1
L1-P1-2-R-DCB-4	128	2268	1	Lobe 1
L1-P1-3-R-DCB-6	118	1854	1	Lobe 1
L4-P1-1	125	2654	0.82	Lobe 4
L4-P1-2	112	2523	0.82	Lobe 4
L4-P1-3	120	2647	0.82	Lobe 4
L4-P1-4	132	2675	0.82	Lobe 4
L4-P1-5 *	124	4192	0.82	Lobe 4
L4-P1-6-R-DCB-8	137	2895	0.82	Lobe 4
L4-P1-7-R-DCB-5	134	2689	0.82	Lobe 4
L4-P2-1	123	2634	0.82	Lobe 4
L4-P2-2	128	2668	0.82	Lobe 4
L4-P2-3	125	2861	0.82	Lobe 4

* represents a specimen that contained foam core splice material, not included in average compressive strength

Average Lobe 1 2185 kPa	Standard Deviation 301 kPa
Average Lobe 4 2696 kPa	Standard Deviation 115 kPa

Numerical Analysis of Honeycomb Fuel Tank Investigation

Motivation

Experimental evaluations of strength and fracture toughness performance were conducted. Due to the complexity of the honeycomb material some verification of the experimental findings was needed. In addition to experimental verification, some validation of the testing techniques was also needed. ASTM standards were followed closely, however the awkward nature of the sandwich construction required some degree of originality with regard to testing methodology.

FEA simulations were constructed for the flat-wise tension, mode I, and mode II testing specimens. Again these simulations were developed to confirm the experimental data reduction and to insure that the testing methodologies were reasonable. Each of these models is addressed individually and compared to experimental findings.

Flatwise Tension

Special care was taken when preparing the flatwise tension specimens. The tabs that were attached were carefully aligned with the aid of a glue fixture to minimize any bending stress. Eccentric loading would produce a combined stress state and simple stress equations would provide conservative but errant results. It is virtually impossible to guarantee exact alignment of loading and very difficult to even measure misalignment. Instead a FE model of the flatwise tension FWT sample was constructed to evaluate the effects of misalignment on the tensile stress state.

Approach

A near replica model was built to represent a FWT test specimen. The model included the tab fixtures, and was solved with the fixtures located in several configurations to estimate the stresses caused by known loading. The model provided a quantitative assessment of the effects of misalignment and was used to confirm experimental results.

Model

A 2-D model was used to represent the FWT specimen. Both the upper and lower tab fixtures were included as well as the face sheet and core regions. Each face sheet region, core, and tab regions were represented by areas. These areas were meshed with Plane82 8 noded elements. Both plane stress and plane strain loading conditions were evaluated. Symmetry was not used to any advantage.

Standard constitutive properties were used for the steel tabs. The modulus for the core material was taken from the experiment, and a Poisson's ratio of 0.3 was assumed. The transverse properties of the face sheet material were not known. The flexural modulus was obtained experimentally for other models and provided a means for estimation. A range of values was used for the transverse modulus of the face sheet material to insure the results produced were not sensitive to this property.

A single node at the bottom center of the lower tab was restricted from horizontal and vertical movement but allowed rotation. This was consistent with the actual experimental apparatus. The failing load was applied to the top center node of the upper

tab. Horizontal displacement was also restricted at this node for stability purposes. A fully meshed and constrained FWT model is shown in Figure 5.20.

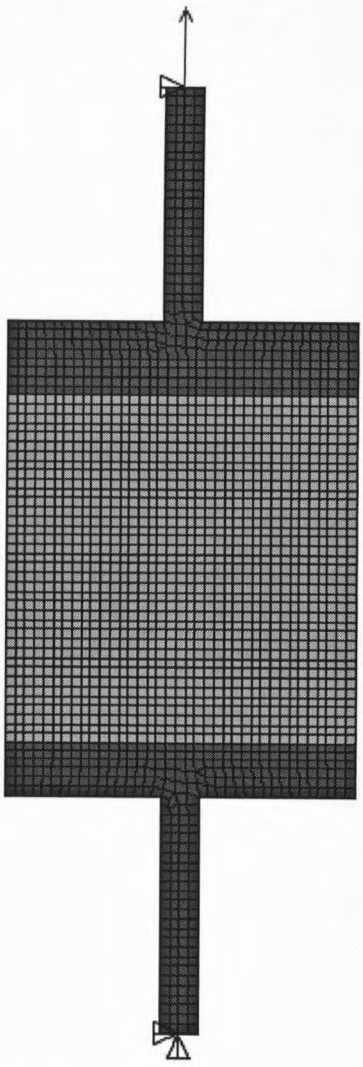


Figure 5.20 Flatwise (Transverse) Tension Model

Results

The model was solved for various alignment cases. The baseline case was perfect alignment. This case was used to confirm solution convergence and mesh refinement.

Both plane stress and plane strain scenarios were applied to the baseline case. Generally plane strain provides conservative results or predicts larger stresses than plane stress for this configuration. Additionally transverse stiffness properties were varied to insure that the estimated values would not corrupt the solution.

Solution and Mesh Convergence

Stress (in the y direction) was plotted for the entire FWT sample and for the core region only (Figure 5.21). Stress singularities were present in the entire sample at material interfaces due to change in stiffness. Stress concentrations were also noticed at edge of the isolated core material.

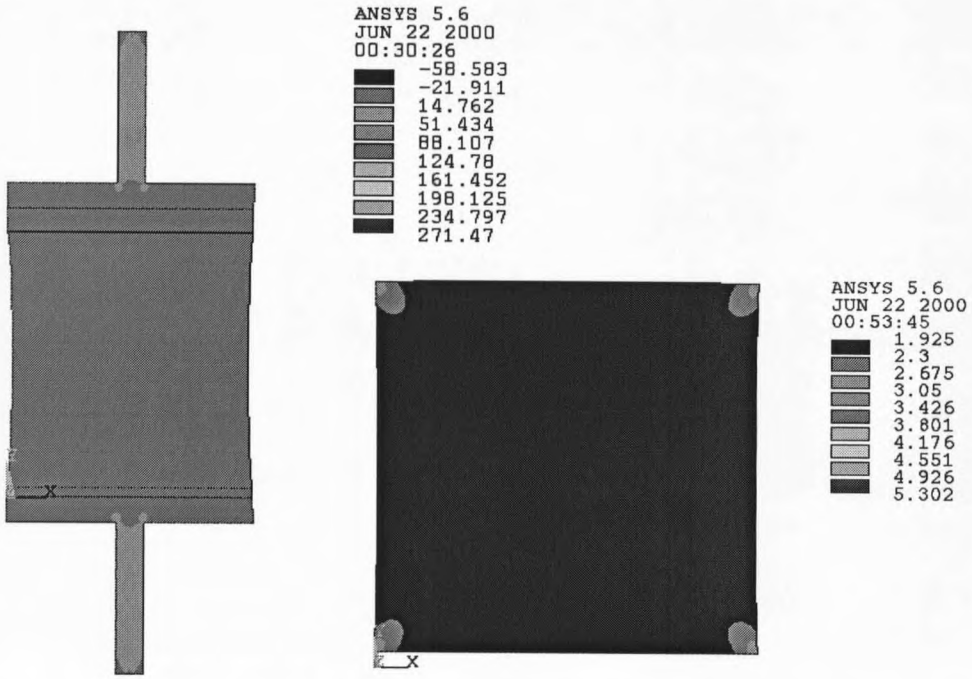


Figure 5.21 FWT Stress Distribution with Core Close-up

The primary regions of interest were at the facesheet/core interface and in the core itself. As a result stress profiles were obtained at these regions.

The baseline case was solved for three different mesh sizes. The stress contour plots of each refinement are shown in Figure 5.34. Similar solutions resulted for each mesh size, but the most sensitive region was that near the edge. The stress was constant across the section except for a concentration near the edge. Also at smaller mesh sizes the curve smoothed and the transition from the isostress state to the concentration was less abrupt. The plane strain results were similar to the plane stress results, Figure 5.22. The primary difference was a larger concentration stress at the edge free edge boundary.

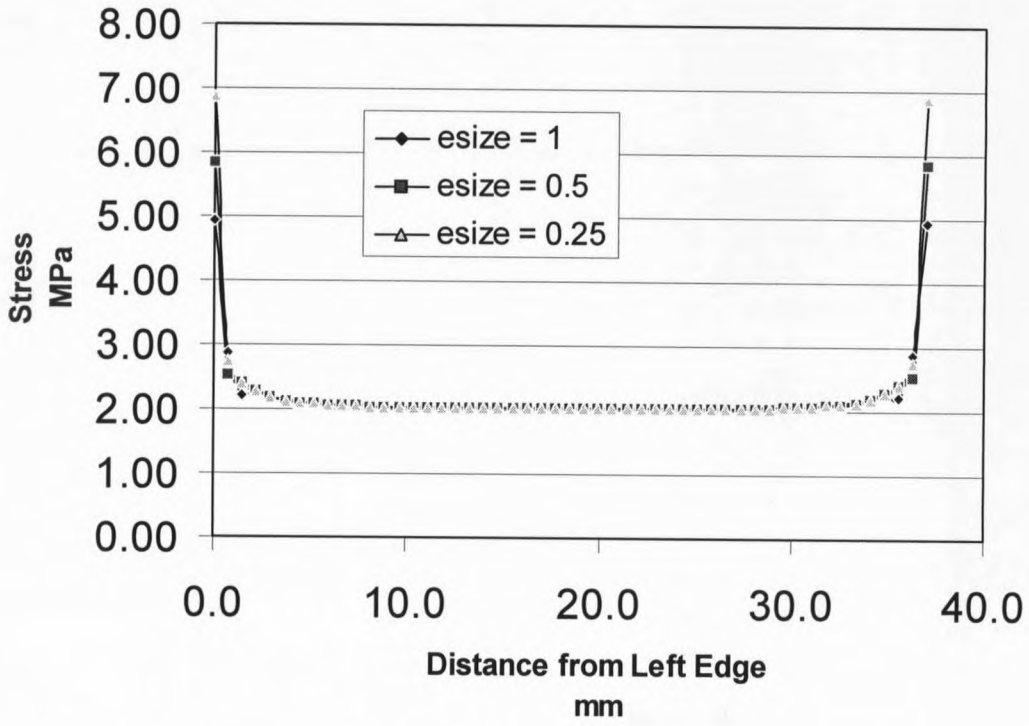


Figure 5.22 FWT Solution Convergence

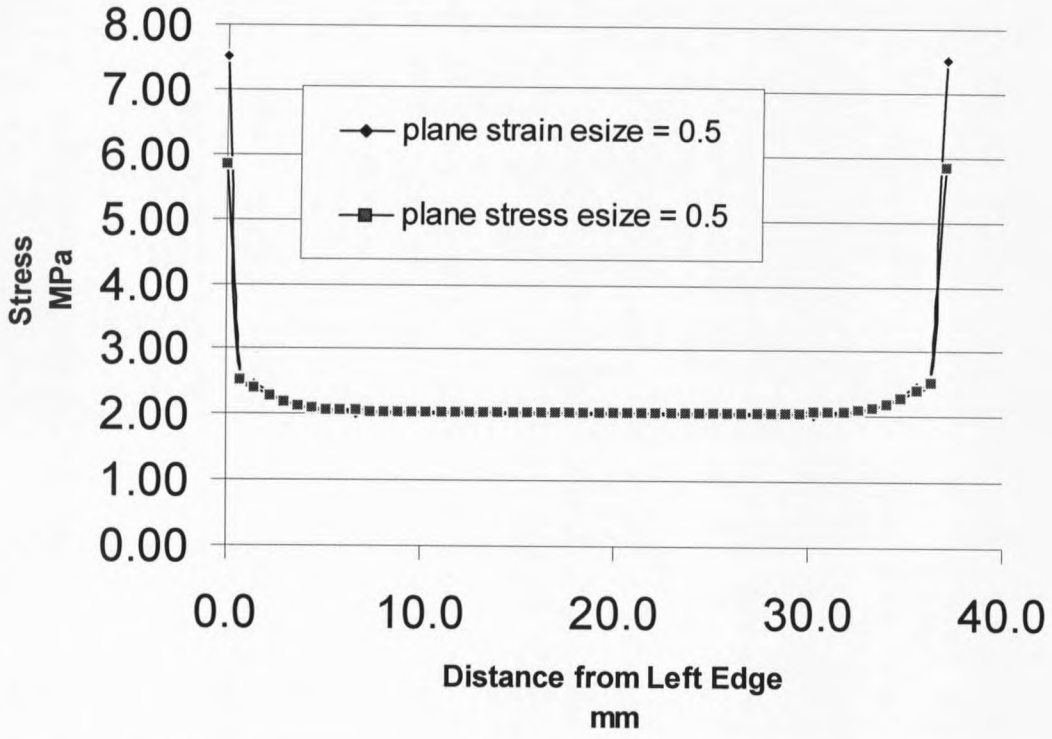


Figure 5.23 Plane Stress vs. Plane Strain

Once a credible solution was obtained with the baseline case, misalignment was evaluated at 1mm, 2mm and 4mm of offset. The stress at the boundary of the facesheet and the core material was used to generate a plot of stress vs. position across the section. The plots provided qualitative and quantitative results of the stress response as a function of misalignment.

The extreme stress concentrations at the boundary of the specimen in Figure 5.45 are related to free edge effects. These extremes were disregarded to produce the plot in Figure 5.24

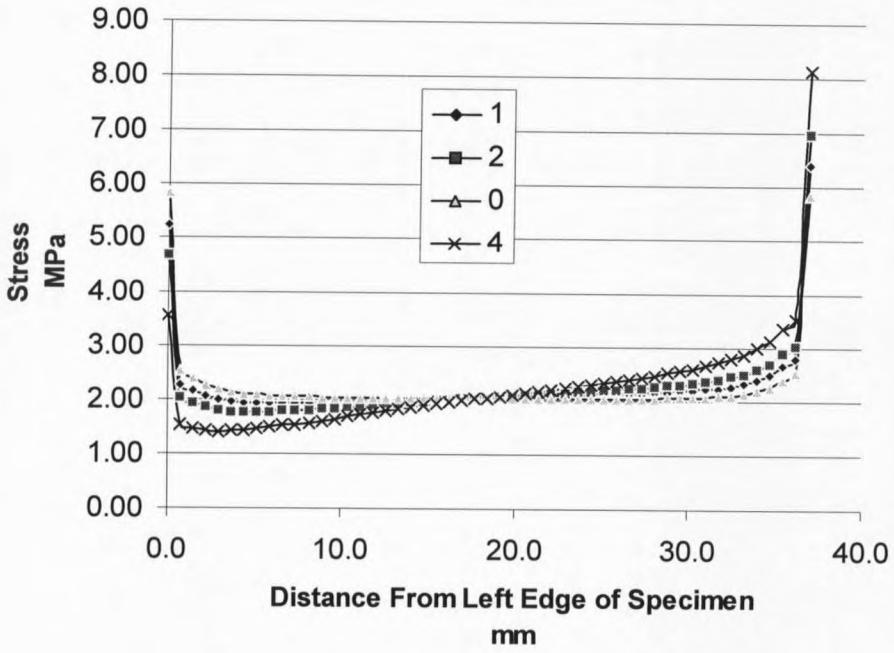


Figure 5.24 Stress Profile Based on Offset Distance

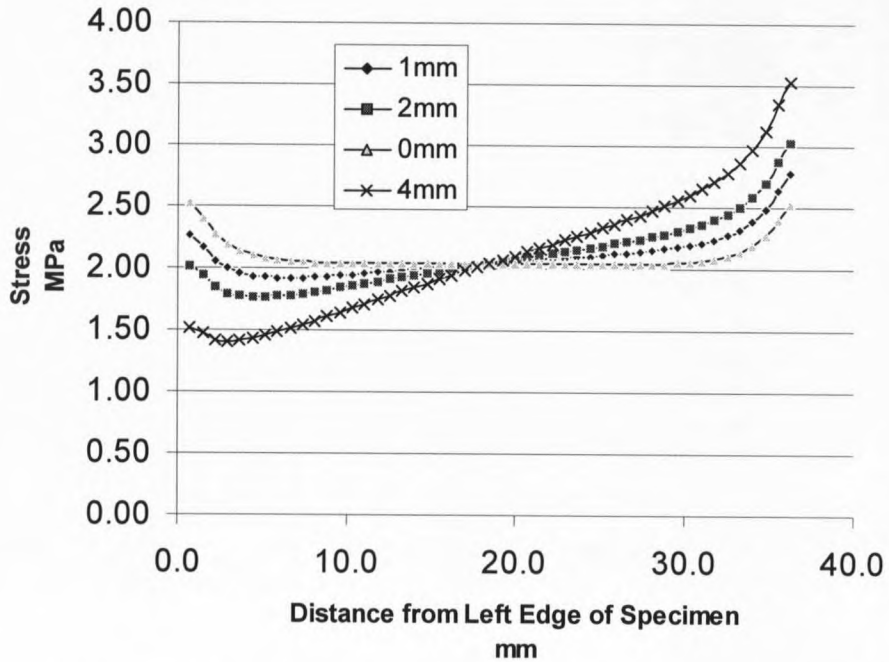


Figure 5.25 Stress Profile without Singularities

The FWT model suggests that the strength values predicted from the experimental data could be conservative by about 8 - 16%. This is assuming that the misalignment was less than 2mm from center.

Mode I

Due to the asymmetric and complex nature of the mode I test specimens, some confirmation of the experimental results was desired. The area method, modified beam equation and derived compliance equation were used to calculate experimental G_{Ic}. Variation in the results was present but not at unacceptable levels. The area method predicted larger G_{Ic} values than the modified beam method. This is common because generally more energy is required to propagate crack growth as the crack grows. Both of these methods predicted a larger G_{Ic} than the derived compliance equation. One explanation for this is that there could have been shear stress present during testing. Due to the specimen dimensions there was a likelihood that the DCB test specimens were not subjected to pure bending. If this were the case, mixed mode fracture may have been the cause of failure for the tested DCB's. The FE model developed would ideally quantify any undesired mode II or shear fracture and provide a means to substantiate experimental results.

Approach

Four techniques were applied to the DCB sandwich specimen. The single and two step crack closure methods were employed as well as the crack extension methods discussed previously. The results for GI_c obtained from these techniques were compared to the experimental findings for GI_c discussed.

Model

Symmetry was immediately abandoned for the DCB analysis. A 2-D model was developed of the entire honeycomb DCB specimen. A parametric macro procedure was employed that generated a geometry, which consisted of three regions. Two regions represented the top and bottom face sheet, and the third region was the core material. Plane82 (plain strain elements) were used to mesh the areas that comprised these regions. The DCB was discretized to allow for a refined mesh near the crack zone, and coarser mesh away from the crack zone. This conserved computational time and maintained appropriate a/da ratios for fracture analysis.

The face sheet constitutive properties were ascertained empirically by performing static flexure tests on face sheets removed from previously tested specimens. The core material properties were estimated and compared to Tri-Core proprietary materials and did not greatly affect the model.

The nodes corresponding to the hinge attachment locations of the DCB specimen were restrained from motion in the horizontal direction. The bottom node corresponding to hinge attachment was additionally constrained from vertical motion, and the critical force was applied to the top node. No other loads or constraints were required except in the case of the unit loads for the two step crack closure method. Figure 5.26 contains a meshed DCB with boundary conditions and loads applied.

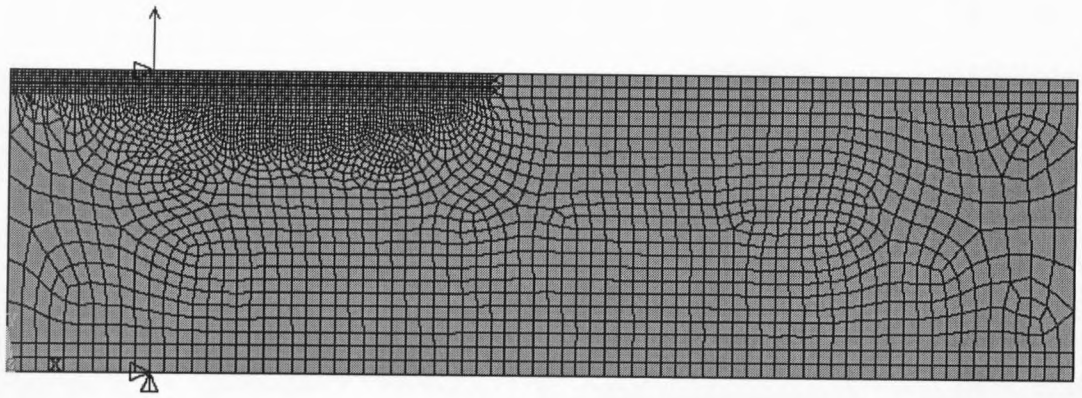


Figure 5.26 DCB Model for Sandwich Material

Solution and Convergence

A static solution was performed and the displacement at the location of the applied load was compared to the experimental value. This confirmed that the flexural modulus used for the face sheets was valid. A typical displacement plot is shown in Figure 5.26. Three mesh sizes were used to confirm convergence. In fracture modeling the a/da ratio is of primary interest. The a/da ratio is simply the number of elements along the length of the modeled crack. The a/da ratios solved for in this study were 60, 100 and 150 elements / unit crack length. These are generally acceptable levels of discretization for the evaluation of G_c [Rybicki and Kanninen (1977)]. The results for the convergence test are shown in Table 5.8.

Table 5.8 Convergence Results for FEA Techniques

a/da ratio	VCCT 1	VCCT 2 mid	VCCT 2 corner	CE
	N/m	N/m	N/m	N/m
60	386	233	332	216
100	374	226	339	204
150	366	229	340	198

Comparison

The bulk of the post processing with this model focused on forces and displacements at the crack tip. The single step virtual crack closure method was followed as described in Chapter 2. Two versions of the two step crack closure method were employed. The virtual loads were applied at the most adjacent node to the crack origin as standard. A modified version, which relocated the virtual loads to the corner node behind the crack front, was also used. Both variations of the crack extension methods were used as well. All of the methods seemed to converge but not to the same solution. The two step methods provided consistent results for each (a/da) increment. The modified version with the unit loads applied at the corner of the compared well with the VCCT 1. The results obtained from these methods were compared to the experimental and analytical findings. The experimental methods included the strain energy method and the modified beam theory equation. An additional relationship for G_I was derived for a sandwich beam and was included in the comparison. The analytical method (equation 6.3) was developed from the basic compliance relationship for G_c (equation 6.2).

$$G_c = \frac{P^2}{2b} \cdot \frac{dc}{da} \tag{5.3}$$

$$G_I = \frac{6P^2a^2}{b^2}\left(\frac{1}{E_1 t_1^3} + \frac{1}{E_2 t_2^3}\right) \tag{5.4}$$

Table 5.9 Comparison of FEA and Experimental Results for G_c

VCCT 1	VCCT 2 corner	CE	Modified Beam Theory	Compliance Equation	Area Method
N/m	N/m	N/m	N/m	N/m	N/m
366	340	198	574	323	797

The VCCT 1, VCCT 2 and the compliance equation all compared closely. These three methods evaluate the energy required to initiate crack growth, and do not account for any R-curve behavior. The area method used averages G_I over the length of crack growth. Generally this value exceeds the compliance and other initiation methods. The modified beam theory results predict larger G_I values. This was thought to be the result of neglecting shear effects. Due to the geometry of the DCB, some induced shear was present. The VCCT 1 method was used to evaluate G_{II} also.

The shear effects were quantified with the VCCT 1 method and compared to the Gtotal. Gtotal is the total strain energy in mode I and II. The percentage of the total strain energy that was responsible for mode II crack growth G_{II} was also reported.

Table 5.10 Shear Effects G_{II} Compared to G_I

Mesh	GI	GII	Gtotal	GII/Gtotal
a/da	N/m	N/m	N/m	
60	386	35	421	0.08
100	374	45	419	0.11
150	366	53	419	0.13

It appears that some mixed mode behavior was present, but the primary failure was mode I. This suggests that the tests conducted were affective at assessing the mode I fracture toughness, but due to the thickness of the specimen shear was also present. The crack closure techniques allow for each behavior to be quantified separately.

Mode II

A similar model was developed to simulate mode II fracture. However the results from this model were considerably errant. The model was very sensitive to the core material properties. These properties were not available and were not easily acquired or approximated.

Summary for Case Study II

The variations of the standard testing techniques applied appear to be reasonable. The screening tests used worked well to characterize the competing material options. The FWT, FWC, mode I peel test and mode II could be applied to rival material combinations. Various core materials, face sheet architectures, and adhesive options could be investigated with these tests and the implementation of the approach provided in chapter III. The design drivers have been established as well as appropriate tests to develop a material database of relevant material properties. From this a screening approach can be applied and potentially some form of analytical prediction may be pursued with additional development.

The finite element models that were developed validated the experimental approach for the FWT and mode I testing. The preliminary results from the mode II model suggest that the experimental G_{II} values are exaggerated. There could have been a considerable amount of core crushing in addition to crack growth. This would elevate the experimental G_{II} values. Improvement would have to be made to the existing mode II FEA model to confirm this suspicion.

The closed form solution developed for evaluating the mode I fracture toughness of sandwich panels compared well with the FEA solutions. This equation is valid for asymmetric panels with face sheets of different dimensions and composition. The equation is valid as long as individual face sheets are not so thin that standard beam formulations no longer apply.

Exploiting sandwich theory to improve specific strength and stiffness works well. However the laminated nature of this construction and the introduction of an adhesive layer can make delamination a considerable mode of failure. It would still be difficult at this point to model and predict discrete crack growth and delamination in primary structure made of this sandwich type construction. This is especially true for mixed mode cases [Valisetty (1988)].

Epilogue

It should be noted that, shortly after this investigation was complete, confidence in honeycomb composite materials had decayed. It was decided to replace the material investigated in this study with Aluminum [HPC (2001)]. This was pursued only briefly before the X-33 space shuttle mission was postponed and effectively abandoned or canceled. This depressing outcome could have most likely been prevented if a thought process such as those discussed in chapter 3 had been employed.

CHAPTER 6

CASE STUDY III
AEROSPACE RESIN SYSTEM EVALUATION

This project also employed a database – screening approach as in the two previous case studies. Basic interlaminar properties were evaluated with the procedures outlined in the background and previous sections. The properties were used to establish a basic database. The database of fracture properties was used to characterize resin systems. Special scanning electron microscopy (SEM) technology was used to isolate the limiting factor of several resin systems.

Project Introduction

ACG is a manufacturer of a complete range of high quality structural prepregs tailored to meet individual process and application requirements. They are pioneers in low temperature molding (LTM) epoxy resin systems, providing chemistry for maximum dimensional accuracy and affordability for both tooling and component applications. Both low (LTM) and high temperature (HTM) cure resin systems are available that have a high T_g or glass transition temperature, which allows for use at elevated temperatures. These systems have unlimited applications but are ideal for aerospace uses.

It is apparent that their lower cure temp high T_g resin systems have significantly lower fracture toughness than the higher cure temp high T_g systems. Generally, lower cure temperature resin systems lend themselves to simpler manufacturing processes for laminate structures, and this makes them desirable.

ACG has performed fracture toughness tests to obtain K_c for neat resin coupons. At this point, the limitation for the performance of the low cure temperature resins is unknown. A variety of problems could effect the fracture performance of the manufactured laminates. Chemical incompatibility with the resin systems chosen and the AS4AP fiber could be a source of limitation. Additionally, the fibers may not be fully encapsulated by the pre-impregnated resin. Flow characteristics such as viscosity and other parameters can also effect the fiber resin bond. As stated the resin itself may be the major limitation and not the resin/fiber interface.

ACG has performed a variety of other tests on prepreg laminates with AS4AP carbon fiber. At this point most of the mechanical properties are promising. The major limitation of laminates tested with the AS4AP fiber has been the fracture toughness. Currently the fracture performance of these combinations has not been optimized and improvements are welcomed. ACG hopes to improve the fracture toughness of their AS4AP systems without sacrificing high temperature capabilities. In addition to meeting these requirements the system should also maintain other mechanical properties such as flexural stiffness and tensile strength.

Problem Statement

The goal of Montana State University was to quantify the interlaminar performance of several resin systems. Standard mode I, static mode II, and dynamic mode II tests were conducted to evaluate the interlaminar fracture toughness. These procedures were applied to 9 different specimen types at several post-cure conditions.

Additionally, scanning electron microscopy was employed to determine the limiting factors in the composite's structural performance.

Material and Specimen Description

To meet these goals ACG provided Montana State University (MSU) with 9 separate laminates. Each laminate was different with respect to resin system used or curing processes applied. Ideally some combination of resin, cure temperature, and cure time should provide improved fracture toughness. A brief description of the laminates and their major variation is included in Table 6.1.

Table 6.1 Specimen Description

	Resin	Fiber	Cure Temp	Cure Time
ID	Type	Type	Celsius	Hours
6863	LTM45EL	AS4AP	80	5
6864	XF9914	AS4AP	80	5
6865	LTM45-1	AS4AP	80	5
6866	XHTM	AS4AP	120	8.5
6867	XF9914	AS4AP	120	2
6868	XHTM45(EF21199)	AS4AP	120	8.5
6869	XHTM45(EF21199)	AS4AP	177	2
6964	EF1800	AS4AP	80	5
6965	EF3300	AS4AP	177	2.5

All of the materials provided are preimpregnated carbon fiber laminates or prepreg. They are all unidirectional architectures constructed of 24 layers of AS4AP carbon fibers and are approximately 60% in fiber volume. They were all autoclave cured at 90 psi at the above specified temperatures and times.

Test Matrix

Each of the above materials were subjected to the tests mentioned. A significant amount of tests were conducted on specimens without post curing. Post cure conditions of 120 °C at two hours and 177 °C at eight hours were used to further cure the laminates. SEM's were only prepared for select materials. A test matrix summarizing the tests performed and quantity for each material is shown in Table 6.2.

Table 6.2 Test Matrix

Sample ID	Resin system	Static Flexure NPC	Mode I DCB NPC	Mode I DCB PC 120C @ 2	Mode I DCB PC 177C @ 8	Static Mode II ENF NPC	Static Mode II ENF PC 120C@2	Static Mode II ENF PC 177C@8	Dynamic Mode II DENF NPC
#		specimen	specimen /cracks	specimen /cracks	specimen /cracks	specimen	specimen	specimen	specimen
6863	LTM45EL	2	3s/3c	1s/3c	1s/3c	6	1	1	4
6864	XF9914	2	3s/3c	1s/3c		6	1		4
6865	LTM45-1	2	3s/3c	1s/3c	1s/3c	6	1	1	4
6866	XHTM	2	3s/3c		1s/3c	6		1	4
6867	XF9914	2	3s/3c		1s/3c	6		1	4
6868	XHTM45 (EF21199)	2	3s/3c		1s/3c	6		1	4
6869	XHTM45 (EF21199)	2	3s/3c			6			4
6964	EF1800	2	3s/3c	1s/3c	1s/3c	6	1	1	4
6965	EF3300	2	3s/3c			6			4

Details regarding the experimental procedures are presented in the following chapter. Material specimens 6863, 6865, and 6866 were subjected to SEM technology to

investigate bond interface issues. This was done at non-postcured state and at the extreme postcure condition of 177 °C for 8 hours.

Experimental Methods

Static flexure experiments were performed in addition to several fracture toughness evaluations. The procedure, data reduction methods, and explanation of the procedures are provided in this chapter.

Static Flexure

Static flexure (SF) experiments were initially performed. The primary material properties obtained from this test, are the flexural modulus and the flexural strength. The major goal of ACG is to improve fracture toughness without compromising strength and stiffness. Additionally, some of the data reduction methods for fracture toughness require the value for the elastic modulus. In the case of composites, the flexural modulus is used for this. Performing static flexure tests also provided a means to establish confidence in testing apparatus and a baseline to compare to ACG's results.

Static Flexure Apparatus

An in-house produced 3-point fixture was used in combination with the model 4206 Instron screw type test device. The device was screw driven and can be used in load or displacement control. The static test apparatus is shown in Figure 4.10. The voltage proportional to load applied and displacement were output and sampled by a SCXI-1200 labview data acquisition system.

Static Flexure Testing Procedure

The specimen was measured for width and thickness and then supported in the fixture as shown. The crosshead was then activated to apply forces in displacement control. An array of force and corresponding displacement was measured via data acquisition described above. Data was recorded until the specimen failed. The force was then plotted vs. displacement. A force – displacement curve is shown in Figure 6.1.

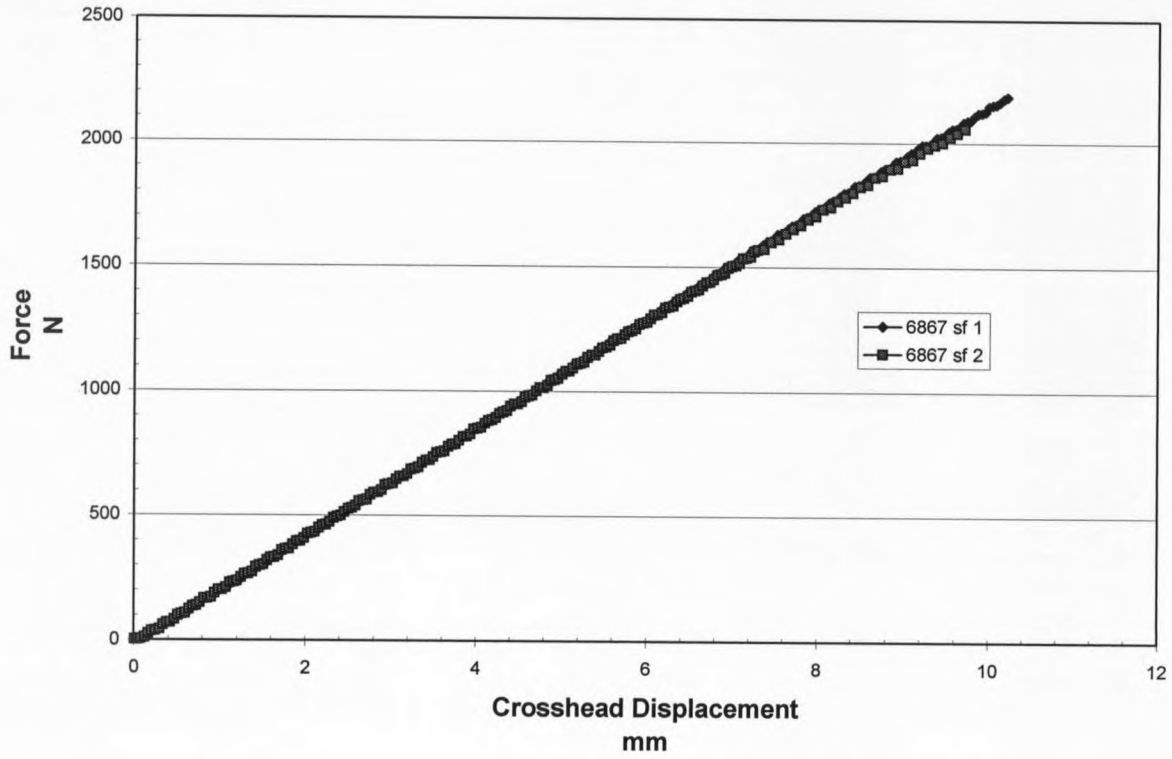


Figure 6.1 Static Flexure Test Results for 6867 Material

Static Flexure Data Reduction

From the graphical output in Figure 6.1 the bending modulus and maximum bending stress were determined using standard beam theory formulations [Gere (1984)] provided in equations (4.4 and 4.7). The bending modulus was obtained by performing a curve fit on the linear portion of the flexure data. This slope was equivalent to the spring stiffness. The maximum load was used to calculate the flexure strength or bending strength of each material.

Fracture Toughness Testing

The fracture toughness tests conducted consisted of static mode I, static mode II, and dynamic mode II. Strain energy release rates were evaluated from each experiment. Strain rate dependencies were investigated, as well as postcure temperature affects. The procedures are discussed briefly here and in more detail in the background (Chapter 2).

DCB Testing Procedure

All of the prepreg laminates supplied had MR1 release film placed at the outer edge. This release film was inserted at the midplane to represent a flaw or crack. Specimens were then sectioned from a composite plate and their dimensions were 150mm x 25mm with a thickness of about 3.2 mm. Once the specimens were acquired from the plate, hinges were attached at the cracked end with Hysol.EA 9309.2NA QT adhesive. A fixture was used to connect the hinge equipped DCB specimen to standard Instron Grips. The specimen was then pulled slowly apart in displacement control at a

rate of 1mm/min until satisfactory crack growth has occurred. At this point the test machine's actuator is reversed to allow specimen unloading. During this entire process, force and corresponding actuator displacement were recorded. The area contained by the force – displacement curve represents the energy absorbed by the specimen. Provided that no damage has occurred beyond crack growth, this energy is directly responsible and related uniquely to crack growth or propagation [Broek (1996)]. Once the specimen was unloaded, additional cracks were grown. A more compliant force – displacement graph resulted. In most cases three cracks were grown for each specimen tested.

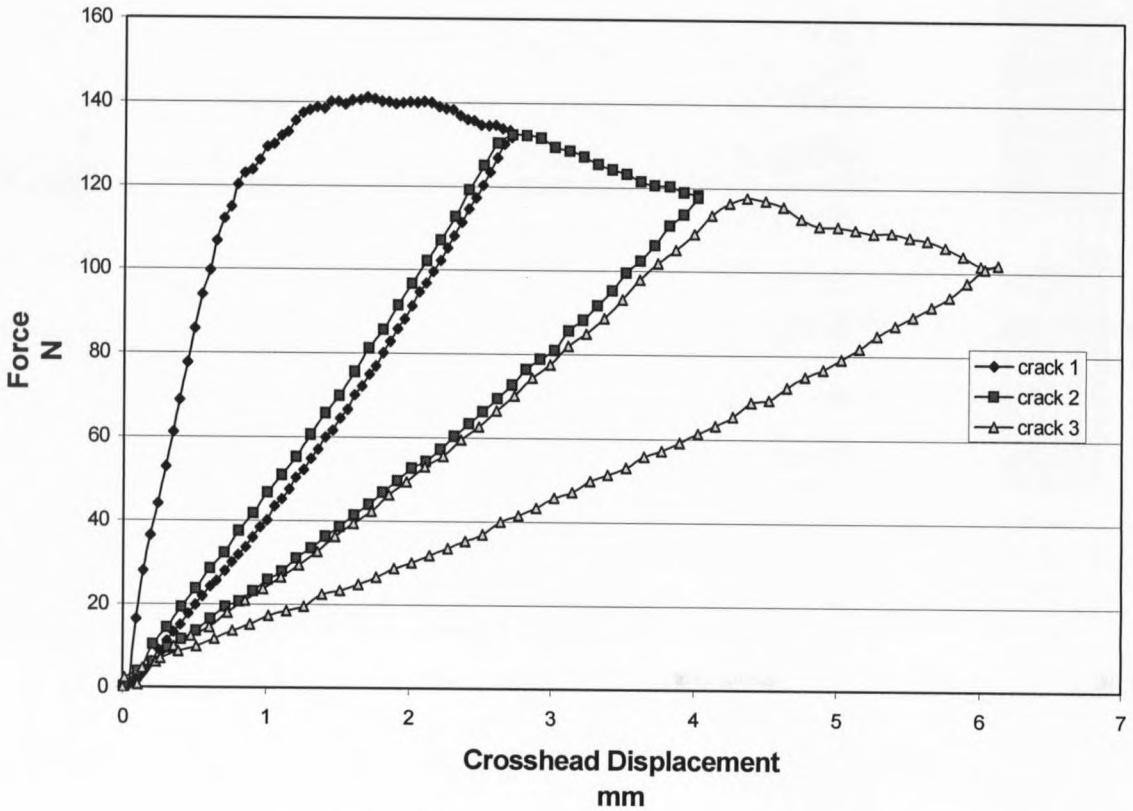


Figure 6.2 Hysteretic Behavior of 6866 DCB – 3 Specimen

DCB Data Reduction Methods

The area method (equation 2.1) was used to evaluate the mode I fracture toughness. Additionally the modified beam method was also used to evaluate G_I (equation 2.2). These methods were applied for each crack growth segment.

Mode II

Mode II fracture is caused by in plane shear or a sliding motion between two surfaces. Bending is one load scenario that induces mode II fracture in laminated composites. This failure mode is more prevalent in composites than metals and polymers due to the laminated construction of composites. To evaluate mode II fracture toughness, a three point bending apparatus is used to conduct an ENF or end notch flexure test [Carlsson (1986)]. A specimen is supported as a simple span beam, and load is applied at center span until crack propagation occurs. A typical test apparatus is shown in Figure 2.7.

ENF Testing Procedure

As with the DCB specimen, an initial crack was required and was already created during manufacture with the insertion of MR1 release film. This initial crack was propagated manually before testing to insure an ideal crack front. The ENF specimen dimensions were 150mm x 25mm and had a thickness of 3.2 mm. The ENF or end notch flexure specimen was supported by a 125 mm span of two rollers. The supported specimen was then loaded at midspan by a loading nose to ensure line contact. A model ENF specimen is shown in Figure 2.8.

The load was incremented in displacement control until the crack propagated. Mode II crack propagation is typically confirmed by the presence of audible cracking and is generally not stable. The crack propagated to the midspan, or further, immediately and repeat crack growths were not possible. The hysteretic behavior of unloading was captured, an example is shown in Figure 6.3.

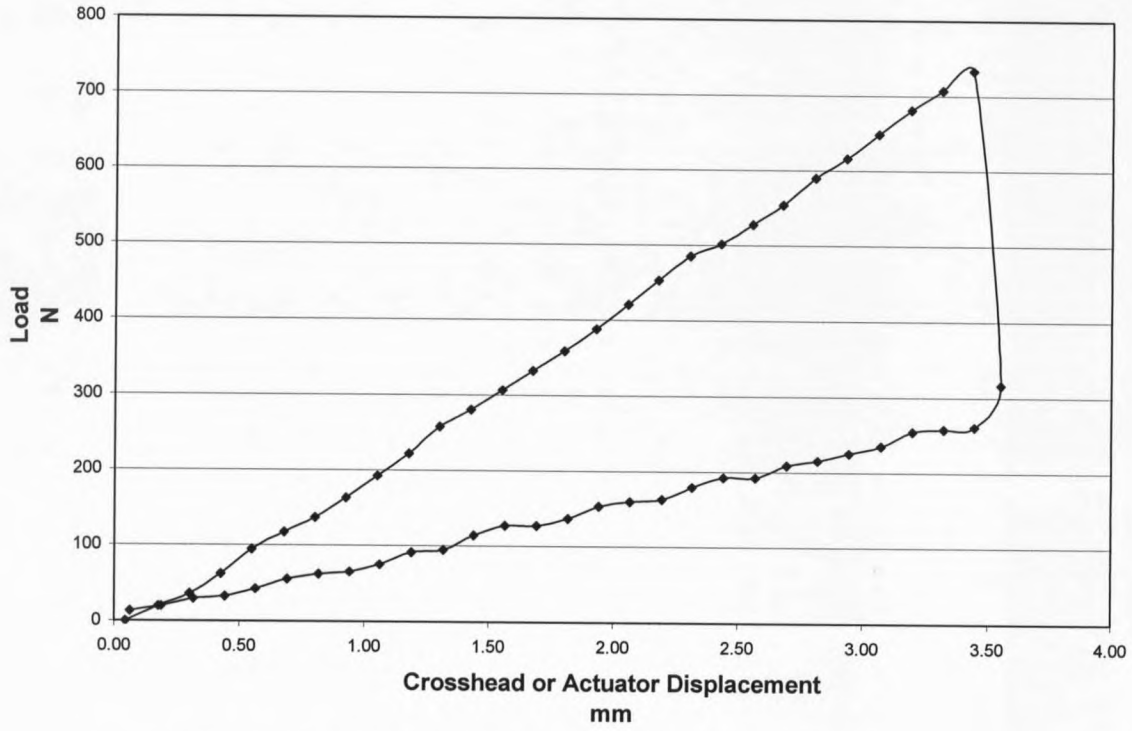


Figure 6.3 Mode II Crack Behavior with Hysteresis Captured

ENF Data Reduction Methods

As in the case of mode I type fracture, the driving element of crack growth is strain energy. The energy method, equation (2.2), is valid for mode II fracture as well.

The load displacement data can be integrated and divided by the crack damage area to calculate a G_{II} or mode II fracture toughness as before.

Dynamic Mode II Testing

Dynamic resistance to delamination was evaluated using dynamic mode II testing. The metric of this experiment is still G_{IIc}, but for dynamic loading conditions. This property accounts for any strain rate dependencies of the material [Cairns (1992)].

Dynamic ENF Apparatus

To conduct a dynamic version of the mode II fracture toughness test, special equipment had to be used [Mackin (1992) and McMichael (1988)]. An impact tower was employed to supply the force and energy to induce crack growth (Figure 4.1). Special data acquisition equipment was also used (Figure 4.2). Details regarding the equipment used follow.

Dynamic ENF Testing Procedure

Most of the procedure and data reduction techniques are similar to the mode II fracture toughness methods outlined in Chapter 2 and for ENF testing. The test specimen geometry is the same as the ENF. An ultrasonic transducer was used to isolate and measure crack fronts before and after testing. The primary difference of the DENF test from the ENF test is method of applying force. As discussed, load is applied by means of an impactor travelling at speeds of about 1 m/s. The impact force is sampled at high frequencies (50 kHz). A typical impact trace is shown in Figure 6.4.

Dynamic ENF Data Reduction

Impact tests provided force vs. time data of the form represented in Figure 6.4. This data was converted to force vs. deflection data by employing a series of numerical integration routines. The force data is used to obtain acceleration, velocity, and displacement all as functions of time. All that is needed to do this is the original force versus time trace and boundary conditions regarding velocity and displacement during the impact. The same methodology was followed as was presented in Chapter 4. Sample output for each step of the process is provided in Figure 6.5 – 6.8. Force as a function of displacement is shown in Figure 6.8.

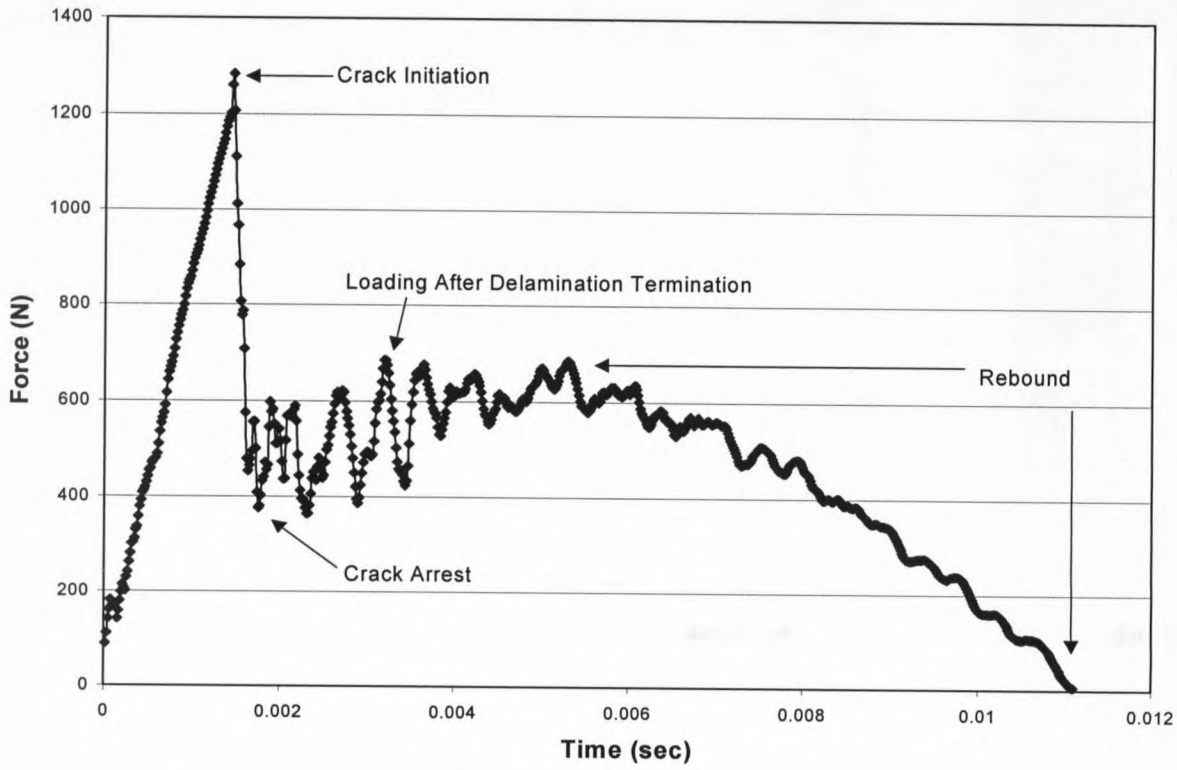


Figure 6.4 Force vs. Time Data for 6868 XHTM Material

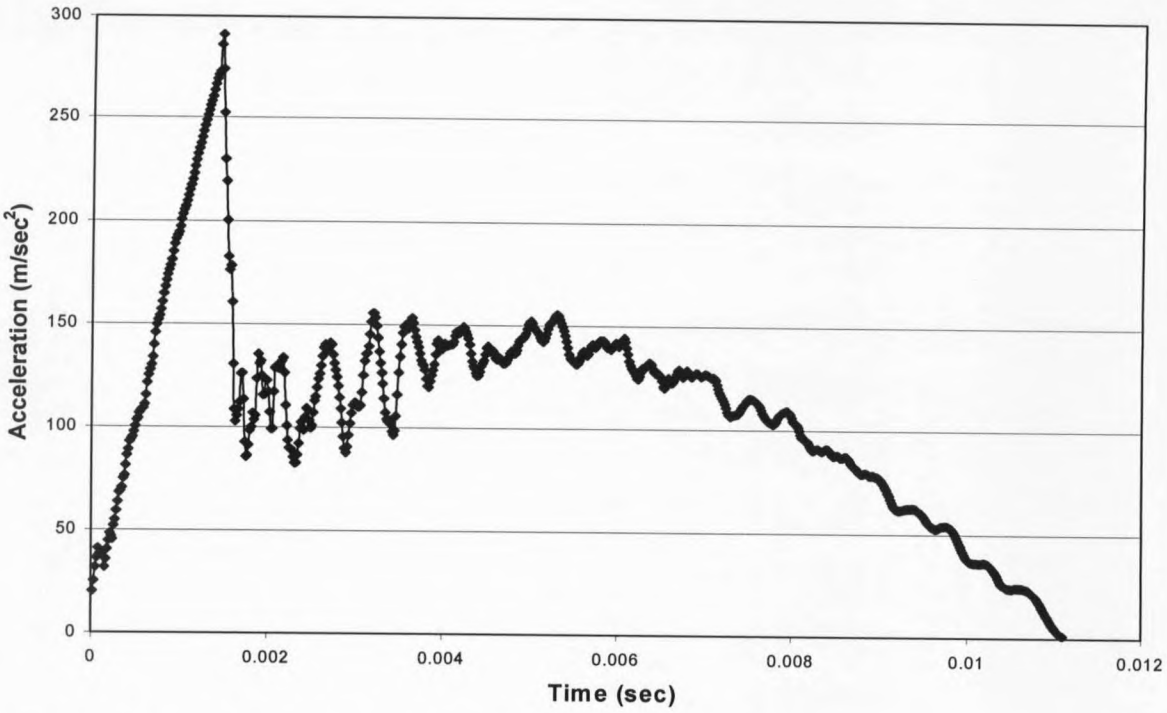


Figure 6.5 Acceleration vs. Time for 6868 XHTM Material

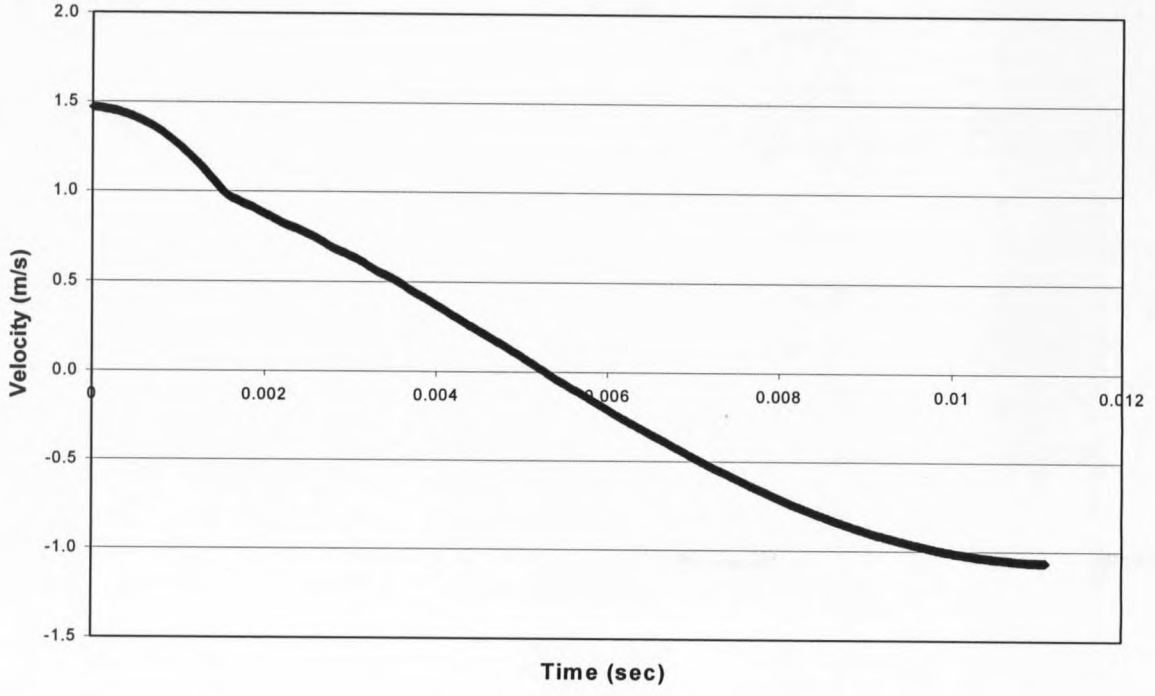


Figure 6.6 Velocity Profile for 6868 XHTM Material

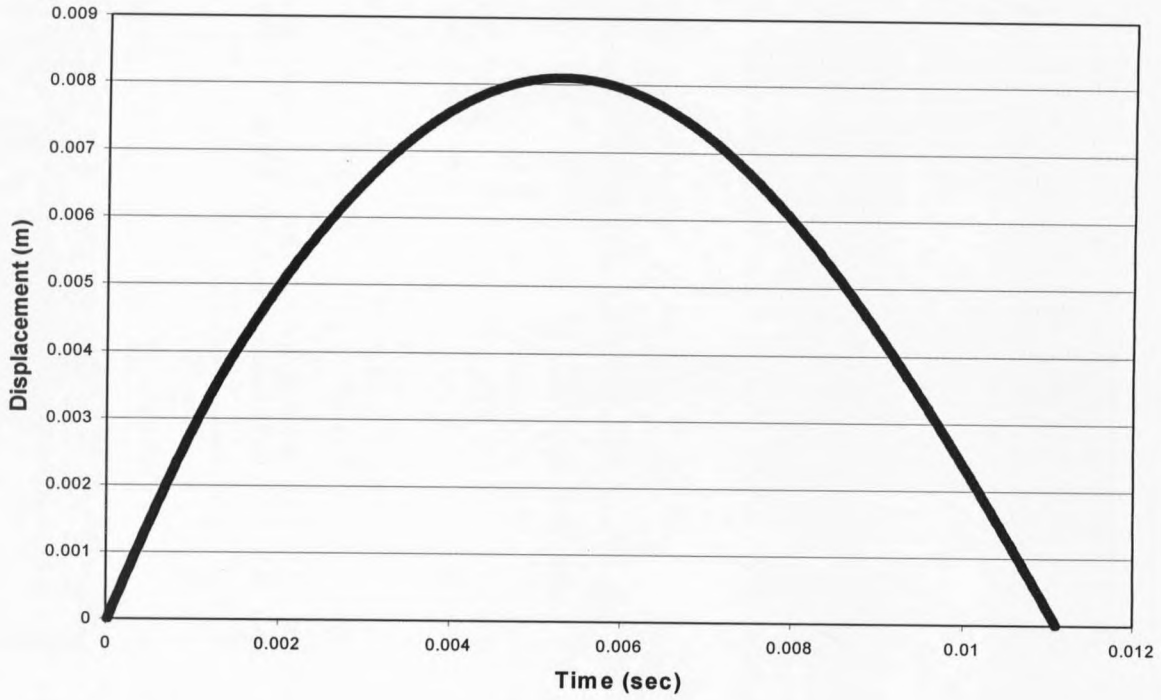


Figure 6.7 Displacement vs. Time for 6868 XHTM Material

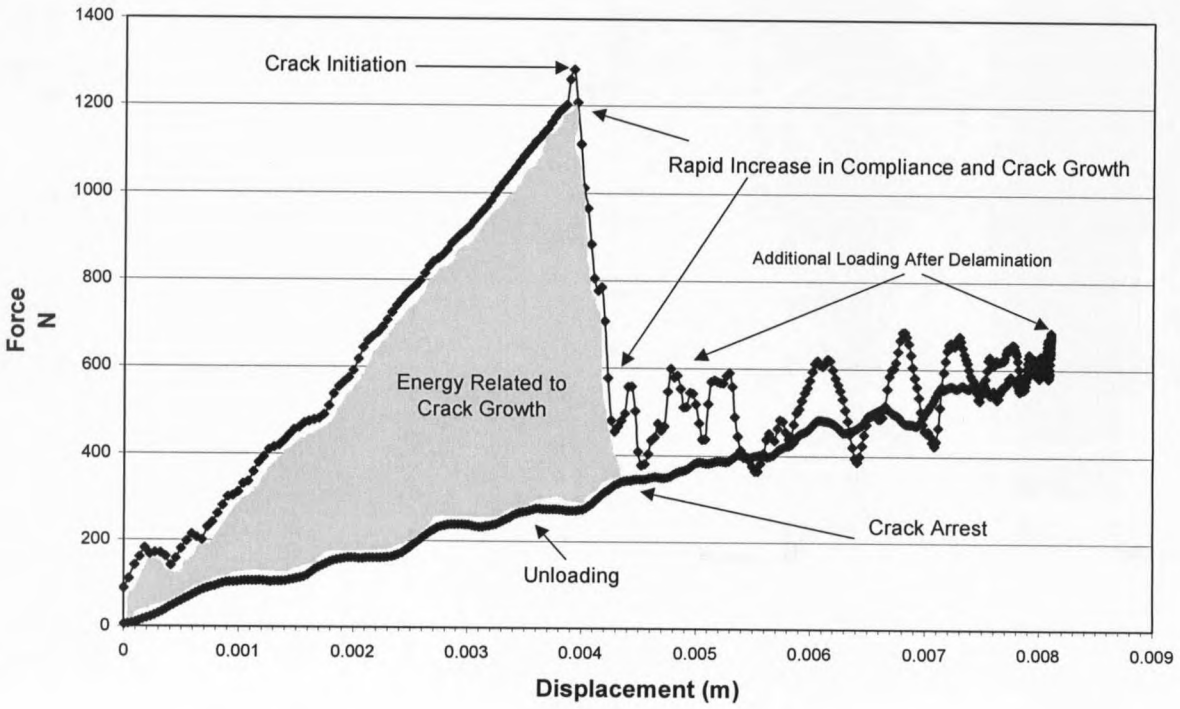


Figure 6.8 Dynamic Load Displacement Curve for 6868 XHTM Material

The data reduction techniques outlined in chapter 2 were followed. Both the area method (equation 2.2) and the compliance method (equation 2.6) were used to obtain experimental G_{II} values.

Scanning Electron Microscopy Evaluations

Scanning Electron Microscopy (SEM) technology was used to isolate the limitation of the interlaminar performance of several select materials provided [Hyer (1998)]. Bondability (or compatibility of the resin and fiber) and brittle resin behavior were the most likely culprits.

SEM Apparatus

Special equipment at the Montana State University (MSU) Image and Chemistry Analysis Laboratory (ICAL) facility were employed to capture images of fracture planes of G_{II} specimens. Special Assistant Nancy Equall and a state of the art scanning electron microscope were the primary components of this system.

SEM Testing Procedure

Samples of three different materials were subjected to SEM evaluations for two extreme postcure conditions (not postcured and postcured at 177 °C for 8 hours). These samples were sectioned from G_{II} specimen remnants. Their dimensions were approximately 12mm x 25mm. Upon sectioning these samples they were sprayed with compressed nitrogen gas to remove debree from sectioning. Once the specimens were cleaned and mounted on aluminum platforms, they were subjected to a "sputtering" process. This process consisted of using argon gas to induce ionic excitement and

subsequent bombardment of gold-polladium. This coats the specimen with a conductive layer which enhances the microstructure of the laminate's constituents. At this point the specimens were loaded into the SEM chamber and inspected. A twelve kV excitation voltage was used and specimens were viewed at both 500 magnification and 1500 magnification levels. Black and white images were sampled and inspected for brittle behavior and bondability characteristics. An example of a SEM photo is shown in Figure 6.9. The stripes are hackle marks which are characteristic of mode II fracture. These are caused by shear at the interlaminar boundary.



Figure 6.9 SEM Photo

Experimental Results

The experimental procedures presented were used to quantify the interlaminar characteristics of the nine materials discussed. Summaries and explanations of those experimental results follow.

Static Flexure Test Results

Two samples were tested for each of the nine different specimen types supplied. The static flexure testing procedures were followed as outlined in Chapter 2. From the load – deflection graph obtained the flexural modulus and flexural strength were obtained. A summary of these results is included in Table 6.3.

Table 6.3 Summary of Static Flexure Results

ACG ID	Sample ID	Resin system	Initial Cure Temp	Initial Cure Time	Post Cure Temp	Flexural Modulus	Flexural Strength
	#		C	Hours	C	GPa	MPa
26,27,28	6863	LTM45EL	80	5	None	137 (0%)	1574
1,2,3	6864	XF9914	80	5	None	143 (1%)	1619
6,7,8	6865	LTM45-1	80	5	None	140 (1%)	1694
12,13	6866	XHTM	120	8.5	None	137 (0%)	1709
4,5	6867	XF9914	120	2	None	139 (.6%)	1605
12,13	6868	XHTM45 (EF21199)	120	8.5	None	138 (.3%)	1652
11	6869	XHTM45 (EF21199)	177	2	None	134 (0%)	1602
14,15,16	6964	EF1800	80	5	None	132 (0%)	1264
20	6965	EF3300	177	2.5	None	135 (0%)	1705

Note the values in ( ) are the standard deviation / average x 100 [coefficient of variation]

The modulus values were very consistent and precise for all of the specimen tested. The flexural modulus values ranged from 132-143 GPa. The flexural strength values followed similarly with greater variation amongst each specimen type and comparatively between all of the specimen. The 6964 series possessed the worst flexural strength of 1290 MPa and the 6866 (XHTM) was the best at 1709 MPa.

Mode I Results from DCB Testing

Three specimen of each type were subjected to standard Double Cantilever Beam (DCB) testing to evaluate (G_I). The testing procedure in Chapter 2 was followed. The crack was initially grown and usually extended two more times. Each specimen provided three samples or data for G_I. The Mode I fracture toughness (G_{II}) was calculated by both methods presented in Chapter 2. The compliance method represents the energy required to initiate crack growth. The area method averages the energy required to extend a crack some distance. Generally, the area method provides a larger value for G_I. This is because of R-curve behavior or a material's inherent ability to arrest crack growth as discussed previously. Fiber bridging and other mechanisms contribute to this. Materials that do not exhibit this behavior will generally have unstable and continuous crack growth in service. The results for the Mode I tests conducted are shown in Table 6.4.

Table 6.4 Static Mode I Test Results

ACG ID	sample ID	Resin system	Cure Temp	Cure Time	Post Cure Temp	G_I MBT Method	G_I Area Method	G_I Average
	#		C	Hours	C	N/m	N/m	N/m
26,27,28	6863	LTM45EL	80	5	None	352	310	331
1,2,3	6864	XF9914	80	5	None	248	264	256
6,7,8	6865	LTM45-1	80	5	None	347	387	367
12,13	6866	XHTM	120	8.5	None	664	579	622
4,5	6867	XF9914	120	2	None	257	237	247
12,13	6868	XHTM45 (EF21199)	120	8.5	None	652	573	613
11	6869	XHTM45 (EF21199)	177	2	None	336	266	301
14,15,16	6964	EF1800	80	5	None	334	406	370
20	6965	EF3300	177	2.5	None	285	247	266

The 6866 and 6868 (XHTM) series performed the best with an average G_I of 622 N/m and 613 N/m respectively. The XF 9914 and EF3300 resin systems had the lowest G_I. All other resin systems ranged in the 300's. The 6969 (XHTM) series sample was initially cured at 177 °C instead of 120 °C. This appears to have had a dramatic effect on G_I. The mode I interlaminar fracture toughness was decreased by a factor of two. The only feasible explanation is the cure temp conditions. There was no apparent R-curve effect so all of the results were grouped.

Mode I tests were also conducted on specimens at varying postcure temperatures. Specimens were subjected to postcure conditions of 120 °C at 2 hours and 177C at 8 hours depending on initial cure temperature. The results for the G_I based on varying postcure temperatures are shown in Figure 6.10. Generally the Mode I fracture toughness diminished with increasing post cure temperature. This was especially true for the materials that performed better at the non-postcured state.

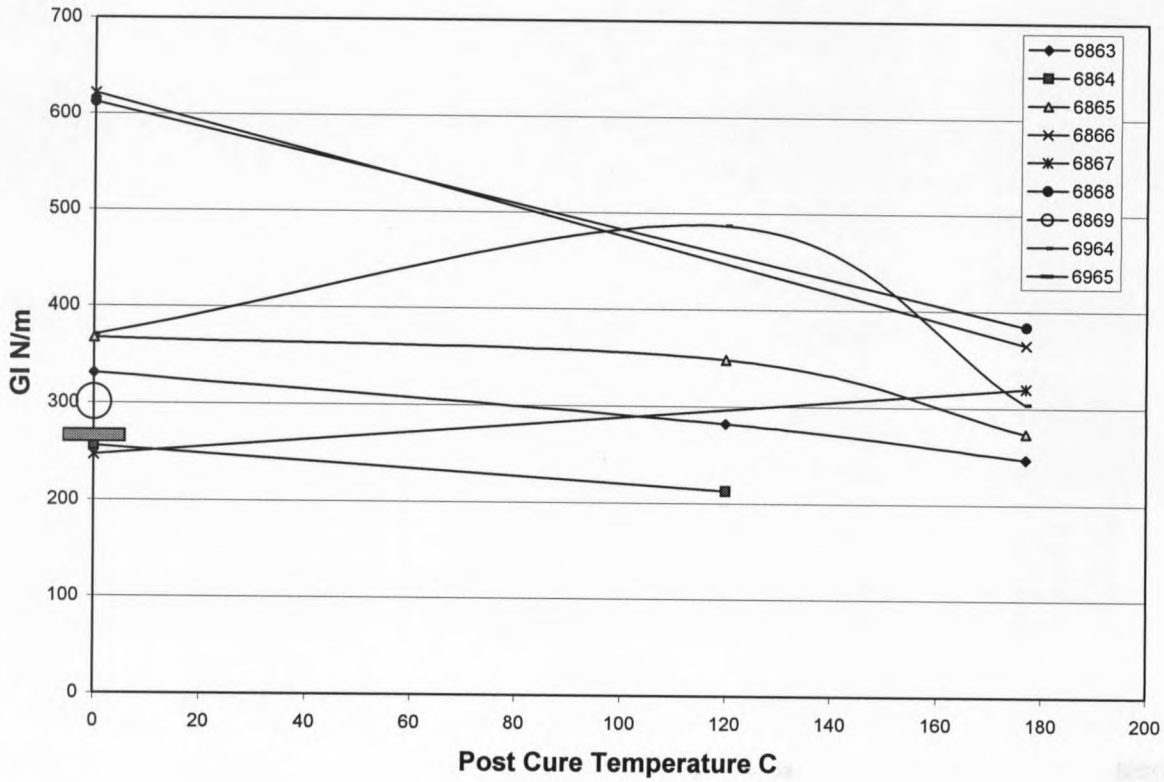


Figure 6.10 Mode I Results for Varying Post Cure Temperatures

Mode II Results from Static ENF Testing

Six specimen of each type were submitted to Static End Notch Flexure (SENF) testing to evaluate Mode II fracture toughness (G_{II}). In Mode II cracks generally grow unstably, across the entire spanned region of the test specimen. This makes it impossible for more than one crack growth session to occur for each specimen. Each specimen provides only one test and approximation for G_{II}. A summary of test results for Mode II interlaminar fracture toughness is included in Table 6.5.

Table 6.5 Summary of Mode II Test Results

ACG ID	sample ID	Resin system	Initial Cure Temp	Initial Cure Time	Post Cure Temp	G_{II} Static MBT Method	G_{II} Static Area Method
#	#		C	Hours	C	N/m	N/m
26,27,28	6863	LTM45EL	80	5	None	438 (36%)	675
1,2,3	6864	XF9914	80	5	None	387 (40%)	396
6,7,8	6865	LTM45-1	80	5	None	452 (28%)	695
12,13	6866	XHTM	120	8.5	None	716 (30%)	1163
4,5	6867	XF9914	120	2	None	384 (23%)	574
12,13	6868	XHTM45 (EF21199)	120	8.5	None	713 (24%)	966
11	6869	XHTM45 (EF21199)	177	2	None	1021 (32%)	1360
14,15,16	6964	EF1800	80	5	None	575 (16%)	730
20	6965	EF3300	177	2.5	None	506 (19%)	631

Note the values in ( ) are the standard deviation / average x 100 [coefficient of variation]

The mode II results indicate that the (XHTM) series, 6866, 6868, and 6869 materials performed the best. For mode II the 6869 material (with the higher initial cure temperature) performed better than the 6866 or 6868. This suggests that increasing the initial cure temperature could improve G_{II} but be detrimental to G_I. In all cases, the area method provided a larger G_{II} value than the compliance equation. This indicates that all the materials possess some inherent crack arresting attributes.

SENF tests were also performed on several of the materials at varying post cure temperatures. Post curing the composites at higher temperatures might have reduced the interlaminar fracture toughness as for mode I. However, SENF tests were conducted at the same conditions as for mode I, and opposite results were obtained. The results of this are shown in Figure 6.11.

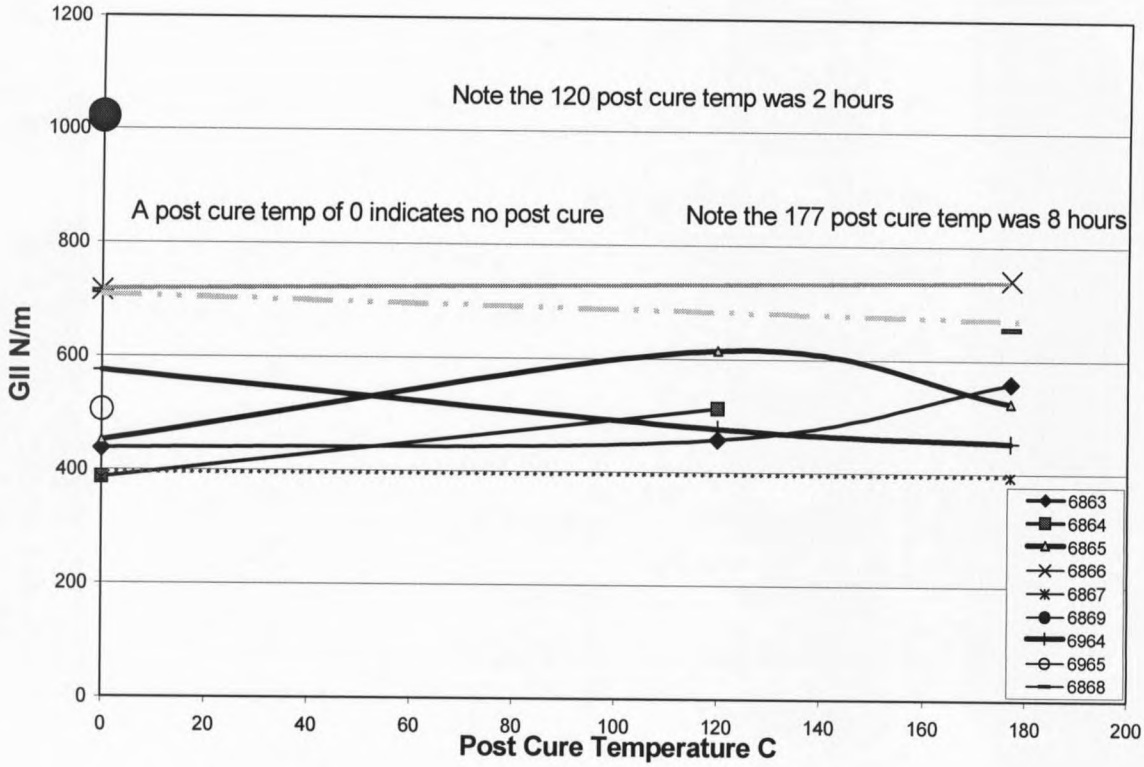


Figure 6.11 Mode II Fracture Toughness as a Function of Postcure Temperature

Mode II Results from Dynamic ENF Testing

Four specimen of each type were subjected to Dynamic End Notch Flexure (DENF) testing to evaluate the strain rate effects on G_{II}. The behavior was similar to the ENF specimen. The primary difference was the method of testing employed. Instead of using a typical Instron or standard static tensile testing machine, an instrumented drop tower was used. The details regarding these testing procedures were described previously in Chapter 4. Extensive data reduction was required to obtain force-deflection graphs. From these the equations presented for the static G_{II} can be applied. The

resulting G_{II} values account for the effects of high strain rate loading. A summary of these test results for non-postcured samples can be found in Table 6.6.

Table 6.6 Summary of Dynamic End Notch Flexure Results

ACG ID	sample ID	Resin system	Cure Temp	Cure Time	Post Cure Temp	G_{II} Dynamic MBT Method	G_{II} Dynamic Area Method	G_{II} Dynamic Average
#	#		C	Hours	C	N/m	N/m	N/m
26,27,28	6863	LTM45EL	80	5	None	489 (14%)	431	460
1,2,3	6864	XF9914	80	5	None	418 (17%)	244	331
6,7,8	6865	LTM45-1	80	5	None	299 (43%)	322	311
12,13	6866	XHTM	120	8.5	None	709 (10%)	806	758
4,5	6867	XF9914	120	2	None	361 (6%)	286	324
12,13	6868	XHTM45 (EF21199)	120	8.5	None	592 (13%)	719	656
11	6869	XHTM45 (EF21199)	177	2	None	701 (17%)	1260	981
14,15,16	6964	EF1800	80	5	None	544 (8%)	508	526
20	6965	EF3300	177	2.5	None	421 (18%)	433	427

Note the values in ( ) are the standard deviation / average x 100 [coefficient of variation]

The dynamic end notch flexure test results follow the static versions. However many of the poorer performing systems maintained their toughness at the high strain rates, while the better materials showed a definite decay. A comparison in static GII and dynamic GII is shown in Table 6.7. The results were obtained from the compliance equation.

Table 6.7 Rate Dependency Comparison for Mode II Testing

ACG ID	Sample ID	Resin system	Initial Cure Temp	Initial Cure Time	Post Cure Temp	G_{II} Static MBT Method	G_{II} Dynamic MBT Method	G_{II} static / dynamic
#	#		C	Hours	C	N/m	N/m	none
26,27,28	6863	LTM45EL	80	5	None	438 (36%)	489 (14%)	0.90
1,2,3	6864	XF9914	80	5	None	387 (40%)	418 (17%)	0.93
6,7,8	6865	LTM45-1	80	5	None	452 (28%)	299 (43%)	1.51
12,13	6866	XHTM	120	8.5	None	716 (30%)	709 (10%)	1.01
4,5	6867	XF9914	120	2	None	384 (23%)	361 (6%)	1.06
12,13	6868	XHTM45 (EF21199	120	8.5	None	713 (24%)	592 (13%)	1.20
11	6869	XHTM45 (EF21199	177	2	None	1021 (32%)	701 (17%)	1.46
14,15,16	6964	EF1800	80	5	None	575 (16%)	544 (8%)	1.06
20	6965	EF3300	177	2.5	None	506 (19%)	421 (18%)	1.20

Note the values in ( ) are the standard deviation / average x 100 [coefficient of variation]

A definite rate dependency was noticed, but not for all of the materials. The LTM-45 (6865) and the XHTM-45 (6868 and 6869) series showed reduced performance in mode II at high strain rates. The other materials were mostly unaffected by the increased strain rate. The dynamic end notch flexure test results have a lower coefficient of variation due to the use of ultrasonic crack detection throughout the course of the experiments.

SEM Results for Selected Systems

Three specimen types were prepared for Scanning Electron Microscope (SEM) analysis. The 6863, 6865, and 6866 materials were prepared based on the procedures presented. The goal of this particular investigation was to determine if the interlaminar performance was linked to or limited by the interface or bond properties of the resin to the fibers.

Photographs were taken at both a 500 magnification and a 1500 magnification. Images were captured for the above specimen types from samples sectioned from mode II remnants. This was done for specimens, which had been post-cured at 177C, and for those that had not been post-cured at all. It was demonstrated that post curing had an effect on the interlaminar fracture toughness. Possibly there might be a relationship between the micro-mechanics of the composites, post cure temperature, and their interlaminar performance.

The results of the SEM photos are very subjective. The goal of the interpretation of these results is to find some evidence of brittle resin behavior and also to investigate the apparent bondability or compatibility of the fibers and resin systems. Each of the three resin systems investigated will be discussed individually.

The 6863 (LTM-45EL) resin system possessed limited interlaminar performance. At a 1500 magnification level the non-postcured material shows definite brittle fracture behavior as shown in Figure 6.13A. At the 500 M view the photo shows some loose fibers which could indicate some problem with bonding (Figure 6.13B). However, the bondability seems effective and the brittle nature of the resin itself is most likely the limiting element of this resin system. The postcured results generally follow and show no apparent improvement or degradation in brittleness and bondability (Figure 6.13C, D).

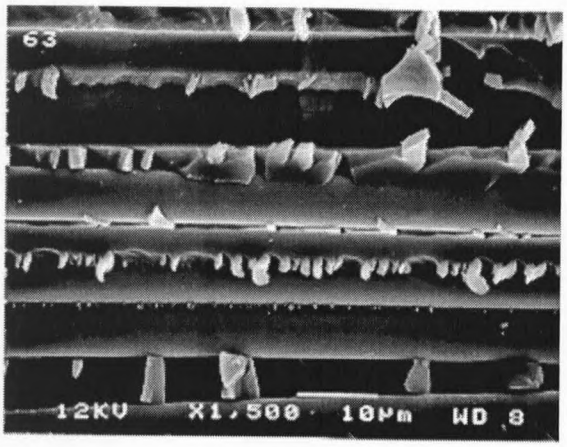


Figure 6.12A 6863 npc at 1500 M



Figure 6.12B 6863 npc at 500 M

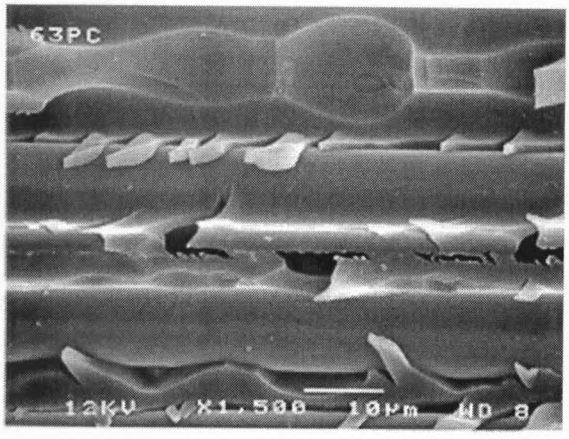


Figure 6.12C 6863 pc177 at 1500 M

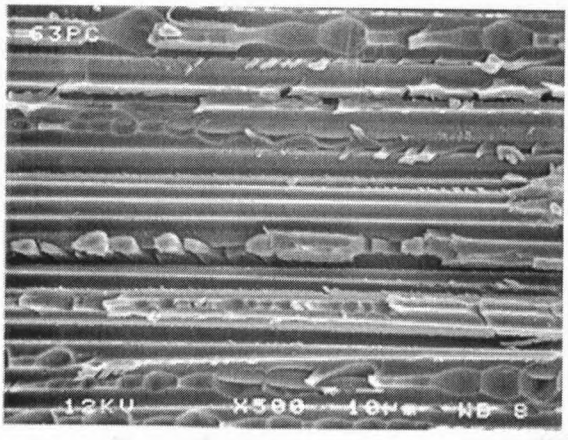


Figure 6.12D 6863 pc177 at 500 M

The 6865 resin had similar results as the 6863 material with regards to interlaminar fracture performance. The SEM results were similar also. Some evidence of brittle behavior was evident for both postcure states. Scattered loose fibers could also be seen for both conditions. The hackle marks are typical for mode II type crack growth. Consequently the 6865 series appears somewhat less brittle than the 6863 material. The bondability appeared reasonable and was most likely not the limiting factor regarding fracture toughness.

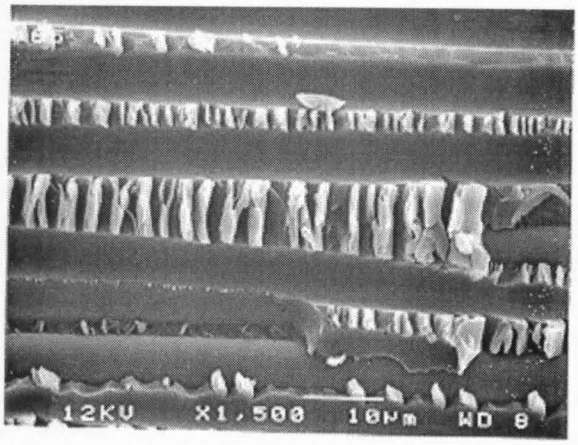


Figure 6.13A 6865 npc at 1500 M



Figure 6.13B 6865 npc at 500 M

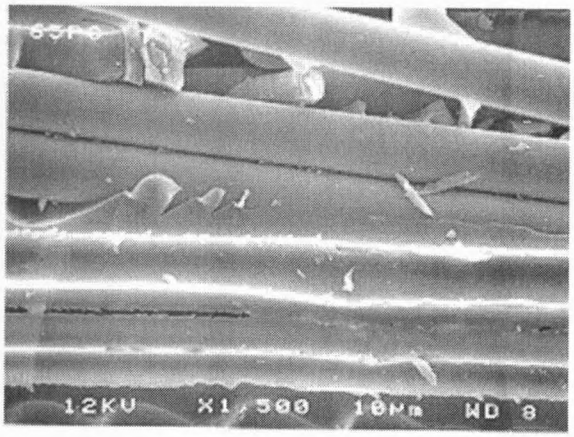


Figure 6.13C 6865 pc177 at 1500 M

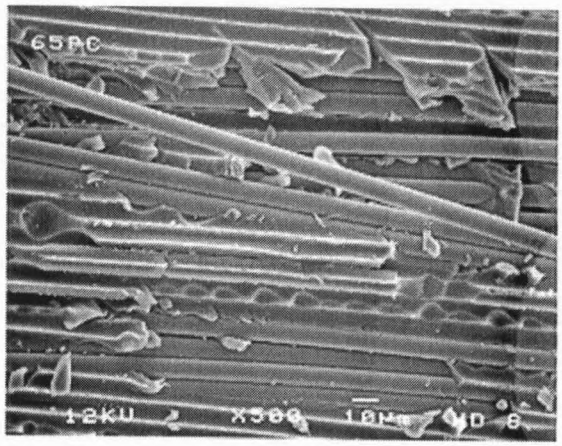


Figure 6.13D 6865 pc177 at 500 M

The 6866 material performed considerably better for both G_I and G_{II} than either of the previous systems. Both magnification levels show minimal brittle fractures and thorough bonding capabilities. Very similar results are shown for both postcure conditions. The Mode II fracture toughness was almost unaffected by the additional postcuring. The SEM results confirm that little change took place. The SEM results also explain the improved fracture toughness over the previous systems. Reduced brittleness and increased bondability most likely contributed to the improved fracture properties.

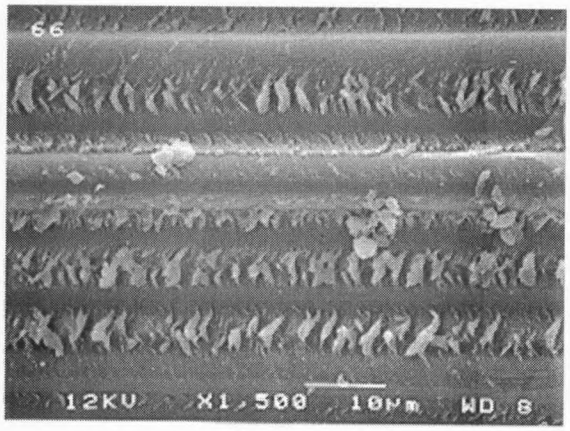


Figure 6.14A 6866 npc at 1500 M

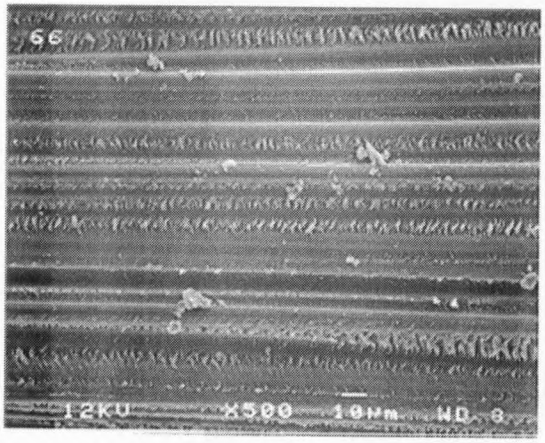


Figure 6.14B npc at 500 M

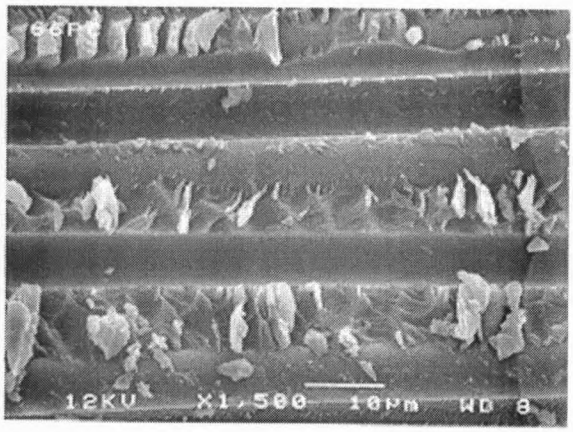


Figure 6.14C 6866 pc177 at 1500 M

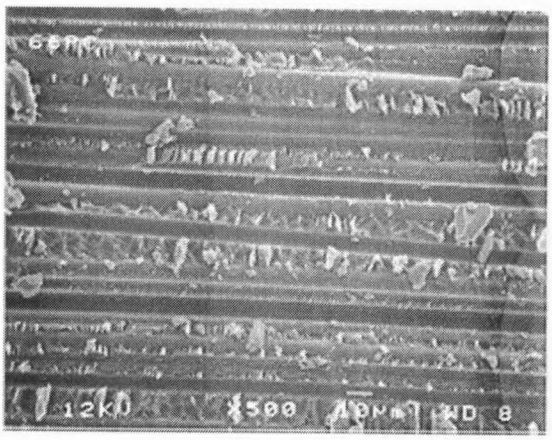


Figure 6.14D 6866 pc177 at 500 M

Summary for Case Study III

Nine separate laminates, of different resin compositions, were provided to MSU by ACG for interlaminar fracture toughness evaluations. Mode I, mode II and dynamic mode II delamination experiments were performed. The results of these experiments indicate that the XHTM resin system or high temperature molded laminates outperformed the LTM systems with regard to overall fracture toughness.

However, when the specimens were subjected to postcuring, most of the materials G_I or mode I fracture toughness decayed. The XHTM systems lost a greater percentage of toughness than the LTM systems. This was not true for mode II, G_{II} values typically held steady or improved with the addition postcuring. Possibly the resins shear strength is less effected than the tensile strength.

Reduced performance at higher strain rates was not noticed for most materials. The dynamic G_{II} values followed the static results closely except for the 6865 or LTM45-1 system and the XHTM45 systems.

The SEM tests provided some correlation between interlaminar fracture performance and microstructure. The 6863, 6865 and 6866 systems were compared. The 6863 (LTM45EL) system and the 6865 (LTM45-1) system were similar in composition and fracture performance. Both showed signs of brittle resin fracture, and some problems with bondability. The 6866 (XHTM45) system outperformed both the 6863 and 6865 system and showed improved bondability and less brittle fracture.

This case study was the perfect application for the database-screening process presented in Figures 3.4 and 3.5. The materials investigated possessed good mechanical properties and all had similar strength and stiffness metrics.

However, significant variation was found with regard to interlaminar fracture performance. The Mode I values did not always follow the Mode II values either. This reinforces the need to conduct both tests. It was also discovered that some of the materials exhibited a definite rate sensitivity. As a result, when composite candidates are to be used in impact or dynamic environments, the dynamic Mode II tests should also be used to characterize the laminate. The resin post cure effects indicate that interlaminar fracture performance can also be altered by processing details. The SEM technology worked well to relate the interlaminar behavior to the micro-mechanics of the laminate. This technique of damage assessment can be used with the database-screening process to optimize a potential laminate composite. Ultimately, the methodology outlined could be employed to further improve and optimize the laminated architectures that are currently being produced as well as future candidate engineering materials.

CHAPTER 7

CASE STUDY IV

METAL INTERFACE

As part of an effort to develop composite wind turbine blades, a sub-structure root section was constructed. The function of this sub-structure was to connect a mostly fiberglass-polyester resin blade to a hub. A specially constructed steel insert shown in Figure 7.1 was employed to make this connection. Significant research has been spent evaluating the performance of this root detail [Skramstad (1999)].

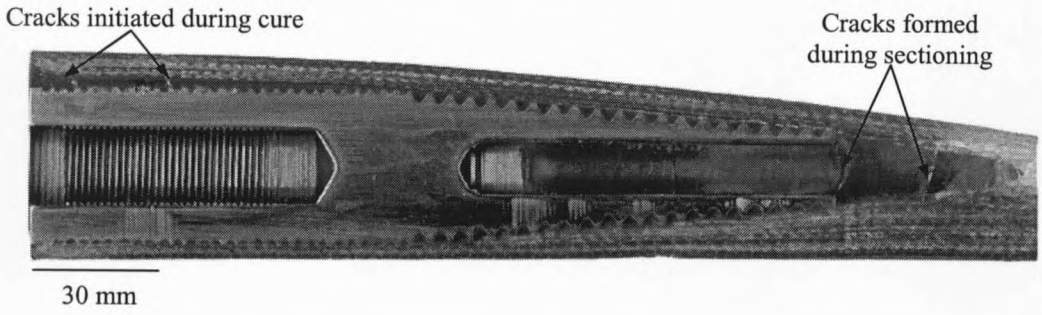


Figure 7.1 Fatigue Specimen, R112 Cross-Section with Steel Insert.

The chosen constituents and composite architecture performed satisfactorily. To improve the existing root configuration a better understanding of metal composite combinations was required.

Bond Components

The interface between the steel insert and the surrounding composite material was not greatly understood. It was certain that some chemical bond adhesion as well as some

structural interlock joined the steel insert to the composite material. The importance and contribution of each was unknown.

Chemical Bond

Since the steel insert was typically placed in the fabric and the resin was then injected via RTM, the steel was primarily held in place by the resin system used. The resin then possessed a molecular or chemical bond to the steel. This bond would allow load in form of shear to transfer from the blade to the root and ultimately the hub. It is surmised that chemical bonding is not solely responsible for this load transfer from the insert material to the surrounding composite. Due to the geometry of the insert a definite structural mechanism also exists that secures the insert to the composite housing.

Structural Interlock

The threaded surface of the insert material provides mechanical interlock. This mechanical interlock enhances the bond strength of the insert material beyond chemical adhesion alone. In fact during initial stages of root development, it was observed that the steel insert would fail before the composite material or the bond itself.

Need for Simpler Structure and Methodology

In order to improve upon existing design or to even understand its success, more information is needed regarding both chemical bond properties and mechanical interface properties. As a screening process, two new test specimens were developed and constructed. These scaled down structures were designed to reduce the burden of constructing an entire root section to evaluate potential modifications. The simplest test

specimen is the shear lap specimen. This test isolates chemical bond strength. A more complex test specimen was developed to account for the mechanical interface between metals and composites. This specimen was called the miniroot. This is a scaled down version of the root section specimen mentioned.

Lap Shear

Two types of lap shear tests were investigated. A single lap shear and a double lap shear test were used. These tests are generally used for adhesives. However, resin systems share some of the same type of structural responsibility as adhesives. Details regarding each are discussed individually.

Single Lap Shear

The single lap shear test specimen has been designed to evaluate bond properties of adhesives. ASTM standards are in place that provide guidelines and procedures for conducting this test [ASTM D1002-72 (1993)]. The shear lap test is used to evaluate and quantify an adhesive strength of a joining material with a given material. Typically, a lap or overlap joint is made by two pieces of parent material and a bond is formed with the adhesive. These are specimen that can then be pulled apart in shear. Shear is the basic mechanism of load transfer for adhesives and glues. A shear strength can then be obtained from the failing load and the bond area.

Generally, this is not a material property and designing with these values can be hazardous [ASTM D4896-89 (1993)]. Other tests exists that provide more meaningful results, but are difficult to conduct and require complicated fixtures [ASTM D3983-92

(1993), E229-92 (1992), 4562-90 (1993), 4027-92 (1993)]. More accurate results can be obtained from lap-joint tests by accounting for the stress gradient. A stress singularity is present at the beginning of the bond interface and the bond area is not under constant stress [Hart-Smith (1990), and Skeist (1977)]. The bond strength will vary linearly as a function of width but not length. A stress gradient is present along the length of the bond surface. This stress gradient behavior can be captured with FEA.

Single Lap Shear Construction

The shear lap specimens were constructed with four pieces of metal, resin, and glue. First the lap joint was formed with the resin material and two pieces of metal 150mm in length. Then to combat any bending stress or out of plane loading, two 75mm long tabs were glued to the lapped piece as spacers. These spacers allowed the specimen to be clamped with the bond line centered. This mitigated most problems associated with eccentric loading and bending.

Single Lap Shear Configuration

An example of a basic shear lap specimen is shown in Figure 7.2. The tabbed region was the area that was actually clamped in the Instron testing device. The bond region is where the resin and metal shared a surface or interface.

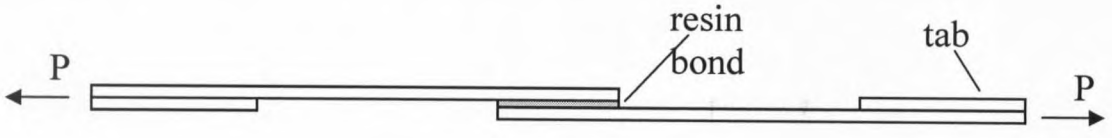


Figure 7.2 Single Lap Shear Specimen

Test Procedure

The shear lap specimens were clamped into the Instron 4206 carefully to avoid any unintended shear stress from clamping. Load was then applied in displacement control until failure occurred. The bond area was estimated before and after failure. The ultimate load was the primary concern since failure occurred suddenly.

Data Reduction

With the bond area and the ultimate load known the max shear stress can be obtained [Gere (1984)] with equation (7.1). This normalized property could be compared between resin systems to evaluate bond strength. However, it was expected that there would be a shear gradient, or distribution along the bond surface.

$$\tau = \frac{P}{A} \tag{7.1}$$

In addition to equation 7.1, a finite element model was developed to capture the shear gradient along the bond surface. The shear gradient was the curve fit and used with the Whitney Nuismer Criterion (equation 7.2) to evaluate a characteristic length [Nuismer (1974)]. This characteristic length is an approximation of how much of the bonded length is operating at the max strength of the resin.

$$\tau = \frac{1}{a_0}\int_0^{a_0} \tau(x)dx \tag{7.2}$$

Double Lap Shear

The single lap shear test coupon provides limited results [ASTM D4896-89 (1993), Hart-Smith (1990), Skeist (1977)]. Many agree that the test results from the SLS specimens are good for screening analysis or baseline comparison only. The primary limitation of this test is the peel stresses induced from eccentric loading of the asymmetric geometry. Other variables that affect the results are; the thickness of the adhesive and adherend, the stiffness of the adherend, and the bond length.

A new lap specimen has been developed to combat these issues [Hart-Smith (1990)] called the inverse skin doubler specimen. The primary limitation of this specimen is its complexity and machining requirements. Features include tapered inside and outside faces of metal adherends to reduce peel stresses at the edge. The specimen is also symmetric which reduces bending stresses.

This study employed a modified shear lap specimen, which has been called a double lap shear specimen (DLS). The double lap shear specimen is a symmetric version of the single lap specimen. It shares some of the same features as the inverse skin doubler specimen, but does not have tapered adherends. The DLS specimen was used to confirm the SLS test results and should provide more accurate results due to the mitigation of bending.

Double Lap Shear Configuration

The DLS specimens were almost as simple as the SLS specimen. The primary difference was that a second bond interface had to be introduced to maintain symmetry.

A spacer shim was also used at the gripped end to reduce bending. An example of a DLS specimen is shown in Figure 7.3.

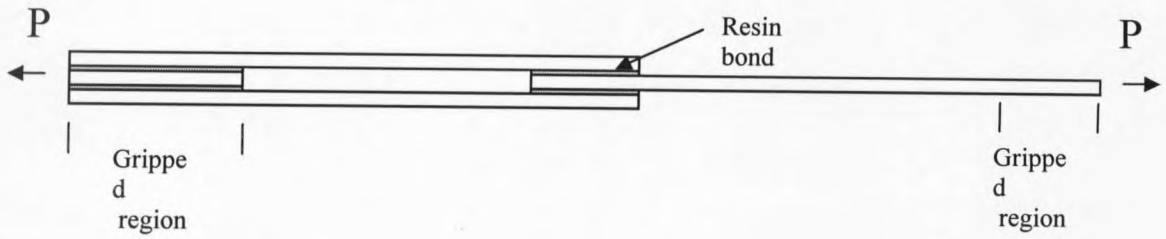


Figure 7.3 Double Lap Shear (DLS) Specimen

Double Lap Shear Construction

Three pieces of parent metal were required for the construction of the DLS. Two metal strips were bonded to the outside of a center adherend to form two bond surfaces. These measures were taken to preserve specimen symmetry. A spacer shim was incorporated into the design to prevent bending stresses from occurring. Similar preparation was applied to the DLS as was to the SLS.

Double Lap Shear Test Procedure and Data Reduction

The testing procedure for the DLS was identical to that of the SLS specimen. Both bond areas had to be measured and spacer shims were used to ensure alignment. The failing load was divided by the total bond area or total bond width, depending on the metric desired.

Miniroot

The miniroot is a three dimensional version of the shear lap specimen. This specimen has the added feature of accommodating mechanically enhanced insert material. This allows for a wide range of mechanical interlock parameters to be evaluated. This specimen also provides an evolutionary step to the more complex root structure shown in Figure 7.1.

Miniroot Construction

A mold with dimensions of 23 x 81 cm was used to make approximately 20 miniroot structures at a time. The final product was made of 16 layers of 0 degree oriented fibers. To manufacture the miniroots 8 layers of fabric would be cut and placed into the mold. At this point, the insert material was placed so that half of the length would be on the eight layers of fabric and half would exceed the gasket boundary. The gasket on this edge was half of the thickness of the three sides that did not have insert material crossing the boundary. With the insert material in place the remaining eight layers of fabric would be placed in the mold on top of the insert. The insert was then "sandwiched" between 16 layers of fabric. The glass half of the mold was then clamped in place and the resin was injected via the RTM method. Typically some curing was required depending on resin system used. Curing involved heating the specimens for usually 1 hour at 60 °C. Once the plate of 20 miniroots was cured it was then cut into individual specimens. A variety of different geometries, resin systems, and insert materials are included in Figure 7.4.

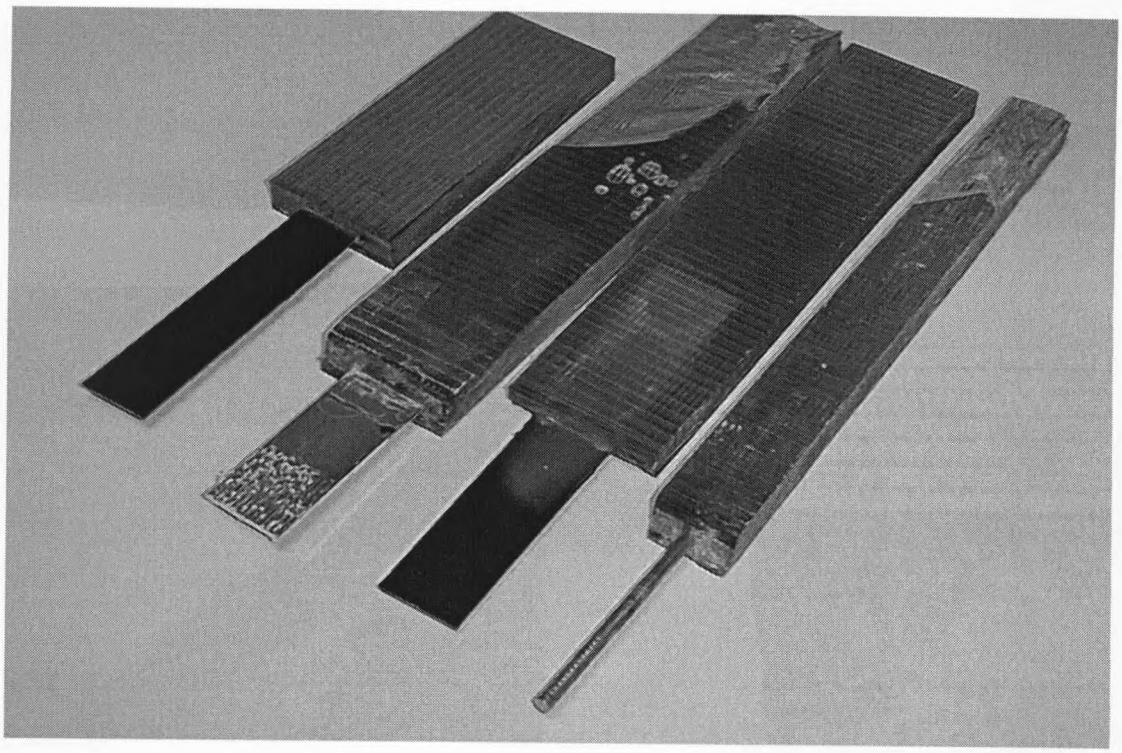


Figure 7.4 Array of Miniroot Variations

Miniroot Configuration

There are three basic regions of the miniroot. There is a metal only grip section. There is the interface test section and there is a composite only grip section. The interface section is the focus of this specimen but the other regions were required to accommodate testing apparatus. These regions are labeled and shown in Figure 7.5.

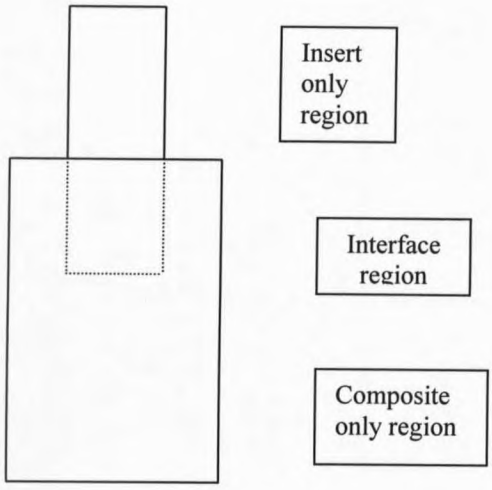


Figure 7.5 Miniroot Configuration

Testing Procedure

The design of the miniroot structure was such that the metal insert could be clamped in an Instron jaw and the composite structure could be clamped in an opposing jaw. The section of the miniroot containing the jaw attached to the crosshead would then be moved upward slowly applying tension to the entire cross-section. Eventually one of three outcomes would occur. The metal specimen would fail; the composite only section would fail; or the bond between the insert and the composite housing would fail. Force and crosshead displacement were tracked and recorded. Generally, either debonding occurred or the metal insert failed. In cases where the metal insert fails, a lower limit of bond strength can be calculated.



Figure 7.6 Lap Shear and Miniroot Testing Apparatus

Data Reduction

The recorded force and deflection were plotted. An average shear stress was calculated and tabulated with equation 7.1. Additionally, an FEA model was developed to evaluate the shear stress distribution at the interface. From this the peak shear stress could be extracted from the gradient and the relationship in equation 7.2 could be used to determine an effective bond length.

Sample Results

Preliminary test results indicate that two distinct phenomena occur when the interface fails. Initially a debonding occurs and then some damage tolerance in form of friction exists. This behavior is clearly demonstrated in Figure 7.7.

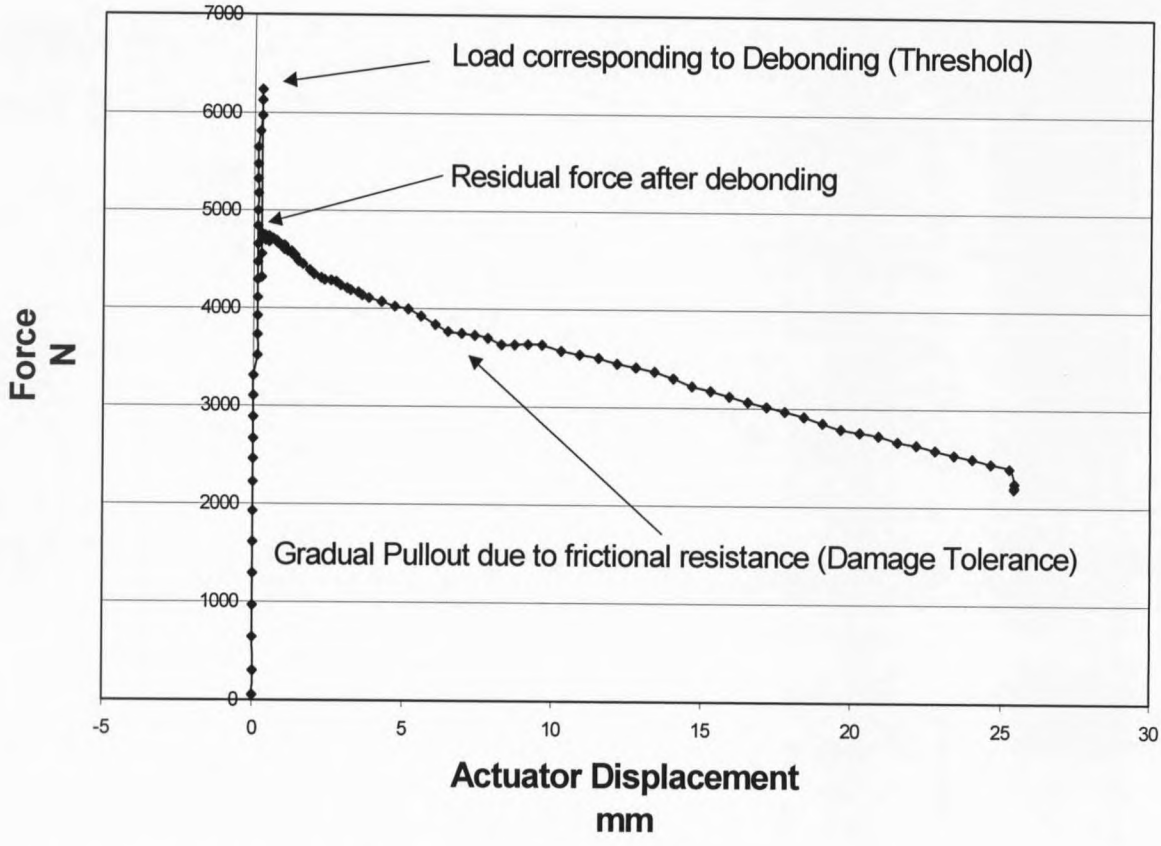


Figure 7.7 Miniroot Failure Characteristics

De-bonding

Test data exists in the form of load-deflection graphs. It has been assumed that the steep relationship(initial slope) between the force and deflection represents the steel insert and the composite behaving as a single structure. The sharp drops represent an

increase in compliance and a subsequent de-bonding of the metal insert from the composite casing. Ideally this threshold load associated with de-bonding should be resolved into a failing stress. Most likely the miniroot structure's interface is failing from shear stress. This is the mechanism most likely transferring load from the insert to the composite.

Pull-out

Once the bond between the resin material and the insert has broken the curve levels off and the load gradually drops off. Damage tolerance exists in the form of friction. Residual stresses create tractions and forces normal to the insert surface, which induce this friction. The tractions responsible for this friction are either from differing elastic properties or residual stresses from curing process, which involves a 40 °C temperature gradient.

Metal Interface Experimental Results

The three specimen described earlier were constructed and tested based on methods outlined. The single lap shear, double lap shear, and miniroot test results will be discussed on an individual basis. The shear lap specimen were used to evaluate chemical bond capabilities, while the miniroot specimen were an evolutionary step used to evaluate mechanical bond capabilities.

Parametric Study

Three different resin systems were used to construct several different SLS, DLS. and miniroot structures. Other variatons included surface treatment, insert or lap

material, and structural alterations. These parameter that were investigated will be briefly discussed as well as the test matrix and specific experimental results.

Surface Treatment

The surface treatment greatly affects the bond characteristics of metals. Chemical alterations in form of etchents can increase bond strength. Phosphoric acid was used for steel and ASTM D 2651-90.was followed for aluminum. Mechanical conditioning, such as sanding and bead blasting increases bond strength as well. Additionally the bond surface can be tapped, knurled, or modified by other machining processes to enhance the structural bond.

Elastic Properties

The elastic properties of the composite affect load sharing. These properties such as shear modulus, Poisson's ratio, and Young's modulus determine the manner in which the force and related stresses are distributed through the material. The magnitude of the interfacial stresses and the associated gradient are strictly a function of the material properties and the miniroot dimensions.

Chemical Bond Characteristics

As stated earlier, the miniroot's ability to with stand loading is based on chemical bond and structural bond characteristics or properties. Each resin system has a unique molecular structure. Vinylesters are different than Polyesters, which vary from Epoxies in molecular structure. Each different type of resin system and particular resin has different bondability with the metals.

Mechanical Bond Characteristics

Measures were taken to improve the overall bond strength by increasing the mechanical bond directly. Alterations were made to the insert surface to enhance the mechanical interlock between the composite and the insert metal. A variety of modifications were made. Ideally each progression of mechanical bond improvement would approach the aggressive root structure.

1. Plain
2. Knurled
3. Threaded

Knurling

This surface treatment was applied to the round specimens only due to ease of machining. Three different patterns were applied. A straight or longitudinal groove was used as well as a criss-cross or diamond pattern similar to a typical knurled handle.

Threading

In addition to knurling, threading was also applied to some specimens. The threads were applied with a simple tap. The threaded specimens provided and evolutionary step from the simple miniroot structure to the complex root structure.

Resin Systems

Three candidate resin systems were used to construct the shearlap and miniroot test specimens. The polyester 63-AX-051 system is an unsaturated, orthophthalic polyester manufactured by Interplastics corporation. Extensive research has been

conducted on this system by DOE/MSU research effort. Due to the abundance of the information available on this system, it was chosen as a baseline [Orozco (1999)]. Another improved version of the above resin system was the isopthalic polyester resin. The vinylester 8084 system is a rubber toughened epoxy vinylester provided by Dow Chemical. This system has shown better performance with regard to fracture toughness and tensile strength compared to the baseline polyester [Orozco (1999)].

Layup Variations

When measures were taken to improve the mechanical interlock between the composite housing and the metal insert, the fiber orientation can play an important role. Orienting the fibers in 45 degree manner could allow an improved interlock between the fibers and the machined insert. The layers of fabric adjacent to the insert were varied in orientation to evaluate the affect of fabric interlock.

Insert Material

The elastic properties and dimensions of the insert material also affect the manner in which load is shared and distributed. The insert materials used in this study were isotropic. The major difference in varying the insert material was the elastic modulus. Steel also has different bond characteristics than aluminum. The insert material can affect both the chemical bond as well as the load sharing properties.

Insert Coating

To provide a reduced shear transition between the insert material and the composite housing material, the inserts were sometimes coated with an epoxy material.

This allowed for a transitional stiffness as well as an enhanced bond. The intermediate material was thought to possess superior bond characteristic to both the composite and the insert as compared to the bond characteristics of the composite to the insert directly. Additionally some mechanical interlock was achieved from this process. Due to the variance in thickness of the coating some structural interference was created.

Test Matrix

At times several of the discussed parameters were evaluated with one test. To provide a more systematic approach of testing, a test matrix was developed. For each resin system and insert material various treatments were evaluated. Additionally different geometries were investigated. Round and rectangular insert shapes were used to construct the miniroot structures. The table below is a test matrix that shows what combinations of parameters were tested.

Table 7.1 Test Matrix for Composite and Metal Interface Investigation

Resin System	Insert Material	Insert Geometry	Etching	Epoxy Coating	Smooth Surface	Knurled Surface	Threaded Surface
Ortho-polyester	steel	Round			M	M	M
		Rectangular	S and D		S,D and M		
	aluminum	Round			M	M	M
		Rectangular	S and D	M	S,D and M		
Vinylester Resin System	steel	Round					
		Rectangular	S and D				
	aluminum	Round					
		Rectangular	S and D	M	S,D and M		
Isopolyester	steel	Round					
		Rectangular	S and D				
	aluminum	Round					
		Rectangular	S and D				
S = Single shear lap, D = Double shear lap, and M = Miniroot							

Single Lap Shear (SLS) Experimental Results

Single lap shear specimens were constructed of aluminum and steel adherend material. The adhesive or resin was one of three resins investigated. An orthopolyester was used as a baseline to compare to an isopolyester and a toughened vinylester. A test matrix shown in Table 7.1 displays the combination of materials tested. The adherends were also prepared with an industry accepted etchant to enhance the bond strength. The SLS samples were then compared to un-etched samples for both metal adherends for all three resin systems. Generally 6 specimen were tested, in some cases there were less.

Each specimen was tested as described. The failing or peak load was recorded and used for data reduction. The experimental strength was based on the failing load and total bond area (equation 7.1). It has been suggested that the length of the bond does not contribute to the strength as much as the width of the bond due to the shear stress gradient [Skeist (1977) and Hart-Smith (1990)]. As a result the failing load was also divided by the width only. The results for both data reduction techniques are included. The load per area results and the load per unit width results are shown in Table 7.2 and 7.3 respectively.

Table 7.2 Single Lap Shear Test Results for Shear Strength

	Vinylester	Orthopolyester	Isopolyester
Adherend Material and Surface Preparation	MPa (cv in %)	MPa (cv in %)	MPa (cv in %)
Aluminum (Not Etched)	3.88 (10.2)	2.61 (14.3)	2.76 (12.0)
Aluminum (Etched)	8.29 (40.4)	2.89 (9.74)	5.41 (25.9)
Steel (Not Etched)	5.4 (19.4)	4.35 (19.7)	4.89 (6.18)
Steel (Etched)	7.66 (19.0)	1.98 (20.3)	3.54 (8.55)

Table 7.3 Single Lap Shear Test Results for Load/Unit Width

	Vinylester	Orthopolyester	Isopolyester
Adherend Material and Surface Preparation	N/mm (cv in %)	N/mm (cv in %)	N/mm (cv in %)
Aluminum (Not Etched)	96.3 (8.21)	67.7 (18.9)	83.5 (12.9)
Aluminum (Etched)	252 (34.1)	157 (11.4)	158 (25.8)
Steel (Not Etched)	139 (20.0)	120 (24.8)	138 (11.4)
Steel (Etched)	224 (17.5)	98.2 (24.7)	112 (11.1)

In almost all cases, the Vinylester system outperformed the Isopolyester and the Orthopolyester resins. The etchant improved the bondability for all three resins when aluminum was used for an adherend material. However, only the vinylester system

showed an improvement from etching for the steel adherend SLS samples. The (load per unit width) results generally follow the shear strength results. Both indicate that steel bonded better than aluminum when no etchents were used. When etchents were used the aluminum SLS specimen exceeded the steel. The load per area results and the load per unit width results compared closely. Since the bond length was consistent the either metric would probably be adequate.

Double Lap Shear (DLS) Experimental Results

The DLS specimen was very similar to the SLS specimen. The primary difference is that the DLS specimen is more symmetric and is less likely to effected by bending. As a result the DLS test results are expected to be a better representation of the upper limit of the bond capabilities. As with the SLS specimens the Double Lap Shear (DLS) specimens were constructed of two different metal adherends and bonded with three different resins. This was done for etched and non-etched variations. A test matrix is provided in Table 7.1 and the test results are shown in Table 7.4.

Table 7.4 Double Lap Shear Test Results for Shear Strength

	Vinylester	Orthopolyester	Isopolyester
Adherend Material and Surface Preparation	MPa (cv in %)	MPa (cv in %)	MPa (cv in %)
Aluminum (Not Etched)	4.26 (10.1)	3.12 (7.10)	3.26 (15.5)
Aluminum (Etched)	7.51 (5.81)	4.49 (13.7)	6.06 (7.82)
Steel (Not Etched)	6.55 (4.92)	6.11 (2.73)	6.58 (30.5)
Steel (Etched)	8.27 (16.9)	4.57 (8.92)	4.76 (18.9)

In general, the DLS results followed the SLS results. The average failing stress was increased due to the reduction in bending. The vinylester resin system exceeded both the polyester systems. The isopolyester system generally performed slightly better than the orthopolyester resin. In the case of the DLS tests, steel consistently outperformed aluminum. The primary exception was the etched steel and polyester resin systems. Pre-treating with acid etchant actually reduced the bond strength for both the SLS and DLS test configurations with steel inserts.

The SLS and DLS test specimen worked well to evaluate parameters such as resin material, insert material, and the effects of etching. These simple tests worked well to evaluate the overall chemical bondability of the resins and metal inserts. In order to

investigate the mechanical effects of various degrees of interlock, the miniroot test was required.

Miniroot Experimental Results

Several interesting comparisons were made with this unique test specimen. The miniroot test configuration accommodated such variations as insert shape, intermediate adhesive coatings, and various levels of mechanical interlock. These parameters will be discussed individually.

Insert Coating Effects

As stated, it was expected that using an intermediate bond material might enhance the overall bond strength. A standard Devcon produced epoxy adhesive was applied to the surface of the metal inserts. This adhesive coating was allowed to dry and the entire ins Figure 7.8 Effects of Using an Epoxy Coating as an Intermediate Adhesive Layer This was done with aluminum inserts and two resin systems. For both the polyester and vinylester systems controls were also tested that were not coated with the epoxy material. The established testing procedure was used to apply force until the specimen debonded or some type of failure occurred. In cases of debond the force was applied after failure to capture the damage tolerance of the bond. Graphical representation of this is shown in Figure 7.8.

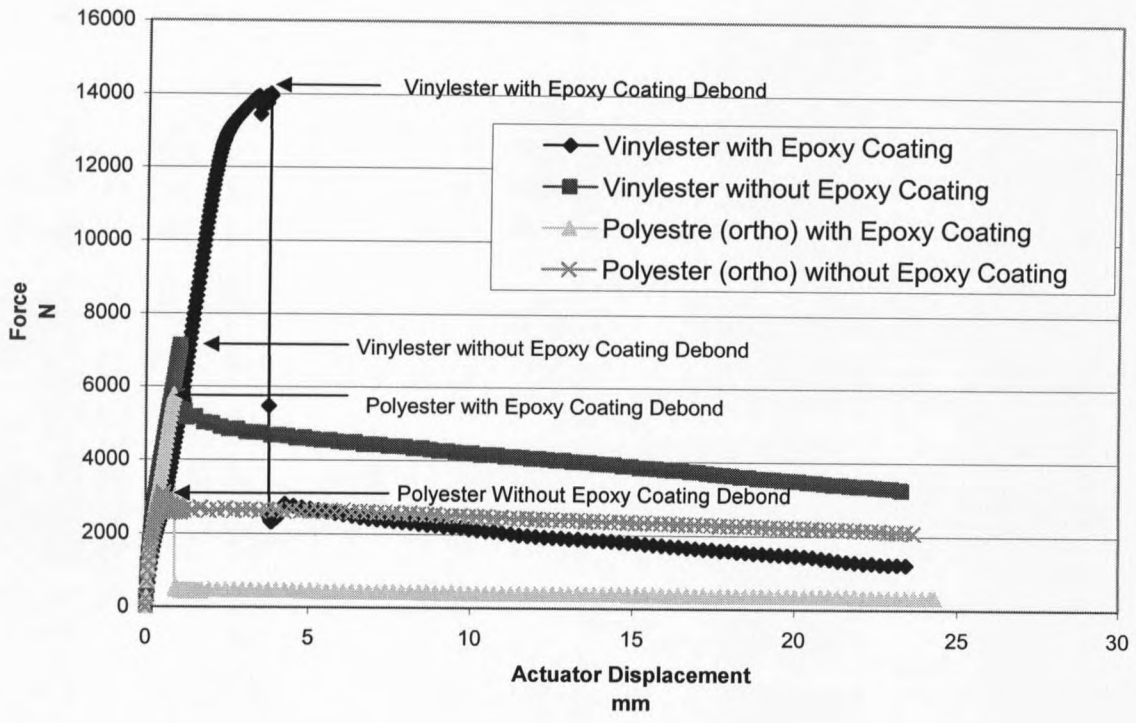


Figure 7.8 Effects of Using an Epoxy Coating as an Intermediate Layer

The epoxy coating improved the debond load for both resin systems by a factor of about 2. As with the SLS and DLS specimens the vinylester exceeded the orthopolyester resin shown. The average shear strength and load per unit width were determined from the experimental data shown in Figure 7.8. This information is summarized in Table 7.5. Four specimen of each type were tested and the average values are displayed with the coefficient of variation included as a percent.

Table 7.5 Results of Including an Epoxy Coating

Resin Type	Insert Material	Insert shape	Coating	Stress MPa	Load/width N/mm
Polyester	Aluminum	Rectangle	None	0.71 (3.2%)	63.6 (1.9%)
Polyester	Aluminum	Rectangle	Devcon Epoxy	1.22 (18%)	108 (15%)
Vinylester	Aluminum	Rectangle	None	1.69 (16%)	135 (10%)
Vinylester	Aluminum	Rectangle	Devcon Epoxy	3.14 (8.4%)	256 (2.4%)
Stress was found as load / total bond area cv shown in (%)					

These results are consistent with the shear lap (SLS and DLS) results qualitatively. The SLS and DLS samples typically withstood more stress than the miniroot versions. This is because the length of the bond does not contribute as much as the width of the bond. Load per unit width metrics were also reported.

Geometry

The special design of the miniroot test coupon provided a means to test round and rectangular inserts. Steel and aluminum rods were sandblasted and specimens were constructed based on the methods previously outlined. It was anticipated that the round specimens would tolerate more stress because of the reduction in stress concentrations associated with the corners of the rectangular inserts. Steel and aluminum round inserts were used to construct polyester miniroots. The specimens were tested using the methods discussed and the apparatus shown in Figure 7.6. Graphical representation of the debond behavior for the round inserts is displayed in Figure 7.9.

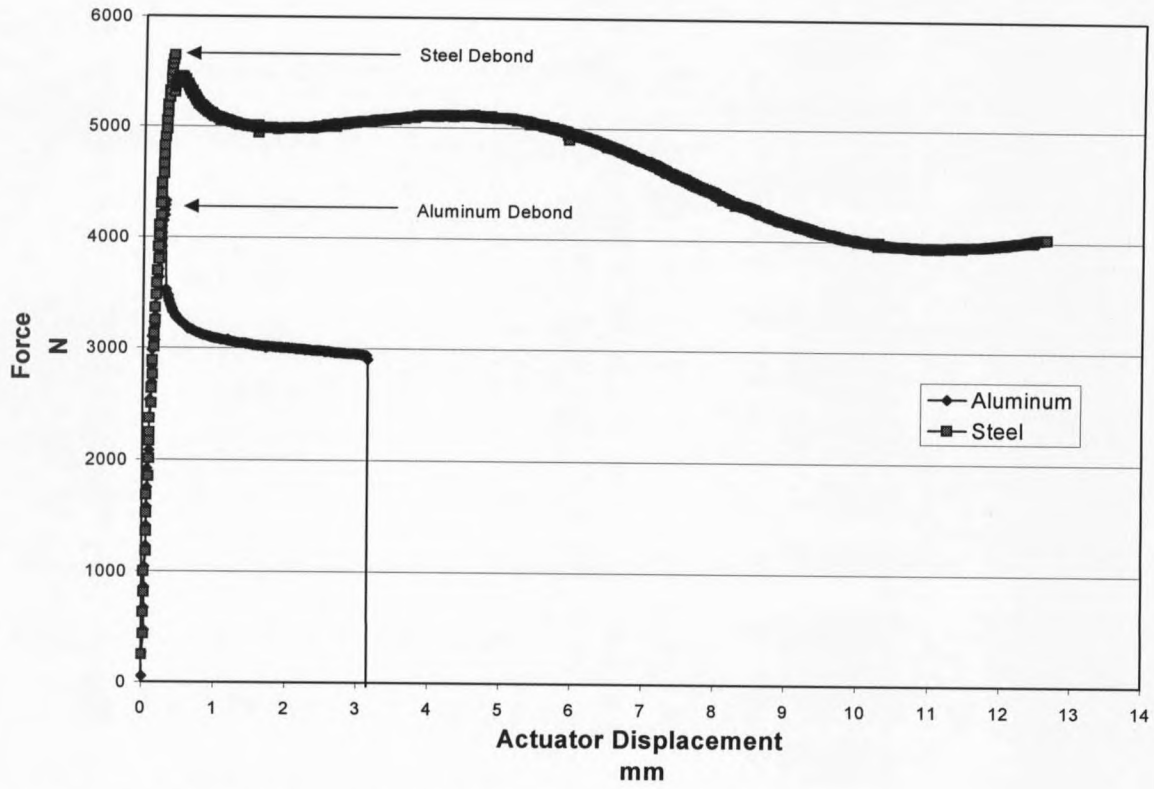


Figure 7.9 Debond Behavior of Miniroots with Round Inserts

The steel material outperformed the aluminum as in previous cases. The overall stress was significantly better for the round geometry than it was for the rectangular miniroots. The load per circumference and average stress or load per area, are shown in Table 7.6.

Table 7.6 Comparison of Aluminum and Steel Rod Miniroots

Aluminum		Steel	
Load / Circumference	Load / Area	Load / Circumference	Load / Area
N/mm	MPa	N/mm	MPa
860	35.1	1123	47.6

Mechanical Interlock

Additional tests were conducted to evaluate the mechanical interlock and parameters that would effect it. Specimens were prepared with varying layups and mechanical enhancements such as knurling. In all cases where some form of mechanical interlock was provided, the steel specimen either yielded or completely failed before any damage occurred at the bond interface. This type of behavior is shown in Figure 7.10.

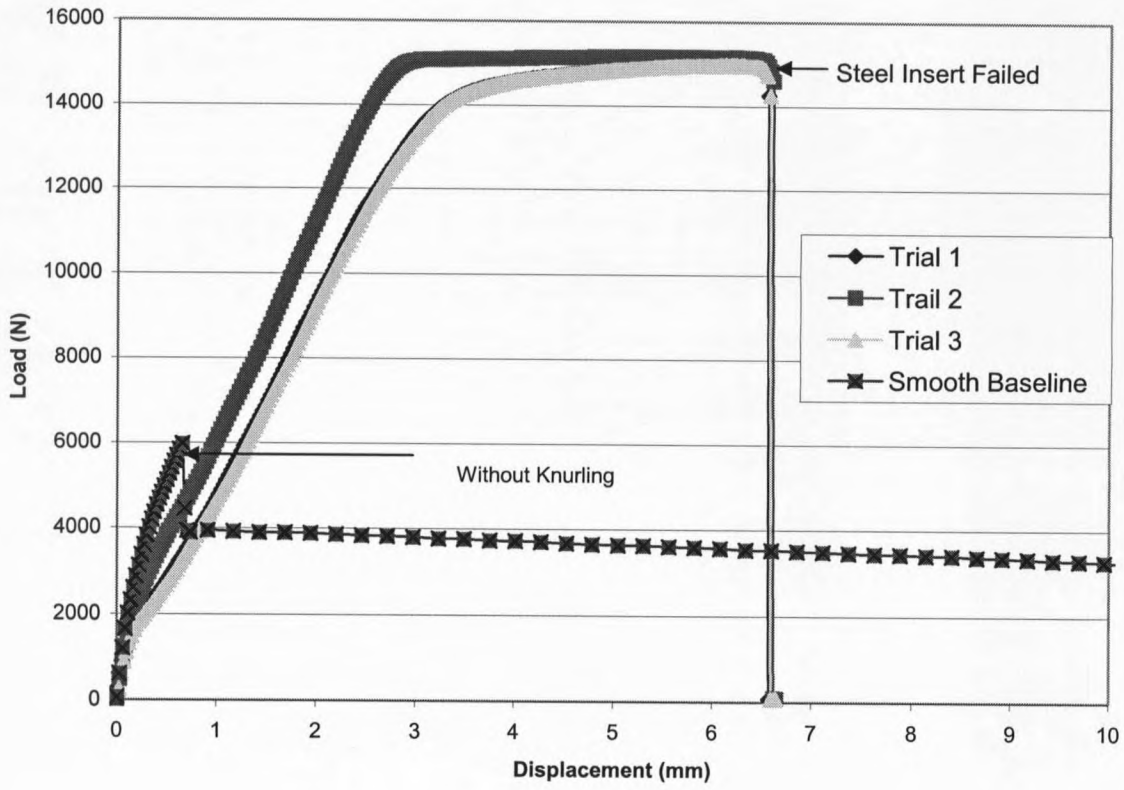


Figure 7.10 Failure of 45 Degree Diamond Knurled Steel Insert Miniroot

Metal Interface Numerical Study

Three separate specimens were developed and used to evaluate the bond performance of composites and metals. The SLS, and the MR specimens required the use FEA for data reduction beyond basic shear relations (equation 7.1). Finite element models were used to extract the shear stress distributions along the metal/resin or metal/composite interface. The distributions provided improved data reduction options and accounted for singularities (equation 7.2). Details regarding the formulation, construction, and execution of these models follow on an individual basis.

SLS Motivation and Approach

A near replica model of the SLS test specimen was constructed. Details regarding the adhesive or resin thickness, bond dimensions and material stiffness were all accounted for in this simulation. The shear distribution along the adherend/adhesive interface was captured and compared to basic elasticity solutions. The stress gradient was expected to be a function of the elastic modulus ratio of adherend to adhesive. A relationship for peak stress singularity based on material stiffness ratios is shown in Figure 7.11

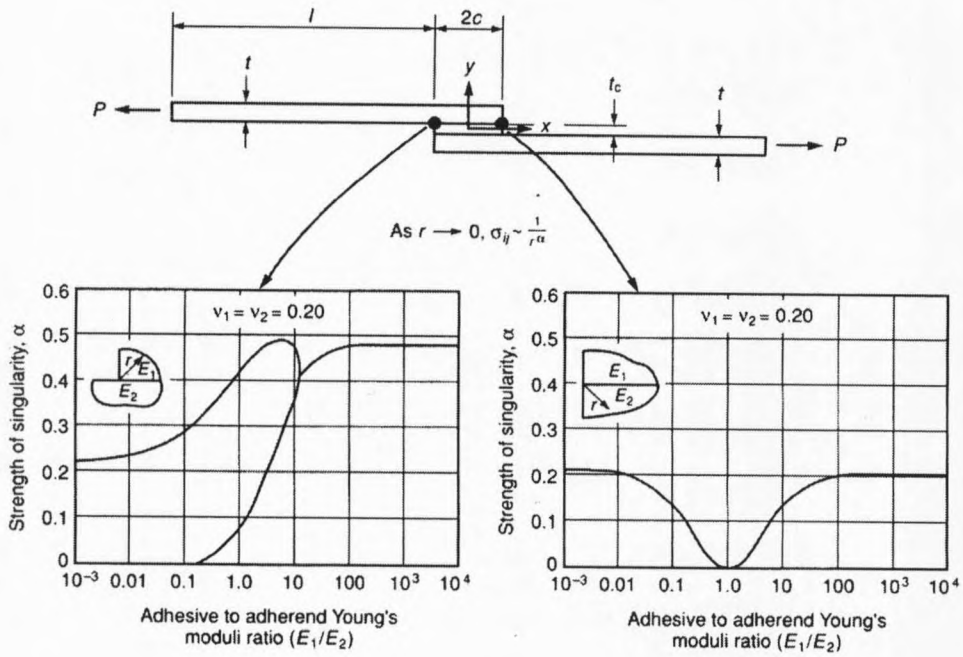


Figure 7.11 Shear Stress Singularity Effects

Model

The FEA model represented both adherend strips and the resin bond region between. Symmetry was not used to any advantage. A two-dimensional analysis was used. Areas were used to model the adherend and resin regions.

Plane82 elements were used with plane stress option activated. Mesh details presented by [Penado and Dropek (1990)] were followed for comparison. Generally at least 3 elements were used through the thickness of the resin bond. The mesh was refined at transition regions at the boundary of the bond. Details regarding the mesh and boundary conditions are included in Figure 7.12.

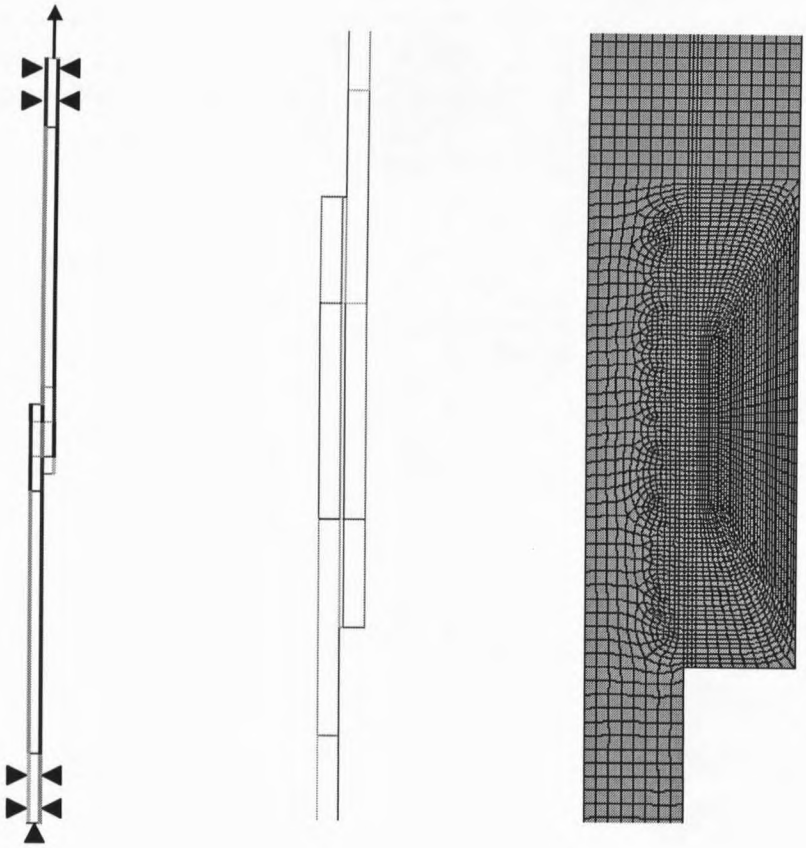


Figure 7.12 SLS FEA Model and Mesh Detail

Results

The model was solved with the maximum load applied and the shear stress distribution along the interface was mapped and plotted. Elasticity solutions provided by Goland and Volkerson were also used for comparison to the FEA solution. From this, the peak shear stress could be determined as well as the entire shear stress gradient along the bond. The results of these solutions are shown in Figure 7.13.

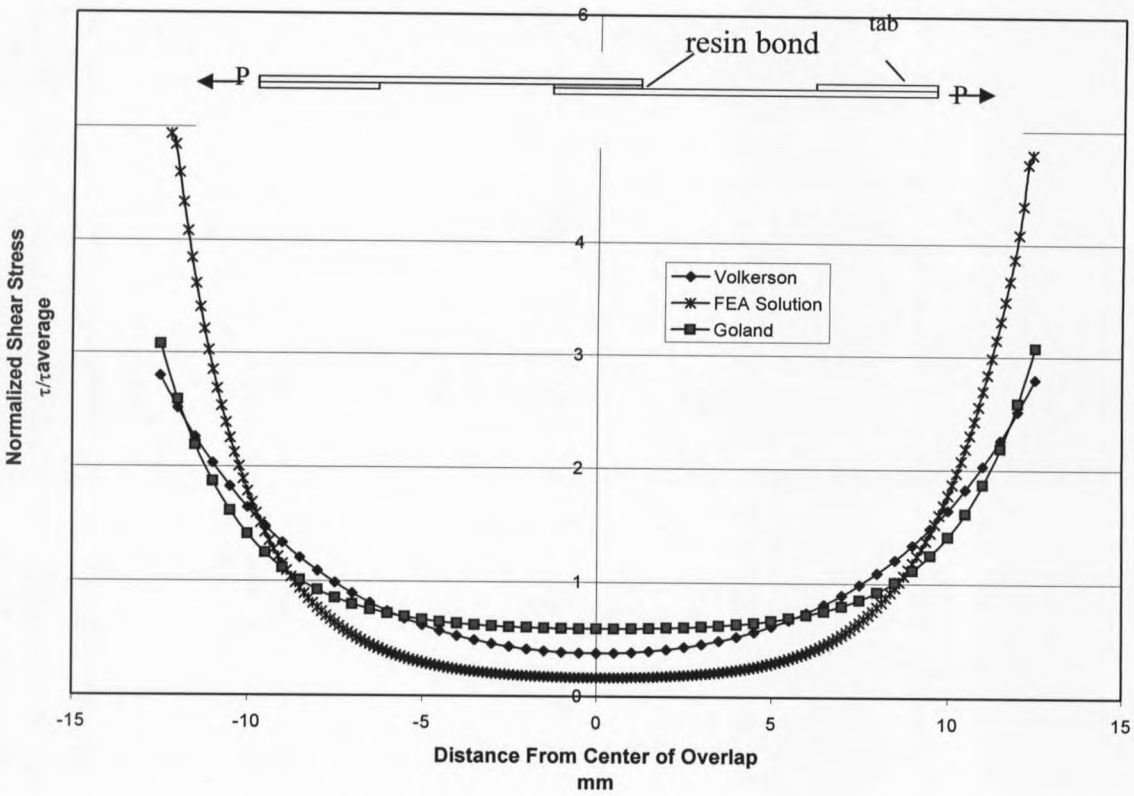


Figure 7.13 Lap Shear Analytical and Numerical Results for Etched Vinylester

The peak stress was typically found to be a factor of 4 to 5 times that of the average stress. The average stress was found with use of equation 7.1. A third order polynomial curve fit was used to approximate the FEA shear stress gradient. This relationship was then used in accordance with equation 7.2. From this, a characteristic length was determined. This represents the length of the bond that performed at the shear strength of the resin. The characteristic length could then be divided by the actual bond length to determine a bond efficiency. This was done for the etched vinylester system shown in Figure 7.13. The characteristic length was found to be 17.7mm with a bond efficiency of 71%.

Miniroot Motivation and Approach

It was known that there would be definite affects of the miniroot's structure on the behavior of the bond. It was assumed that a shear stress gradient between the composite surface and the insert surface was responsible for the debonding of the insert. Experimentally the debond load was resolved into a bond strength by dividing the force by the penetrated surface area. However it was suspect that a uniform stress state did not exist, as was shown by the lap shear results.

To better assess the material behavior and to develop a means to quantify the bond strength, FEA was implemented. The intent was to capture the stress behavior at the interface and ultimately use the model to explain this behavior and possibly predict performance.

Model

The ANSYS code was used to evaluate all test cases. A macro was developed to generate geometry, mesh elements, constrain and load the miniroot structure. Brick (solid 45) elements were used to compose a full 3-D model for the De-bonding model. Quarter symmetry was utilized to reduce the number of elements required. Several solutions were obtained with differing meshes, order of element, and geometry. Initially 16,880 elements were required for this model. This provided 1mm x 1mm elements which corresponded to 5 elements through the thickness for the composite and 1 element through the thickness for the steel insert. The model was resolved with a solid 95 element to test convergence. That second solution verified the original.

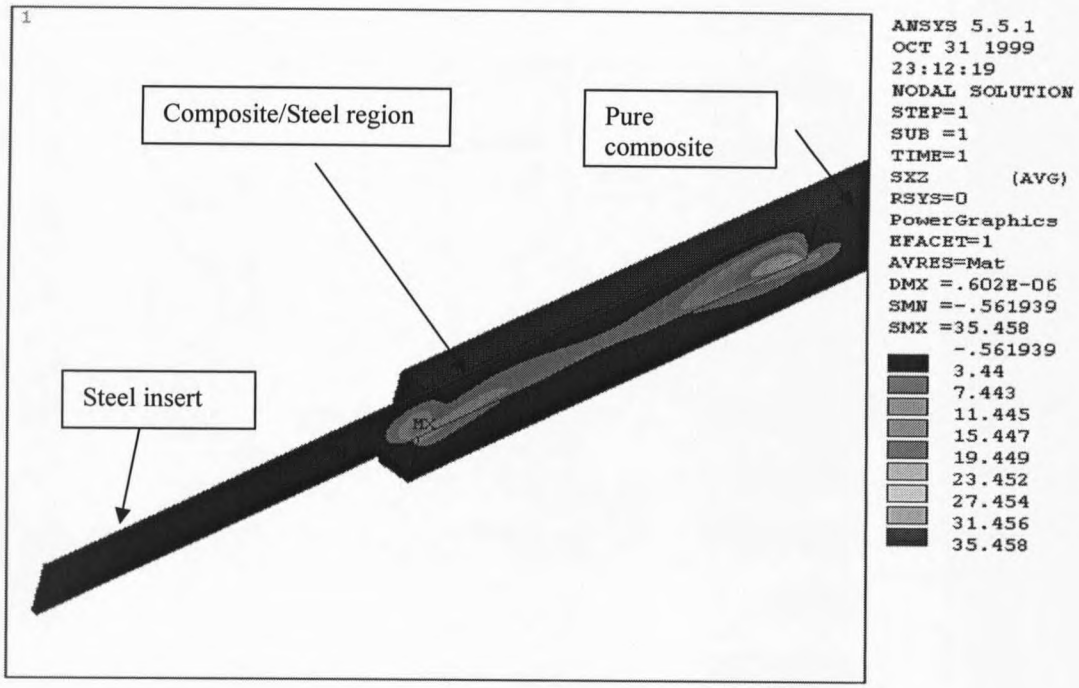


Figure 7.14 Miniroot FEA Shear Stress Plot for Vinylester

Results

The model was then solved in load control with a pressure applied to the leading insert edge proportional to the experimental debond load. In the ANSYS post processor, the insert volume removed to reveal the stress gradient on the composite bond surface. The peak stress was found to be 35 MPa. The shear stress gradient was also plotted for the miniroot specimen. This is shown in Figure 7.15 for the vinylester system without etching and an aluminum insert.

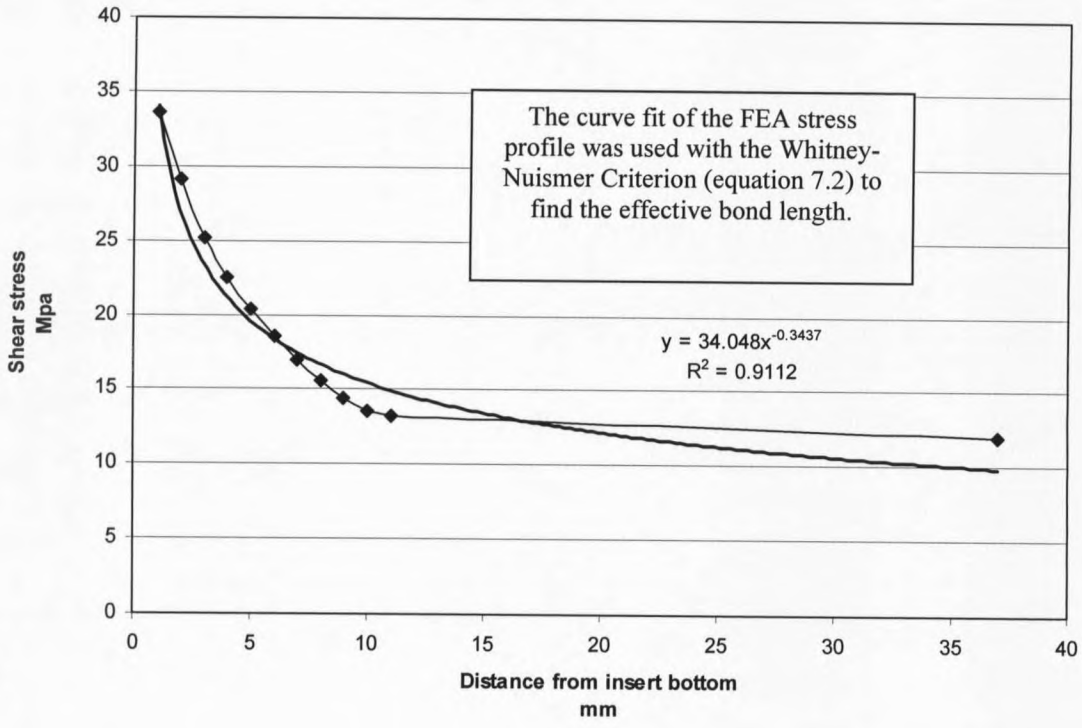


Figure 7.15 Shear Stress Distrubution From Peak to Level Stress

Equation 7.2 was used on the profile in Figure 7.15 to produce an effective bond length of 19mm. Dividing this by the total length of the bond produced a bond efficiency of 25.2%. The etched lap shear specimen had a much better bond efficiency than the miniroot version without the etching process [ASTM D2651-90 (1993)].

Summary for Case Study IV

The data base-screening approach was applied to this case study. The primary goal was to develop a series of tests that could be used to test various parameters that relate to the bond performance of composite and metal interfaces. An additional goal of this study was to determine if the bond performance could be quantified as a material property and used as an analytical design tool. A special evolution of test specimen and testing procedures were developed to evaluate the performance of metal to composite bond interfaces.

Unique data reduction techniques were employed to characterize and quantify the bond performance. In general, the length of the interfacial bond contributes less to the strength than does the width of the bond. As a result experimental load limits were compared to overall bond area as well as bond width. Another hypothesis was that a peak stress singularity might be a consistent limit for bonds of the type investigated. A final method of reduction investigated was the Whitney-Nuismer Criterion. This approach determines an effective bond efficiency based on a stress distribution extracted from a finite element analysis.

At the onset of the project these four techniques were to be applied at each level of test geometry (single shear lap, double shear lap, and miniroot specimen). Potentially, a technique that showed promise could be extended to root test specimen and ultimately to a blade design detail.

From the experimental test results obtained and the applied data reduction techniques, no clear quantity proved to be repeatable at all levels of geometry

development. A primary problem with the testing conducted was that the metal adherends were routinely the limiting factor of the test specimen evaluated. Even in the case of the single and double shear lap specimen the bond typically would not fail until the metal insert began to yield and contract away from the bond. Similar behavior was observed for the smooth rectangular miniroots. For the mechanically interlocked versions of the miniroot, the insert material always failed completely before the bond would break. This behavior is consistent at the full-size root level also.

The screening process experimentally provided useful qualitative results. It was found that etching the adherends improved the chemical bond characteristics significantly. Additionally, the intermediate epoxy coating improved the chemical bond strength by a factor of almost 2. The vinylester resin system exceeded the polyester competitors for bond strength. The screening shear lap test used worked well to investigate these modifications quickly and affordably.

This investigation reinforces the need to test composite structures and materials substantially. The behavior of the bond failures was predictable but, the load levels could not presently be predicted.

CHAPTER 8

CONCLUSIONS AND FUTURE WORK

A general methodology was developed to quantify the interlaminar fracture toughness of composite materials. Four separate case studies were investigated to help establish and validate the approach. The approach consisted of two distinct paths. An analytical approach that employed the use of FEA and basic G (strain energy release rate) properties was investigated as well as a screening approach that compared candidate composites at a material level and other subsequent stages of structural development. Ideally, some blend of these two options is most desirable. It was found that substantial experimental validation is required to establish confidence in FEA models. Occasionally FEA was required for basic data reduction and experimental interpretation when the analytical approach was abandoned. The experimental (screening) approach and the FEA analytical approach were very complementary. Neither approach uniquely quantifies the complex behavior of composites. The database-screening approach proved worthy for every project and required limited resources.

This chapter contains conclusive results from each case study that can generally be applied to other topics and projects. Additionally, a structured approach to composite design is offered. The majority of the conclusions and suggestions are related to screening processes and their importance to composite material design.

Composite Material Design Process

1. Apply analytical methods available to evaluate forces and stresses on component desired. With intended use of structure known, evaluate design drivers and potential weaknesses.
2. With the aid of classical lamination theory, develop an architecture scheme that best addresses the above critical loading scenario. Details such as fiber type, resin system, fiber volume, and fiber orientation should be decided at this stage. Other criteria should also be met, such as glass transition temperature, environmental affects of moisture, and other material properties that were not addressed by this study.
3. With ideal architecture candidates formed, the initial construction of simple plates should be conducted. Specimens can be sampled from these plates which can then be subjected to tensile testing, mode I fracture testing, static flexure testing, etc…
4. Empirical methods should be applied to test data to evaluate basic strength and fracture toughness properties. Damage should be inspected to assess the limitation of the materials performance. Empirical testing of these plates should provide important estimates of material properties. Knowing these properties will be important, because these will need to be implemented into FEA models or used with other means to predict and avoid structural failure.

Rival materials can be compared at this point. This serves as a screening process. The materials that show the most promise at the completion of step 4 should then be developed into desired geometry or structure. FEA Models of test specimens should be developed to confirm testing results. These models can eventually evolve to predict the behavior of complex structures that will be made from the composite materials.

5. Iterate and adjust parameters to refine and improve the overall performance of the composite material.
6. Construct actual part or component. Some intermediate testing and screening may be necessary.

Importance of the Screening Process

Fracture mechanics as applied to composites is not an exact science. It is difficult to first assess fracture related material properties, and to second use them as a predictive tool in design. Using the test and analysis methods outlined can serve as an effective approach to compare candidate materials at a developmental level. The material properties obtained from this methodology could then be used with the FEA techniques presented to predict damage or failure in simple structures.

Case Study Review

Case study I and case study II were material property investigations that resulted from full-scale failures. At the point of failure, little was known about the actual properties of the materials used. Additionally, limited structural analysis had been conducted with regard to the final product.

The developmental screening process provided both of these sponsors with a means to compare simple composite architecture alternatives. It also would have provided them with important material properties to use for failure analysis.

Case study III was a good example of a classic application. Even in cases where initial attempts are successful, a screening process has value. In case study IV the root structure developed was performing satisfactorily. However, there were several unknown parameters. Limited iterations were made to arrive at the successful root structure. Improving on this design required some backtracking and down scaling.

Case Study I Composite Aerofan Blade Evaluation

- Excessive through thickness reinforcement of composite architectures sacrifices in plane properties to unacceptable levels.
- Through thickness reinforcement significantly increases fracture toughness. Some optimized percentage of cross-stitching could provide an ideal blend of delamination resistance and necessary in plane properties.
- Most of the reinforced material behaved in a bilinear fashion. Ideally, an Aerofan blade should maintain crisp linearity up to threshold. This is because in the event of a collision, blade survival and engine survival would be greatly reduced due to an unbalanced deformed semi-damaged blade.
- The 5 series material possessed the most impressive static and dynamic flexure strength of 845 MPa and 745 MPa respectively. MSU produced materials have rivaled this performance with equal or greater fracture toughness. Some investigation should be conducted with other resin systems,

because possibly the difficult processing requirements of PR 520 may be inhibiting bonding performance or other process events.

Case Study II X-33 Fuel Tank Investigation

- The usage of sandwich theory to increase stiffness and strength introduces a bond layer. This bond layer possesses some fracture toughness but still may limit the overall performance of the material.
- The lobe 1 replacement material performed better in all regards except transverse compression. This exception was most likely related to the aspect ratio of the specimens. The compression test was effectively a critical buckling analysis. The interfacial bond was improved for lobe 1 to the point that core failure occurred during mode I, and transverse tension testing.
- G_{II} values were typically a factor of 10 larger than the G_I values. This might indicate that any fracture type failure would most likely be mode I. However this depends greatly on the loading, not just the fracture resistance. It should be noted that some shear was present during mode I testing due to the geometry of the test specimen this was observed and confirmed with the aid of FEA analysis.
- Foam reinforcement material outperformed the honeycomb core. Foam splices were able to detour cracks from the core into the facesheet.
- Employing these testing techniques could have prolonged the X33 space program since its ultimate limitation was the honeycomb fuel tanks.

Case Study III Aerospace Composite Resin Characterization

- Strength properties were not necessarily proportional or inversely proportional to interlaminar properties. This requires a dedicated assessment or testing to characterize the composite's fracture toughness.
- Mode I performance did not always follow Mode II.
- Impact testing provided a means to evaluate strain rate sensitivity as it relates to interlaminar fracture.
- Relationship between laminate microstructure and interlaminar fracture observed with SEM technology.

Case Study IV Metal Interface Evaluation

- Simple tests provided the most results.
- FEA worked well for data reduction and aided in the overall understanding of the load sharing behavior.
- The evolution of tests developed worked well.

Future Recommendations

The scope of this study was broad, and several of the details investigated could be further pursued. These details as well as the global focus of interlaminar fracture characterization will be discussed.

In general, the screening process developed was sensible and simple. The mentality and methodology associated with the process could be extended to other design issues relating to composite materials. Ideally, a generalized design process needs to be established that addresses strength, stiffness, interlaminar fracture, environmental conditions, and fatigue considerations of composite materials. This process could then be applied to optimize a potential composite candidate material.

To implement the screening approach of comparison, design drivers and limitations need to be identified. Pertinent material properties that are related to intended performance can be acquired through subsequent testing. The acquired material properties can be used as a material database for analysis. Analysis can be closed form mathematical solutions, empirical formulas, or finite element codes. Ultimately the analysis can be used as a design tool to minimize expensive testing and construction iterations. The FEA methods presented could be used to avoid interlaminar fracture in damage tolerant structures. However, the current technology needs to be advanced and further validated with examples like those in Case study I and II.

REFERENCES CITED

ANSYS (1998). "Engineering Analysis System", (10th ed) Canonsburg, PA: ANSYS Inc.

ASM V19 (1997) "Fatigue and Fracture" ASM International, Materials Park, OH.

ASTM C 297-94 (1997). "Standard Test Method for Flatwise Tensile Strength of Sandwich Constructions, C 297-94", 1997 Annual Book of ASTM Standards, Vol 15.03, 1997, pp.9-10.

ASTM C 365-94 (1997). "Standard Test Method for Flatwise Compressive Properties of Sandwich Cores, C 365-94", 1997 Annual Book of ASTM Standards, Vol 15.03, 1997, pp.15-17.

ASTM C 393-94 (1997). "Standard Test Method for Flexural Properties of Sandwich Constructions, C 393-94", 1997 Annual Book of ASTM Standards, Vol 15.03, 1997, pp.21-26.

ASTM D 1002-72 (1993). "Standard Test Method for Strength Properties of Adhesives in Shear by Tension Loading (Metal to Metal), D 1002-72", 1993 Annual Book of ASTM Standards, Vol 15.06, 1993, pp.47-49.

ASTM D 2651-90 (1993). "Standard Guide for Preparation of Metal Surfaces for Adhesive Bonding, D 2651 – 90", 1993 Annual Book of ASTM Standards, Vol 15.06, 1993, pp.170-174.

ASTM D 3983-92 (1993). "Standard Test Method for Measuring Strength and Shear Modulus of Nonrigid Adhesives by the Thick-Adherend Tensile-Lap Specimen, D 3983-92", 1993 Annual Book of ASTM Standards, Vol 15.06, 1993, pp.309-317.

ASTM D 4027-92 (1993). "Standard Test Method for Measuring Shear Properties of Structural Adhesives by the Modified-Rail Test, D 4027-92",1993 Annual Book of ASTM Standards, Vol 15.06, 1993, pp.319-332.

ASTM D 4562-90 (1993). "Standard Test Method for Shear Strength of Adhesives Using Pin-and-Collar Specimen, D 4562-90", 1993 Annual Book of ASTM Standards Vol 15.06, 1993, pp.378-380.

ASTM D 4896-89 (1993). "Standard Guide for Use of Adhesive-Bonded Single Lap-Joint Specimen Test Results D 4896 - 89", 1993 Annual Book of ASTM Standards, Vol 15.06, 1993, pp.419-423.

ASTM D 5528-94a (1997). "Standard Test Method for Mode I Interlaminar Fracture Toughness of Unidirectional Fiber-Reinforced Polymer Matrix Composites, D 5528 – 94a", *1997 Annual Book of ASTM Standards*, Vol. 15.03, 1997, pp.271-279.

ASTM E 229-92 (1993). "Standard Test Method for Shear Strength and Shear Modulus of Structural Adhesives, E 229-92", 1993 Annual Book of ASTM Standards, Vol 15.06, 1993, pp.454-458.

ASTM E 399-90 (1992). "Standard Test Method for Plane-Strain Fracture Toughness of Metallic Materials, E 399 – 90", *1992 Annual Book of ASTM Standards*, Vol. 15.03, 1997, pp.509-539.

ASTM E 813-89 (1991). "Standard Test Method for J_{Ic}, A Measure of Fracture Toughness, E 399-90," 1991 *Annual Book of ASTM Standards*, Vol. 03.01, 1991, pp. 738-752.

Astrom, B.T., (1997) "Manufacturing of Polymer Composites". *1st ed.* London, England: Chapman & Hall.

Broek, D. (1996). "Elementary Engineering Fracture Mechanics" (4th edition). Boston, Massachusetts: Kluwer Academic Publishers.

Cairns, D.S., (1999) "Personal Interview," Montana State University-Bozeman, Bozeman, Montana.

Cairns, D.S., (1992) "Static and Dynamic Mode II Strain Energy Release Rates in Toughened Thermosetting Composite Laminates," ASTM Journal of Composites Technology & Research, Volume 14, No. 1, Spring 1992, pp. 37-42.

Cairns, D.S. (1990) "Mechanisms of Fracture and Toughening in Multiphase Materials," 22nd International SAMPE Technical Conference, November 6-8, 1990.

Cairns, D.S. and Lagace, P. A. (1992) "A Consistent Engineering Methodology for the Treatment of Impact in Composite Materials," Journal of Reinforced Plastics and Composites, Vol. 11 April 1992, pp. 395-412.

Carlsson, L.A. (1991) "On the Design of the Cracked Sandwich Beam (CSB) Specimen," Journal of Reinforced Plastics and Composites, Volume 10, July 1991, pp. 434-443.

Carlsson, L.A., Sendlein, L.S., and Merry, S.L., (1986) "Characterization of Face Sheet/Core Shear Fracture of Composite Sandwich Beams," Journal of Composite Materials, 25(1)" 101-116.

Carlsson, L.A.,Gillespie, L.A., and Pipes, R.B., (1986) "On the Analysis and Design of the End Notch Flexure Specimen (ENF) specimen for mode II testing," Journal of Composite Materials, Volume 20, November 1986, pp. 594-603.

Freitas, G. and Fusco,T., (1995) "Z-Fiber Technology and Products for Enhancing Composite Design," Waltham, MA: Aztec Inc.

Gere, J.M.and Timoshenko, S.P. (1984). "Mechanics of Materials" (3rd edition). Boston, MA: PWS-KENT Publishing Co.

Gillespie, J.W.,Carlsson, L.A., and Pipes, R.B., (1986) "Finite Element Analysis of the End Notch Flexure Specimen for Measuring Mode II Fracture Toughness," Composites Science and Technology, Volume 27, pp.177-197.

Griffith A.A., (1920). "Philos. Trans. R. Soc." Vol. A221, London, England, p.163.

Hart-Smith, L.J. (1990). "Rating and Comparing Structural Adhesives: A New Method" Engineering Materials Handbook(Adhesives and Sealants) Vol 3, 1990, pp.471-476.

Haugen D. (1998). "Fracture of Skin Stiffener Intersections in Composite Wind Turbine Blade Structures" Master's Thesis, Montana State University-Bozeman, Bozeman MT.

Hyer, M. W. (1998). "Stress Analysis of Fiber Reinforced Composite Materials" . Boston, Massachusetts: McGraw-Hill.

HPC (2000). "X-33 Update (Experimental Composite Tanks)" High Performance Composites, Volume 8 number 1, Jan/Feb 2000, page 9.

HPC (2001). "X-33 Update (Composite Tanks to be Replaced with Aluminum)" High Performance Composites, Volume 9 number 1, Jan/Feb 2001, page 15.

Irwin, G.R. (1949). "Fracturing of Metals, American Society for Metals," Cleveland. Ohio. pp. 146 – 148.

Jarmon, D.C., Weeks, C.A., Naik, R.A., Kogstrom, C.L., Logan, C.P., and Braun, P.F. (1998). "Mechanical Property Comparison of 3-D and 2-D Graphite Reinforced Epoxy Composites Fabricated by RTM," 43rd International SAMPE Symposium/Exhibition.

Jones, R. M. (1999). "Mechanics of Composite Materials" (2nd edition). Leviitown, PA: Taylor and Francis.

Mackin, T.J., (1992) "A Comparison of Instrumented Impact Testing and Gardner Impact Testing," Santa Barbara, CA: Dynatup Products Division General Research Corp.

Mandell J.F., and Samborsky D.D. (1997). DOE/MSU composite material fatigue database: Test methods, materials, and analysis (Contractor Report No. SAND97,3002). Albuquerque, NM: Sandia National Laboratories.

McMichael, S., and Fischer, S., (1989) "Understanding Materials with Instrumented Impact," Santa Barbara, CA Dynatup Products Division. General Research Corp.

Morehead, R.B. (2000). 'Fatigue of Skin Stiffener Intersections in Composite Wind Turbine Blade Structures" Master's Thesis, Montana State University-Bozeman, Bozeman MT.

Naik, R.A. Jarmon, D.C., Weeks, C.A., and Logan, C.P. (1998). "Characterization and Modeling of Advanced Architecture Woven Materials," 43rd International SAMPE Symposium/Exhibition.

Norton, R. L. (1996). "Machine Design (An Integrated Approach)". Upper Saddle River, NJ: Prentice Hall.

Orozco, R. (1999). "Effects of Toughened Matrix Resins on Composite Materials for Wind Turbine Blades" Master's Thesis, Montana State University-Bozeman, Bozeman MT.

Penado, F.E. and Dropek, R.K. (1990). "Numerical Design and Analysis", Engineering Materials Handbook(Adhesives and Sealants) Vol 3, 1990, pp.477-500.

Russel, A.J. and Street, K.N. (1987). "The Effect of Matrix Toughness on Delamination: Static and Fatigue Fracture Under Mode II Shear Loading of Graphite Fiber Composites," Toughened Composites, ASTM STP 937, ASTM, Philadelphia, PA. pp 275.

Rybicki, E.F. and Kanninen, M.F. (1977). "A Finite Element Calculation of Stress Intensity Factors by a Modified Crack Closure Integral," *Engineering Fracture Mechanics*, Vol. 9, 1977, pp. 931-938.

Skeist, I. (1977). "Handbook of Adhesives" (2nd Ed). Livingston, NJ: Van Nostrand Reinhold Company.

Skramstad, J.D. (1999). "Evaluation of hand lay-up and resin transfer molding in composite wind turbine blade manufacturing", Master's Thesis, Montana State University-Bozeman, Bozeman MT.

Sun, T.C. (1997). "Calculation of Stress Intensity Factors for Interlaminar Cracks in Composite Laminates," *Composites Science and Technology*, Vol. 57, 1997, pp 637-650.

Tsai, S.W. (1971). A General Theory of Strength for Anisotropic Materials, J. Composite Materials, January, 1971, pp. 58-80.

Tsai, S.W. (1988). Composite Design 4th edition, Think Composites. Dayton, OH.

Valisetty, R.R. and Chamis, C.C. (1988). "Sublaminate or Ply-Level Analysis of Composites and Strain Energy Release Rates of End-Notch and Mixed-Mode Fracture Specimens,"*Composite Materials: Testing and Design(8th conference)*, ASTM STP 972, ASTM, Philadelphia, Pennsylvania, pp. 41-56.

Weeks, C.A., Naik, R.A., and Kogstrom, C.L. (1998). "Analysis of Damage in Through Thickness Reinforced Composites Induced by Soft Body Impact," 43rd International SAMPE Symposium/Exhibition.

Whitney, J.M. and Nuismer, R.J. (1974). "Stress Fracture Criteria for Laminates Containing Stress Concentrations," Journal of Composites, vol. 8, pp. 253-265.

APPENDIX A

FINITE ELEMENT CODES

Static Flexure FEA Macro

```
/PREP7
!This Model Constructs a representation of a basic 3-pt Bending Apparatus
!and Static Flexure Specimen.  Symmetry is employed at the midplane
!The effects of friction due to the testing fixture are also captured

!Initial Dimensions of Test Geometry

!Specimen
halfspan=63.5
thick=6.135
overhang=22

!Support Fixture
rad=9.50
sloprad=9.70`

!Keypoints to Construct  Specimen
K,1,0,0,0
K,2,overhang,0,0
K,3,halfspan+overhang,0,0
K,4,halfspan+overhang,thick,0
K,5,0,thick,0

!Lines Required to Construct Specimen
LSTR,1,2
LSTR,2,3
LSTR,3,4
LSTR,4,5
LSTR,5,1

!Area Representing  Specimen
AL,1,2,3,4,5

!Element Declaration
ET,1,PLANE 82
KEYOPT,1,3,3
R,1,25.4

!Material Properties
MP,EX,1,74.5E3
MP,PRXY,1,.3
```

```
!Element Sizing
ESIZE,thick/6

!Meshing of Specimen
TYPE,1
MAT,1
AMESH,1

!Stability and Symmetry Boundary Condition
DL,3,1,UX,0


!Steel Properties for Fixture
MP,EX,2,209E3
MP,PRXY,2,.3

!Roller Generation
CYL4,OVERHANG,-RAD,RAD

!Roller Meshing
MSHAPE,1,2D
MSHKEY,0
TYPE,1
MAT,2
AMESH,2

!Construction of Fixture Using Keypoints
K,22,OVERHANG-SLOPRAD,-RAD,0
K,23,OVERHANG+SLOPRAD,-RAD,0
K,24,OVERHANG+25.4,-RAD,0
K,25,OVERHANG-25.4,-RAD,0
K,26,OVERHANG,-RAD,0
K,27,OVERHANG-25.4,-35.1,0
K,28,OVERHANG+25.4,-35.1,0

!Lines from Keypoints
LARC,22,23,9
LSTR,22,25
LSTR, 23,24

LSTR,25,27
LSTR,27,28
```

```
LSTR,28,24

!Area from Lines
AL,10,11,13,14,15,12

!Meshing of Fixture
MSHAPE,1,2D
MSHKEY,0
TYPE,1
MAT,2
AMESH,3

!Application of Jig constraints
DA,3,ALL,0

!The contact wizard should then be employed to produce
!2 flexible-flexible 2-D contact pairs or surfaces
!One between the roller and fixture and the other between the roller and sample

!Apply Load to Specimen Center and Solve
```

ENF FEA Macro

```
/PREP7
!This Model is a Representation of the ENF Test Specimen

!Specimen Dimensions
SUPPORT=11
CRACK=39
L=171
T=6.135

!Construction of Keypoints for Geometry
K,1,0,0,0
K,2,L,0,0
K,3,L,T/3,0
K,4,4/3*CRACK,T/3,0
K,5,CRACK,T/3,0
K,6,0,T/3,0
K,7,L,2*T/3,0
K,8,4/3*CRACK,2*T/3,0
K,9,CRACK,2*T/3,0
K,10,0,2*T/3,0
K,11,0,T/2,0
K,12,CRACK,T/2,0
K,13,L,T,0
K,14,0,T,0
K,15,0,T/2,0
K,16,SUPPORT,T/3,0
K,17,SUPPORT,T/2,0
K,18,SUPPORT,2*T/3,0
K,19,SUPPORT,T/2,0
K,20,4/3*CRACK,T/2,0

!Construction of Areas From Keypoints
A,6,16,17,11
A,16,5,12,17
A,19,12,9,18
A,15,19,18,10
A,5,4,20,12
A,12,20,8,9

A,4,3,7,8
A,1,2,3,4,5,16,6
A,10,18,9,8,7,13,14
```

```
!Declaration of Element Type
ET,1,PLANE 82
KEYOPT,1,3,3
R,1,1

!Assignment of Material Properties
MP,EX,1,75E3
MP,PRXY,1,.3

!Meshing
ESIZE,.5
TYPE,1
MAT,1
AMESH,5
AMESH,6
AMESH,3
AMESH,2

ESIZE,1
TYPE,1
MAT,1
AMESH,1
AMESH,4

ESIZE,1
TYPE,1
MAT,1
AMESH,7
AMESH,8
AMESH,9

!Use Contact Wizard to Generate Contact Surfaces on the Lines that Form the Crack
!Apply Y Constraints at the Roller Locations and an X Constraint at the Node with the
!Critical Load and Solve
```

Flatwise Tension FEA Macro

```
/PREP7
!FEA Model of Flat Wise Tension Specimens
!TOL variable allows for the shifting of the steel tabs
!FWT properties determined from test scraps.
!Flexure used to Assess face sheet properties
!Assumed modulus from FWT experiment used for core material

!The model can be ran with different values of TOL
!Geometric Parameters for Face Sheet and Core Thicknesses and Specimen Width

WIDTH=37
T1=1.6
T2=37
T3=4
TTOTAL=T1+T2+T3

!Geometric Parameters for Steel Fixture or Tab
FLANGE=4
WEBT=4
HEIGHT=29
TOL=0

!Declaration of Element Size
ESIZE,1

!Keypoints
K,1,0,0,0
K,2,WIDTH,0,O
K,3,WIDTH,T1,O
K,4,0,T1,O
K,5,0,T1+T2,0
K,6,WIDTH,T1+T2,0
K,7,WIDTH,T1+T2+T3,0
K,8,0,T1+T2+T3,0

!Generating Areas from Keypoints
A,1,2,3,4
A,3,4,5,6
A,5,6,7,8

!Assignment of Material Core Properties
MP,EX,1,21
```

```
MP,PRXY,1,.3

!Assignment of Material
MP,EX,2,43400
MP,PRXY,2,.3


!Declaration of Element Type
ET,1,PLANE 82
KEYOPT,1,3,3
R,1,37

!Meshing of Core Region
TYPE,1
MAT,1
AMESH,2

!Meshing of Face Sheets
TYPE,1
MAT,2
AMESH,1
AMESH,3

!Construction of Steel Tabs
K,9,0,-FLANGE,0
K,10,WIDTH/2-WEBT/2+TOL,-FLANGE,0
K,11,WIDTH/2-WEBT/2+TOL,-HEIGHT,0
K,12,WIDTH/2+WEBT/2+TOL,-HEIGHT,0
K,13,WIDTH/2+WEBT/2+TOL,-FLANGE,0
K,14,WIDTH,-FLANGE,0

A,1,2,14,13,12,11,10,9

K,15,0,FLANGE+TTOTAL,0
K,16,WIDTH/2-WEBT/2,FLANGE+TTOTAL,0
K,17,WIDTH/2-WEBT/2,HEIGHT+TTOTAL,0
K,18,WIDTH/2+WEBT/2,HEIGHT+TTOTAL,0
K,19,WIDTH/2+WEBT/2,FLANGE+TTOTAL,0
K,20,WIDTH,FLANGE+TTOTAL,0

A,7,8,15,16,17,18,19,20

!Material Properties for Steel
MP,EX,3,200000
```

```
MP,PRXY,3,.3

Meshing of Steel Tabs
TYPE,1
MAT,3
AMESH,4
AMESH,5

!Constrain center node at bottom with DN,UX,0 and DN,UY,0
!Where N is the node number.
!Constrain center node at top iwth DN,UX,0
!Apply Appropriate Force to Top Node.
!Solve

!Use Map Function to Map Membrane stress to x location and extract for plots
```

DCB Specimen FEA Macro

```
/PREP7
!This Model Represents the DCB Sandwich Panel Test Specimen

!Specimen Dimensions
!L=Length, C=Crack length, W=width, T1,T2, and T3 are face sheet and core thicknesses
L=150
C=50
T1=4
T2=37
T3=1.64
W=37.5

!Creation of Keypoints for Geometry
K,1,0,0,0
K,2,L,0,0
K,3,L,T1,0
K,4,0,T1,0
K,5,L,T1+T2-T3,0
K,6,4/3*C,T1+T2-T3,0
K,7,C,T1+T2-T3,0
K,8,0,T1+T2-T3,0
K,9,L,T1+T2,0
K,10,4/3*C,T1+T2,0
K,11,C,T1+T2,0
K,12,0,T1+T2,0
K,13,L,T1+T2+T3,0
K,14,4/3*C,T1+T2+T3,0
K,15,C,T1+T2+T3,0
K,16,0,T1+T2+T3,0
K,17,0,T1+T2,0

!Creation of Areas from Keypoints
A,1,2,3,4
A,4,3,5,6,7,8
A,8,7,11,12
A,7,6,10,11
A,6,5,9,10
A,10,9,13,14
A,11,10,14,15
A,17,11,15,16
```

```
!Declaration of element type
ET,1,PLANE 82
KEYOPT,1,3,3
R,1,W

!Material Properties
!Elastic Modulus
MP,EX,1,42200
MP,PRXY,1,.3
MP,EX,2,50
MP,PRXY,2,.3

!Declaration of Element Size and Meshing
ESIZE,.2
TYPE,1
MAT,1
AMESH,8
AMESH,7

TYPE,1
MAT,2
AMESH,3
AMESH,4

ESIZE,2
TYPE,1
MAT,1
AMESH,6
AMESH,1

TYPE,1
MAT,2
AMESH,5

ESIZE,6
TYPE,1
MAT,2
AMESH,2

!Restrain x and y displacement at node corresponding to hinge location at bottom
!Restrain x displacement at node corresponding to hinge location at top
!Apply critical load and solve
```

Shear Lap Specimen FEA Macro

```
/PREP7
!This model replicates the Shear lap specimen

!Shear Lap Specimen Properties
!TM = Metal thickness, TR = Resin thickness, LR = Length of the bond, LM Length of
Metal.
TM=1.43
TR=.070
LR=29
LM=150
GRIP=25

!Keypoints for Geometry
K,1,0,0,0
K,2,TM,0,0
K,3,TM,LM-5/4*LR,0
K,4,0,LM-5/4*LR,0
K,5,TM,LM-3/4*LR,0
K,6,0,LM-3/4*LR,0
K,7,TM,LM-LR/4,0
K,8,0,LM-LR/4,O
K,9,TM,LM,0
K,10,0,LM,0
K,11,TM,LM-LR,0
K,12,TM+TR,LM-LR,0
K,13,TM+TR,LM-3/4*LR,0
K,14,TM+TR,LM-LR/4,0
K,15,TM+TR,LM,0
K,16,2*TM+TR,LM-LR,0
K,17,2*TM+TR,LM-3*LR/4,0
K,18,2*TM+TR,LM-LR/4,0
K,19,2*TM+TR,LM+LR/4,0
K,20,2*TM+TR,2*LM-LR,0
K,21,TM+TR,2*LM-LR,0
K,22,TM+TR,LM+LR/4,0
K,23,TM,GRIP,0
K,24,0,GRIP,0
K,25,TM+TR,2*LM-LR-GRIP,0
K,26,2*TM+TR,2*LM-LR-GRIP,0

!Creating Areas from Keypoints
A,1,2,23,24
```

```
A,24,23,3,4
A,4,3,11,5,6
A,6,5,7,8
A,8,7,9,10


A,11,12,13,5
A,5,13,14,7
A,7,14,15,9


A,12,16,17,13
A,13,17,18,14
A,14,18,19,22,15
A,19,26,25,22
A,25,26,20,21

!Assignment of Material Properties
MP,EX,2,200000
MP,PRXY,2,.3
MP,EX,1,3250
MP,PRXY,1,.35

!Element Declaration
ET,1,PLANE82
ESIZE,TR/3

!Meshing of Resin Region
TYPE,1
MAT,1
AMESH,6
AMESH,8

ESIZE,TM/8
TYPE,1
MAT,1
AMESH,7

!Meshing of Steel
TYPE,1
MAT,2
AMESH,4
AMESH,10
```

```
AMESH,3
AMESH,5
AMESH,9
AMESH,11

ESIZE,TM/2
TYPE,1
MAT,2
AMESH,1
AMESH,2
AMESH,12
AMESH,13

!Application  of Constraints
DL,1,1,ALL,0
DL,2,1,UX,0
DL,4,1,UX,0

DL,36,13,UX,0
DL,38,13,UX,0

!Apply load and Solve
```

Miniroot FEA Macro

```
/PREP7
!This Model Replicates the Miniroot Test Specimen
!13 Volumes were Required to Provide Regions of Varying Discretization
!and to Ensure Element Continuity

!Creation of Keypoints for All of the Volume Segments that Formulate the Miniroot
K,1,0,0,0
K,2,24,0,0
K,3,24,6,0
K,4,0,6,0
K,5,0,0,138
K,6,24,0,138
K,7,24,6,138
K,8,0,6,138
K,9,24,1,138
K,10,12,1,138
K,11,12,0,138
K,12,24,0,280
K,13,24,1,280
K,14,12,1,280
K,15,12,0,280
K,16,0,0,210
K,17,12,0,210
K,18,12,1,210
K,19,24,1,210
K,20,24,6,210
K,21,0,6,210
K,22,0,1,210
K,23,0,1,138
K,24,12,6,210
K,25,12,6,138
K,26,0,0,120
K,27,24,0,120
K,28,24,6,120
K,29,0,6,120
K,30,24,0,210
K,31,24,1,120
K,32,12,6,120
K,33,12,1,120
K,34,12,0,120
K,35,0,1,120

K,36,24,1,0
```

```
K,37,12,0,0
K,38,12,1,0
K,39,12,6,0
K,40,0,1,0

!Creation of the Volume from the Keypoints
V,11,6,9,10,34,27,31,33
V,10,9,7,25,33,31,28,32
V,5,11,10,23,26,34,33,35
V,23,10,25,8,35,33,32,29
V,35,33,32,29,40,38,39,4
V,26,34,33,35,1,37,38,40
V,34,27,31,33,37,2,36,38
V,33,31,28,32,38,36,3,39
V,17,30,19,18,15,12,13,14
V,17,30,19,18,11,6,9,10
V,5,11,10,23,16,17,18,22
V,10,9,7,25,18,19,20,24
V,23,10,25,8,22,18,24,21

!Assignment of Material Properties for the Composite Regions
MP,EX,1,28.3E9
MP,EY,1,7.75E9
MP,EZ,1,7.38E9
MP,PRXY,1,.32
MP,PRYZ,1,.33
MP,PRXZ,1,.44
MP,GXY,1,3.30E9
MP,GYZ,1,2.82E9
MP,GXZ,1,2.55E9

!Assignment of Material Properties for the Metal Insert
MP,EX,2,209E9
MP,PRXY,2,.3
MP,GXY,2,75.5E9

!Declaration of Element Type and Meshing of Composite Regions
ESIZE,1
ET,1,SOLID45
TYPE,1
MAT,1
VMESH,1
VMESH,2
VMESH,3
```

```
VMESH,4
VMESH,11
VMESH,12
VMESH,13

!Meshing of Metal Insert
ESIZE,1
TYPE,1
MAT,2
VMESH,9
VMESH,10

ESIZE,6
ET,1,SOLID45
TYPE,1
MAT,1
VMESH,5
VMESH,6
VMESH,7
VMESH,8

!Application of Constraints
DA,25,ALL
DA,29,ALL
DA,33,ALL
DA,36,ALL
DA,3,UX
DA,8,UX
DA,31,UX
DA,34,UX
DA,39,UX
DA,44,UX
DA,51,UX
DA,2,UY
DA,13,UY
DA,26,UY
DA,30,UY
DA,38,UY
DA,43,UY
DA,47,UY

SFA,42,1,PRES,-160

/SOLVE
```

MONTANA STATE UNIVERSITY - BOZEMAN
3 1762 10352909 3